Stony Brook University

Synthesis of Carbon-11 Radiopharmaceuticals and Their Evaluations

A Dissertation Presented

by

Kun-Eek Kil

to

The Graduate School

In Partial Fulfillment of the

Requirements

for the Degree of

Doctor of Philosophy

in

Chemistry

Stony Brook University

December 2008

Stony Brook University

The Graduate School

Kun-Eek Kil

We, the dissertation committee for the above candidate for the

Doctor of Philosophy degree, hereby recommend

Acceptance of this dissertation.

Joanna S. Fowler – Dissertation Advisor

Professor, Department of Chemistry

Yu-Shin Ding – Dissertation Co-Advisor

Professor, Department of Chemistry
Yale University School of Medicine

Iwao Ojima – Chairperson of Defense

Distinguished Professor, Department of Chemistry

Philip M. Johnson – Third Member

Professor, Department of Chemistry

Anat Biegon – Outside Member

Senior Scientist, Brookhaven National Laboratory

This dissertation is accepted by the Graduate School

Lawrence Martin

Dean of the Graduate School

Abstract of the Dissertation

Synthesis of Carbon-11 Radiopharmaceuticals and Their Evaluations

by

Kun-Eek Kil

Doctor of Philosophy

in

Chemistry

Stony Brook University

2008

Positron emission tomography (PET) is a medical imaging method which measures the distribution and movement of radiotracers labeled with positron emitting isotopes in the living animal and human body. Its use to measure biochemical transformations and the movement of drugs in the body requires the development radiopharmaceuticals labeled with short lived positron emitting isotopes. Among the positron emitting isotopes, carbon-11 is a very attractive isotope for molecular imaging and drug research. However, because of its short half life (t1/2 = 20.4 min), the chemist must produce the isotope and incorporate it into a radiopharmaceutical in less than 60 minutes

Imatinib (Gleevec) and letrozole, both are manufactured by Novartis Pharmaceuticals, and are FDA approved drugs for chronic myeloid leukemia and breast cancer, respectively. Because imatinib is an inhibitor of bcr-abl tyrosine kinase, we developed a synthesis of carbon-11 imatinib as a potential diagnostic for bcr-abl tyrosine kinase positive chronic myeloid leukemia. On the other hand, letrozole, an aromatase inhibitor, blocks the last step of estrogen bio-synthesis mediated by aromatase. Carbon-11 labeled letrozole was developed to image aromatase. Both [^{11}C]imatinib and [^{11}C]letrozole are also of interest for measuring drug pharmacokinetics.

We synthesized the unlabeled precursor and product of both imatinib and letrozole. [^{11}C]Methyl iodide and [^{11}C]hydrogen cyanide are generated in their own modules, and used in the syntheis of [*N*-^{11}C-methyl]imatinib and [^{11}C-cyano]letrozole in around 80% radiochemical yield by methylation and palladium(0)-mediated cyanide coupling, respectively. When [*N*-^{11}C-methyl]imatinib was evaluated in a healthy female baboon for pharmacokinetic study, increased carbon-11 uptake was observed in gall bladder, liver, kidneys, and bladder which might represent hepatobiliary and urinary excretion. There was minor carbon-11 uptake that was observed in a spinal cord where the malignancy of chronic myeloid leukemia develops. On the other hand, PET images of baboon brain using [^{11}C-cyano]letrozole indicated non-specific binding throughout the brain with no elevated accumulation in the amygdala where aromatase is abundant. These two labeled drugs provide the opportunity to examine the distribution and pharmacokinetics these two drugs in the brain and peripheral organs in humans.

Table of Contents

List of Figures·····xiii

List of Schemes·····xvi

List of Tables·····xvii

Table of Abbreviation·····xviii

Acknowledgement·····xx

Part I Introduction: PET and development of radiopharmaceuticals·····1

1. Principles of PET ·····1

2. Production of isotopes and radiochemistry·····2

2.1 Radiochemistry and isotopes for PET·····2

2.2 Units of radioactivity and radiation dose·····3

2.3 Production of positron emitting isotopes·····4

2.4 Specific activity·····5

3. Synthesis of carbon-11 labeling precursors and labeling chemistry·····6

3.1 Synthesis of carbon-11 labeling precursors·····6

3.2 Labeling chemistry·····9

4. Fluorine-18 chemistry·····11

4.1 Electrophilic reactions·····11

4.2 Nucleophilic reactions·····14

5. Quality control of radiopharmaceuticals for PET·····15

5.1 Physicochemical tests·····15

5.2 Biological tests·····17

6. Evaluation of PET radiopharmaceuticals for brain studies·····18

7. Advantages of PET·····23

Figures, Tables, and Schemes ·····24

Part II Synthesis and PET studies of carbon-11 labeled imatinib (Gleevec®)·····34

Abstract·····34

1. Introduction·····35

2. Material and Methods·····38

2.1 General·····38

2.2 Chemistry·····38

2.2.1 Norimatinib synthesis from Gleevec® capsule·····38

2.2.1.1 Recovering imatinib free base from Gleevec® capsules·····38

2.2.1.2 Preparation of 4-[(piperazinyl)methyl]-*N*-[4-methyl-3-[[4-(3-pyridyl)-2-pyrimidinyl] amino]phenyl benzamide (**2**) from imatinib free base (**1**) ····39

2.2.2 Preparation of *N*-(5-amino-2-methylphenyl)-4-(3-pyridyl)-2-pyrimidinamine for norimatinib (**2**) and imatinib (**1**) ·····40

2.2.2.1 3-(*N*,*N*-dimethylamino)-1-(3-pyridyl)-2-propen-1-one (**3**) ·····40

2.2.2.2 2-Methyl-5-nitrophenylguanidine nitrate (**4**) ·····41

2.2.2.3 *N*-(2-methyl-5-nitrophenyl)-4-(3-pyridyl)-2-pyrimidinamine (**5)** 42

2.2.2.4 *N*-(5-amino-2-methylphenyl)-4-(3-pyridyl)-2-pyrimidinamine (**6**) 43

2.2.2.5 Benzyl 4-(4'-hydroxycarbonylbenzyl)-1-piperazine carboxylate (**7**) 43

2.2.2.6 4-(4-Methylpiperazinomethyl)benzonitrile (**8**) 44

2.2.2.7 4-(4'-hydroxycarbonylbenzyl)-1-methylpiperazine (**9**) 45

2.2.2.8 Preparation of imatinib (**1**) and 4-[(4-benzyloxycarbonyl-1-piperazinyl)methyl]-*N*-[4-methyl-3-[[4-(3-pyridyl)-2-pyrimidinyl] amino]phenylbenzamide (**10**) by amide bond formation·····45

2.2.2.9 Preparation of norimatinib (4-[(piperazinyl)methyl]-*N*-[4-methyl-3-[[4-(3-pyridyl)-2-pyrimidinyl]amino]phenyl benzamide, **2**) by deprotection reaction·····47

2.3 Radiolabeling·····47

2.4 Quality control of collected [*N*-^{11}C-methyl]imatinib hydrochloride·····48

2.5 Determination of log D·····49

2.6 PET studies of [*N*-^{11}C-methyl]imatinib in baboon·····50

2.7 HPLC determination of fraction of [*N*-^{11}C-methyl]imatinib in plasma·····51

2.8 Plasma protein binding (PPB) of [*N*-^{11}C-methyl]imatinib·····52

2.9 Image analysis·····52

3. Results and Discussion·····53

3.1 Chemistry and carbon-11 labeling·····53

3.2 Evaluation of [*N*-^{11}C-methyl]imatinib with PET·····54

3.3 [*N*-^{11}C-methyl]imatinib pharmacokinetics after pretreatment with a therapeutic dose of imatinib·····56

4. Conclusions·····56

Figures and Schemes·····57

NMR Spectra·····65

Part III Synthesis and PET studies of [^{11}C-cyano]letrozole (Femara®), an aromatase inhibitor drug·····85

Abstract·····85

1. Introduction·····86

2. Materials and Methods·····90

2.1 General·····90

2.2 Chemistry·····91

2.2.1 1-(4-cyanobenzyl)-1*H*-1,2,4-triazole (**1**) and 1-(4-bromobenzyl)-1*H*-1,2,4-triazole (**2**) ·····91

2.2.2 4-[(4-bromophenyl)-1*H*-1,2,4-triazol-1-ylmethyl]benzonitrile (**3)** ···92

2.2.3 1-[Bis-(4-cyanophenyl)methyl]-1*H*-1,2,4-triazole (Letrozole) ·····93

2.3 Model reaction for the synthesis of letrozole from 4-[(4-bromophenyl)-1*H*-1,2,4-triazol-1-ylmethyl]benzonitrile (**3**) and cyanide. (General) ·····94

2.3.1 4-(4'-bromobenzoyl)benzonitrile (**4**) ·····95

2.3.2 4-(Phenyl-1*H*-1,2,4-triazol-1-ylmethyl)benzonitrile (**5**) ·····95

2.3.3 4,4'-dicyanobenzophenone (**6**) ·····95

2.4 Radiolabeling·····96

2.5 Quality control and radiochemical yield determination of [^{11}C-cyano]letrozole·····97

2.6 Determination of log D of [^{11}C-cyano]letrozole·····98

2.7 PET studies of [^{11}C-cyano]letrozole in baboon·····98

2.8 HPLC determination of [^{11}C-cyano]letrozole fraction in blood plasma·····99

2.9 Plasma protein binding (PPB) of [^{11}C-cyano]letrozole·····100

2.10 Image and data analysis·····100

3. Results and Discussion·····100

3.1 Chemistry and Carbon-11 Labeling·····100

3.2 Evaluation of [^{11}C-cyano]letrozole with PET image in the baboon brain···103

4. Conclusions·····105

Figures and Schemes·····106

NMR Spectra·····114

Part IV Synthesis and Labeling of Monoamine Oxidase (MAO) Inhibitors·····128

1. Introduction·····128

2. Chemistry·····133

2.1 General·····133

2.2 Experimental·····133

2.2.1 Synthesis of Ro 41-1049·····133

2.2.1.1 Ethyl 2-amino-5-bromo-1,3-thiazole-4-carboxylate (**2**) ·····133

2.2.1.2 Ethyl 2-amino-5-chloro-1,3-thiazole-4-carboxylate (**3**) ·····134

2.2.1.3 Ethyl 5-bromo-1,3-thiazole-4-carboxylate (**4**) ·····134

2.2.1.4 Ethyl 5-chloro-1,3-thiazole-4-carboxylate (**5**) ·····135

2.2.1.5 Ethyl 5-(3'-fluorophenyl)-1,3-thiazole-4-carboxylate (**6**) ·····135

2.2.1.6 5-(3'-fluorophenyl)-1,3-thiazole-4-carboxamide (**7**) ·····136

2.2.1.7 5-(3'-fluorophenyl)-1,3-thiazole-4-(*N*-hydroxymethyl) carboxamide (**8**) ·····137

2.2.1.8 5-(3'-fluorophenyl)-1,3-thiazole-4-(*N*-acetoxymethyl) carboxamide (**9**) ·····137

2.2.1.9 5-(3'-fluorophenyl)-1,3-thiazole-4-(*N*-cyanomethyl)carboxamide (**10**) ·····138

2.2.1.10 5-(3'-fluorophenyl)-1,3-thiazole-4-(*N*-2'-aminoethyl) carboxamide (Ro 41-1049) ·····139

2.2.1.11 5-(3'-fluorophenyl)-1,3-thiazole-4-(*N*-2'-aminoethyl) carboxamide (Ro 41-1049) from Compound **6**·····140

2.2.2 Synthesis of Ro 19-6327 and its precursor·····140

2.2.2.1 5-Chloropyridine-2-carboxamide (**12**) ·····140

2.2.2.2 5-Chloropyridine-2-(*N*-hydroxymethyl)carboxamide (**13**) ·····141

2.2.2.3 5-Chloropyridine-2-(*N*-acetoxymethyl)carboxamide (**14**) ·····141

2.2.2.4 5-Chloropyridine-2-(*N*-cyanomethyl)carboxamide (**15**) ·····142

2.2.2.5 5-chloropyridine-2-(*N*-2-aminoethyl)carboxamide (Ro 19-6327) 142

2.3 Synthesis of [*N*-(2-^{11}C-2-aminoethyl)]Ro 41-1049·····143

2.4 5-Chloropyridine-2-(*N*-^{11}C-cyanomethyl)carboxamide ([^{11}C]**15**) ·····144

2.5 Hydrogen [^{11}C]cyanide synthesis·····145

3. Results and Discussion·····147

4. Conclusions and Future Work ·····154

Figures, Schemes and Table·····155

NMR Spectra·····167

References·····195

List of Figures

Figure 2-1. Structure of Imatinib (The active ingredient of Gleevec®)

Figure 2-2. PET image of baboon brain with [*N*-^{11}C-methyl]imatinib. Summed frames over 90 minutes after injection of 3.9 mCi of [*N*-^{11}C-methyl]imatinib showing lack of uptake of carbon-11 into the brain probably due to P-glycoprotein mediated efflux [51, 52]. Anesthesia was ketamine followed by isoflurane.

Figure 2-3. PET image of torso of the anesthetized baboon with [*N*-^{11}C-methyl]imatinib. PET images (summation of frames over 90 minutes) of the baboon torso after the injection of 4.71 mCi of [*N*-^{11}C-methyl]imatinib showing accumulation of carbon-11 in the heart and lungs (top row); liver and beginning of the gall bladder (second row); liver and gall bladder (third row); gall bladder and spleen (fourth row); kidneys and spleen (fifth row). Note the high accumulation in the gall bladder. Anesthesia was ketamine followed by isoflurane.

Figure 2-4. Time-Activity curves for two different anestized baboons (panels (a) and (b)) who each received two injections of [*N*-^{11}C-methyl]imatinib cover the brain through the urinary bladder.

Figure 2-5. The comparison of time-activity curves of (a) gall bladder, (b) liver, (c) heart, (d) lungs, (e) spleen and (f) kidneys before and after pretreatment with 32 mg of imatinib administration by intravenous injection. Time-activity curves normalized for the area under the plasma time-activity curve are shown in the insets.

Figure 2-6. (a) Time-activity curve at baseline and after imatinib pretreatment for [*N*-^{11}C-methyl]imatinib in plasma showing the first 5 minutes, and (b) the plasma integral over 90 minutes. Pretreatment delayed [*N*-^{11}C-methyl]imatinib peak, and reduced its accumulated concentration in plasma by 10-15%.

Figure 3-1. The function of aromatase

Figure 3-2. Representative aromatase inhibitors (AI)

Figure 3-3. HPLC profile of [^{11}C-cyano]letrozole synthesis showing UV and radioactivity traces.

Figure 3-4. (a) TAC's of plasma from two baseline studies for the first two minutes. (b) Area under the curve (AUC) of [^{11}C-cyano]letrozole concentration in plasma over a 90 minute experiment for the two repeated baseline scans. (c) TAC's of plasma from baseline study and blocking study (0.1 mg/kg of unlabeled letrozole co-administration) for the first two minutes (d) AUC of [^{11}C-cyano]letrozole concentration in plasma over a 90 minute experiment at baseline and after letrozole treatment.

Figure 3-5. Summed frames PET images of baboon brain (0-90 min) from dynamic baseline scan. Carbon-11 uptake was observed in thalamus, striatum, temporal cortex, and cerebellum.

Figure 3-6. TAC's from baseline study showed that even if there are some differences in initial uptake depending on the region, the wash-out was fast for 10 minutes after peak time, but slowed down after 15 minutes.

Figure 3-7. Comparison of first and second dynamic scan for reproducibility in various brain regions.

Figure 3-8. TAC's from baseline study and blocking studies for thalamus (a), striatum (b), cerebellum (c), and amygdala (d). There was some movement of the head during the period 35-60 min necessitating deletion of two time frames for the small ROI's (striatum, thalamus, and amygdala).

Figure 4-2. An example of monoamine oxidation by monoamine oxidase (MAO).

Figure 4-3. Representative substrates for MAO A and MAO B.

Figure 4-4 Representative MAO inhibitors.

Figure 4-5. Representative PET radiotracers for MAO.

Figure 4-5. Diagram of [^{11}C]Hydrogen Cyanide Module

Figure 4-6. Diagram of ammonia removal test.

Figure 4-7. HPLC profile of substitution step to give [^{11}C]**10**.

Figure 4-8. Diagram of Synthesis for [*N*-(2-[^{11}C]-2-aminoethyl)]Ro 41-1049.

Figure 4-9. HPLC profile of [*N*-(2-^{11}C-2-aminoethyl)]Ro 41-1049 synthesis: Cyanide reduction eluting with 25% acetonitrile + 75% 0.1 M ammonium formate until 10 minutes and 50% acetonitrile + 50% 0.1 M ammonium formate after 10 minutes.

Figure 4-10. HPLC profile to synthesize 5-chloropyridine-2-(*N*-^{11}C-cyanomethyl) carboxamide ([^{11}C]**15**) eluting with 30% acetonitrile + 70% 0.1 M ammonium formate.

List of Schemes

Scheme 1-1. Synthesis of carbon-11 precursor from carbon-11 generation.

Scheme 1-2. Representative carbon-11 labeling method using various carbon-11 labeling precursors.

Scheme 1-3. Synthesis of fluorine-18 precursor from [^{18}F]fluorine.

Scheme 1-4. Examples of fluorine-18 labeling using electrophilic addition or substitution reactions.

Scheme 1-5. Fluorine-18 labeling reactions with [^{18}F]fluoride using nucleophilic substitution.

Scheme 1-6. Mechanism of irreversible binding of [^{11}C]clorgyline.

Scheme 2-1. Synthetic scheme of norimatinib, imatinib and [*N*-^{11}C-methyl]imatinib.

Scheme 3-1. Synthesis of letrozole and bromo-precursor (**3**) for [^{11}C-cyano]letrozole.

Scheme 3-2. Palladium catalyst mediated cyanide coupling reaction using potassium cyanide or [^{11}C]hydrogen cyanide in various solvents.

Scheme 4-1. Synthesis of Ro 41-1049, [^{11}C]Ro 41-1049 and its acetate precursor (**9**)

Scheme 4-2. Synthesis of [^{11}C]Ro 19-6327 and its precursor (**14**)

Scheme 4-3. Literature method to synthesize Ro 41-1049 [51, 52].

List of Tables

Table 1-1. The units of radioactivity and radiation dose.

Table 1-2. Properties of representative positron emitting isotopes.

Table 1-3. Quality Control Specification for ^{18}FDG [60] and 6-[^{18}F]-L-FluoroDOPA [61].

Table 4-1. Ammonia removal test with various trapping material.

Table of Abbreviation

Abbreviation	Full Name
PET	Positron Emission Tomography
MRI	Magnetic Resonance Imaging
CT	Computerized Tomography
^{18}FDG	2-deoxy-2-[^{18}F]fluoro-D-glucose
EOB	End of Bombardment
EOS	End of Synthesis
TOI	Time of Injection
FDA	Food and Drug Administration
LAL Test	*Limsulus Amebocyte Lysate* Test
SAR Study	Structure-Activity Relationship Study
MAO	Monoamine Oxidase
BP	Binding Potential
DV	Distribution Volume
DVR	Distribution Volume Ratio
ROI	Region of Interest
CML	Chronic Myeloid Leukemia
GIST	Gastrointestinal Stromal Tumors
^{18}FLT	3-Deoxy-3-^{18}F-Fluorothymidine
WBC	White Blood Cell
PDGF	Platelet Derived Growth Factor
ICC	Interstitial Cells of Cajal
AD	Alzheimer's Disease

Abbreviation	Full Name
Aβ	Amyloid-β-Peptide (Aβ)
HRMS	High Resolution Mass Spectrometry
TLC	Thin Layer Chromatography
RCY	Radiochemical Yield
PPB	Plasma Protein Binding
mCPBA	3-Chloroperbenzoic Acid
CYP	Cytochrome P450
AI	Aromatase Inhibitor
CNS	Central Nervous System
HPLC	High Performance Liquid Chromatography
TAC	Time Activity Curve
DMF	*N*, *N*-Dimethylformamide
USP	United States Pharmacopeia
SPECT	Single Photon Emission Computed Tomography
fMRI	Functional Magnetic Resonance Imaging
GC	Gas Chromatography
DMSO	Dimethyl Sulfoxide
Kd	Dissociation Constant of Ligand
DMAP	4-*N*, *N*-dimethylaminopyridine
NBS	*N*-Bromosuccimide
NCS	*N*-Chlorosuccimide
Kryptofix222	4,7,13,16,21,24-Hexaoxa-1,10-diazabicyclo[8.8.8]-hexacosane

Acknowledgement

First of all, I would like thank my advisor, Dr. Joanna S. Fowler, for her support and advice regarding my PhD degree. She guided many projects throughout my period at Brookhaven National Laboratory. I would also like to thank my co-advisor Dr. Yu-Shin Ding for guidance of research projects. She guided and helped me greatly even after she left Brookhaven. I would also like to appreciate my defense committee members, Dr. Iwao Ojima, chairperson, Dr. Philip Johnson, third member, and Dr. Anat Biegon, outside member, for instructing me to become a qualified Ph.D. I would like to appreciate my former advisors in Korea, Dr. Deok-Chan Ha in Korea University, and Dr. Yong Tae Park in Kyungpook National University for encouraging me to be a Ph.D.

The former and present members of Dr. Fowler's group in Brookhaven have been a big help to me in many ways during my research at Brookhaven. First, I would like to thank to Dr. Kuo-Shyan Lin, Dr. Sung Won Kim, Dr. Jacob M. Hooker, Dr. Alicia Reid, and Dr. Haitao Wu. They have become my friends and have helped me to solve problems during my research. I would also like to appreciate the staffs of cyclotron and PET facility at Brookhaven. Dr. David Schlyer, Richard Ferrieri, Colleen Shea, Youwen Xu, Lisa Muench, David Alexoff, Michael Schueller, Pauline Carter, Donald Warner, and Payton King helped support my research when I performed research at the cyclotron. Dr. Stephen L. Dewey, Dr. Wynne Schiffer, Dr. Jean Logan, Vinal Patel, Diane Lee, Douglas Marsteller, Nicole Barbarich-Marsteller, Martin M Mirrione, and Courtney Liebling also helped me in many ways to be a good member in the PET group at Brookhaven. Especially, I would like to thank Michael Schueller and David Schlyer for operation of the cyclotron, Donald Warner for PET operations, Payton King, and Pauline Carter for

performing the baboon studies. I am also grateful to Colleen Shea, Youwen Xu, and Lisa Muench for performance of *in-vitro* studies.

I would also like to thank my Korean friends in Brookhaven. Dr. Yang Soo Kim, Dr. Hyung Chul Kim, Dr. Jun Beom Park, Dr. Yong Man Choi, Dr. Sang June Park, Do Hyun Kim, Dr. Suk Kyung Lee, Dr. Young Suk Choi, Dr. Hwan Jin Noh, Dr. Yong-Jae Lee, Dr. Kyung Yoon Chung, Dr. Won Sub Yoon, Dr Sang Moon Park, and Dr. Kyung Ha Kang became my friends, and helped me relax during the tough research period.

I am also indebted to my Korean friends at Stony Brook in many ways. Dr. Myung Hwa Kim, Dr. Kyung Hwan Yoon, Dr. Nam June Kim, Young Suk Park, Dr. Jong Kahk Keum, Yeon Joo Lee, Dr. Tae Jin Park, Jong Sik Kim, Dr. Sung Jong Kwak, You Jin Ghang, Keun Soo Kim, Eun Jung Lee, Jun Yong Choi, You Kyung Chung, Jung Yong Lee, Young Chun, Keun Young Kim, Eun Young Lee, Jun Suk Yoon, Dr. Joo Yeon Chung, Dr. Kwang Suk Kim, Dr. Kwang Wook Ahn, Gun Woo Kim, Chan Hang Lee, Dong Hwan Kim, Eun Young Kim, Yeon Joo Jang, Yoon Hyun Oum, and Si Yeon Lee enriched my life during my Ph.D. period.

I would like to thank my eternal friends in Korea. Jae Hoon Kim, Dr. Jae Woong Lee, Sang Chul Shin, Jung Hwan Bae, Byung Soo Lee, Won Chan Kim, Dr. Chang Soo Yun, Dr. Eun Sung Kim, Joo Hwan Chung, Dr. Won Jong Noh, Dae Suk Jung, Tae Yeol Ahn, Jung Ho Jang, and Dae Sik Kim were always by my side, and encouraged me even when I was tired during my research.

Finally, I would like to thank my family in Korea. My parents and my brother supported me mentally and financially all the time. My parents-in-law and brother-in-law provided

me great support during my Ph.D. period. Their presence gave me full strength everyday. Above all, I would like to thank my wife. I could not survive without her encouragement and guidance. I would like to dedicate my thesis to my wife, my true love.

PART I

Introduction: PET and development of radiopharmaceuticals

1. Principles of PET

Positron emission tomography (PET) is an advanced medical imaging method which detects and quantifies the distribution and movement of positron emitting isotope labeled in a volume element of tissue or other material. The PET scanner detects annihilation radiation which comes from positron emitting isotope. When a chemical compound labeled with a positron emitting isotope is introduced into the body, it travels, distributes, and localizes within the living system. When a positron emitting isotope decays, positron is emitted from the nucleus, which combines with an electron within millimeters of its origin, and annihilates into two γ-rays emitted 180 degrees apart. The two γ-rays generated by annihilation radiation have enough energy to penetrate living system even the skull, and to reach the detector which shapes like ring to register the concurrent antiparallel signal. The sophisticated image reconstruction technique produces two or three-dimensional images. Whereas other medical imaging devices such as magnetic resonance imaging (MRI) and computerized tomography (CT), largely impart the anatomical information, PET delivers various functional information on the images in spite of relatively poor image resolution. Functional magnetic resonance imaging (fMRI) also measures brain activity by measuring the differences in the magnetic properties of hemoglobin and deoxyhemoglobin whose levels are determined by blood flow and oxygen consumption during activation, but it is not versatile like PET. PET can display various biochemical information depending on the labeled radiotracer administered to the

living organism. For example, 2-deoxy-2-[^{18}F]fluoro-D-glucose (^{18}FDG) displays information on glucose metabolism in vivo [1]. [^{11}C]Raclopride reveals the distribution and availability of dopamine receptors in the living system [2].

A PET study involves three major steps. One is the production of positron emitting isotopes by nuclear reaction by bombardment of a target with small particles such as protons, and deuterons using a cyclotron. The next step is generation of labeling precursor and labeling the molecule to produce a radiopharmaceutical. The final step is the performance of a PET scan followed by quantification with appropriate kinetic modeling. The following sections will discuss the details of each step to produce and translate PET image.

2. Production of isotope and radiochemistry

2.1 Radiotracer chemistry and isotopes for PET

Radioisotopes emit positive or negative charged particles such as α particle or β particles or carry out electromagnetic radiation because of unstable nucleus. Some radiation decay mode such as α- and β-decay are not useful for medical imaging because the emitted particles have too little energy to exit tissue and reach the detector.

However, positron-emitting isotopes which PET uses for imaging are neutron-deficit. They stabilize their nuclei by turning a proton into a neutron as a result of positron emission. The positron released from positron emitting isotopes such as ^{11}C, ^{18}F, ^{13}N, and ^{15}O travels within tissue for short distance, and then undergoes annihilation with an electron to generate two γ-rays which proceed antiparallel to each other. The two γ-rays feature unique energy (511 KeV) no matter what the isotope is. On the other hand, some neutron deficit nuclei also undergo electron capture to turn an extra proton into a neutron

by capturing an electron in K shell. Because both positron emission and electron capture are carried out by neutron-deficit isotopes, the two decay modes compete with each other. For example, 97% of fluorine-18 undergoes positron emission, and 3% of fluorine-18 undergoes electron capture. However, carbon-11 decay is exclusively by positron emission.

2.2 Units of radioactivity and radiation dose

To understand radioactivity, it is important to know the units of radiation and radiation exposure. These are summarized in Table 1. The unit of radioactivity is expressed as Curie (C_i) or Becquerel (Bq, SI unit). One Bq is defined as one disintegration (decay) per second (dps). 1 C_i is equal to 37 GBq. It is roughly the same radioactivity from 1 g of ^{226}Ra.

Absorbed radiation dose in a biological system is expressed as a Sievert (Sv, SI unit) or rem (Röntgen equivalent in man). Sievert is defined as 1 J/kg. 1 Sv is equal to 100 rem. Whereas sievert is the unit for biological system to measure radiation dose, gray (Gy, SI unit) is the unit for non-biological system to measure absorbed radiation dose. 1 Gy is equal to 1 J/kg, and equal to 100 rad. 1 rad is defined as 100 ergs of energy absorbed by 1 g of material.

Radiation exposure can be expressed as coulomb per kilogram (C/kg) or Röntgen (R). 1 R is equal to 2.58×10^{-4} C/kg. This unit can be converted to radiation dose, rem by multiplying Q factor (rem=Q×R). Q factor is determined by the type of ionization radiation. For example, Q factor of electron, X-ray and γ-ray is 1. Proton and α particle are 5 and 20, respectively. Neutron varies from 5 to 20 depending on its energy.

2.3 Production of positron emitting isotope

PET uses several different isotopes. The most representative positron emitters are ^{11}C ($t_{1/2}$=20.4 min), ^{18}F ($t_{1/2}$=109.8 min), ^{13}N ($t_{1/2}$=9.98 min), ^{15}O ($t_{1/2}$=2.03 min), ^{68}Ga ($t_{1/2}$=68.1 min), ^{64}Cu ($t_{1/2}$=12.7 hr), and ^{124}I ($t_{1/2}$=4.2 days). Among them, ^{11}C, ^{13}N, and ^{15}O are particularly important because isotopic labeling is possible; their incorporation might not alter the original property of non-radioactive analogues. ^{18}F can substitute for H or OH in some cases. The properties of these four common positron emitting isotopes are summarized in Table 2 [3] (See Page 24).

Carbon-11 is generated by the proton bombardment of a nitrogen target. Carbon-11 is obtained as either [^{11}C]methane or [^{11}C]carbon dioxide. When proton bombardment of nitrogen target is performed in 5% hydrogen in nitrogen, the major carbon-11 product is [^{11}C]methane [4]. [^{11}C]Carbon dioxide is obtained by proton bombardment of nitrogen target with intentional addition of trace amount of oxygen [4].

Fluorine-18 is generated by either deuteron bombardment of neon gas or proton bombardment of oxygen-18 water. When fluorine-18 is generated in neon gas ($^{20}Ne(d,\alpha)^{18}F$), the major form of the fluorine-18 element is fluorine gas (F_2) which is directly used in the synthesis. When fluorine-18 is produced in the $H_2{}^{18}O$ ($^{18}O(p,n)^{18}F$), the major form is fluoride. Fluoride is further separated from target water by anion exchange [5] allowing recovery of ^{18}O enriched target water ($H_2{}^{18}O$). The reactivity of [^{18}F]fluoride can be enhanced by addition of large counterion such as rubidium, cesium, potassium with kryptofix222 [6], and tetrabutylammonium salt [7]. Carbonate is a good anion because of its low nucleophilicity and basicity.

When carbon powder or carbon-13 powder is irradiated with deuterons or protons respectively, nitrogen-13 can be obtained as [^{13}N]N_2 [8, 9]. However, it is not a useful labeling agent because nitrogen itself is not very reactive. When water is irradiated with protons, nitrogen-13 is obtained as [^{13}N]NO_3^- [10] which is further reduced to [^{13}N]ammonia by DeVarda's alloy, which is useful for labeling [11].

Oxygen-15 is obtained by the proton bombardment of [^{15}N]nitrogen or deuteron bombardment of nitrogen. It is not only produced as [^{15}O]oxygen, but also obtained as [^{15}O]water when hydrogen and nitrogen mixture is irradiated with deuterons (^{14}N(*d*, n)^{15}O) [12]. Oxygen-15 usually has too short half-life to incorporate the isotope into the substrate. Therefore [^{15}O]oxygen is rapidly converted into [^{15}O]carbon monoxide, or [^{15}O]carbon dioxide for measurement of metabolism and distribution in blood circulation.

As mentioned before, the positron emitting isotopes are typically generated by nuclear reactions which irradiate the target with either protons or deuterons of helium-3 nuclei. To trigger a nuclear reaction, the approaching two nuclei must overcome the repulsive coulomb energy. This is called the coulomb barrier. The yield of a nuclear reaction is dependent on the energy of beam, the thickness of the target, the concentration of target atoms, beam intensity, and irradiation time. The capacity of a cyclotron to produce isotopes is dependent on the energy range of the protons, deuterons, or helium-3 nuclei, and the beam current. Low energy cyclotrons can accelerate the protons to 10-19 MeV. Larger cyclotrons can accelerate many kinds of nuclei to greater energies.

2.4 Specific activity

Specific activity is usually defined as the ratio of the radioactivity of an isotope to the amount of carrier, which is normally the non-radioactive counterpart of the isotope or

labeled compound. When isotopes are produced from a cyclotron target, they are usually diluted with their non-radioactive counterparts because those isotopes are present as impurities in the target materials or other external sources. For example, carbon-11 or fluorine-18 is usually diluted with carbon-12 or fluorine-19. These non-radioactive isotopes also undergo the same chemical transformations as their radioactive counterparts. Therefore, the carrier can be non-radioactive version of target molecule or labeling agent. In this case, it is called no-carrier-added because the isotope impurities were not deliberately added to the cyclotron system.

According to Table 3, the theoretical maximum specific activity of carbon-11 is 9218 $C_i/\mu mol$. If actual specific activity of carbon-11 is 1 $C_i/\mu mol$, approximately one carbon-11 atom is present in every 9200 carbon-12 atoms. Whereas the radioisotope decays as time passes, the number of non-radioactive isotope remain constant. Therefore, specific activity decreases as time passes. Normally, specific activity is calculated by decay correction to a specific time point such as end of bombardment (EOB), end of synthesis (EOS), or time of injection (TOI). For carbon-11, the synthetic process must be performed in less than three half-lives from EOB to EOS in order to have enough carbon-11 left for an imaging study. Quality control for radiopharmaceutical must be carried out in less than one half-life from EOS to TOI.

3. Synthesis of carbon-11 labeling precursor and labeling chemistry

3.1 Synthesis of carbon-11 labeling precursor

Because of the versatility of carbon chemistry, various carbon-11 labeling precursors have been developed, and have been used to incorporate carbon-11 isotopes into different molecules by various methodologies. Scheme 1 shows the chemical synthesis of carbon-

11 labeled precursors. As was discussed in sec 2.3, carbon-11 is generated either as [^{11}C]carbon dioxide or [^{11}C]methane. Alternatively, [^{11}C]methane can be synthesized by reducing [^{11}C]carbon dioxide [4]. [^{11}C]Carbon dioxide can also be reduced to [^{11}C]methanol which can be further converted into [^{11}C]methyl iodide [13, 14] or [^{11}C]formaldehyde [14]. This procedure requires inert conditions to block the absorption of carbon dioxide from air by lithium aluminum hydride. Carbon dioxide contamination from air reduces the specific activity of [^{11}C]carbon dioxide. Recently, rapid conversion of [^{11}C]methyl iodide into [^{11}C]formaldehyde from using trimethylamine N-oxide was reported [15]. Zinc catalyst is used to convert [^{11}C]carbon dioxide into [^{11}C]carbon monoxide [4] which can be further transformed into [^{11}C]phosgene by platinum tetrachloride [16]. [^{11}C]Phosgene is important for labeling the carbonyl moiety in carbamate, carbonate, or urea derivatives. Alternatively, [^{11}C]phosgene can be synthesized from [^{11}C]methane via [^{11}C]carbon tetrachloride [17]. [^{11}C]Phosgene also reacts with liquid ammonia to change into [^{11}C]urea [16] which can be alternatively obtained from [^{11}C]hydrogen cyanide via [^{11}C]cyanate [18]. When [^{11}C]carbon dioxide is treated with methyllithium, [^{11}C]acetone is obtained and applied to various labeling reactions [19]. [^{11}C]Carbon dioxide, itself, is useful reagent to react with Grignard reagents or alkyl or aryl lithium to synthesize labeled carboxylic acids. [^{11}C]Carbon dioxide is also important radiotracer for photosynthesis. [^{11}C]Carbon monoxide has been used in transition metal assisted insertion reactions to synthesize ketone labeled compound [20].

[^{11}C]Methane is not reactive by itself, but it is a very important intermediate in the syntheses of other labeling reagents such as [^{11}C]methyl iodide and hydrogen

[^{11}C]cyanide. As we mentioned previously, it can be directly obtained from nuclear reaction by irradiating 5% hydrogen in nitrogen with protons. [^{11}C]Methane can be obtained from [^{11}C]carbon dioxide by reduction with hydrogen mediated by nickel [4]. Iodination of the resulting [^{11}C]methane at 720^{o}C produces [^{11}C]methyl iodide, an important labeling agent for methylation [21]. The synthesis of [^{11}C]methyl iodide from [^{11}C]methane is preferred synthetic pathway because of high specific activity. [^{11}C]Methyl iodide can be subsequently changed into other carbon-11 precursors. [^{11}C]Methyl iodide is passed through a silver triflate-impregnated graphitized carbon at 150^{o}C to convert into [^{11}C]methyl triflate, a mild methylation labeling agent [22]. [^{11}C]Methyl iodide can also be converted into [^{11}C]methyl lithium by butyl lithium [23], and [^{11}C]mesyl chloride is subsequently generated from [^{11}C]methyl lithium after treatment of sulfuryl chloride [24]. [^{11}C]Methyl iodide is also changed into [^{11}C-methyl]methyl isocyanate by silver cyanate [25]. [^{11}C]Nitromethane which has acidic α-hydrogen is also obtained from [^{11}C]methyl iodide by reaction with silver nitrite [26].

[^{11}C]Hydrogen cyanide, another versatile labeling precursor, is obtained by the reaction of [^{11}C]methane and ammonia mediated by platinum at 920^{o}C [4]. The cyanide group can be further chemically converted into carboxylic acid, amide, or amine moieties. [^{11}C]Hydrogen cyanide is passed through quartz tube containing pyridinium bromide and antimony to form [^{11}C]cyanogen bromide, a useful labeling agent to transfer cyanide group [27]. [^{11}C]Diazomethane is synthesized from [^{11}C]methane via [^{11}C]chloroform for selective methylation [28].

3.2 Labeling chemistry

Because of short half-lives of carbon-11, fluorine-18, and nitrogen-13, labeling reactions must be as rapid as possible, and the label should be incorporated in the final step of the synthesis. Ideally, the reaction should be finished within one-half life of the isotope. The reactivity of a labeling reaction is enhanced by the excess amount of substrate compared with the amount of labeling agent. Therefore, the reaction rate follows pseudo-first order kinetics. The labeling reaction owes its reactivity to a high concentration of substrate in small volume of solvent. A sealed reaction vessel might be another factor to run the labeling reaction at high temperature to increase the rate. Other methods to increase reaction rate are the use of microwaves and solid supports.

Radiochemical yield is expressed as decay corrected or decay uncorrected yield. Decay uncorrected radiochemical yield is expressed following equation: $A_P \times 100/A_L$. Decay corrected radiochemical yield is following equation: $A_P \times \exp(\lambda t) \times 100/A_L$ where A_P is radioactivity of product, A_L is radioactivity of labeling agent, and λ is decay constant.

The most versatile carbon-11 labeling method is carbon-11 methylation with [^{11}C]methyl iodide or [^{11}C]methyl triflate. Many radiopharmaceuticals such as [^{11}C]raclopride and [^{11}C]DASB are labeled by O-methylation or N-methylation [29, 30] (Scheme 1-2 (a, b)). Methyl coupling by Stille coupling has also been carried out in the presence of palladium catalyst. For example, [^{11}C]FMAU was synthesized by Stille coupling with [^{11}C]methyl iodide [31] (Scheme 1-2 (c)).

[^{11}C]Carbon dioxide can be directly used to make carboxylic acid derivatives. [^{11}C]WAY 100635 was synthesized by carboxylation followed by amide coupling after

labeling with [^{11}C]carbon dioxide shown in Scheme 1-2 (d) [32]. [^{11}C]Carbon monoxide is labeled by transition metal mediated insertion reaction. After insertion reaction, the carbonyl carbon can be further functionalized to amide, ester, carbamate, and urea. Scheme 1-2 (e) shows one example of labeling reaction with [^{11}C]carbon monoxide to synthesize a quinazolinone derivative [33]. [^{11}C]Phosgene is used as a precursor for the synthesis of labeled carbamates, carbonates, or ureas. [^{11}C]Befloxatone, a reversible MAO A inhibitor, was labeled with [^{11}C]phosgene to form a carbamate ring [34] (Scheme 1-2 (f)). 2-[^{11}C]Thymidine was synthesized from [^{11}C]urea via [^{11}C]thymine [17] (Scheme 1-2 (g)).

[^{11}C]Formaldehyde can be incorporated into ring such as adenine and imidazole. [^{11}C]Adenosine 5-monophosphate ([^{11}C]AMP) was synthesized using [^{11}C]formaldehyde [35] (Scheme 1-2 (h)). [^{11}C]Diazomethane and [^{11}C]methyl triflate are useful labeling precursor for mild methylations. Both of them carried out selective methylation in presence of competing functional groups with high yield [36, 37] (Scheme 1-2 (i, j)). [^{11}C]Methyl lithium is used as labeling agent for coupling reactions. [21-^{11}C]Progesterone is synthesized from [^{11}C]methyl iodide via [^{11}C]methyl lithium and [^{11}C]methyl(2-thienyl)cuprates(LiCN) in 30-35% radiochemical yield based on [^{11}C]methyl iodide [38] (Scheme 1-2 (k)). [^{11}C]Acetone is used for labeling at isopropyl amine by imine formation followed by reduction [39, 40]. [^{11}C]Bisoporolol and [^{11}C]pindolol were synthesized using [^{11}C]acetone [39, 40] (Scheme 1-2 (l)). [^{11}C]Nitromethane forms a corresponding carbanion and attacks carbonyl group such as aldehyde to form condensation product. [^{11}C]-(±)-Norepinephrine was prepared from [^{11}C]nitromethane shown in Scheme 1-2 (m) [41].

Hydrogen [^{11}C]cyanide is versatile precursor which can be used as a labeling reagent by S_N2 reaction or aromatic nucleophilic substitution. We will discuss more details about cyanide labeling by aromatic nucleophilic substitution and aliphatic nucleophilic substitution followed by reduction in Part III and Part IV, respectively. On the other hand, [^{11}C]cyanogen bromide generated from hydrogen [^{11}C]cyanide rapidly transfers the [^{11}C]cyanide group to heteroatom very fast by nucleophilic substitution. For example, the cysteine and lysine residues in human serum albumin and transferrin were labeled with [^{11}C]cyanogen bromide and further hydrolyzed to carbamyl group [42] (Scheme 1-2 (n)).

4. Fluorine-18 chemistry

4.1 Electrophilic reaction

Fluorine-18 has several advantages over carbon-11. A fluorine-18 labeled radiotracer enables us to investigate the biological or pharmacological effects for longer time period. The maximum travel distance of a positron from fluorine-18 is shorter than that from carbon-11. (See Table 1-3) Therefore, the PET images from fluorine-18 potentially have higher resolution than those from carbon-11. Isotopic labeling with fluorine-18 is possible for the drug containing fluorine. Because many isothetic structures containing fluorine are available, non-isotopic labeling with fluorine does not perturb the original property of the target molecule [43]. For example, fluorovinyl group can be interchangeable with peptide bond [44], and fluorine is similar to hydroxyl group in electronic structure and hydrogen bonding properties. Therefore, fluorine can sometimes be substituted for a hydroxyl group. Because of relatively long half-life, fluorine-18 labeled radiotracers can be distributed from a central radiopharmacy to other institutions.

As described above, fluorine-18 is generated either from neon gas irradiated with deuterons in a nickel target or from [^{18}O]water irradiated with protons. When the fluorine-18 is generated from neon gas by deuteron bombardment, the fluorine-18 is absorbed by the target walls to form nickel fluoride. For efficient recovery of fluorine-18, 1% of fluorine gas is deliberately added to the target to recover the fluorine-18 as ^{18}F-F [45]. Therefore, high specific activity is sacrificed for efficient recovery of fluorine-18. On the other hand, [^{18}F]fluoride ion can be obtained from proton bombardment with [^{18}O]water. The [^{18}F]fluoride is easily recovered by evaporation or absorption on an anion exchange resin. However, the [^{18}O]water should not contain some metal ions such as chromium, iron, and cobalt. These ions can form stable fluoride salts which kill the reactivity of [^{18}F]fluoride. The precious [^{18}O]water can be recycled after distillation. This process does not involve the addition of a carrier such as fluorine gas. Therefore, very high specific activities can be achieved with high yield.

[^{18}F]Fluorine can also be obtained from a [^{18}O]water target after several chemical changes from [^{18}F]fluoride via [^{18}F]fluoromethane [46] or from an [^{18}O]oxygen target [47]. This process also involves the intentional addition of fluorine to recover [^{18}F]fluorine from [^{18}F]fluoromethane [46]. [^{18}F]Fluorine undergoes electrophilic addition, substitution, and radical reactions. Solvents for elemental fluorine reactions are limited because of its high reactivity. Therefore, the reaction with fluorine can result in low selectivity in stereochemistry and regiospecificity. [^{18}F]Fluorine can be transformed into other fluorine-18 precursors with strong electron withdrawing groups which can undergo electrophilic addition or substitution. Scheme 1-3 shows the summary of fluorine-18 precursors which can be synthesized from [^{18}F]fluorine.

As mentioned above, [^{18}F]fluorine can be directly added to alkene substrate by electrophilic addition. The synthesis of ^{18}FDG is an example of this type of reaction [48]. (See Scheme 1-4(a)). There are also many fluorine transferring labeling agents available. Many fluorine-18 radiopharmaceuticals such as [^{18}F]-2-fluorophenylalanine were synthesized using [^{18}F]acetylhypofluorite by electrophilic addition followed by elimination reaction [49] (See Scheme 1-4(b)). ^{18}FDG was synthesized by many methods. Among them, it was synthesized electrophilic addition of [^{18}F]xenon difluoride which can be prepared from either [^{18}F]fluorine or [^{18}F]fluoride [50]. 1-[^{18}F]fluoro-2-pyridone prepared by the reaction between [^{18}F]fluorine and 2-(trimethylsiloxy)pyridine successfully transfer fluorine to methyllithium [51] (See Scheme 1-3). N-[^{18}F]fluoropyridinium triflate synthesized from [^{18}F]fluorine and N-(trimethylsilyl)-pyridinium triflate transfers [^{18}F]fluorine to carbanion [52] (see Scheme 1-4(c)). [^{18}F]Perchloryl fluoride was prepared as an electrophilic fluorine transfer agent (Scheme 1-3), and labeled phenyl derivatives with fluorine-18 after lithiation [53] (see Scheme 1-4(d)). N-[^{18}F]fluoro-N-alkylsulfonamides is designed for mild and regioselective electrophilic fluorine-18 labeling (Scheme 1-3). These reagents were labeled by various yields from 1% to 61% [54] (Scheme 1-4(e)).

Fluorodemetallation is another class of labeling method for [^{18}F]fluorine or [^{18}F]fluorine derivatives to label electron rich aromatic ring with fluorine-18. The driving force of this class of reaction comes from labile bond character between aryl carbon and metals such as mercury, tin, germanium, lead, and silicon relative to stable bond character between aryl carbon and fluorine. The advantage of this class of reactions owes to its regiospecificity in spite of low yield and specific activity. 6-[^{18}F]Fluoro-

DOPA synthesized by fluorodestannylation reaction is a good example for this class of reactions [55] (See Scheme 1-4(f)).

4.2 Nucleophilic reaction

[^{18}F]Fluoride generated from [^{18}O]water has an advantage over [^{18}F]fluorine in high yield and specific activity, but the reactivity of fluoride is very sensitive to the presence of water. Therefore, the recovery of anhydrous [^{18}F]fluoride from aqueous medium in the presence of appropriate large counterion such as rubidium, cesium, and kryptofix222-potassium complex is a critical step to acquire enough reactivity in aprotic solvent such as DMSO, DMF, and acetonitrile.

^{18}FDG is synthesized most efficiently by stereospecific aliphatic substitution reactions shown in Scheme 1-5(a) [56]. Fluorine-18 labeling by aromatic nucleophilic substitution is another labeling method for [^{18}F]fluoride. Halide, nitro, or trialkylammonium groups can be the leaving groups for the reaction. Electron-withdrawing groups such as formyl, nitro, nitrile, amide, and ester group activate the reactivity of aromatic ring. Epibatidine derivatives, a nicotinic acetylcholine receptor agonist, labeled with [^{18}F]fluoride, is prepared by scheme shown in Scheme 1-5(b) [57]. To avoid possible side products, the formyl group directs labeling position of fluorine-18, and is then removed by rhodium catalyst shown in Scheme 1-5(c) [58]. The formyl group activates the leaving group (NO_2) for displacement via the nucleophilic aromatic substitution. [^{18}F]Fluoride can also be incorporated into small alkyl group which can be further incorporated into large molecule by nucleophilic substitution. For example, [^{18}F]N-fluoroethyl-spiperone was obtained by the alkylation of spiperone with 2-[^{18}F]-

fluoroethyl bromide, which was prepared by nucleophilic substitution with 1,2-dibromoethane or 2-bromoethyl mesylate and [^{18}F]fluoride [59] (Scheme 1-5(d)).

5. Quality control of radiopharmaceuticals for PET

After production of radiotracer for PET, quality control should be performed to verify the safety and purity of radiopharmaceuticals before injection into human and animal. Because of short half-life, some time-consuming tests are performed on a 'after the fact' basis. Quality control for radiotracers for PET consists of physicochemical tests and biological tests. Physicochemicals tests consist of seven catagories; specific activity, physical appearance, pH, isotonicity, radionuclidic purity, chemical purity, and radiochemical purity. Biological tests are performed based on two test items; sterility, and pyrogenicity. Table 1-3 shows standard of quality control of ^{18}FDG [60] and 6-[^{18}F]-L-fluoroDOPA [61].

5.1 Physicochemical test

Specific activity: The concept of specific activity is discussed in Sec. 2.4. The amount of radiopharmaceutical is determined by calibration curve which is previously measured with unlabeled reference compound.

Appearance: The color, turbidity, and clarity of radiopharmaceuticals should be checked visually. The solution should be clear by appearance.

pH: Ideal pH of the solution containing radiopharmaceutical is 7.4, the pH of physiological system. Normally, there is tolerance around 7.4 depending on the type of radiopharmaceutical. For example, ^{18}FDG is 4.5-8.5 [60]. If pH of the solution is out of range, it is adjusted by a buffer solution.

Isotonicity (Ionic strength): The radiopharmaceutical should have adequate range of ionic strength to administer to human and animal model. Isotonicity is also adjusted by adding appropriate electrolytes.

Radionuclidic purity: Radionuclidic purity is the ratio of desired radioisotope to total radioisotopes in the product. The undesired radioisotope can be generated because of side nuclear reaction or impurities in the target molecule. However, this is rarely a problem with the short lived isotopes which decay rapidly and chemical processes and purification steps which are required in the labeling exclude other isotopes. One can determine the presence of undesired radionuclei using a multichannel spectrometer or by measuring the half-life of the radioactivity in the product.

Chemical purity: Chemical purity is evaluated by the fraction of radiopharmaceutical in total chemical species present in the sample. Chemical impurities which might be generated during the reaction or introduced from various sources can cause undesirable effects on the radiopharmaceuticals. Chemicals purity is determined by various analysis techniques such as spectroscopy, HPLC and gas chromatography (GC).

The USP also requires to check residual solvent such as acetonitrile in radiopharmaceutical solution by GC. The content of residual solvent should not be over 0.05% or 5 mg/ml [62].

Radiochemical purity: Radiochemical purity is the percentage of total radioactivity which is present as desired radiotracer. The presence of a contaminating side product labeled with the radioisotope can perturb biological system, mislead the data, and expose extra radiation dose in the subject. Therefore, the United States Pharmacopeia (USP) and Food and Drug Administration (FDA) require to check radiochemical purity of each

production. Radiochemical purity is typically determined by HPLC and thin layer chromatography (TLC).

5.2 Biological tests

Sterility: Sterility test of PET radiopharmaceutical confirms the absence of bacteria or microorganism in the solution. All radiopharmaceuticals must be sterilized by passing through 0.22 μm membrane filter or by being heated to 120^{o}C for 20 minutes in a pressurized container (18 lb/in^{2}) before injection into subject or animal. For PET radiopharmaceuticals, filter treatment is preferred sterilization because of the short half-life of the radioisotopes. To test the sterility, the sample solution of radiopharmaceutical is cultured in a fluid thioglycollate medium at 30-35^{o}C for 14 days or in a soybean-casein digest medium at 20-25^{o}C for 14 days. This test is reported as after-the-fact basis because of short half-life of positron emitting isotope. If neither one of the tests is positive, the sample is considered sterile.

FDA also requires to perform filter membrane integrity test for instant indirect sterility evidence. The filter membrane is subjected to stream of air, and it is supposed to stand against air flow. The test device is commercially available, but each laboratory must develop its own method to minimize radiation from radioactive filter membrane [62].

Pyrogenicity: Contamination of a radiotracer by the polysaccharides or proteins metabolized by microorganism causes fever, sweating, chill, diarrhea, or malaise 0.5-2 hour after administration. Technically, there is no established method to prevent pyrogens, but well-managed sterile setup during the run can prevent such a contamination. Conventionally, a pyrogen test was performed using rabbit whose rectal temperature is

monitored after administration of radiopharmaceutical solution. More recently, *limsulus amebocyte lysate* (LAL) test was adopted for fast and simple check-up. A sample solution of radiopharmaceutical was added to the lysate of amebocyte from the blood of horseshoe crab, and incubated at 37^{o}C. If the test is positive, an opaque blue gel will be formed in 15-60 minutes depending on the concentration of pyrogens. For PET radiopharmaceuticals, this test is reported by after-the-fact basis. A new 20 minutes version of the test is now FDA approved.

6. Evaluation of PET radiopharmaceuticals for brain study

The development of a PET radioligand starts from identifying the well-characterized molecular data such as *in-vitro* or *ex-vivo* pharmacological data such as specificity for the molecular target, and binding affinity. If the structure-activity relationship (SAR) study is available, modification of structure based on original molecule will be possible to improve the properties as a PET radiotracer. Another important criterion is that the molecular target should have sufficient concentration for PET imaging. For example, receptor densities (B_{max}) of serotonin (5-HT) transporter measured by [^{3}H]DASB and [^{3}H]citalopram is 66±8 and 83±22 fmol/mg protein respectively [63]. Therefore, receptor densities of target are typically over 60 fmol/mg protein to get reliable PET images in the PET study.

If detailed mechanism is available, further modification will be possible to investigate the mechanism of binding *in vivo*. For example, [^{11}C]clorgyline and [^{11}C]deprenyl bind to monoamine oxidase (MAO) irreversibly [64]. The binding mechanism is well explained using a model compound [65], and shown in scheme 1-6. It involves breaking of the C-H bond on the propargyl group in the rate limiting step, and forms a covalent

bond between oxidized form of flavin and terminal acetylene carbon [65]. Therefore, substitution of deuterium at propargyl hydrogen in [^{11}C]clorgyline and [^{11}C]deprenyl produces an isotope effect during irreversible binding to MAO, and induces changes in kinetic parameters [66]. We will discuss more details in Part IV.

To be a good PET radioligand for brain study, the candidate molecule should satisfy several criteria [67]. The molecule should follow Lipinski's rule of five [68]. This rule provides insights to predict if a chemical will be an orally active drug. This rule can be further applied to a standard for a chemical to cross blood-brain barrier. Lipinski's rule defines the following criteria. (1) Molecular weight of the molecule should be lower than 500. Large molecules cannot cross the blood-brain barrier. (2) Log P should be under 5. More specifically, log P should be 1-4 to be adequate for penetrating blood-brain barrier. The chemical should be hydrophilic enough to dissolve in blood which contains 95% water, and it has to be lipophilic enough to penetrate the blood-brain barrier. If log P is over 4, non-specific binding typically is dominant for the molecule. (3) The molecule should have less than five hydrogen bond donors such as hydroxyl group or amine group. (4) The molecule should have less than 10 hydrogen bond acceptors.

The target molecule should have high affinity with K_d values of nanomolar or subnanomolar range where K_d are dissociation constant of the ligand. Especially, low receptor density requires a radioligand with very high affinity. The relationship between B_{max} and K_d is defined by binding potential (BP); $BP=B_{max}/K_d$. To acquire the good contrast, BP of the target molecule is over four. If BP is under one, the molecule does not usually accumulate on the target tissue that represents non-specific binding and low signal to noise ratio [69].

As mentioned before, a good radiotracer has high specificity and selectivity. Specificity represents the property of radioligand to bind to desired target with high affinity. Selectivity is associated with the ability of radioligand to avoid binding to other targets except desired target. To find out the specificity, the unlabeled compound is pretreated or co-injected with the radiopharmaceutical. Other blocking agents which are known to the bind to the desired target can also be pretreated or co-injected with the radiopharmaceutical. If the radiopharmaceutical is specific, binding to the target in the regions will be reduced. To find out the selectivity, a blocking agent which is known to specifically bind to other target enzymes is pretreated or co-injected with the radiopharmaceutical. If the radiopharmaceutical has selectivity, its binding will not be affected by the injection of a blocking agent.

The radiopharmaceutical should have an optimal uptake in target tissue and clearance from the non-target tissue over 90 minutes of scan time for the carbon-11 case [70]. High uptake ratio between the region of interest (ROI) and reference region (where the target receptors are not present) should be achieved during scan time [70].

Another important property for reversibly binding radiotracers is distribution volume (DV) which tells drug concentration in the ROI compared to the concentration in blood. Distribution volume ratio (DVR) between ROI and reference region has following relationship.

$$DVR = \frac{(DV)_{ROI}}{(DV)_{Ref}} = \frac{B_{max}}{K_d} + 1 = BP + 1$$

DV can also be derived by Logan plot which establishes time-activity curves of ROI and plasma into a linear relationship by setting up appropriate model [71, 72]. Cp is plasma concentration of radiotracer.

$$\frac{\int ROI\,(t')dt'}{ROI(t)} = DV\,\frac{\int Cp(t')dt'}{ROI(t)} + int$$

Those equations derive binding potential and distribution volumes in ROI to evaluate the new radioligand.

Rapid metabolism of radiopharmaceuticals to form metabolites which are labeled and which penetrate the brain will contaminate the PET image and make quantification difficult if not possible. However, well-characterized metabolism can be beneficial to design a new radioligand and understand the PET image underlying mechanism. For example, ^{18}FDG is designed based on glucose metabolism. FDG derivatives were also synthesized, and found that fluorine instead of hydroxyl group at 2-position does not alter the property of D-glucose to serve as a substrate for hexokinase [73]. ^{18}FDG behaves same way like glucose until its hydroxyl group at 6-position is phosphorylated by hexokinase, but further metabolism is hampered by the presence of a fluorine atom at 2-position. Therefore, ^{18}FDG accumulates in tissue depending on the cell activity.

Radiopharmaceuticals should also have low affinity to P-glycoprotein. P-Glycoprotein is molecular efflux system developed in several organs including brain and cancer [74]. Therefore, P-glycoprotein is one of major mechanism to develop drug resistance [75]. A radiopharmaceutical with P-glycoprotein resistance does not accumulate in the tissue such as brain and tumor [76].

As mentioned above, 60 fmol/mg protein or 6 fmol/mg tissue of receptor density is required to get reliable image in the PET study [63]. To accomplish noninvasiveness of a PET study, the radiopharmaceutical must be present in tracer amounts so that it does not produce a pharmacological effect. In other words, the radiopharmaceutical is supposed to occupy very small portion of receptors. However, radiopharmaceutical also contains nonradioactive isotope which is 9,200 times more abundant than radioisotope for 1 mCi/nmol of carbon-11 case. To reduce the possibility to cause pharmacological effect, a radiopharmaceutical with high specific activity is required. Generally, a specific activity of 0.3-1 mCi/nmol is needed to perform PET study though this varies with different receptor concentrations.

Another important criterion is toxicology test. Some radiopharmaceuticals would be predicted to have high toxicity because of the high toxicity of the parent unlabeled compound. Such radiopharmaceuticals can alter the function of organ or potentially cause serious adverse reactions after administration unless they are administered in very high specific activity. Classically, toxicity is determined by LD_{50}, a lethal dose which puts to death of a half of animal models 60 days after administration. LD_{50} is established at least two species before human use. Most radiopharmaceuticals do not reach lethal dose because its injection dose is well below the pharmacological dose. Although general radiopharmaceutical has too low concentration to go beyond toxic effect, the toxicology of the parent unlabelled compound is an important consideration in the initial approval of a radiotracer for human studies. Generally, the labeling of exceptionally toxic molecules is avoided.

7. Advantage of PET

The big virtue of PET study is noninvasiveness and the fact that it can safely be used to image biochemical transformations and the movement of drug in humans. PET creates *in-vivo* functional image without perturbing the biological system.

PET is especially useful in oncology for the diagnosis, monitoring and staging of cancerous tumor. It is also useful tool to find tumor by metastases. As a result, FDG PET gives excellent results in various cancers, especially in lung cancer and Hodgkin's lymphoma. PET is also applied to brain research, and FDG PET visualizes brain activity. Many radioligands such as [^{11}C]raclopride and [^{11}C]DASB have been developed, and these radioligands display the activity of neurotransmitters receptors or transporters such as dopamine D_2 receptor and serotonin transporter, respectively [2, 70, 77]. Besides oncology and neuroscience, PET is also a useful clinical tool in cardiology. For example, FDG PET was reported to detect atherosclerosis, which increases the risk of stroke [78].

PET is also used in drug development, and to evaluate candidate drugs by various studies including pharmacokinetics. PET can monitor the drug metabolism, distribution, and elimination from the body using either the labeled drug or a radiotracer with molecular specificity. Therefore, PET can reduce previous efforts to sacrifice and dissect the animals for the same study reducing the cost of drug development, and also providing scientific basis to determine the effectiveness of drugs at various development of stages.

PET is also evolving into new medical instrument by combining with CT or MRI to complement anatomical information. PET-CT and PET-MRI will expand the boundary of medicinal and clinical research, and will provide more accurate cancer diagnosis.

The following three sections discuss the effective synthesis of unlabeled and labeled drugs. We will also discuss about the evaluation of new radiopharmaceuticals by test/retest and saturability study. These three studies will be good examples how to develop radiopharmaceuticals and labeling methods, and how to determine the usefulness of radiotracers from PET image data and time-activity curves derived from PET images.

Figures, Tables, and Schemes

	Unit	SI Unit	Comment
Radioactivity	C_i (Curie)	Bq (Becquerel) 1Bq=1 decay/sec	1Ci=37 GBq
Radiation Dose (living matter)	rem (Röntgen equivalent in man)	Sv (Sievert) 1 Sv=1 J/kg	1 Sv=100 rem
Absorbed Dose (non-living matter)	rad	Gy (Gray) 1 Gy=1 J/kg	1 Gy=100 rad
Radiation	R (Röntgen)	C/kg	1 R=2.58 x 10^{-4} C/kg

Table 1-1. The units of radioactivity and radiation dose.

	^{11}C	^{18}F	^{13}N	^{15}O
Half-life	20.4 min	109.8 min	9.98 min	2.03 min
Maximum β^+ Energy	0.96 MeV	0.69 MeV	1.19 MeV	1.7 MeV
Maximum Range in water	4.1 mm	2.4 mm	5.4 mm	8.0 mm
Maximum Specific Activity at EOB (Theoretical) $C_i/\mu mol$	< 20 (9218)	< 5.4 (1713)	< 10.8 (18843)	(92638)
Radiochemical Reaction	$^{14}N(p, \alpha)^{11}C$	$^{18}O(p, n)^{18}F$ $^{20}Ne(d, \alpha)^{18}F$	$^{13}C(p, n)^{13}N$ $^{12}C(d, p)^{13}N$ $^{16}O(p, \alpha)^{13}N$	$^{15}N(p, n)^{15}O$ $^{14}N(d, n)^{15}O$
Target	Nitrogen	$H_2{}^{18}O$ (O-18 Water) or Neon gas	^{13}C carbon powder, Carbon powder, Water	Nitrogen or ^{15}N Nitrogen
Decay Product	^{11}B	^{18}O	^{13}C	^{15}N

Table 1-2. Properties of representative positron emitting isotopes.

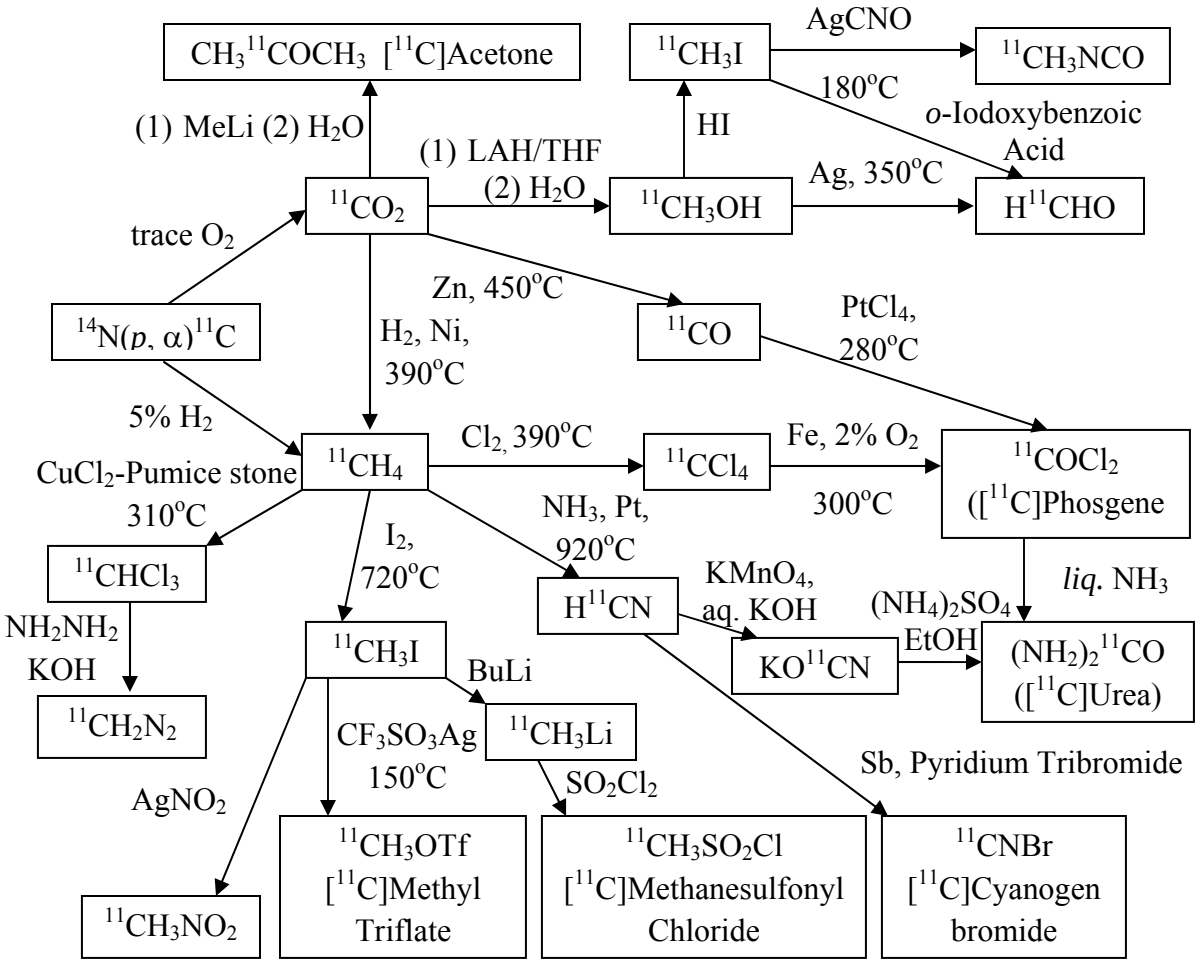

Scheme 1-1. Synthesis of carbon-11 precursor from carbon-11 generation

(a) [29]

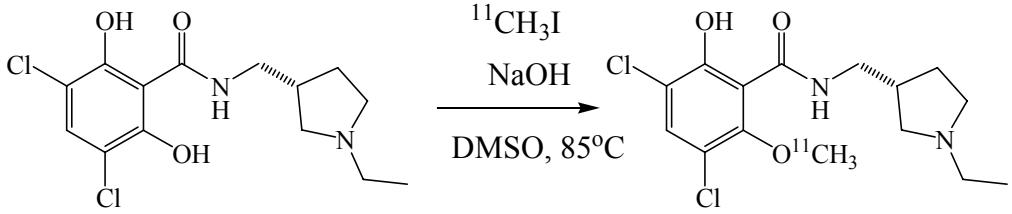

[^{11}C]Raclopride

(b) [30]

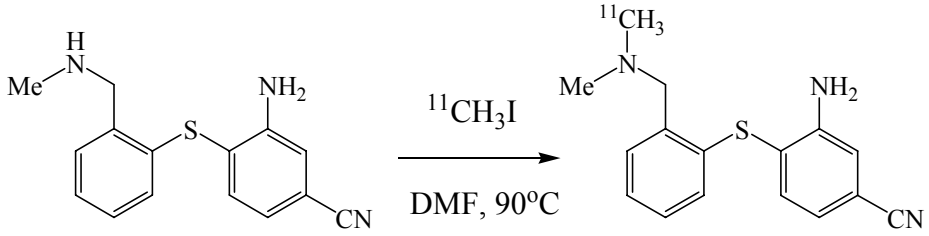

[^{11}C]DASB

(c) [31]

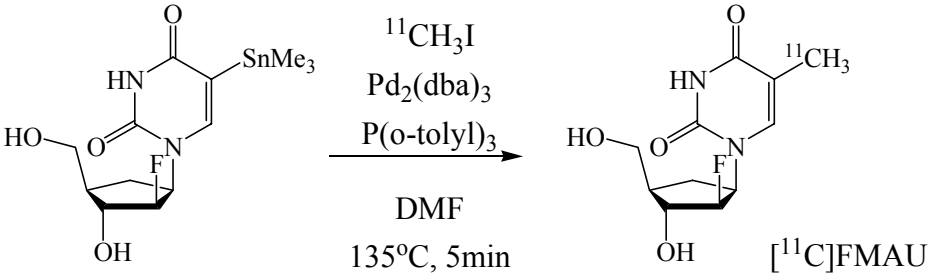

[^{11}C]FMAU

(d) [32]

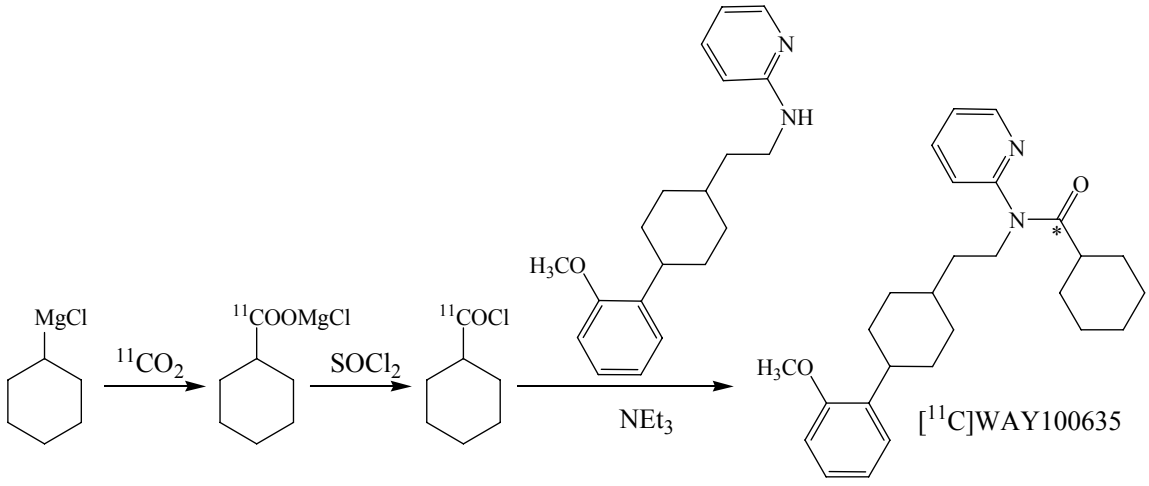

[^{11}C]WAY100635

(e) [33]

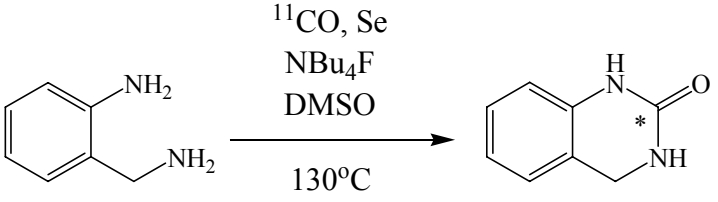

3,4-Dihydroquinazolin-
[2-^{11}C]-2(1H)-one

(f) [34]

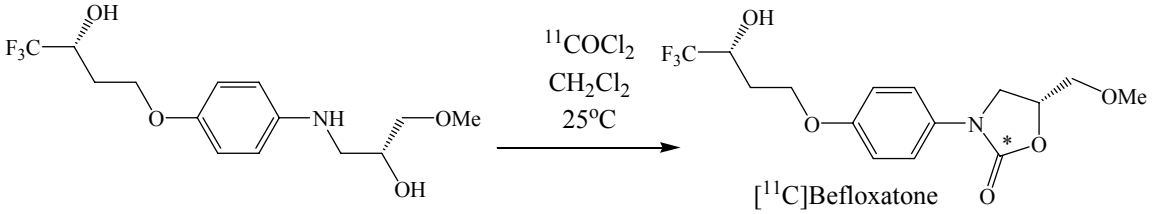

[^{11}C]Befloxatone

(g) [17]

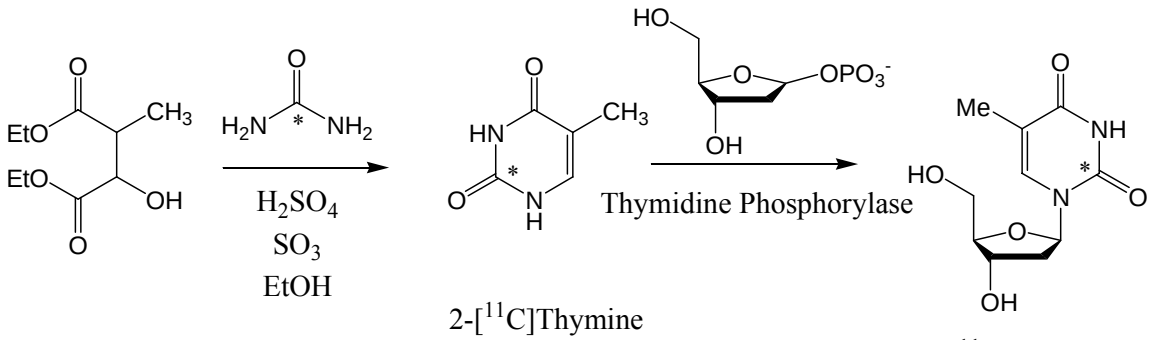

2-[^{11}C]Thymine

2-[^{11}C]Thymidine

(h) [35]

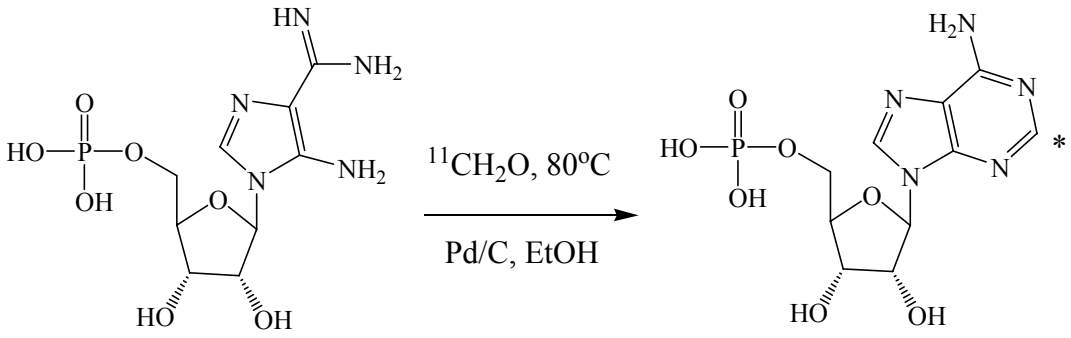

[^{11}C]AMP

(i) [36]

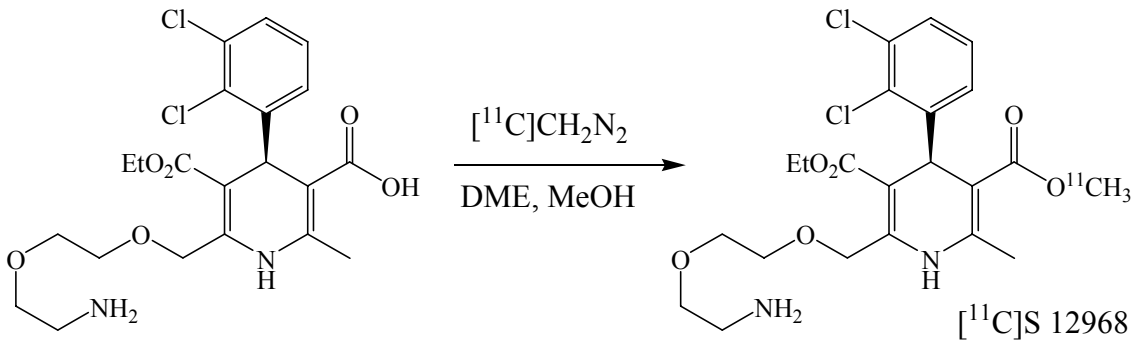

(j) [37]

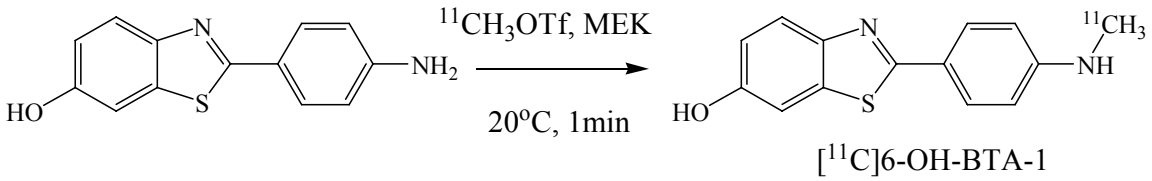

(k) [38]

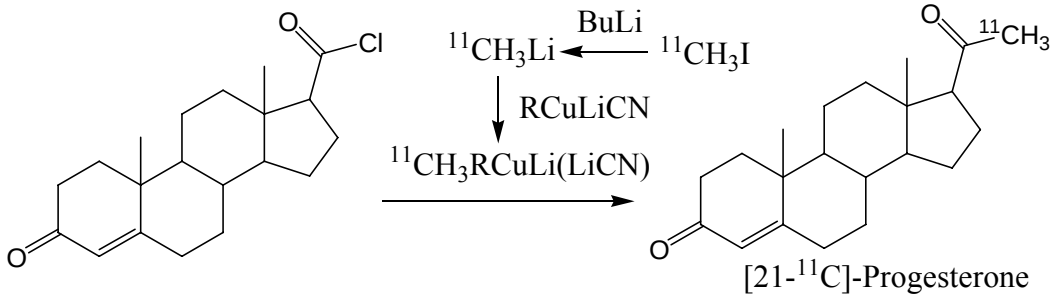

(l) [39]

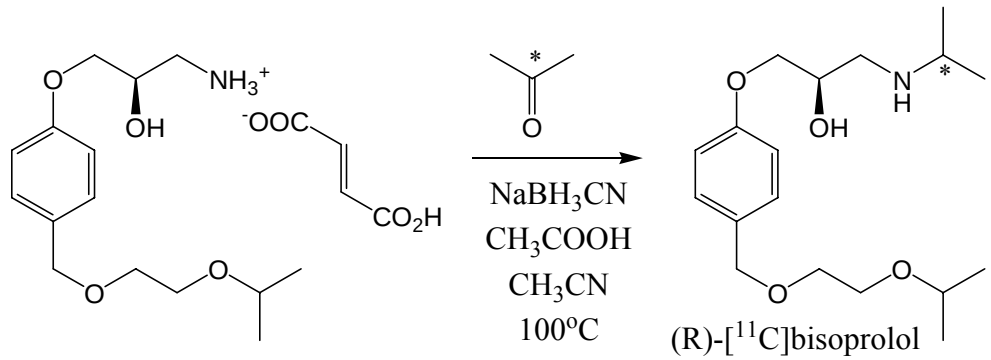

(m) [41]

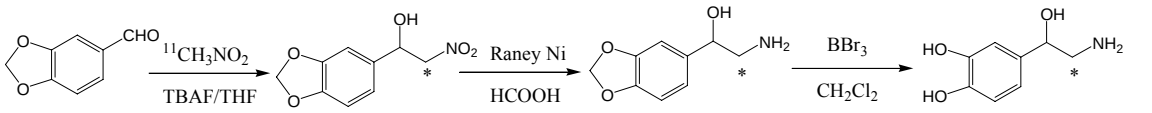

(n) [42]

$$\text{Protein-SH} + {}^{11}\text{CNBr} \rightarrow \text{Protein-S}{}^{11}\text{CN}$$

$$\text{Protein-NH}_2 + {}^{11}\text{CNBr} \rightarrow \text{Protein-NH}{}^{11}\text{CN}$$

$$\text{Protein-NH}{}^{11}\text{CN} + \text{H}_2\text{O} \rightarrow \text{Protein-N}{}^{11}\text{CONH}_2$$

Scheme 1-2. Representative carbon-11 labeling method using various carbon-11 labeling precursors.

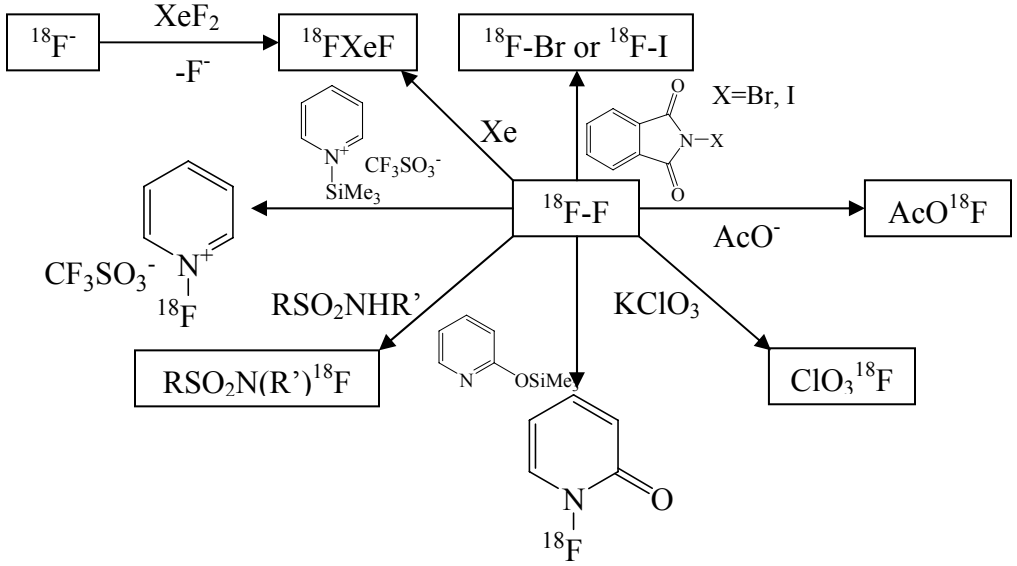

Scheme 1-3. Synthesis of fluorine-18 precursor from [^{18}F]fluorine.

(a) [48]

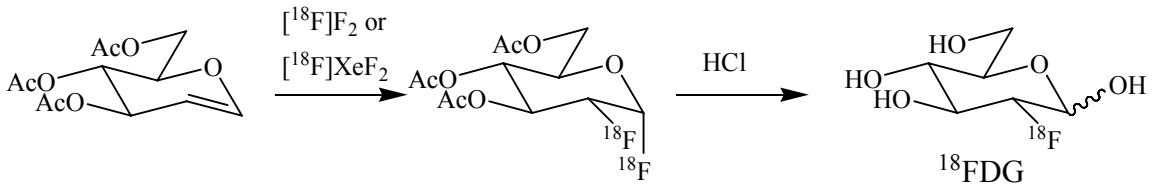

(b) [49]

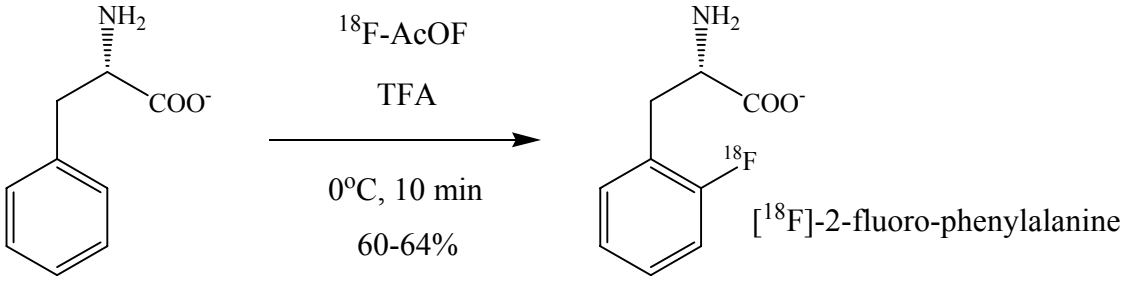

(c) [52]

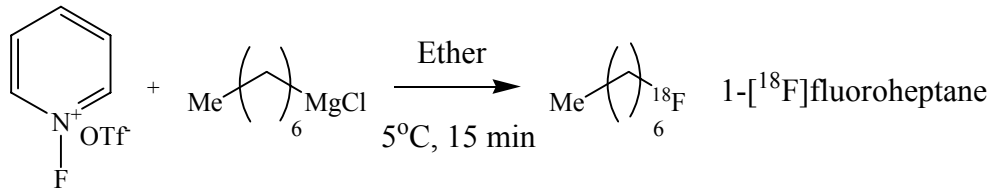

(d) [53]

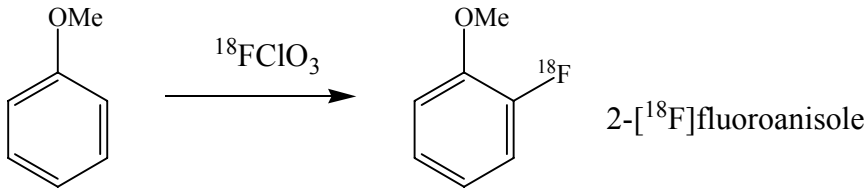

(e) [54]

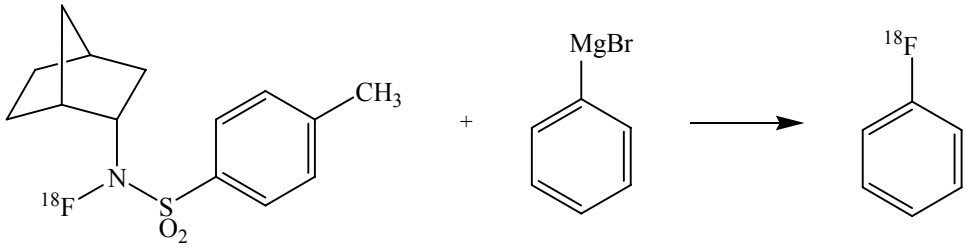

(f) [55]

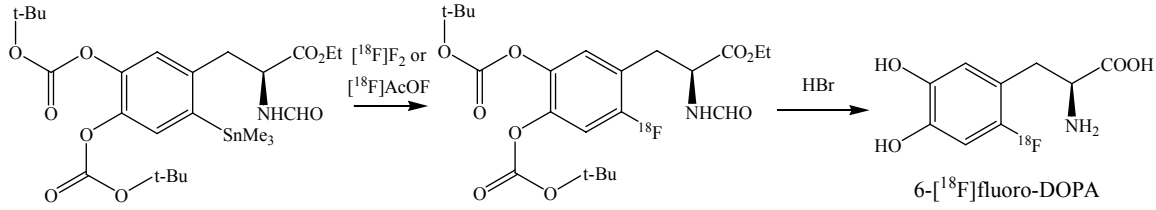

Scheme 1-4. Examples of fluorine-18 labeling using electrophilic addition or substitution reactions.

(a) [56]

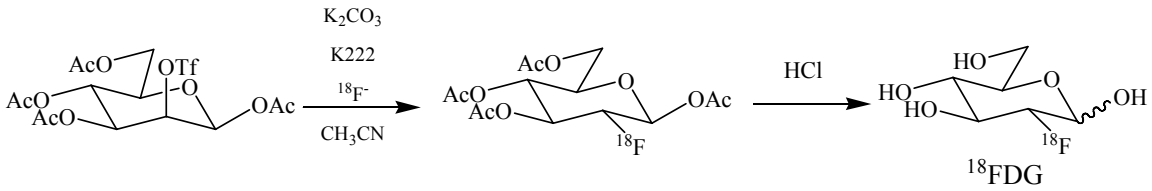

(b) [57]

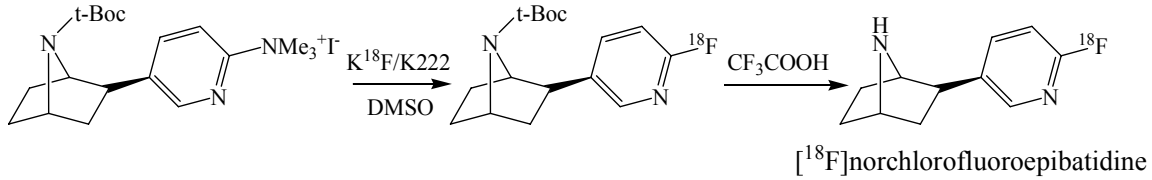

(c) [58]

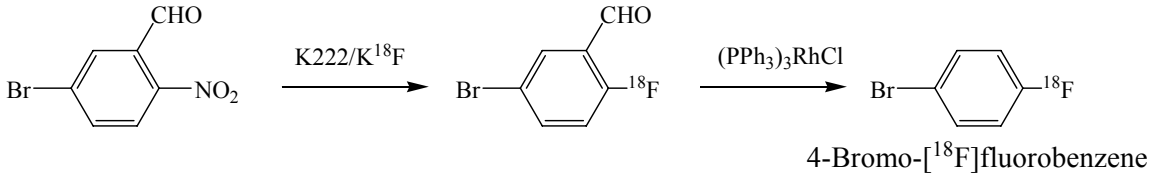

(d) [59]

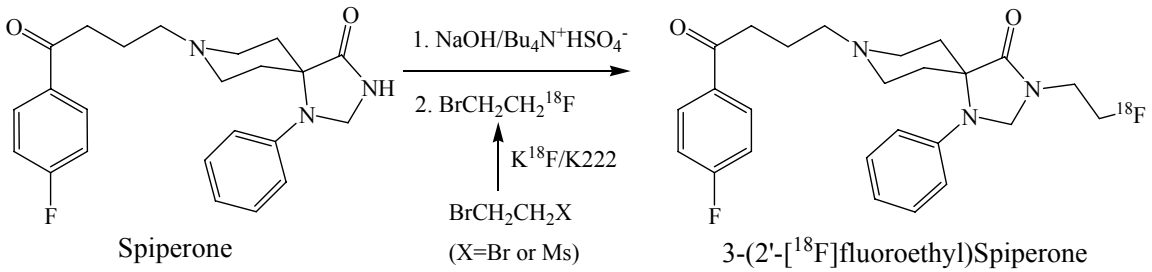

Scheme 1-5. Fluorine-18 labeling reactions with [^{18}F]fluoride using nucleophilic substitution.

	^{18}FDG [60]	6-[^{18}F]-L-FluoroDOPA [61]
Appearance	Clear, colorless, no visible matter	Clear, colorless, no visible matter
pH	4.5-8.5	6-7
Specific Activitry	>1 Ci/μmol	>0.1 Ci/μmol
Radionuclidic Purity	>99.5% 0.511 MeV + 1.022 MeV + Compton scatter	>99.5% 0.511 MeV + 1.022 MeV + Compton scatter <0.1% individual impurity
Chemical Purity	Acetonitrile: <0.04% (w/v) Ethanol: <0.5% (w/v) Chlorodeoxyglucose: <0.5 mg/dose FDG: <10 mg/dose	<0.5 μg/ml Hg
Radiochemical Purity	>90% ^{18}FDG <4% [^{18}F]fluoride	>95% 6-[^{18}F]-L-fluoroDOPA
Sterility	Sterile	Sterile

Table 1-3. Quality Control Specification for ^{18}FDG [60] and 6-[^{18}F]-L-FluoroDOPA [61]

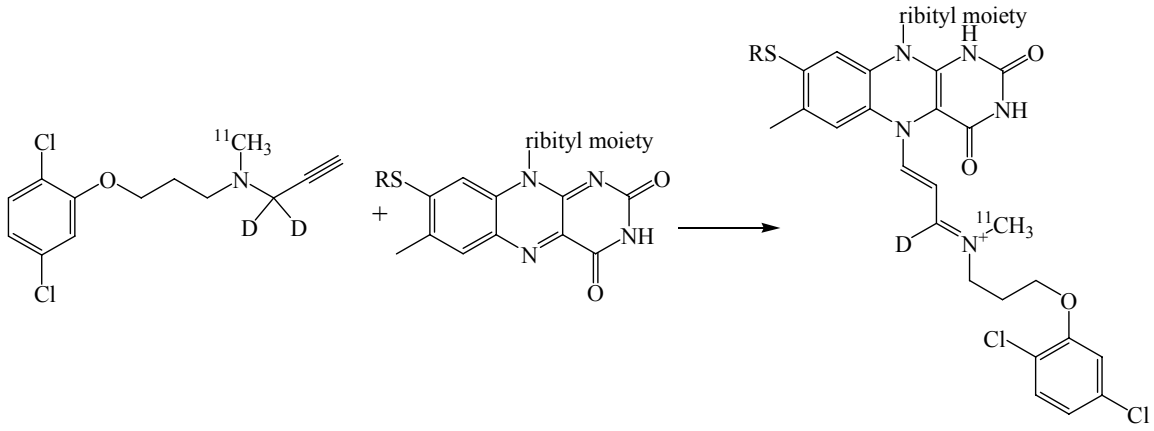

Scheme 1-6. Mechanism of irreversible binding of [^{11}C]clorgyline.

PART II

Synthesis and PET studies of carbon-11 labeled imatinib (Gleevec®)

Abstract:

Introduction: Gleevec® (imatinib mesylate) is well-known drug for treating chronic myeloid leukemia (CML) and gastrointestinal stromal tumours (GIST). Its active ingredient, imatinib, ([4-[(4-methyl-1-piperazinyl)methyl]-*N*-[4-methyl-3-[[4-(3-pyridyl)-2-pyrimidinyl]amino]phenyl]benzamide) blocks the activity of several tyrosine kinases. Here we labeled imatinib with carbon-11 as a tool for determining drug distribution and pharmacokinetics of imatinib and carried out PET studies in the baboon.

Methods: [*N*-^{11}C-methyl]imatinib was synthesized from [^{11}C]methyl iodide and norimatinib synthesized by demethylation of imatinib (isolated from Gleevec® tablets) according to a patent procedure [79]. Norimatinib was also synthesized from the corresponding amine and acid. PET studies were carried out in three baboons to measure

pharmacokinetics in the brain and peripheral organs and to determine the effect of a therapeutic dose of imatinib. Log D and plasma protein binding were also measured.

Results: [*N*-^{11}C-methyl]imatinib uptake in brain is negligible (consistent with P-glycoprotein mediated efflux) and it peaks and clears rapidly from the heart, lungs and spleen. Peak uptake and clearance occurs more slowly in the liver and kidneys followed by accumulation in the gall bladder and urinary bladder. Pretreatment with imatinib did not change uptake in heart, lungs, kidneys, and spleen and increased uptake in liver and gall bladder.

Conclusions: [*N*-^{11}C-methyl]imatinib has potential for assessing the regional distribution and kinetics of imatinib in the human body to determine whether the drug targets tumor and to identify other organs to which the drug or its labeled metabolites distributes. Paired with tracers such as ^{18}FDG and 3-deoxy-3-^{18}F-fluorothymidine (^{18}FLT), [*N*-^{11}C-methyl]imatinib may be a useful radiotracer in planning chemotherapy, in monitoring response to treatment and for assessing the role of drug pharmacokinetics in drug resistance.

1. Introduction

PET coupled with a radiolabeled drug is a powerful tool for determining drug distribution and pharmacokinetics [80] This information would be of major importance in determining whether a chemotherapeutic drug targets a tumor and also in determining other organs where the drug or its metabolites accumulate [81]. In addition a study design in which a labeled chemotherapeutic drug is paired with a functional radiotracer

such as ^{18}FDG or ^{18}FLT offers the potential to both plan and monitor therapy and to make changes depending on individual response.

Gleevec® (Figure 2-1, also known as imatinib mesylate ([4-[(4-methyl-1-piperazinyl)methyl]-*N*-[4-methyl-3-[[4-(3-pyridyl)-2-pyrimidinyl]amino]phenyl] benzamide methanesulfonate), STI571) is a member of new class of signal transduction inhibitors to treat CML and GIST. It was the first drug which was rationally designed based on molecular abnormality in CML, and was approved by the FDA in 2001 after remarkable success in the treatment of chronic phase CML patients [82, 83]. In fact PET studies with ^{18}FDG have documented a dramatic reduction in ^{18}FDG uptake after oral administration of 300-400 mg/day of imatinib mesylate in GIST patients [84, 85].

CML is a myeloproliferative disorder [86] triggered by genetic translocation between chromosome 9 and chromosome 22 to produce aberrant Philadelphia chromosome [87, 88]. This chromosome expresses the abnormal protein enzyme, bcr-abl tyrosine kinase. Bcr-abl tyrosine kinase is constitutively altered so that it is no longer dependant on normal signal transduction induced by interaction between cytokine (Interleukin-3, IL-3) and its receptor. Therefore the hematopoietic stem cell comprising bcr-abl tyrosine kinase exerts enhanced cell function to produce white blood cell (WBC) and blast as well as cell proliferation. For these reasons, bcr-abl tyrosine kinase serves as good molecular target for CML treatment.

Imatinib, the active ingredient of Gleevec®, was originally designed as a competitive inhibitor of bcr-abl tyrosine kinase in leukemic cell and c-abl tyrosine kinase in normal cells (IC_{50}=0.025 μM for both cells). Since c-abl tyrosine kinase doesn't play

an important role in cell survival of normal cell, imatinib spares normal cells while killing leukemic cells [89, 90, 91]. However, in spite of its efficacy, treatment resistance emerges due to mutation of the bcr-abl tyrosine kinase which interferes with drug binding [92, 93].

Imatinib also blocks other tyrosine kinases such as c-kit and platelet derived growth factor (PDGF) [89, 94] (IC_{50} (c-kit=0.41 μM, PDGF=0.38 μM)). c-Kit contributes to the unique pathology of GIST [95] which is initiated in interstitial cells of Cajal (ICC) which plays an essential role in intestinal motility [96]. c-Kit undergoes a gain of function mutation in GIST [97, 98, 99]. Imatinib reduces tumor size in a significant fraction of GIST patients [100]. Unfortunately, similar to CML, resistance against imatinib also occurs in GIST by a secondary mutation. From this perspective, we reasoned that [*N*-^{11}C-methyl]imatinib may be useful in determining whether drug pharmacokinetics change when drug resistance develops.

In addition to chemotherapeutic applications for CML and GIST, preclincal studies show that imatinib has some potency against deposition and accumulation of amyloid-β-peptide (Aβ), a characteristic peptide plaque found in the brain of Alzheimer's disease (AD) patients though blood-brain barrier penetration is a limitation [101, 102]. Other conditions where imatinib shows promise are hepatocellular carcinoma [103, 104], liver fibrosis [105, 106], and pulmonary fibrosis [107, 108] which are characterized by the expression of abl kinase, c-kit kinase or PDGF kinase.

Here we synthesized [*N*-^{11}C-methyl]imatinib according to a recent patent procedure in which the nor-precursor was prepared via demethylation of imatinib [79].

We also prepared norimatinib from the corresponding amine and acid. We measured the distribution of [*N*-^{11}C-methyl]imatinib and/or its labeled metabolites in the brain and in peripheral organs in the baboon at tracer doses and after treatment with a single dose of imatinib. This information is of relevance in determining the organs targeted by imatinib and its labeled metabolites.

2. Material and Methods

2.1 General

All chemicals used in the synthesis were purchased from Sigma Aldrich Chemical Company (Milwaukee, WI), and were used without any further purification. ^{1}H-NMR spectra were obtained in $CDCl_3$ solution (unless specified) using Bruker Avance 400 MHz NMR spectrometer (400 MHz for ^{1}H and 100 MHz for ^{13}C) (Bruker Instruments Inc., Billerica, MA) and were reported in part per million downfield from tetramethylsilane as internal standard. Melting points were measured by Fisher-Johns melting point apparatus (Fisher Scientific Co., Pittsburgh, PA). High resolution mass spectrometry (HRMS) experiments were obtained by VG 7070 high resolution mass spectrometer in UCR Mass Spectrometry Facility (Riverside, CA). All reactions are monitored by analytical thin layer chromatography (TLC), and spots were detected using UV light (254 nm) and, if appropriate, detected by 0.1% ninhydrin solution in isopropanol. An unlabelled standard of imatinib mesylate was generously provided by Dr. Brian J. Druker, and recovered from the capsules.

2.2 Chemistry

2.2.1 Norimatinib synthesis from Gleevec® capsule

2.2.1.1 Recovering imatinib free base from Gleevec® capsules

A 100 mg of Gleevec® capsule contains 100 mg of imatinib and 218.5 mg of inert ingredients [109]. To recover the imatinib, the cover of one capsule of Gleevec® was removed and powder was dissolved in 3 ml of distilled water. The suspension was filtered, and washed with 2 ml of distilled water. Sodium bicarbonate aqueous solution (0.2 M, 10 ml) was added to the filtrate drop by drop until it was fully suspended. After the solution was crystallized overnight, it was filtered. For further purification, the solid was recrystallized from methylene chloride-hexane co-solvent. The product was collected by filtration and dried *in vacuo* to give 0.0879 g of imatinib (**1**) as a white powder. (Yield: 87.9%) mp 208-209^{o}C (lit. 207-212^{o}C [110, 111]). NMR spectrum was consistent with previous literature [111]. ^{1}H NMR (DMSO-d_6): δ 2.14 (s, 3H), 2.22 (s, 3H), 2.33 (broad s, 4H), 3.33 (s, 4H), 3.52 (s, 2H), 7.19-7.21 (d, J=8.8 Hz, 1H), 7.42-7.43 (d, J=5.6 Hz, 1H), 7.42-7.44 (d, J=8.4 Hz, 2H), 7.47-7.50 (dd, J= 7.6 Hz, 2.4 Hz, 1H), 7.50-7.53 (dd, J=7.6 Hz, 4.8 Hz, 1H), 7.90-7.92 (d, J=8.8 Hz, 2H), 8.08 (d, J=1.2 Hz, 1H), 8.46-8.49 (dt, J=8.0 Hz, 2.4 Hz, 1H), 8.50-8.51 (d, J= 4.8 Hz, 1H), 8.67-8.69 (dd, J=4.4 Hz, 1.2 Hz, 1H), 8.97 (s, 1H), 9.27 (d, J=2.0 Hz, 1H), 10.17 (s, 1H). ^{13}C NMR (Methanol-d_4): δ 168.64, 163.88, 162.80, 160.48, 151.94, 149.20, 143.00, 139.19, 138.36, 136.96, 135.59, 134.73, 131.73, 130.71, 129.38, 128.85, 125.54, 118.85, 118.57, 108.88, 63.37, 55.84, 53.59, 49.79, 45.99, 17.99.

*2.2.1.2 Preparation of 4-[(piperazinyl)methyl]-N-[4-methyl-3-[[4-(3-pyridyl)-2-pyrimidinyl]amino]phenyl benzamide (**2**) from imatinib free base (**1**)*

Norimatinib **2** was obtained from imatinib (**1**) by non-classical Polonovski demethylation [112] according to the procedure in US patent [79]. Briefly, to a stirred solution of imatinib (0.20 g, 0.405 mmol) in methylene chloride (2.0 ml) was added 3-chloroperbenzoic acid (m-CPBA, 0.14 g, 0.810 mmol) and the mixture was stirred for 3 hours at room temperature. After the solvent was evaporated, the residue was diluted with methanol (2.0 ml). Ferrous sulfate (0.451 g, 1.621 mmol) was added, and the mixture solution and stirred for 2 hours at 4^{o}C. The solution was diluted with 7 ml of sodium carbonate solution (3.5 ml of saturated sodium carbonate solution diluted with 3.5 ml of distilled water) and extracted three times with ethyl acetate. The organic layers were dried by anhydrous magnesium sulfate, filtered and evaporated. The residue was purified by column chromatography eluting with methanol, and then with methanol:28-30% ammonia solution=100:1 co-solvent to give norimatinib (**2**) (0.067 g, 34.5%) as a white powder. mp: 145-149^{o}C. LC-MS (**2**) m/z calcd for $C_{27}H_{29}N_7O$ (M^+), 479.24; found (MH^+), 480.3 ^{1}H NMR: δ 2.36 (s, 3H), 2.46 (s, 4H), 2.91-2.94 (t, J=4.8 Hz, 4H), 3.56 (s, 2H), 3.58 (s, 1H), 7.06 (s, 1H), 7.19-7.20 (d, J=3.6 Hz, 1H), 7.21-7.23 (d, J=8.3 Hz, 1H), 7.30-7.33 (dd, J=8.1 Hz, 1.9 Hz, 1H), 7.42-7.47 (m, 3H), 7.84-7.86 (d, J=8.2 Hz, 2H), 7.90 (s, 1H), 8.52-8.53 (d, J=5.2 Hz, 1H), 8.60 (d, J=1.3 Hz, 1H), 8.70-8.72 (dd, J=4.8 Hz, 1.6 Hz, 1H), 9.25-9.26 (d, J=1.5 Hz, 1H). ^{13}C NMR (DMSO-d_6): δ 165.27, 161.59, 161.18, 159.47, 151.38, 148.19, 142.11, 137.78, 137.21,

134.41, 133.70, 132.20, 130.01, 128.66, 127.58, 128.52, 123.78, 117.19, 116.71, 107.50, 62.41, 54.14, 45.58, 17.65.

*2.2.2 Preparation of N-(5-amino-2-methylphenyl)-4-(3-pyridyl)-2-pyrimidinamine for norimatinib (**2**) and imatinib (**1**)*

*2.2.2.1 3-(N,N-dimethylamino)-1-(3-pyridyl)-2-propen-1-one (**3**)*

The procedure to synthesize β-(dimethylamino)vinyl 2-pyridyl ketone was adapted to synthesize 3-(*N*,*N*-dimethylamino)-1-(3-pyridyl)-2-propen-1-one (**3**) [113]. Briefly, to a stirred solution of 3-acetylpyridine (18.19 mmol, 2.0 ml) in 10 ml of toluene at room temperature was added *N*,*N*-dimethyl formamide dimethyl acetal (21.83 mmol, 2.90 ml), and the mixture was refluxed for 2 days. The solvent was removed *in vacuo*. The residue was dissolved ethyl acetate and filtered. For further purification, the filtered solution was evaporated, and crystallized by ethyl acetate-hexane co-solvent to afford Compound **3** as an orange solid (2.432 g, 75.9%). mp 80-81^{o}C (lit. 81-82^{o}C [114]) GC/MS (**3**) m/z calcd for $C_{10}H_{12}N_2O$ (M^+), 176.09; found 176. NMR spectra were consistent with previous literature [115]. ^{1}H-NMR: δ 2.91 (s, 3H), 3.13 (s, 3H), 5.62-5.65 (d, J=12 Hz, 1H), 7.29-7.33 (qd, J=4.4 Hz, 1.0 Hz, 1H), 7.78-7.81 (d, J=12 Hz, 1H), 8.13-8.16 (dt, J=8 Hz, 1.2 Hz, 1H), 8.61-8.63 (dd, J=5.2 Hz, 1.6 Hz, 1H), 9.04-9.05 (dd, J=2.4 Hz, 0.7 Hz, 1H). ^{13}C NMR: δ 186.74, 155.08, 151.85, 149.30, 136.03, 135.46, 123.68, 92.21, 45.61, 37.78.

*2.2.2.2 2-Methyl-5-nitrophenylguanidine nitrate (**4**)*

The procedure for the synthesis of 3-nitrophenyl-guanidine nitrate was adapted to synthesize 2-methyl-5-nitrophenylguanidine nitrate (**4**) from 2-methyl-5-nitroaniline [116]. To a solution of 2-methyl-5-nitroaniline (30.0 mmol, 4.61 g) in ethanol (10 ml) at room temperature was slowly added nitric acid (70% aqueous solution, 30.0 mmol, 1.92 ml). After the exothermic reaction subsided, cyanamide (50% aqueous solution, 45.0 mmol, 3.50 ml) was added, and the reaction mixture was refluxed for 1 day. The reaction mixture was cooled to 0^{o}C, and filtered. The filtered solid was washed with ethanol:ether (1:1) and dried *in vacuo* to give Compound **4** (4.114 g, 56.3%) as a yellowish solid. mp 218-219^{o}C (lit. 214-220^{o}C [117]) NMR spectra were consistent with previous literature [111]. ^{1}H NMR (DMSO-d_6): δ 2.32 (s, 3H), 7.42 (s, 4H), 7.63-7.65 (d, J=8.8Hz, 1H), 8.10 (d, J=2.8Hz, 1H), 8.15-8.17 (dd, J=8.0Hz, 3.2Hz, 1H), 9.45 (s, 1H). ^{13}C NMR (DMSO-d_6): δ 158.51, 148.60, 145.50, 135.54, 133.68, 124.56, 124.36, 18.06.

*2.2.2.3 N-(2-methyl-5-nitrophenyl)-4-(3-pyridyl)-2-pyrimidinamine (**5**)*

Phenylamino-pyrimidine (**5**) was prepared from enaminone (**3**) and guanidine derivative (**4**) according to the procedure in Zimmerman *et. al* [118]. To a solution of 3-dimethylamino-1-(3-pyridyl)-2-propen-1-one (**3**, 1.70 mmol, 0.3 g) and 2-methyl-5-nitrophenylguanidine nitrate (**4**, 1.70 mmol, 0.415 g) in isopropanol (2.0 ml) at room temperature was added sodium hydroxide (1.87 mmol, 0.075 g), and the mixture was refluxed for 2 days. The solution was cooled to room temperature, filtered, and the solid was washed with isopropanol. The filtered product was suspended in water, and stirred for 30 minutes at room temperature. The suspended solution was filtered, and washed with ethyl alcohol, and then ether. The remaining residue was dried *in vacuo* to give

Compound **5** (0.291 g, 55.6%) as a yellow powder. mp 194-195°C (lit. 193-198°C [117]). NMR spectra were consistent with previous literature [111]. ^{1}H NMR (DMSO-d_6): δ 2.43 (s, 3H), 7.51-7.53 (d, J=8.4Hz, 1H), 7.54-7.58 (qd, J=4.0Hz, 0.8Hz, 1H), 7.58-7.59 (d, J=4.8Hz, 1H), 7.89-7.91 (dd, J=8.8Hz, 2.0Hz, 1H), 8.48-8.50 (dt, J=8.4Hz, 2.0Hz, 1H), 8.62-8.63 (d, J=6.0Hz, 1H), 8.71-8.72 (dd, J=5.6Hz, 2.0Hz, 1H), 8.80 (d, J=2.0Hz, 1H), 9.24 (s, 1H), 9.32 (dd, J=2.0Hz, 0.8Hz, 1H). ^{13}C NMR (DMSO-d_6): δ 161.98, 160.98, 160.09, 152.02, 148.54, 146.19, 139.26, 139.16, 134.69, 132.26, 131.63, 124.28, 118.35, 117.88, 109.28, 18.76.

*2.2.2.4 N-(5-amino-2-methylphenyl)-4-(3-pyridyl)-2-pyrimidinamine (**6**)*

Pyrimidinamine (**6**) is prepared by reduction of nitro group in phenylamino-pyrimidine (**5**) using a modification of the procedure by Satoh *et. al* [119]. To a mixture of *N*-(2-methyl-5-nitrophenyl)-4-(3-pyridyl)-2-pyrimidiamine (**5**, 2.84 mmol, 0.874 g), cobalt(II) chloride (5.69 mmol, 1.35 g), and sodium borohydride (28.4 mmol, 1.08 g) was added methanol (17 ml) with a syringe. The reaction mixture was refluxed for 2 hours, and diluted with saturated sodium bicarbonate solution, and extracted three times with ethyl acetate. The organic layers were dried by anhydrous $MgSO_4$, filtered, and evaporated. The residue was purified by column chromatography eluting with ethyl acetate to give Compound **6** as a yellow powder (0.566 g, 71.8%). mp 137-139°C (lit. 141-144°C [110]). NMR spectra were consistent with previous literature [111]. ^{1}H NMR (DMSO-d_6): δ 2.06 (s, 3H), 4.85 (s, 2H), 6.32-6.34 (dd, J= 8.0Hz, 1.6Hz, 1H), 6.78 (d, J=2.0Hz, 1H),

6.85-6.87 (d, 7.6Hz, 1H), 7.36-7.37 (d, J=4.8Hz, 1H), 7.52-7.55 (dd, J=8.0Hz, 4.8Hz, 1H), 8.40-8.42 (dt, J=7.6Hz, 1.6Hz, 1H), 8.46-8.47 (d, J=5.2Hz, 1H), 8.69 (s, 1H), 8.695 (t, J=1.2Hz, 1H), 9.24-9.25 (d, J=2.0Hz, 1H). ^{13}C NMR (DMSO-d_6): δ 161.44, 161.26, 159.32, 151.30, 148.09, 146.73, 137.90, 134.23, 132.26, 130.29, 123.79, 119.28, 111.07, 110.87, 107.03, 17.20.

2.2.2.5 Benzyl 4-(4'-hydroxycarbonylbenzyl)-1-piperazine carboxylate (7)

The procedure of Metcalf *et. al.* was adapted to synthesize benzyl 4-(4'-hydroxy-carbonylbenzyl)-1-piperazine carboxylate (**7**) from 4-hydroxycarbonylbenzyl bromide and benzyl piperazine-1-carboxylate [120]. To a mixture of 4-hydroxycarbonylbenzyl bromide (4.65 mmol, 1.00 g) and potassium carbonate (23.3 mmol, 3.21 g) in ethanol (20 ml) at room temperature was added benzyl piperazine-1-carboxylate (5.58 mmol, 1.08 ml) and the mixture was refluxed for 2 hours. After the solution was filtered, the filtrate was evaporated *in vacuo*, and the residue was dissolved in 25% sodium hydroxide solution. After the solution was extracted three times with ether, the aqueous solution was acidified to pH2 with 10% HCl solution. The solution was extracted three times with ether. The organic layer was dried by anhydrous magnesium sulfate, filtered, and then evaporated *in vacuo* to give Compound **7** as a white powder (0.634 g, 39.4%). mp: 180-182^{o}C, ^{1}H NMR (DMSO-d_6): δ 2.33-2.36 (t, J=5.2 Hz, 4H), 3.40 (s, 4H), 3.55 (s, 2H), 5.07 (s, 2H), 7.29-7.39 (m, 5H), 7.42-7.44 (d, J=7.6 Hz, 2H), 7.89-7.91 (d, J=7.6 Hz, 2H), 12.85 (s, 1H). ^{13}C NMR (DMSO-d_6): δ 167.27, 154.40, 143.13, 136.92, 129.79, 129.31, 128.83, 128.44, 127.86, 127.56, 66.19, 61.46, 52.31, 43.48. HRMS (DCI/NH_3) m/z calcd for $C_{20}H_{23}N_2O_4$ (MH^+), 355.1652; found 355.1672.

*2.2.2.6 4-(4-Methylpiperazinomethyl)benzonitrile (**8**)*

4-(4-Methylpiperazinomethyl)benzonitrile (**8**) was prepared from α-bromo-*p*-tolunitrile and 1-methylpiperazine by the procedure of previous literature [121]. To a stirred solution of α-bromo-*p*-tolunitrile (10.2 mmol, 2.00 g) in chloroform (15 ml) was added a solution of 1-methylpiperazine (28.6 mmol, 3.17 ml) in chloroform (15 ml) dropwise, and stirred for 3 hours at room temperature. The resulting solution was diluted with saturated sodium bicarbonate solution (30 ml), and stirred for 30 minutes at room temperature, then extracted three times with methylene chloride (30 ml). The organic extracts were combined, dried with anhydrous magnesium sulfate, filtered, and evaporated. The residue was purified with hexane by recrystallization to afford Compound **8** as a white powder (1.55 g, 71%). mp (**8**): 66-67^{o}C (lit. 66-68^{o}C [121]). NMR spectra were consistent with previous literature [121]. ^{1}H NMR: δ 2.29 (s, 3H), 2.47 (broad s, 8H), 3.55 (s, 2H), 7.44-7.46 (d, J=7.8 Hz, 2H), 7.59-7.61 (d, J=7.7 Hz, 2H). ^{13}C NMR: δ 144.46, 132.29, 129.69, 119.18, 111.03, 62.61, 55.27, 53.36, 46.23.

*2.2.2.7 4-(4'-hydroxycarbonylbenzyl)-1-methylpiperazine (**9**)*

4-(4'-Hydroxycarbonylbenzyl)-1-methylpiperazine (**9**) was prepared from 4-(4-methylpiperazinomethyl)benzonitrile (**8**) by the procedure of previous literature [121]. To a stirred solution of 4-(4-methylpiperazinomethyl)benzonitrile (**8**, 3.72 mmol, 0.80 g) in methanol (18 ml) was added 10% sodium hydroxide solution (75.0 mmol, 30 g) and stirred for three hours at 60-70^{o}C. The resulting solution was cooled down to room temperature, and methanol was removed *in vacuo*. After the solution was washed with ether, the aqueous was acidified to pH1 with HCl (conc) at 0-10^{o}C. The suspended

product was filtered and dried *in vacuo* to give Compound **9** as a white powder. (0.564 g, 49%) LC-MS m/z calcd for $C_{13}H_{18}N_2O_2$ (M^+), 234.14; found (MH^+), 235.3 ^{1}H NMR (**9**, D_2O): δ 3.03 (s, 3H), 3.66 (broad s, 8H), 4.54 (s, 2H), 7.64-7.66 (d, J=6.2 Hz, 2H), 8.11-8.13 (d, J=6.2 Hz, 2H). ^{13}C NMR (**9**, D_2O): δ 169.91, 132.91, 131.84, 131.40, 130.43, 59.82, 50.25, 48.35, 42.74.

*2.2.2.8 Preparation of imatinib (**1**) and 4-[(4-benzyloxycarbonyl-1-piperazinyl) methyl]-N-[4-methyl-3-[[4-(3-pyridyl)-2-pyrimidinyl]amino]phenylbenzamide (**10**) by amide bond formation*

Imatinib (**1**) and cbz-protected imatinib (**10**) were prepared by amide bond formation with pyrimidamine (**6**) and their corresponding acids (Compounds **9** and **7** respectively) using a modification of procedure by Lee *et al* [122]. A benzyl 4-(4'-hydroxycarbonylbenzyl)piperazine-1-carboxylate (**7**, 2.0 mmol, 0.709 g) or 4-(4'-Hydroxycarbonylbenzyl)-1-methylpiperazine (**9**, 2.0 mmol, 0.469 mmol) solution in thionyl chloride (5.0 ml) was refluxed for one hour. After the remaining thionyl chloride was removed *in vacuo*, *N*-(2'methyl-5'-amino-phenyl)-4-(3'-pyridyl)-2-pyrimidiamine (**9**, 1.80 mmol, 0.504 g), triethylamine (4.30 mmol, 0.60 ml), and methylene chloride (6.0 ml) were added to the residue. The reaction mixture was stirred overnight at room temperature. The solution was diluted with 10ml of sodium carbonate solution (5 ml of saturated sodium carbonate solution was diluted with 5ml of water) and extracted three times with 10 ml of ethyl acetate. The extracted solution was dried by anhydrous magnesium sulfate, filtered, and evaporated. Column chromatography with ethyl acetate gave imatinib (**1**, 0.368 g, 41%), and Compound **10** (0.602 g, 54%). Both compounds

were obtained as a white powder. mp 208°C (**1**), 160-162°C, (**10**). NMR spectra of imatinib (**1**) were consistent with previous experiment (Sec. 2.2.1.1). ^{1}H NMR (**10**): δ 2.37 (s, 3H), 2.43 (s, 4H), 3.52-3.55 (t, J=5.2 Hz, 4H), 3.58 (s, 2H), 5.14 (s, 2H), 7.10 (s, 1H), 7.20-7.21 (d, J=5.2 Hz, 1H), 7.22-7.24 (d, J=8.0 Hz, 1H), 7.31-7.38 (m, 6H), 7.43-7.47 (m, 3H), 7.84-7.87 (d, J=7.2 Hz, 2H), 7.87 (s, 1H), 8.52-8.55 (m, 2H), 8.59-8.60 (d, J=2.4 Hz, 1H), 8.71-8.73 (dd, J=4.8 Hz, 2.8 Hz, 1H), 9.27 (dd, J=1.6 Hz, 0.8 Hz, 1H). ^{13}C NMR (**10**): δ 165.53, 163.01, 160.77, 159.23, 155.46, 151.66, 148.71, 142.23, 138.03, 136.92, 136.74, 135.23, 134.34, 132.92, 131.04, 129.54, 128.71, 128.24, 128.11, 127.31, 124.48, 123.98, 115.51, 113.30, 108.62, 67.35, 62.71, 53.01, 44.00, 17.92. HRMS (**10**, FAB) m/z calcd for $C_{36}H_{36}N_7O_3$ (MH^+), 614.2874; found 614.2879.

*2.2.2.9 Preparation of norimatinib (4-[(piperazinyl)methyl]-N-[4-methyl-3-[[4-(3-pyridyl)-2-pyrimidinyl]amino]phenyl benzamide, **2**) by deprotection reaction*

Norimatinib (**2**) was prepared from Compound **10** by a modified procedure from the literature [123]. To a solution of 4-[(4-benzyloxycarbonyl-1-piperazinyl)methyl]-*N*-[4-methyl-3-[[4-(3-pyridyl)-2-pyrimidinyl]amino]phenylbenzamide (**10**, 0.326 mmol, 0.20 g) in methanol (6.5 ml) at room temperature was added 10% palladium on charcoal (0.038 mmol, 0.040 g) in a Parr shaker. The solution was shaken for 3.5 days under 65 psi of hydrogen. The reaction mixture was filtered and evaporated *in vacuo*. The remaining residue was purified by column chromatography eluting with methanol:28-30% ammonia solution=100:1 co-solvent to give norimatinib as a white powder (**2**, 0.062 g, 40.9%). mp 145-149°C. NMR spectra of norimatinib (**2**) were consistent with previous experiment (Sec. 2.2.1.2).

2.3 Radiolabeling

[N-^{11}C-methyl]Imatinib hydrochloride (**1**) was prepared by modifying the method published in US patent in 2003 [79]. [^{11}C]Methyl iodide was generated from GE PETtrace MeI Microlab, and transferred into long neck V-shaped vessel containing 0.2 mg of Compound **2** in 0.20 ml of dimethyl sulfoxide (DMSO). When carbon-11 radioactivity peaked in the reaction vessel as determined by NaI detector, the reaction vessel was sealed, and heated at 80^{o}C for 10 minutes in an oil bath. The reaction mixture was diluted with 1 ml of 0.06 N HCl solution, and the product was eluted with 27% acetonitrile:73% 0.1 M ammonium formate co-solvent at a flow rate of 4.5 ml/min on a Phenomenex Luna C18 semi-preparative column (250 mm×10 mm, 5 μm) with Knauer HPLC system (Sonntek Inc., Woodcliff Lake, NJ) equipped with model K-500 pump, a model 87 variable wavelength monitor (UV 254 nm), a NaI radioactivity detector and two Hewlett-Packard 3390A integrators. Norimatinib eluted around 14.5-18.5 min. The product was collected around 18.8-23.1 min after injection, and transferred to a rotary evaporator preloaded with 50 μl of 1 N HCl to co-evaporate with acetonitrile. The residue was dissolved in 4 ml of 5% ethyl alcohol solution in saline and passed though a 0.22 μm Millipore® filter (Millipore Corp., Billerica, MA) into a sterile vial for PET study. Synthesis time was one hour from the end of cyclotron bombardment (EOB) to delivery. The radiochemical yield (RCY) was 76.7±6.9% (n=6) based on total [^{11}C]methyl iodide activity. The specific activity ranged from 1.1-1.4 Ci/μmol at the EOB and was determined as the ratio of the total carbon-11 eluted with the product peak to the mass of imatinib determined from the area under the HPLC peak referred to a standard curve.

2.4 Quality control of collected [N-^{11}C-methyl]imatinib hydrochloride

The radiochemical purity of purified [*N*-^{11}C-methyl]imatinib hydrochloride was determined by both analytical HPLC system and TLC. An aliquot of the [^{11}C]product (10 μl) was eluted with 35% acetonitrile:65% 0.1 M ammonium formate solution at a flow rate of 1.0 ml/min in the analytical HPLC system to check radiochemical purity. Its retention time was 6.1±1.6 min, and the radiochemical purity was >98% as determined by comparing the radioactivity in the peak to the total carbon-11 injected. When product aliquot (15 μl) was co-injected with unlabeled imatinib free base standard solution (7 μl) and 0.3 N HCl (30 μl) to form one ionic species, labeled product and unlabeled standard co-eluted (Retention time: 5.6±0.6 min).

TLC in which the labeled product and an authentic standard were co-spotted also showed that the radiochemical purity was >98% and the R_f value (0.48). (Solvent: methanol: 28-30% NH_4OH solution=20:1 on Macherey-Nagel Polygram® Sil G/UV254 plastic-back TLC plate). The TLC plate was scanned by Bioscan System 200 Imaging Scanner (Bioscan Inc., Washington DC). The UV spot was checked with 254 nm short wave UV.

2.5 Determination of log D

Log D was determined by modification of a literature procedure [124]. [*N*-^{11}C-methyl]imatinib hydrochloride solution (50 μl) was added to a test tube containing 2.5 ml of octanol and 2.5 ml of pH 7.4 phosphate buffer solution. The solution was vortexed for 2 minutes and centrifuged for 2 minutes at maximum speed. An aliquot (0.1 ml) was

taken from organic layer, and another aliquot (1.0 ml) was taken from aqueous layer. Then 2.0 ml of sample from organic layer was added to second test tube containing 0.5 ml of octanol and 2.5 ml of pH 7.4 phosphate buffer solution. The same treatment is applied to the second test tube. These repeated procedures were applied to six test tubes so that 12 samples (six from aqueous layer and six from organic layer) were obtained. Each sample was counted by well counter (Picker, Cleveland, OH) to yield the ratio of decay-corrected counts in the octanol:buffer. log D=log (Decay corrected radioactivity in octanol layer×10 / decay corrected radioactivity in phosphate buffer layer)

2.6 PET studies of [N-^{11}C-methyl]imatinib in baboon

The study was performed under the strict control of the NIH guide for the Care and Use of Laboratory Animals (US Department of Health and Human Services) and approved by the Brookhaven National Laboratory Institutional Animal Care and Use Committee. Three female baboons (*Papio anubis*) were prepared and anesthetized according to a procedure published previously [125]. An intramuscular injection of ketamine hydrochloride (10 mg/kg) was given and the animal was intubated and transported to PET facility in a temperature controlled transfer cage. Oxygen (800 ml/min), nitrous oxide (1500 ml/min), and isoflurane (1-4%) were provided to keep the animal sedated. Catheters were inserted in an antecubital vein for radiotracer injection, and another line in the radial artery for blood sampling. Vital signs such as heart rate, respiration rate, arterial partial pressure of oxygen, and temperature were monitored during the study. A transmission scan performed with a ^{68}Ge rotating rod source, before [*N*-^{11}C-methyl]imatinib was injected. Two intravenous injections of [*N*-^{11}C-methyl]imatinib were administered to each animal. In one of the animals a dynamic

brain scan and a dynamic torso (encompassing liver through kidneys) scan were carried out two hours apart; in the second animal two dynamic torso scans were performed at different positions to optimize coverage of peripheral organs from the heart through the urinary bladder; in a third animal, two dynamic torso scans were performed (covering heart through kidneys) with an intervening therapeutic dose of 32 mg (i.v.) free imatinib (as imatinib hydrochloride which is equivalent to a 400 mg oral dose of imatinib mesylate [126]) infused over a 60 minute time period prior to the second tracer dose. Imatinib hydrochloride solution was synthesized according to Scheme 2-1 by dissolving free imatinib (32 mg) in 1.95 ml of 0.1 N hydrochloride solution. The excess amount of hydrochloric acid was removed by co-evaporation with acetonitrile to give imatinib hydrochloride salt which was dissolved in 5 ml of sterile water and passed through a Millipore® filter. Doses of [*N*-^{11}C-methyl]imatinib ranged from 2.8-6.2 mCi (n=6) and specific activity ranged from 0.1-0.13 Ci/μmol at the time of injection for the six PET studies.

Scanning was carried out for 90 minutes with a high-resolution PET (Siemens HR+; 63 slices; 4.5×4.5×4.5 mm at the center of field of view) in 3D mode. Scanning sequences were following; 10 frames of 1 min, 4 frames of 5 min, 8 frames of 7.5 min except one of the torso scans which was terminated at 71 minutes. Arterial blood sampling was conducted every 2.5 sec (OleDich blood sampling machine, Hvidore, Denmark) for first 2.5 minutes and then obtained at 5, 10, 20, 30, 60 min and at the end of scanning. All samples were centrifuged to obtain plasma samples which were measured radioactivity in a well counter calibrated with a ^{68}Ge/^{68}Ga source. Plasma

samples at 1, 5, 10, 30, 60, and 90 min were subjected to HPLC analysis to determine the fraction of carbon-11 present as parent radiotracer. (See Sec 2.7)

2.7 HPLC determination of fraction of [N-^{11}C-methyl]imatinib in plasma

Arterial plasma samples were added to 0.3 ml of acetonitrile containing 20 μl of standard unlabeled imatinib solution (1 mg/ml). After measuring total activity, each solution was homogenized for 10 sec, and centrifuged for 5 minutes. The resulting supernatant (A_{total}), was counted, and injected into analytical HPLC system (Phenomenex Luna C18 analytical column (250 mm×4.6 mm, 5 μm) with UV detector (254 nm)) eluting with 35% acetonitrile : 65% 0.1 M ammonium formate solution at a flow rate of 1.0 ml/min. The fraction of unchanged parent radiotracer determined as a ratio of counts in the imatinib fraction (A) to the total carbon-11 injected onto the column (A_{total}): A/A_{total}.

2.8 Plasma protein binding (PPB) of [N-^{11}C-methyl]imatinib

The free fraction of [*N*-^{11}C-methyl]imatinib in plasma was measured according to the literature procedure [127]. A diluted aliquot (10 μl) of [*N*-^{11}C-methyl]imatinib was added to baboon plasma (0.8 ml), and incubated for 10 minutes at room temperature. An aliquot (20 μl) was counted in a well counter (unspun aliquots). A portion of the sample (0.2 ml) was charged into the upper level of a Centrifree® tube (Amicon Inc., Beverly, MA) and centrifuged for 10 minutes. The top part of Centrifree® tube was removed and an aliquot of the solution remaining in the bottom cup was counted in the well counter (unbound sample). The free fraction is the ratio of the decay-corrected counts of the unbound aliquot to the decay-corrected counts of the unspun aliquot.

2.9 Image analysis

Time frames were summed over the experimental period and planes were summed in groups of two for the purpose of region of interest placement. Regions of interest (ROI's) were placed over the brain and peripheral organs (heart, lungs, spleen, liver, gall bladder, kidneys, urinary bladder and spinal cord) and then projected onto the dynamic images to obtain time activity curves. Carbon-11 concentration in each region of interest was divided by the injected dose to obtain the %dose/cc. For the pretreatment study, we compared the time-activity curves at baseline and after pretreatment. We also compared the time activity curves for unchanged tracer in plasma and the area under the curve for the plasma at baseline and after treatment. For the pretreatment study we also normalized the time-activity curves in each organ for the area under the plasma time-activity curve at each time point (% dose/cc/AUC(t)) to determine whether changes were driven by treatment-induced changed in the plasma.

3. Results and Discussion

3.1 Chemistry and carbon-11 labeling

Demethylation of imatinib with m-CPBA and iron sulfate by nonclassical Polonovski reaction according to the patent procedure gave a modest yield (34.5%) [79, 112]. Norimatinib (**2**) and imatinib (**1**) were also synthesized from commercially available starting materials adapting a series of literature methods [111] (Scheme 2-1). While imatinib was built up from amine (**6**) to imatinib (**1**) step by step following the patent [111, 117], the amine (**6**) and acids (**7** and **9**) were synthesized separately from commercially available chemicals to reduce the steps from starting chemicals to

norimatinib in a new procedure. Compound **6** was prepared from Compound **3** and Compound **4** in three steps by known or modified procedures [116, 118]. Compound **3** was prepared from 3-acetylpyridine and 3-(*N*,*N*-dimethylamino)-1-(3-pyridyl)-2-propen-1-one in one step by literature procedure [113]. Compound **7** was prepared from commercially available 4-bromomethylbenzoic acid and benzyl 1-piperazine carboxylate in one step by applying a literature procedure [120] (39% yield). On the other hand, Compound **9** was prepared from commercially available *p*-bromotolunitrile and 1-methylpiperazine in two step by previous literature [121]. Amide bond formation from Compounds **6** and **7** gave cbz-protected norimatinib (**10**) by modifying literature procedure [122] (54% yield). Removal of the cbz-group with palladium charcoal under hydrogen atmosphere afforded norimatinib (**2**) [123] (41% yield). Thus norimatinib was synthesized in 3 to 4 steps from commercially available starting materials. Imatinib was also synthesized by amide coupling reaction with Compounds **6** and **9** [122]. Norimatinib was labeled successfully at 80^{o}C for 10 minutes without any base by modifying labeling scheme in published patent [79] (Scheme 2-1). [*N*-^{11}C-methyl]Imatinib was obtained in 76.7±6.9% (n=6) yield based on total [^{11}C]methyl iodide activity. Radiochemical purity determined by TLC and HPLC analytical system was over 98%. The specific activity ranged from 1.1-1.4 Ci/μmol at the EOB, and the synthesis time was one hour from EOB. The experimental value of log D was 2.34±0.17.

3.2 Evaluation of [N-^{11}C-methyl]imatinib with PET

As can be seen in the summed PET images of baboon brain after injection of 3.9 mCi of [*N*-^{11}C-methyl]imatinib, carbon-11 was not taken into the brain but was

concentrated in sinus and tissues surrounding the brain (Figure 2-2). Even though imatinib satisfies Lipinski's rule of five [128] with a log D of 2.34±0.17 which is ideal for blood-brain barrier penetration and 11.4% unbound in plasma, its brain distribution is known to be limited by P-glycoprotein mediated efflux [129, 130]. P-Glycoprotein-mediated efflux contributes not only blood-brain barrier elimination of imatinib, but also to the development of imatinib resistance [131]. A summed PET image of the baboon torso showed that [*N*-^{11}C-methyl]imatinib and/or its labeled metabolites concentrated mainly in the liver, kidneys and gall bladder after i.v. injection (Figure 2-3).

Time-activity curves for these organs are shown in Figure 2-4(a) and Figure 2-4(b) for two baboons in which four scans were performed to cover the entire torso from the brain to the urinary bladder. We found that [*N*-^{11}C-methyl]imatinib and/or its labeled metabolites peaked early in the heart, lungs, and spleen and cleared rapidly while the liver and kidney peaked and cleared more slowly and gall bladder accumulated carbon-11 over the time course of the study.

Carbon-11 accumulation in the gall bladder may represent the excretion of imatinib or its labeled metabolite(s). We note that imatinib is mainly metabolized by cytochrome P450 3A4 (CYP3A4) and CYP3A5 isoenzyme system [132, 133, 134]. The time-activity curve for the urinary bladder shows a transient large peak between 50 and 70 minutes which is likely to represent urinary excretion (Figure 2-4(b)).

There was very little uptake of carbon-11 in the spinal cord (data not shown) as well as the lungs. Thus it may be possible to determine whether [*N*-^{11}C-methyl] imatinib accumulates in tumors occurring in these regions. [*N*-^{11}C-methyl]imatinib may be a

useful tool for planning chemotherapy in the GIST patient and in other conditions where imatinib therapy may be warranted.

Labeled imatinib and its labeled metabolites cleared rapidly from the plasma. Treatment of plasma samples with acetonitrile in preparation for HPLC analysis yielded 80% of the total carbon-11 in the supernatant. The percentage of unchanged imatinib as measured by HPLC was 93.8±3.9%, 85.1±6.2%, 79.6±2.9%, 64.6±6.8%, 47.9±17.3% at 1, 5, 10, 30, and 60 min respectively (n=3).

3.3 [N-^{11}C-methyl]imatinib pharmacokinetics after pretreatment with a therapeutic dose of imatinib

Since imatinib is given at therapeutic doses in cancer treatment, we also compared the pharmacokinetics of [*N*-^{11}C-methyl]imatinib before and after an intravenous dose of 32 mg imatinib (equivalent to a 400 mg typical oral chemotherapeutic dose scaled from a 70 kg human to a 15 kg baboon [126].

After pretreatment, we found reduced uptake in heart, lungs, kidneys, and spleen at early times whereas the time-activity curves for these organs paralleled one another after 40 minutes; in contrast, uptake was higher in the liver and gall bladder after imatinib treatment (Figure 2-5). We also found reduced concentration of [*N*-^{11}C-methyl]imatinib in plasma after pretreatment (Figure 2-6). However, when the time-activity curves for the heart, lungs, kidneys, and spleen were normalized for the plasma, there were no differences indicating that reductions in uptake are driven by reductions in plasma. In contrast, normalized time-activity curves in liver and gall bladder showed increased carbon-11 uptake which may reflect increased accumulation of labeled metabolites (see

insets in Figure 2-5). We note a recent report of imatinib induced cardiotoxicity [135], which could result from high heart tissue exposure from chronic administration.

4. Conclusions

[*N*-^{11}C-methyl]imatinib has potential for assessing the regional distribution and kinetics of imatinib in the human body to determine whether the drug targets tumor and to identify other organs to which the drug or labeled metabolites distributes. Paired with tracers such as ^{18}FDG and ^{18}FLT, [*N*-^{11}C-methyl]imatinib may be a useful radiotracer in planning chemotherapy, in monitoring response to treatment and for assessing the role of drug pharmacokinetics in drug resistance. Though the use of [*N*-^{11}C-methyl]imatinib as a biomarker for mutant tyrosine kinases may be possible, this would need to be validated in vivo preferably in the cancer patient to determine if carbon-11 uptake is associated with the presence of abnormal tyrosine kinases, if uptake is saturable and if pharmacokinetics change with drug resistances.

Figures and Schemes

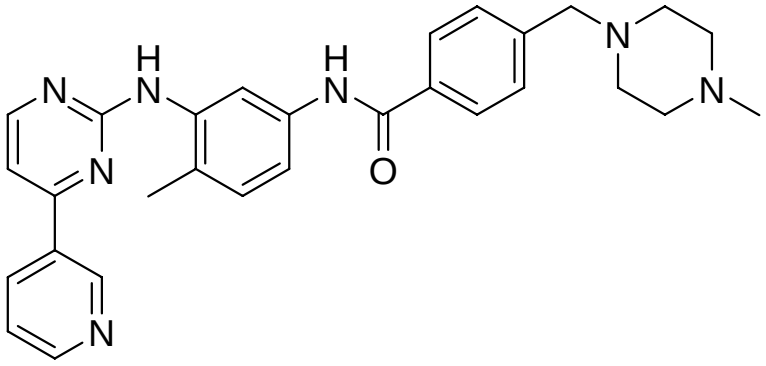

Figure 2-1. Structure of Imatinib (The active ingredient of Gleevec®)

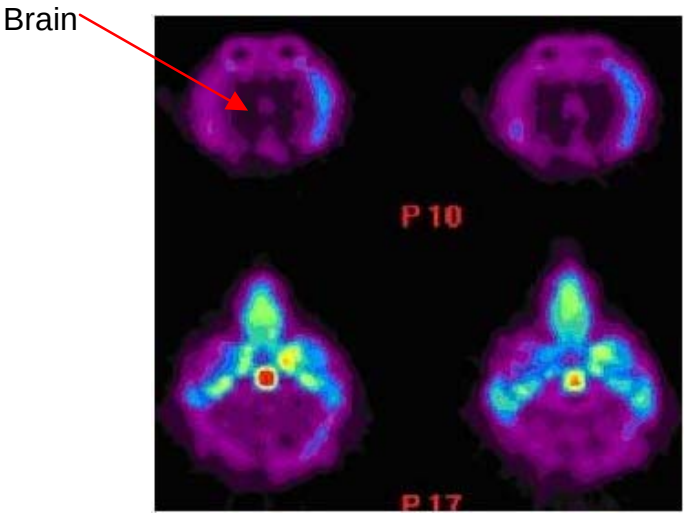

Figure 2-2. PET image of baboon brain with [*N*-^{11}C-methyl]imatinib. Summed frames over 90 minutes after injection of 3.9 mCi of [*N*-^{11}C-methyl]imatinib showing lack of uptake of carbon-11 into the brain probably due to P-glycoprotein mediated efflux [129, 130]. Anesthesia was ketamine followed by isoflurane.

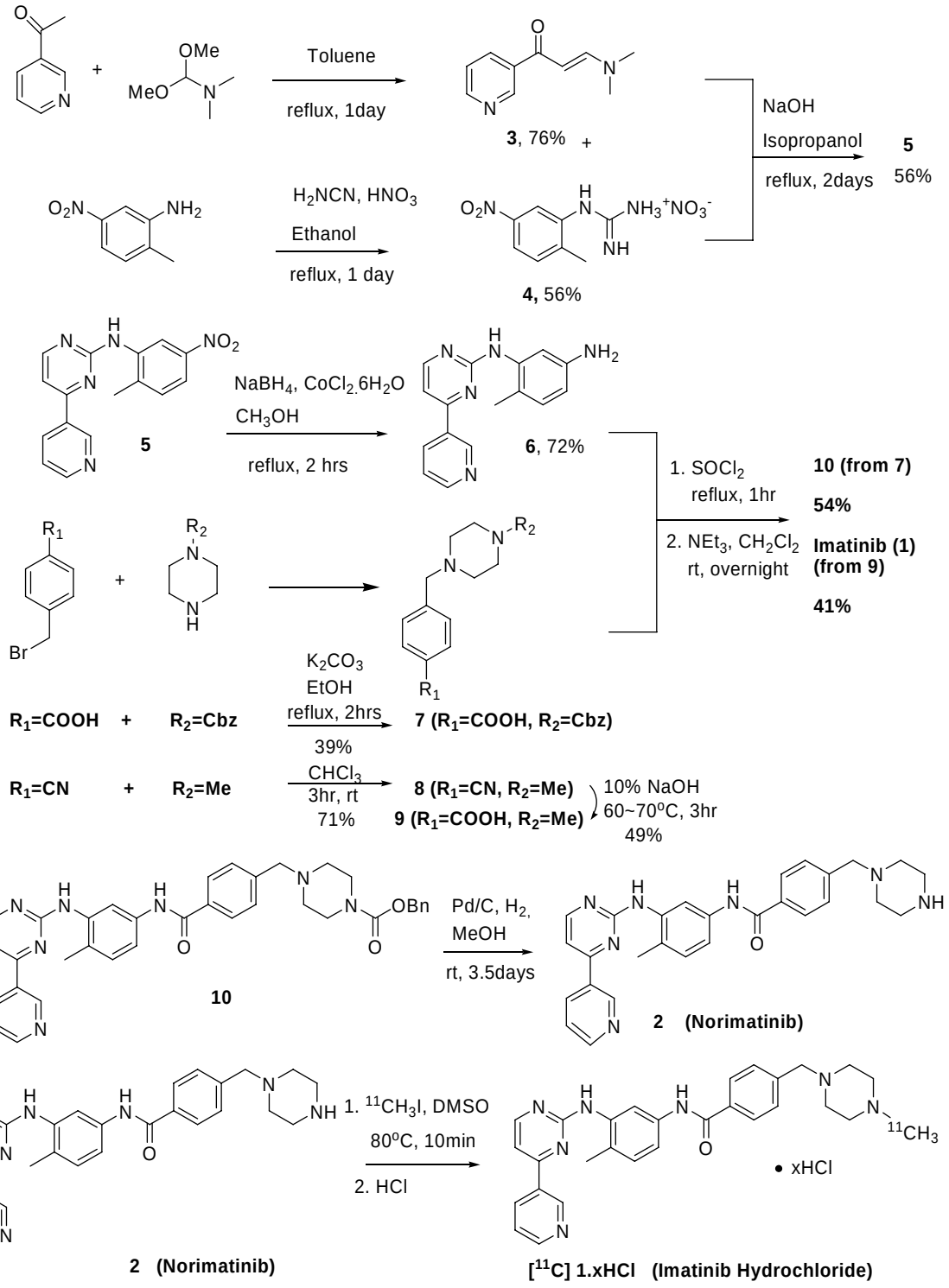

Scheme 2-1. Synthetic scheme of norimatinib, imatinib and [*N*-^{11}C-methyl]imatinib

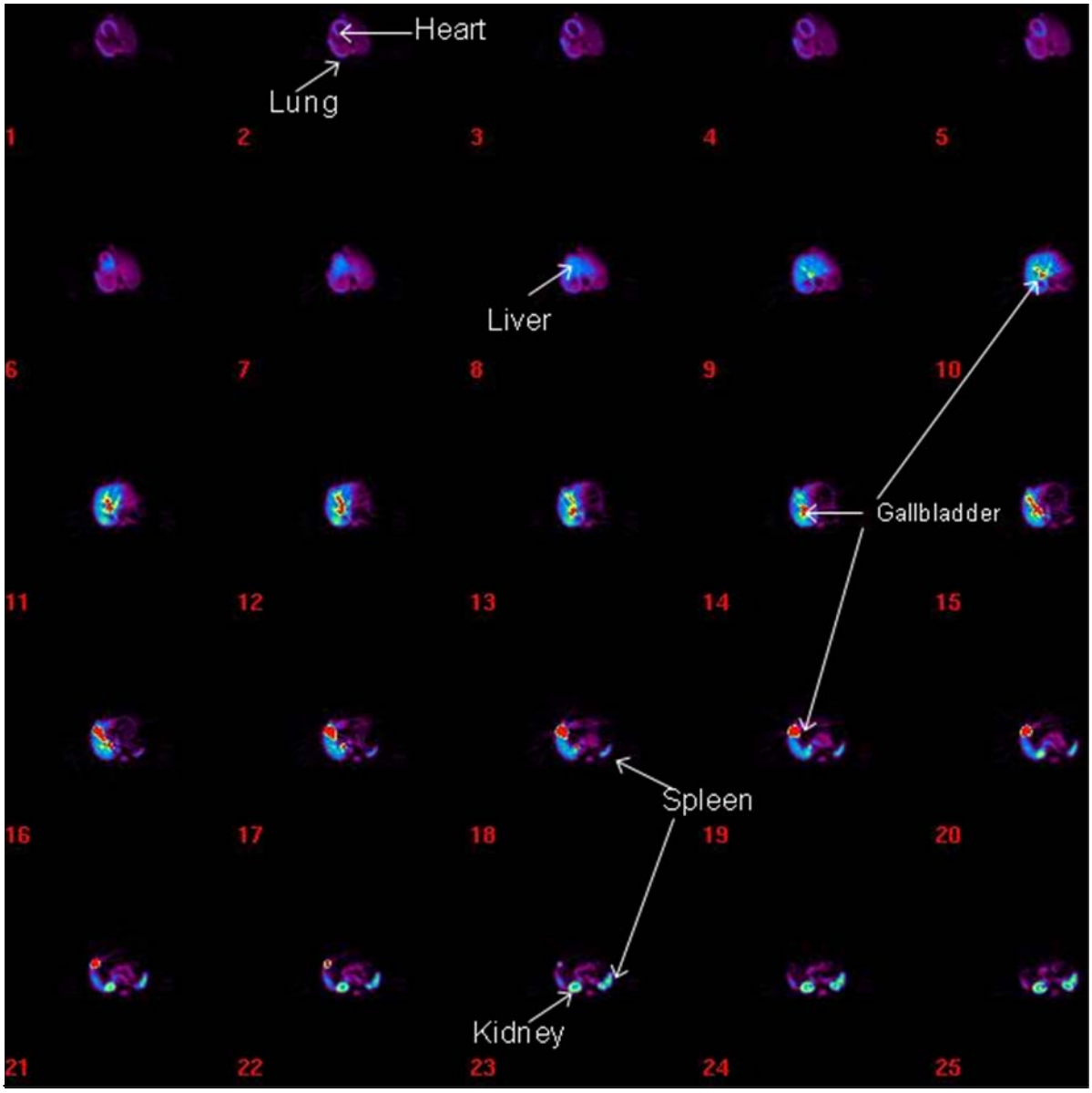

Figure 2-3. PET image of torso of the anesthetized baboon with [*N*-^{11}C-methyl]imatinib. PET images (summation of frames over 90 minutes) of the baboon torso after the injection of 4.71 mCi of [*N*-^{11}C-methyl]imatinib showing accumulation of carbon-11 in the heart and lungs (top row); liver and beginning of the gall bladder (second row); liver and gall bladder (third row); gall bladder and spleen (fourth row); kidneys and spleen (fifth row). Note the high accumulation in the gall bladder. Anesthesia was ketamine followed by isoflurane.

(a)

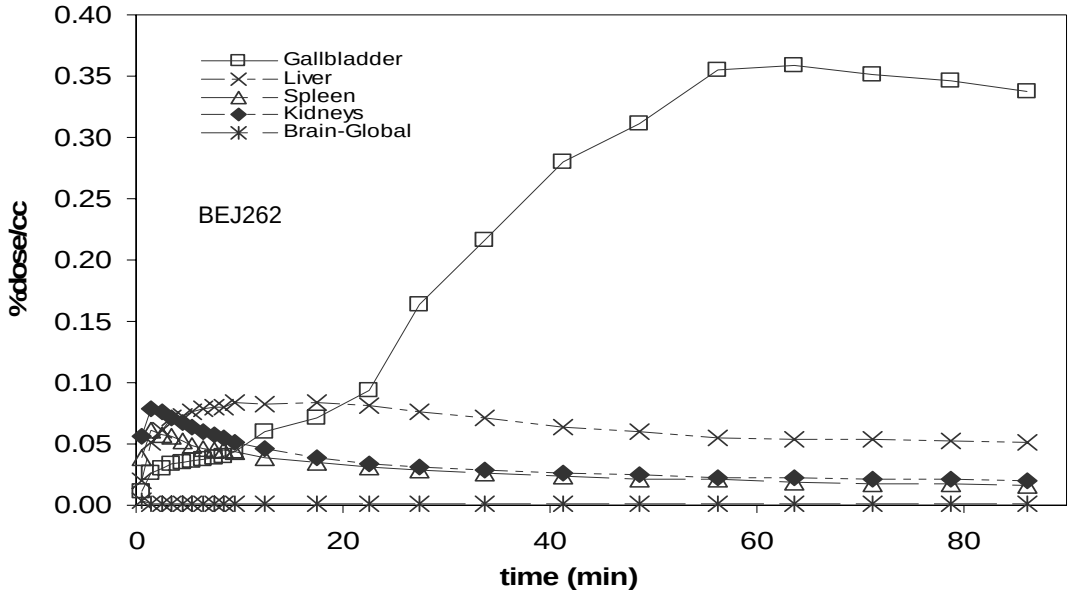

(b)

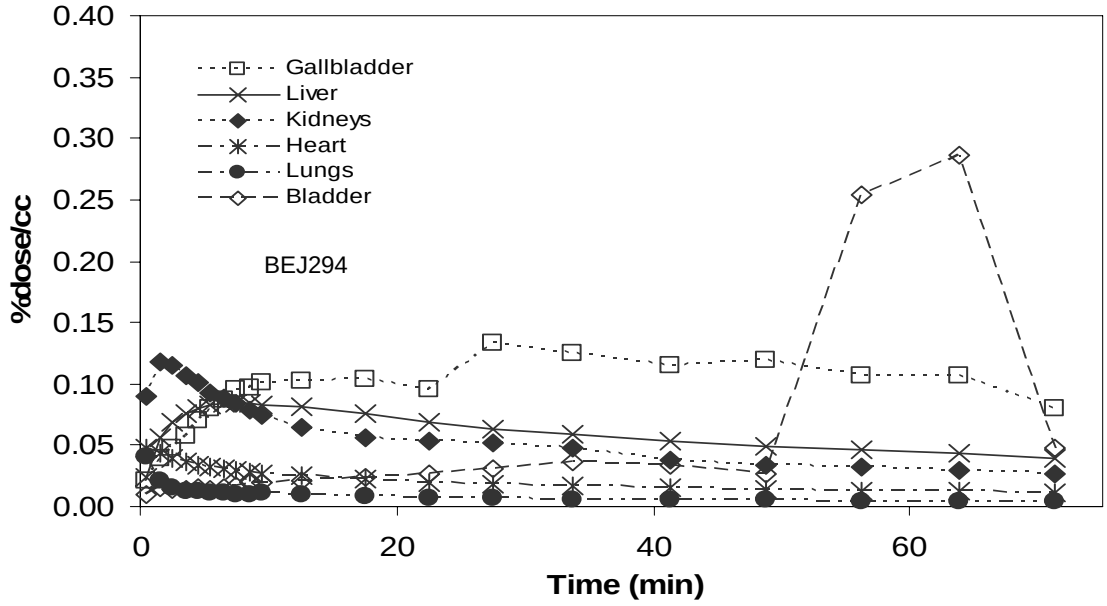

Figure 2-4. Time-Activity curves for two different anestized baboons (panels (a) and (b)) who each received two injections of [*N*-^{11}C-methyl]imatinib cover the brain through the urinary bladder.

(a) Gall Bladder

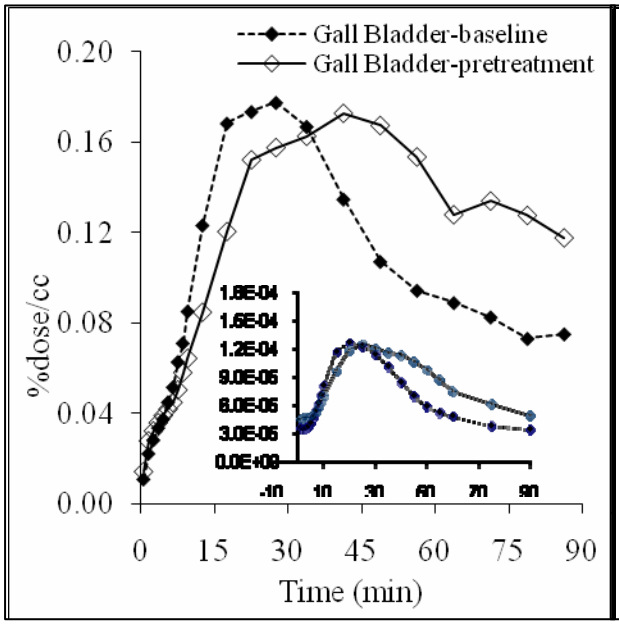

(b) Liver

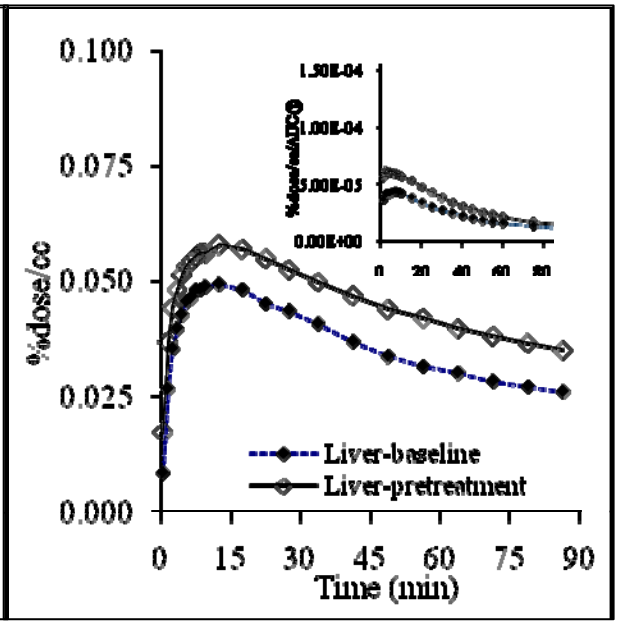

(c) Heart

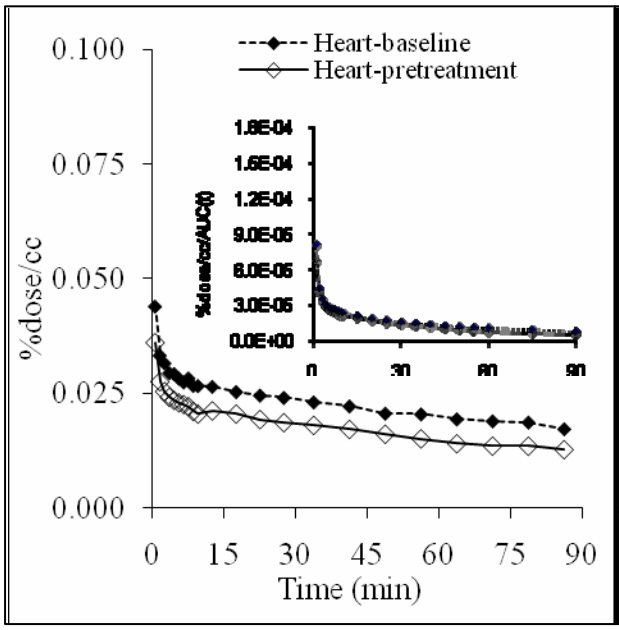

(d) Lungs

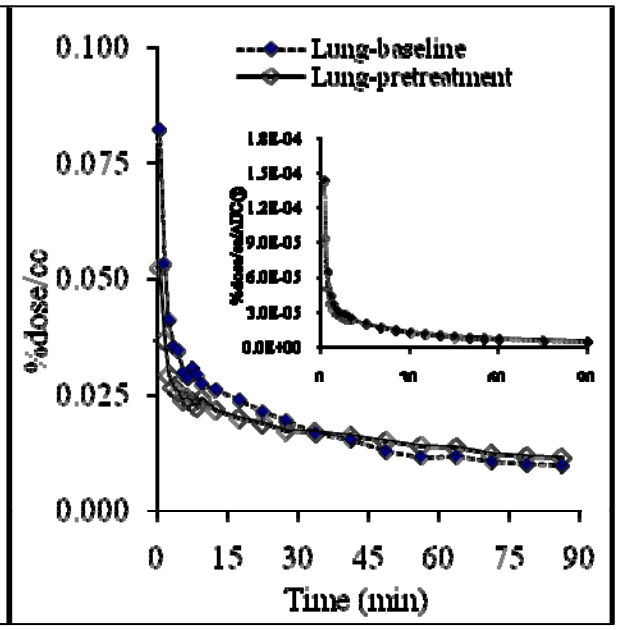

(e) Spleen

(f) Kidneys

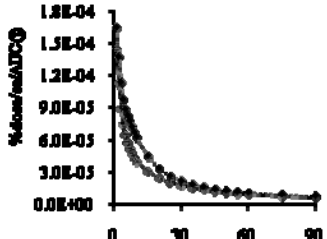

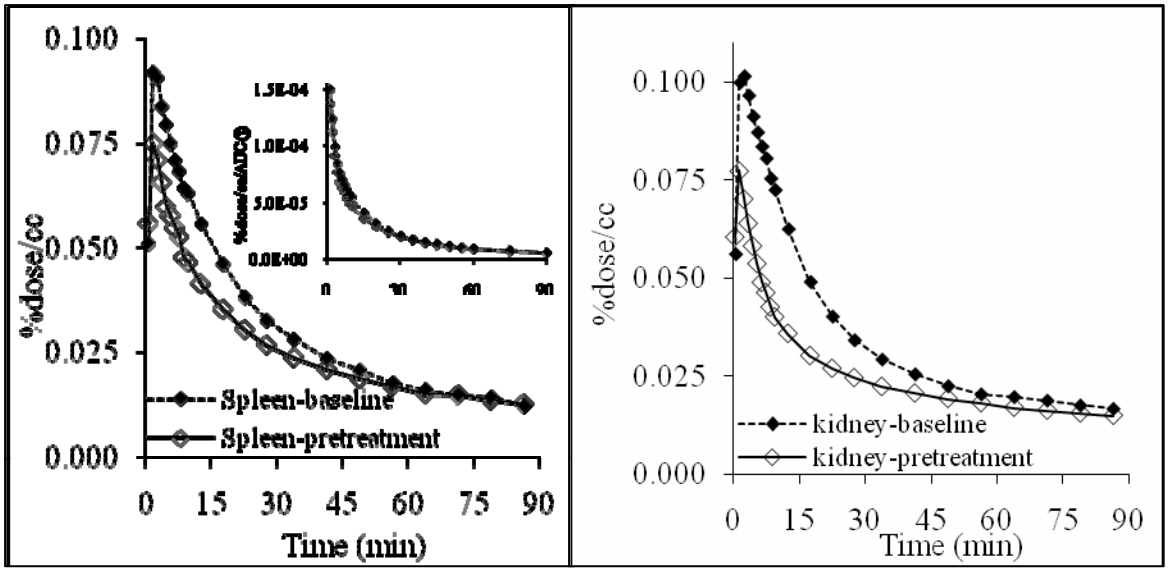

Figure 2-5. The comparison of time-activity curves of (a) gall bladder, (b) liver, (c) heart, (d) lungs, (e) spleen and (f) kidneys before and after pretreatment with 32 mg of imatinib administration by intravenous injection. Time-activity curves normalized for the area under the plasma time-activity curve are shown in the insets.

.

(a)

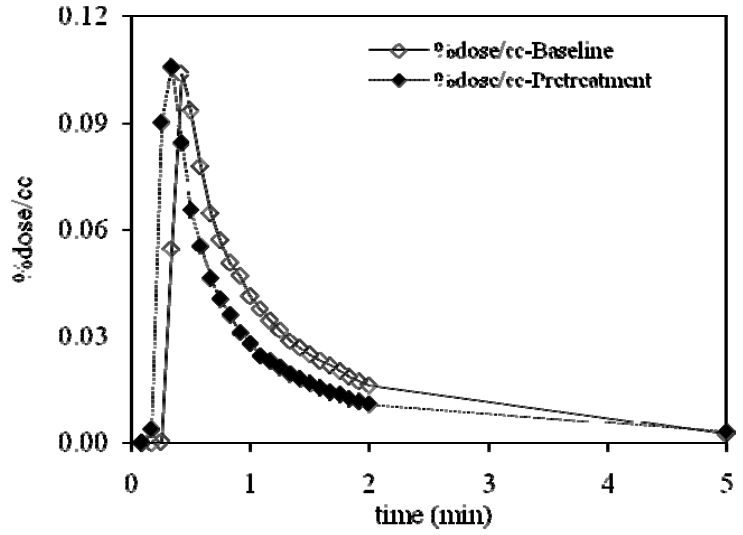

(b)

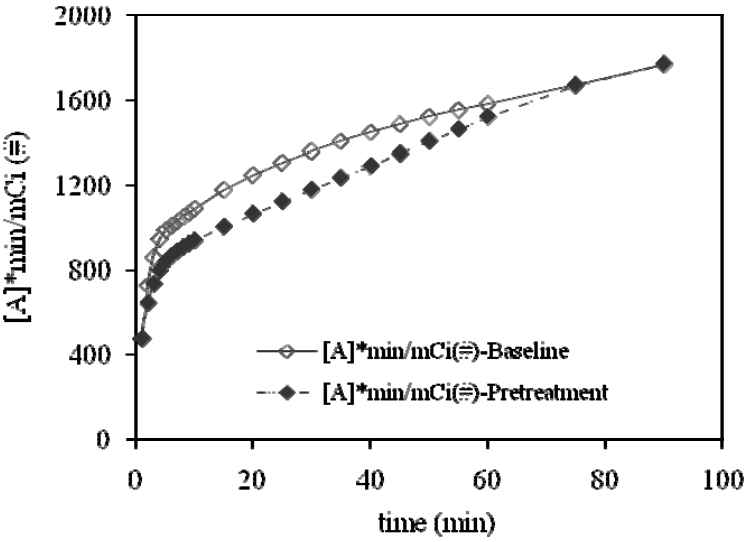

Figure 2-6. (a) Time-activity curve at baseline and after imatinib pretreatment for [*N*-^{11}C-methyl]imatinib in plasma showing the first 5 minutes, and (b) the plasma integral over 90 minutes. Pretreatment delayed [*N*-^{11}C-methyl]imatinib peak, and reduced its accumulated concentration in plasma by 10-15%.

NMR Spectra

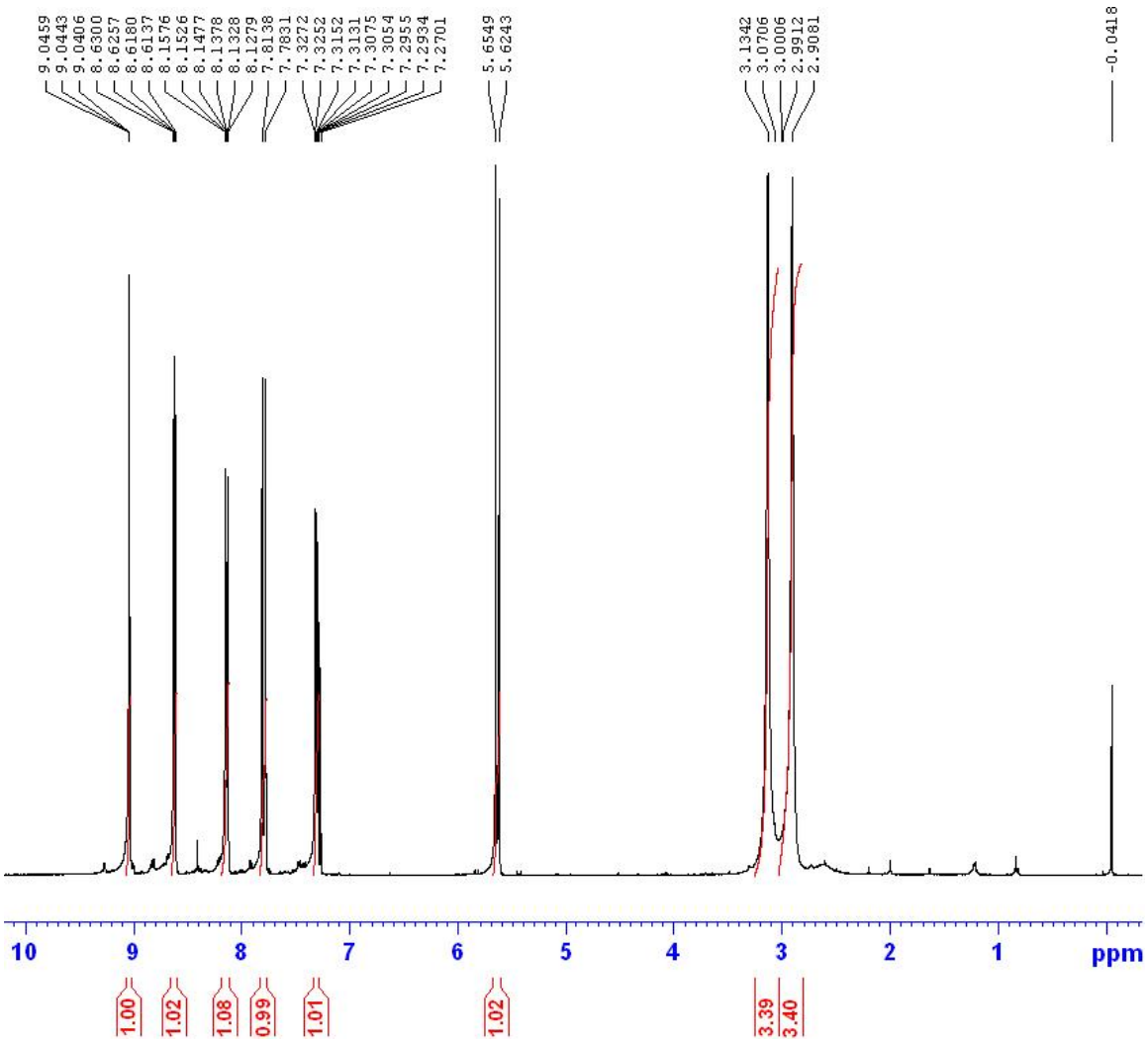

^{1}H-NMR Spectrum of 3-(*N*,*N*-dimethylamino)-1-(3-pyridyl)-2-propen-1-one (**3**)

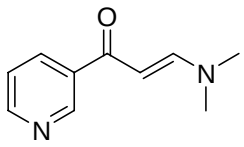

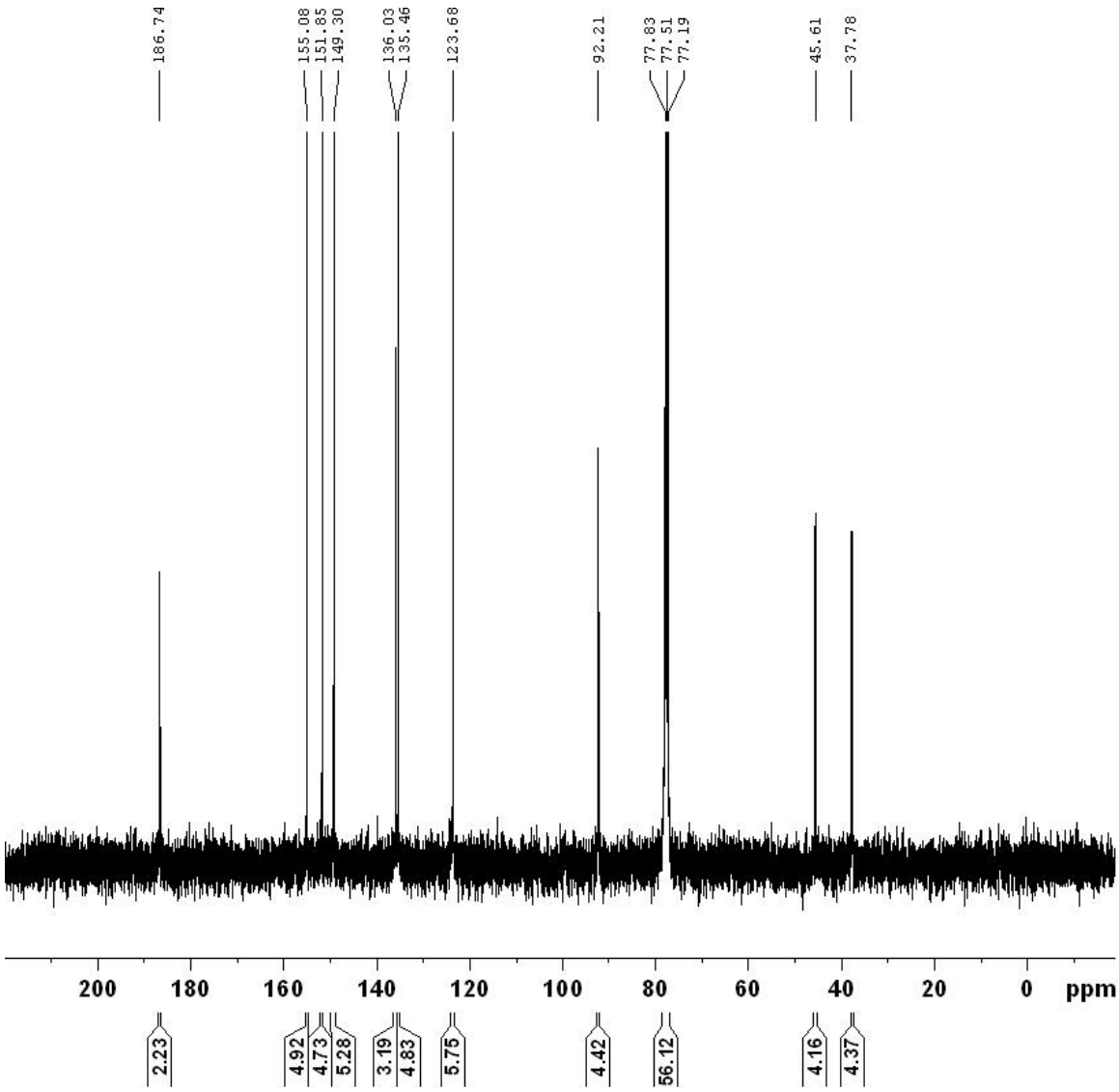

^{13}C-NMR Spectrum of 3-(*N*,*N*-dimethylamino)-1-(3-pyridyl)-2-propen-1-one (**3**)

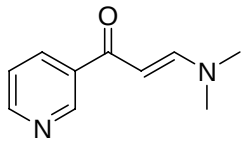

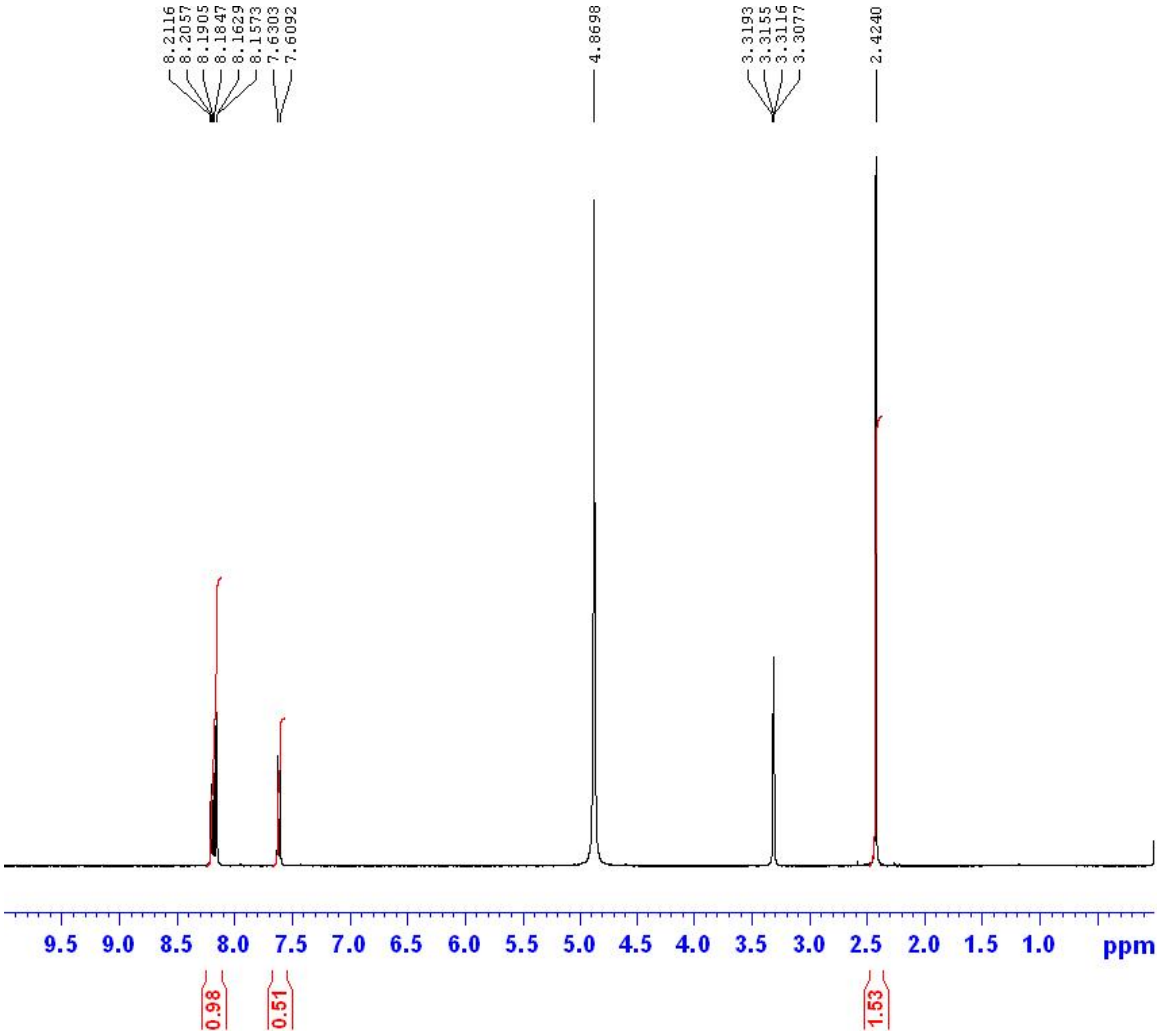

^{1}H-NMR Spectrum of 2-Methyl-5-nitrophenylguanidine nitrate (**4**, MeOH-d_4)

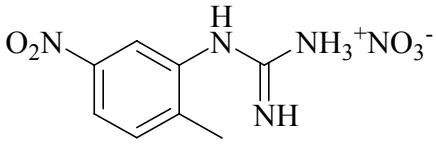

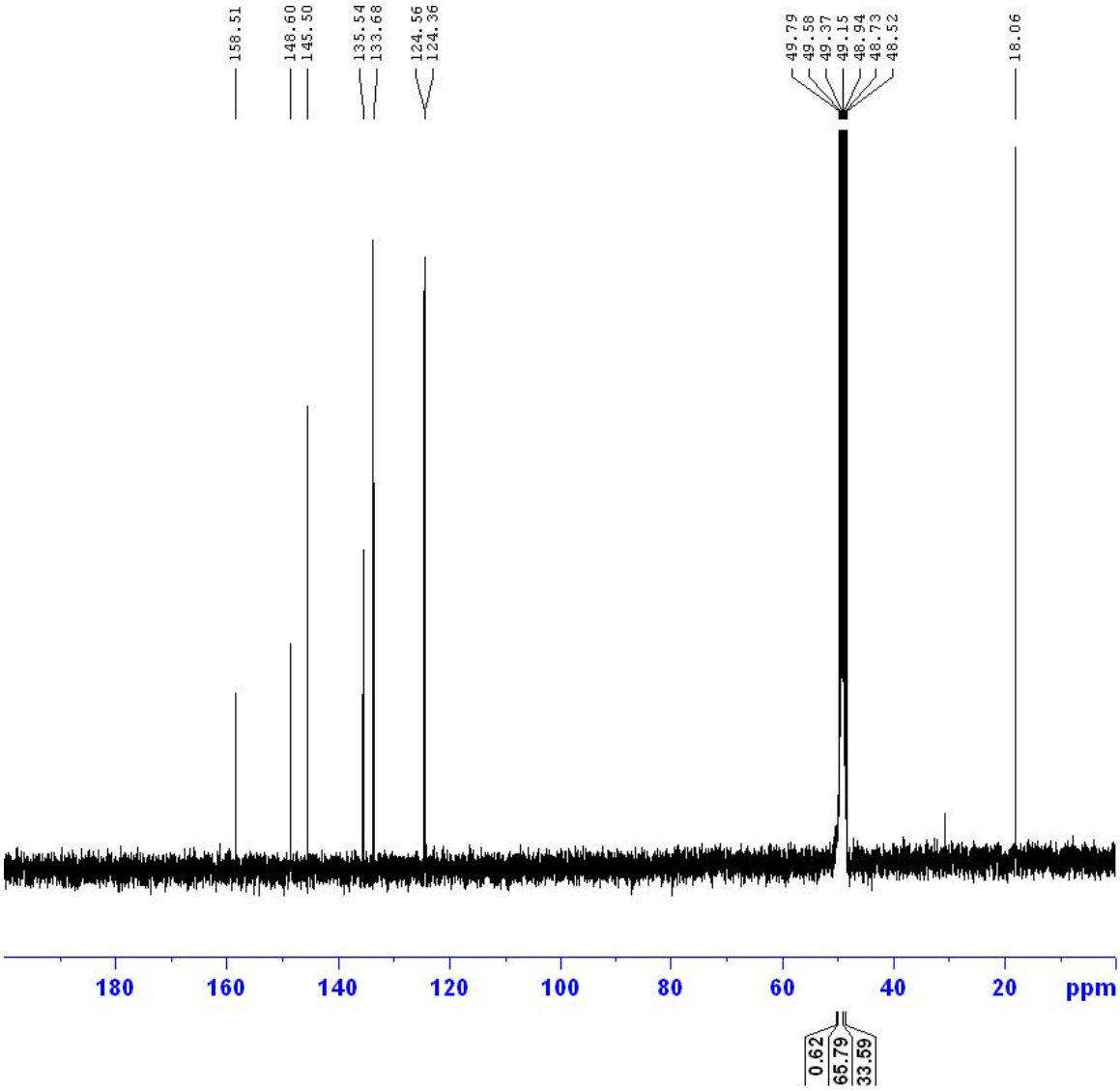

^{13}C-NMR Spectrum of 2-Methyl-5-nitrophenylguanidine nitrate (**4**, MeOH-d_4)

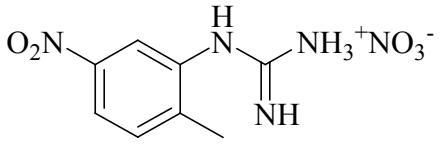

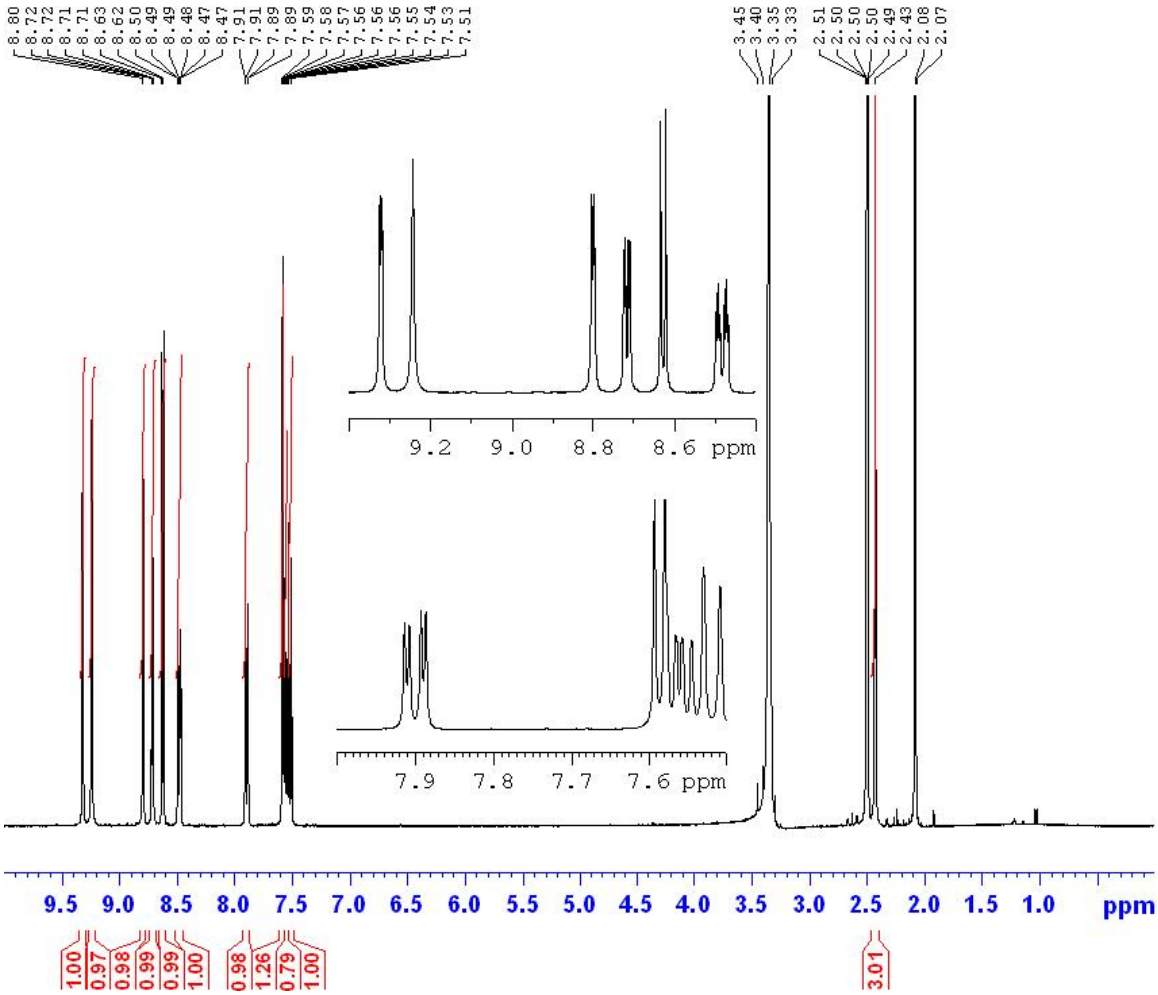

^{1}H-NMR Spectrum of *N*-(2-methyl-5-nitrophenyl)-4-(3-pyridyl)-2-pyrimidinamine (**5**, DMSO-d_6)

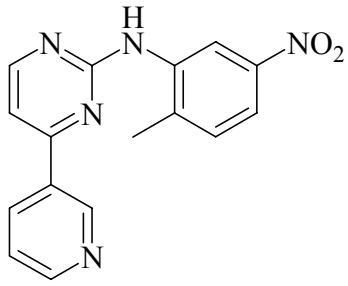

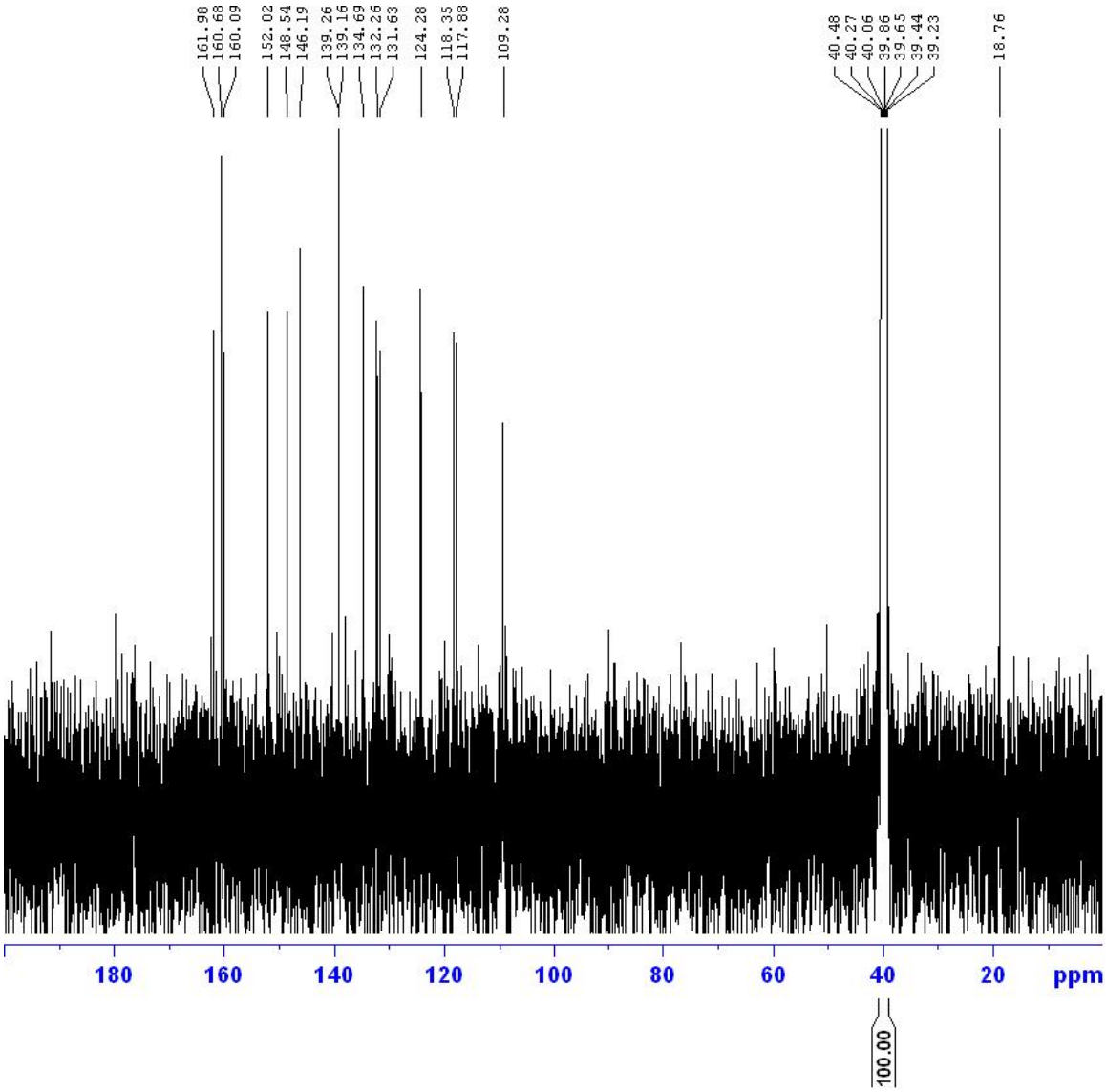

^{13}C-NMR Spectrum of *N*-(2-methyl-5-nitrophenyl)-4-(3-pyridyl)-2-pyrimidinamine (**5**, DMSO-d_6)

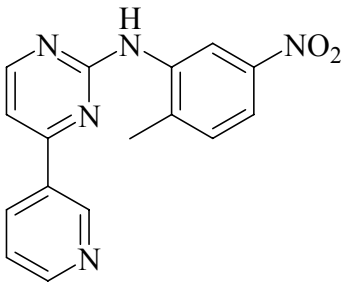

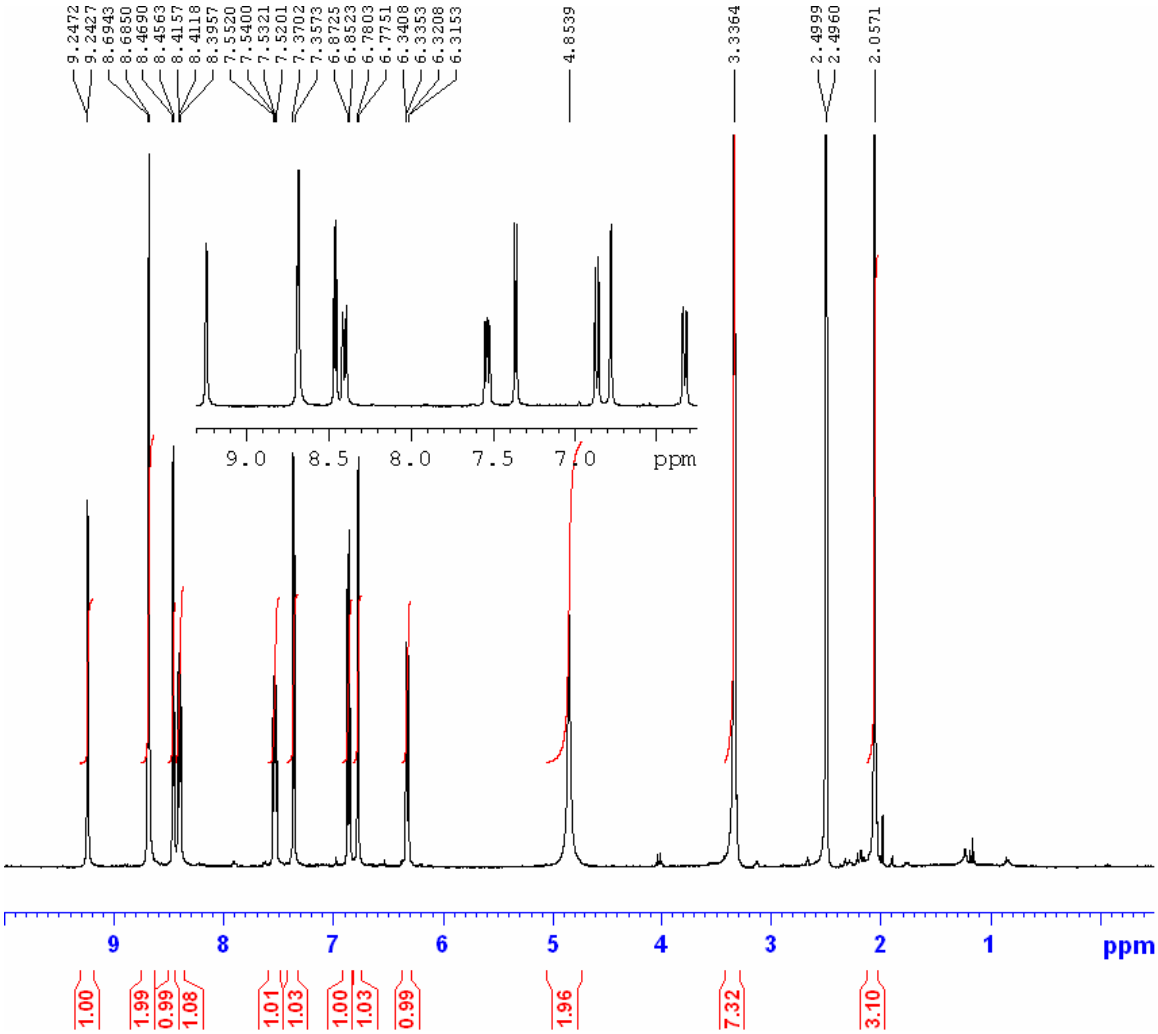

^{1}H-NMR Spectrum of *N*-(5-amino-2-methylphenyl)-4-(3-pyridyl)-2-pyrimidinamine (**6**, DMSO-d_6)

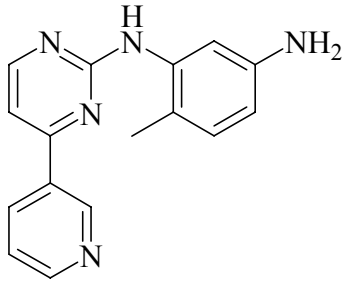

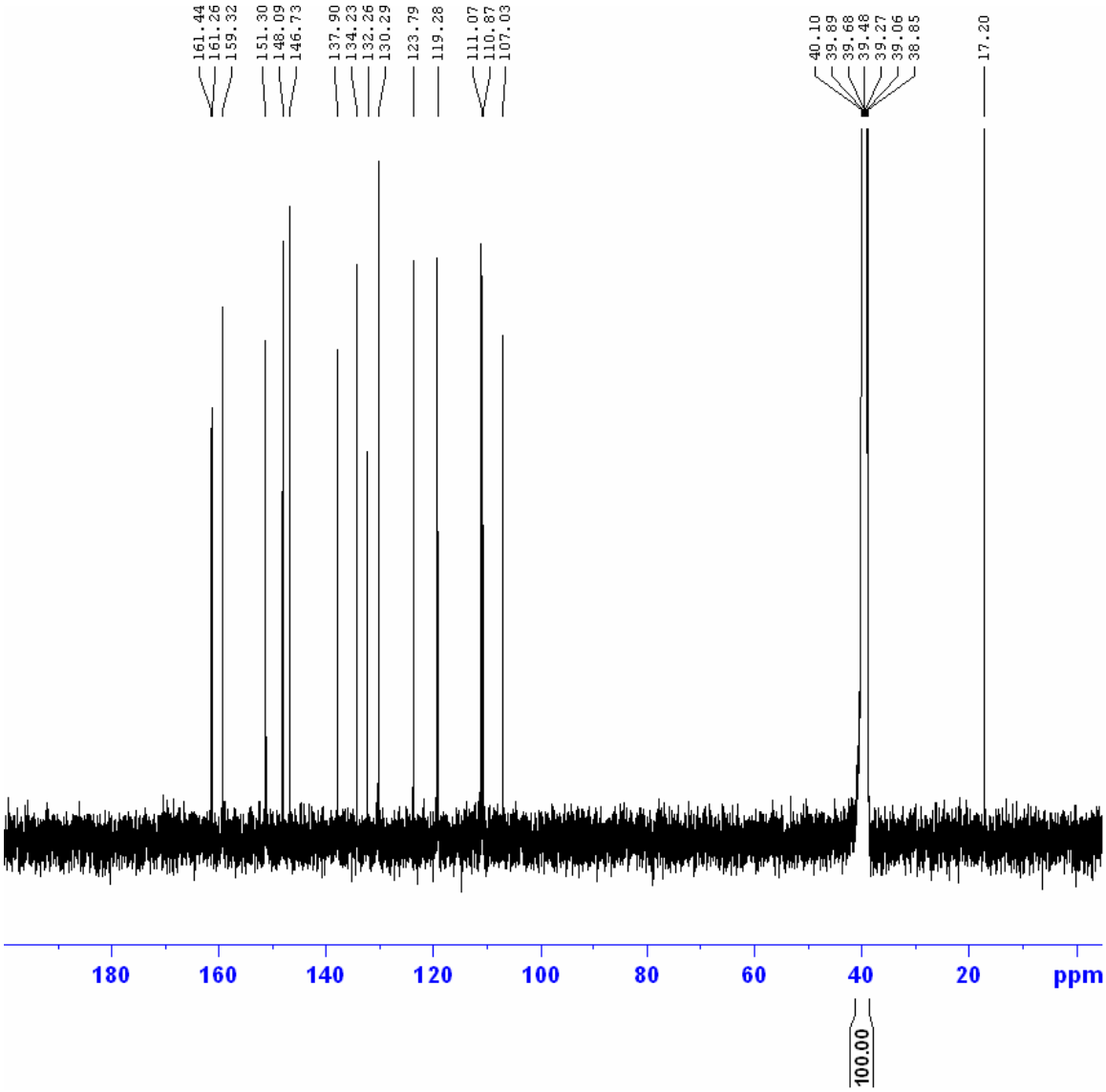

^{13}C-NMR Spectrum of *N*-(5-amino-2-methylphenyl)-4-(3-pyridyl)-2-pyrimidinamine (**6**, DMSO-d_6)

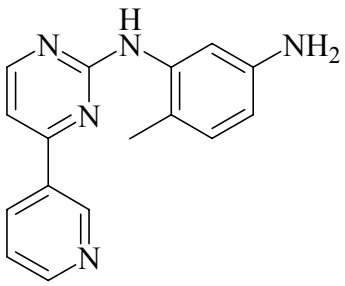

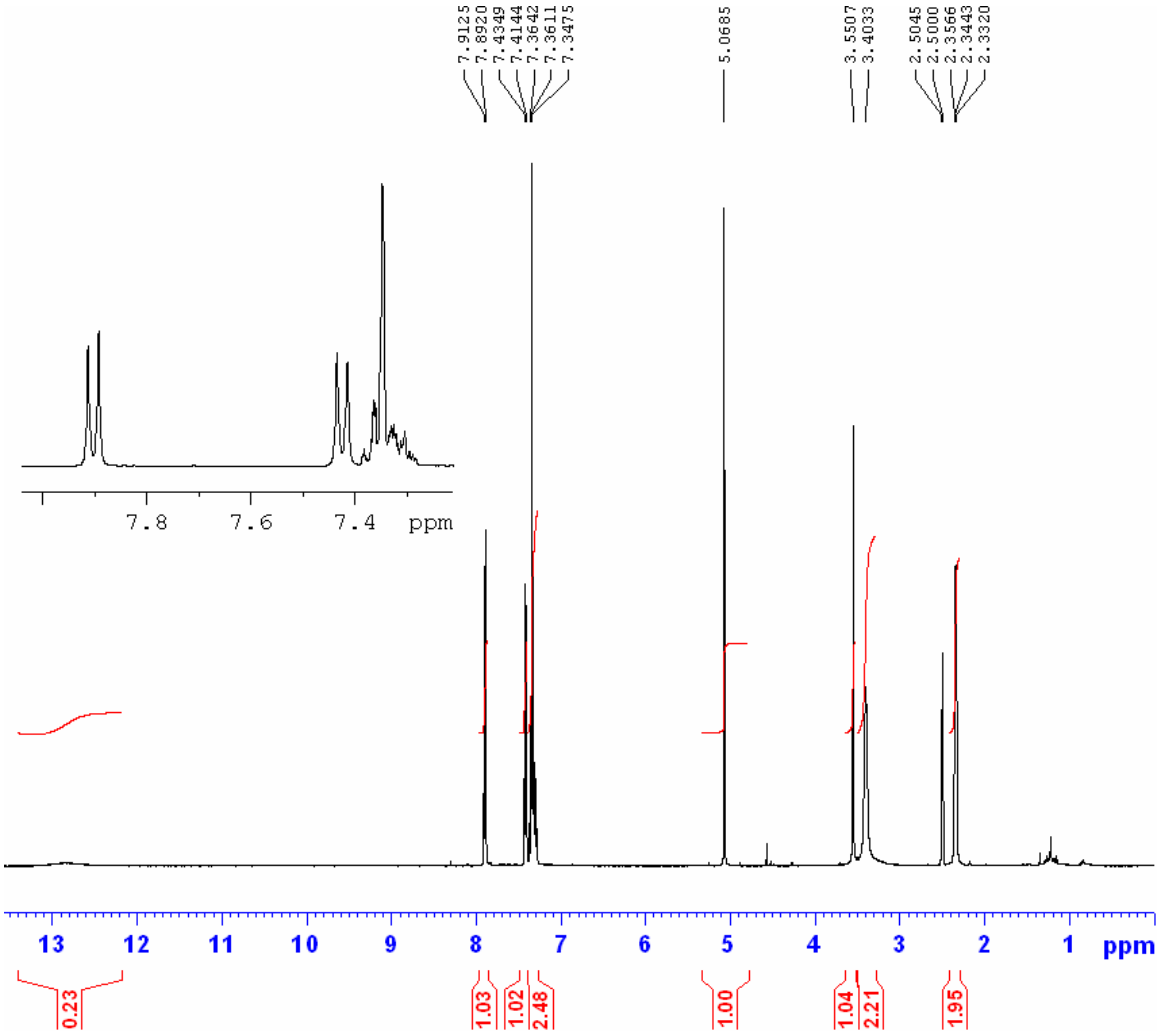

^{1}H-NMR Spectrum of Benzyl 4-(4'-hydroxycarbonylbenzyl)-1-piperazine carboxylate (**7**, DMSO-d_6)

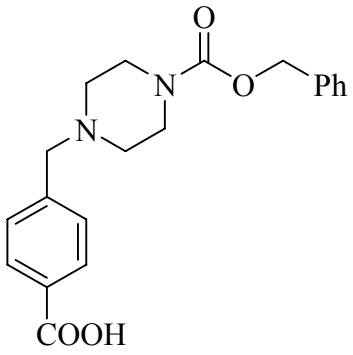

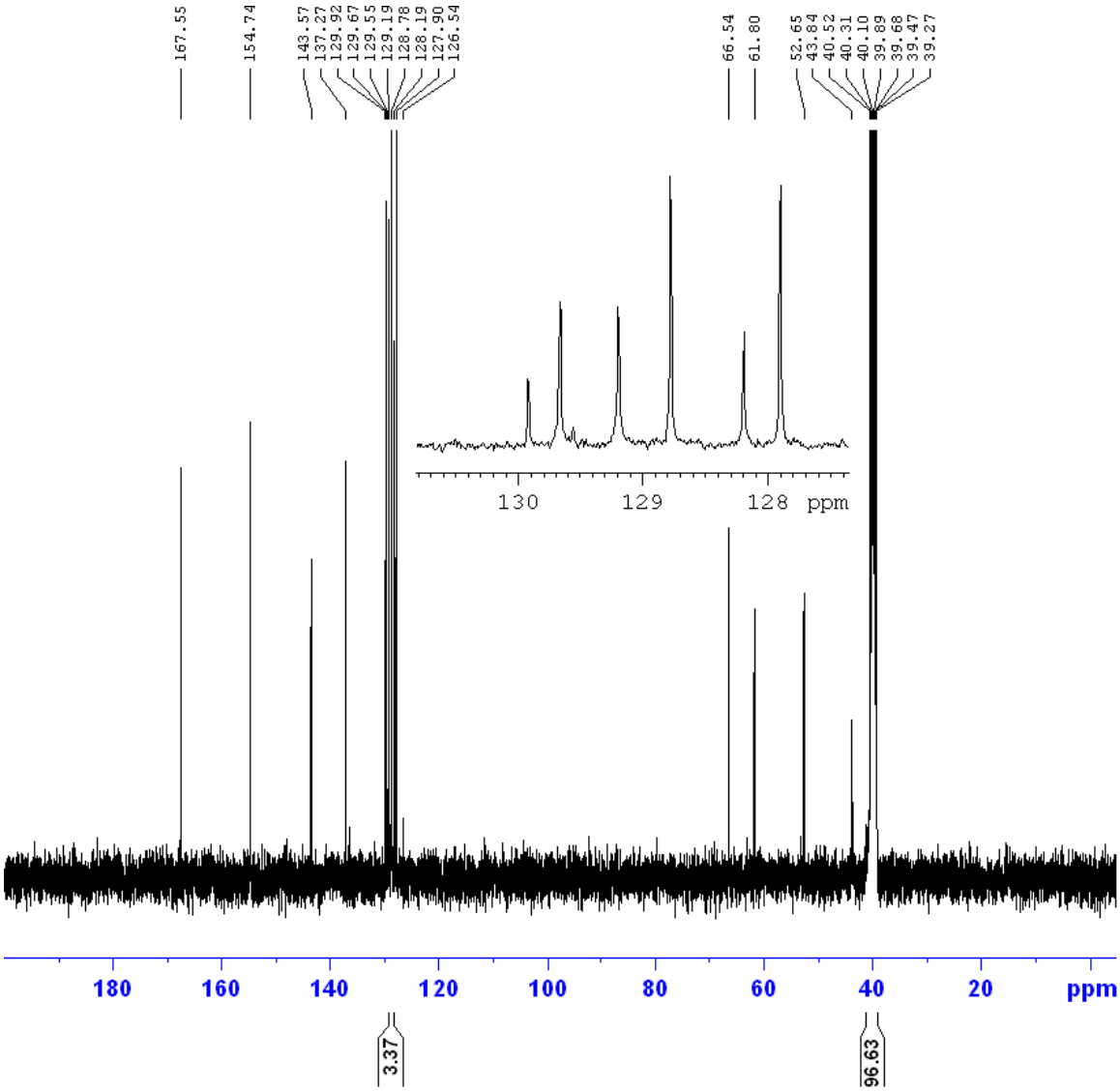

^{13}C-NMR Spectrum of Benzyl 4-(4'-hydroxycarbonylbenzyl)-1-piperazine carboxylate (**7**, DMSO-d_6)

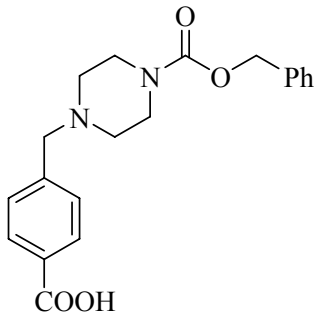

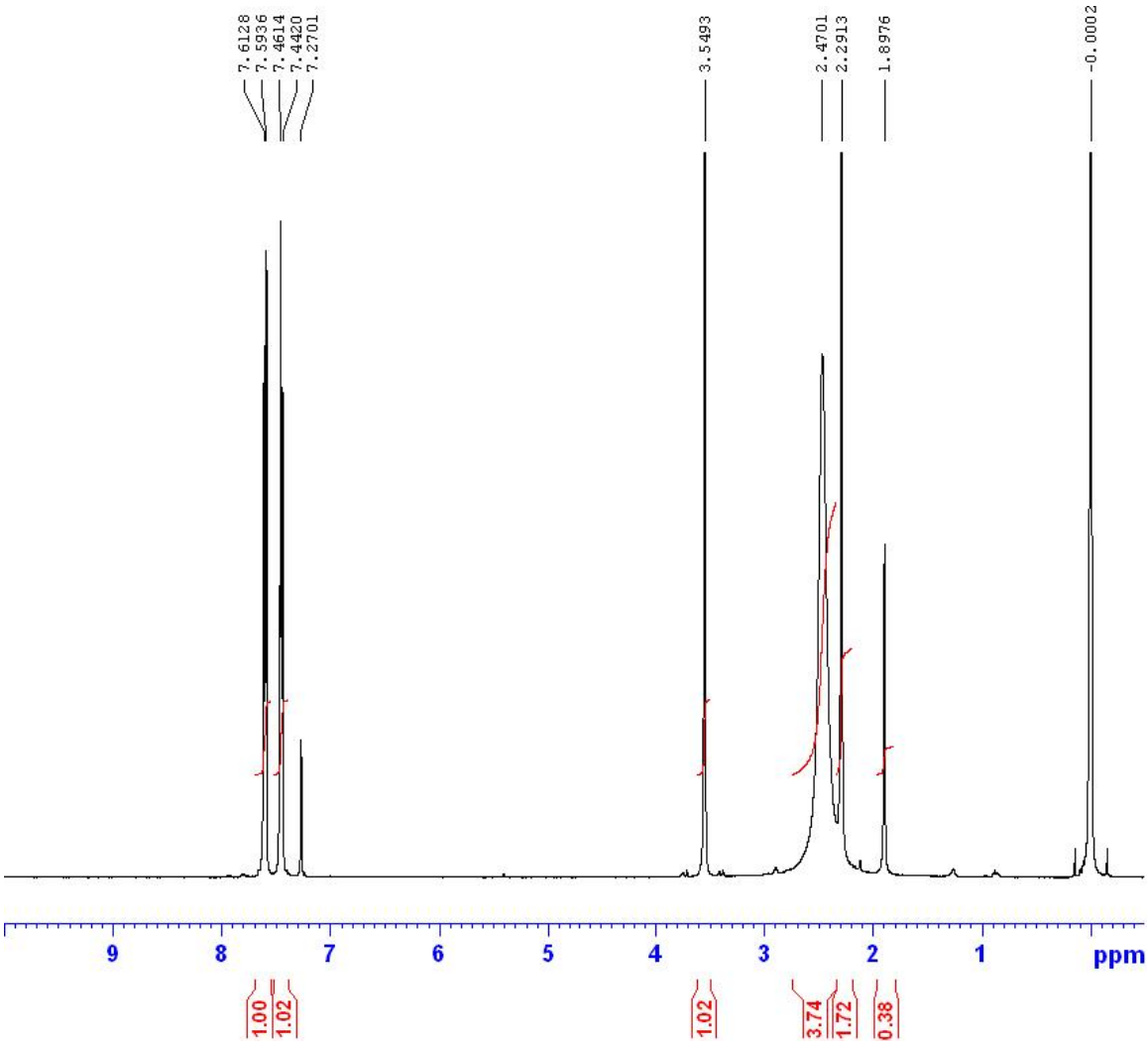

^{1}H-NMR Spectrum of 4-(4-Methylpiperazinomethyl)benzonitrile (**8**)

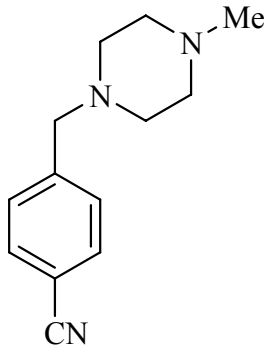

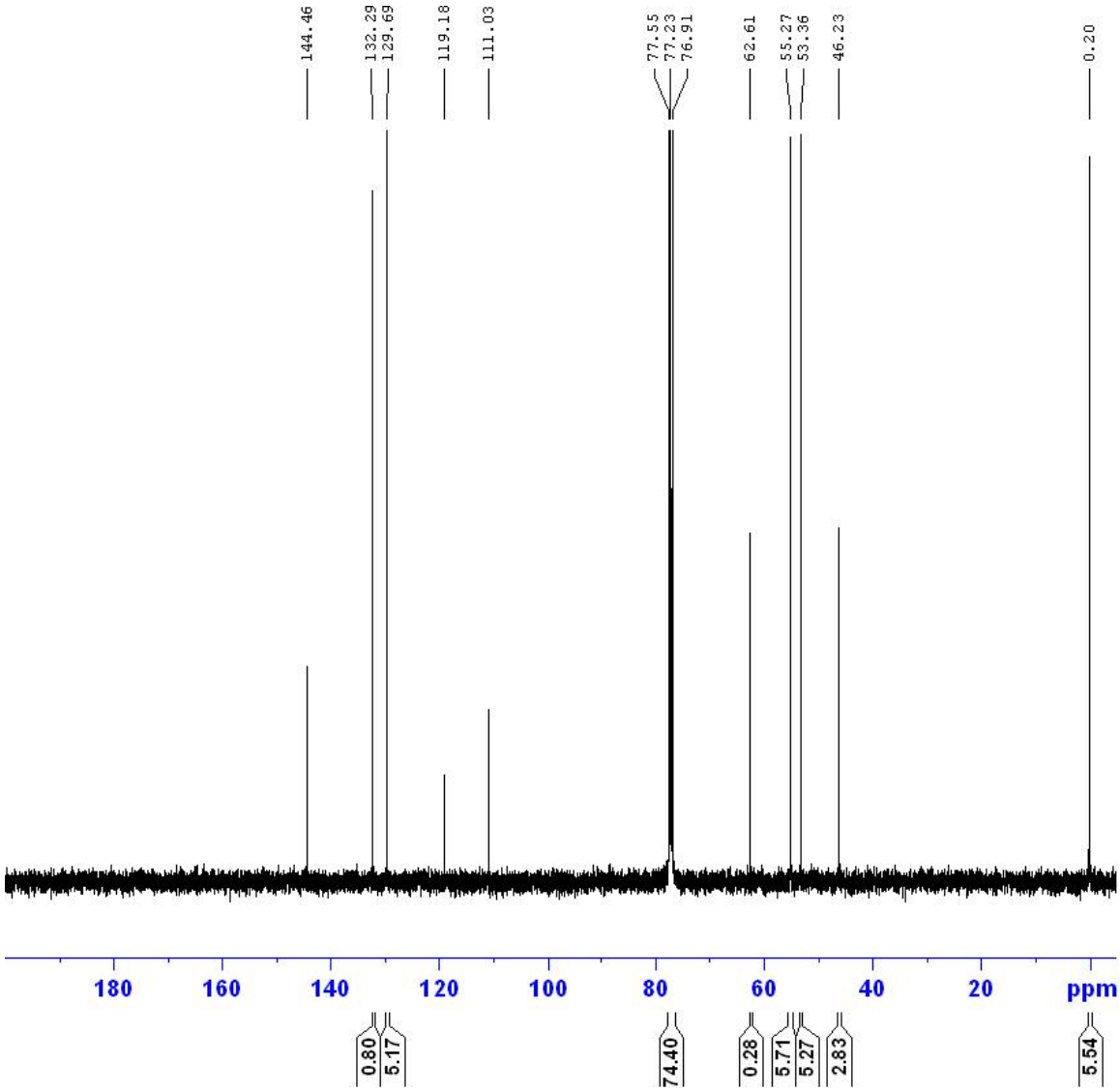

^{13}C-NMR Spectrum of 4-(4-Methylpiperazinomethyl)benzonitrile (**8**)

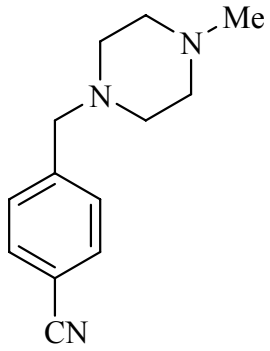

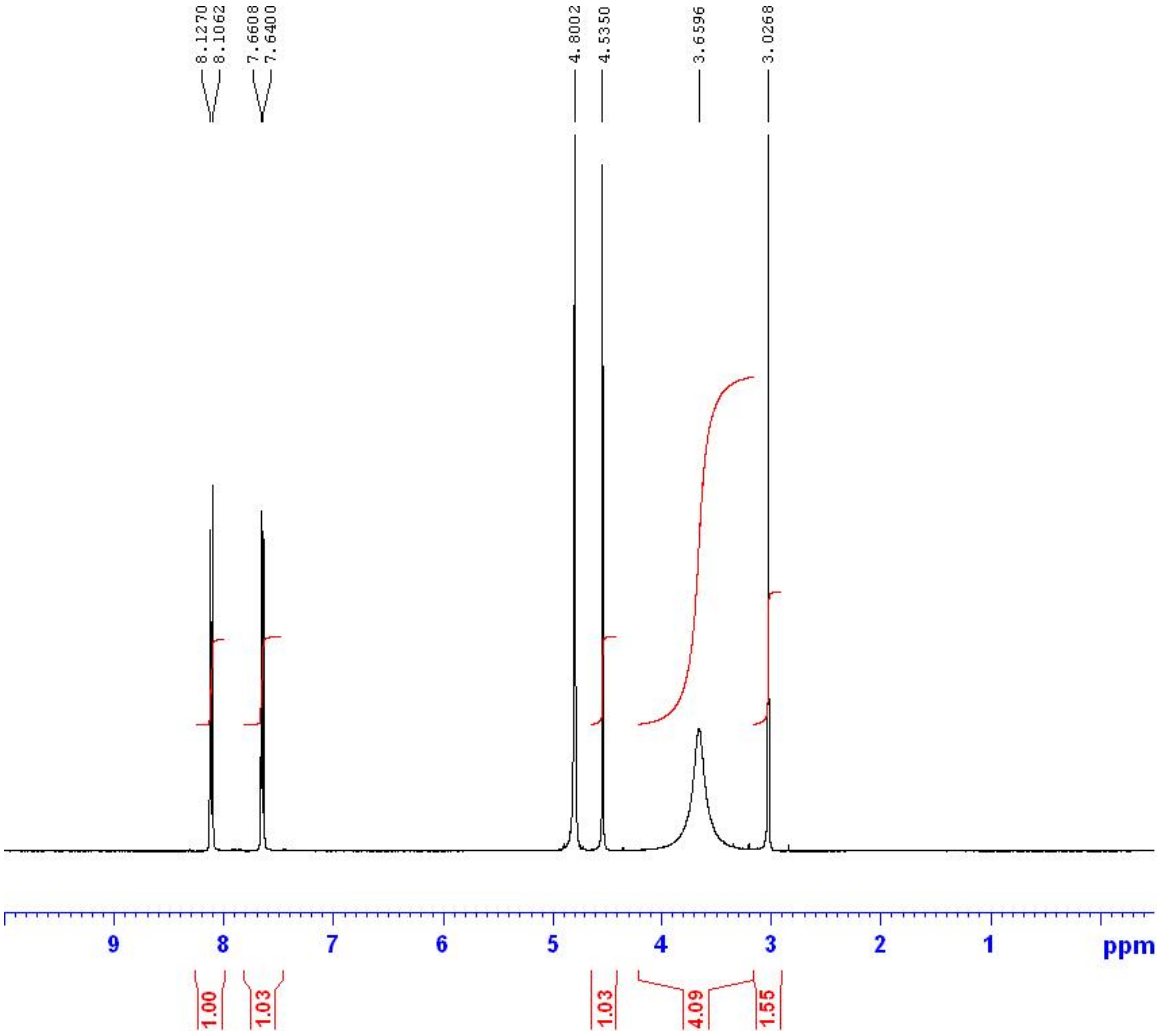

^{1}H-NMR Spectrum of 4-(4'-hydroxycarbonylbenzyl)-1-methylpiperazine (**9**, D_2O)

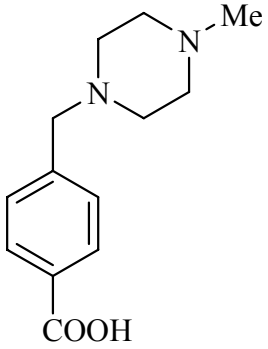

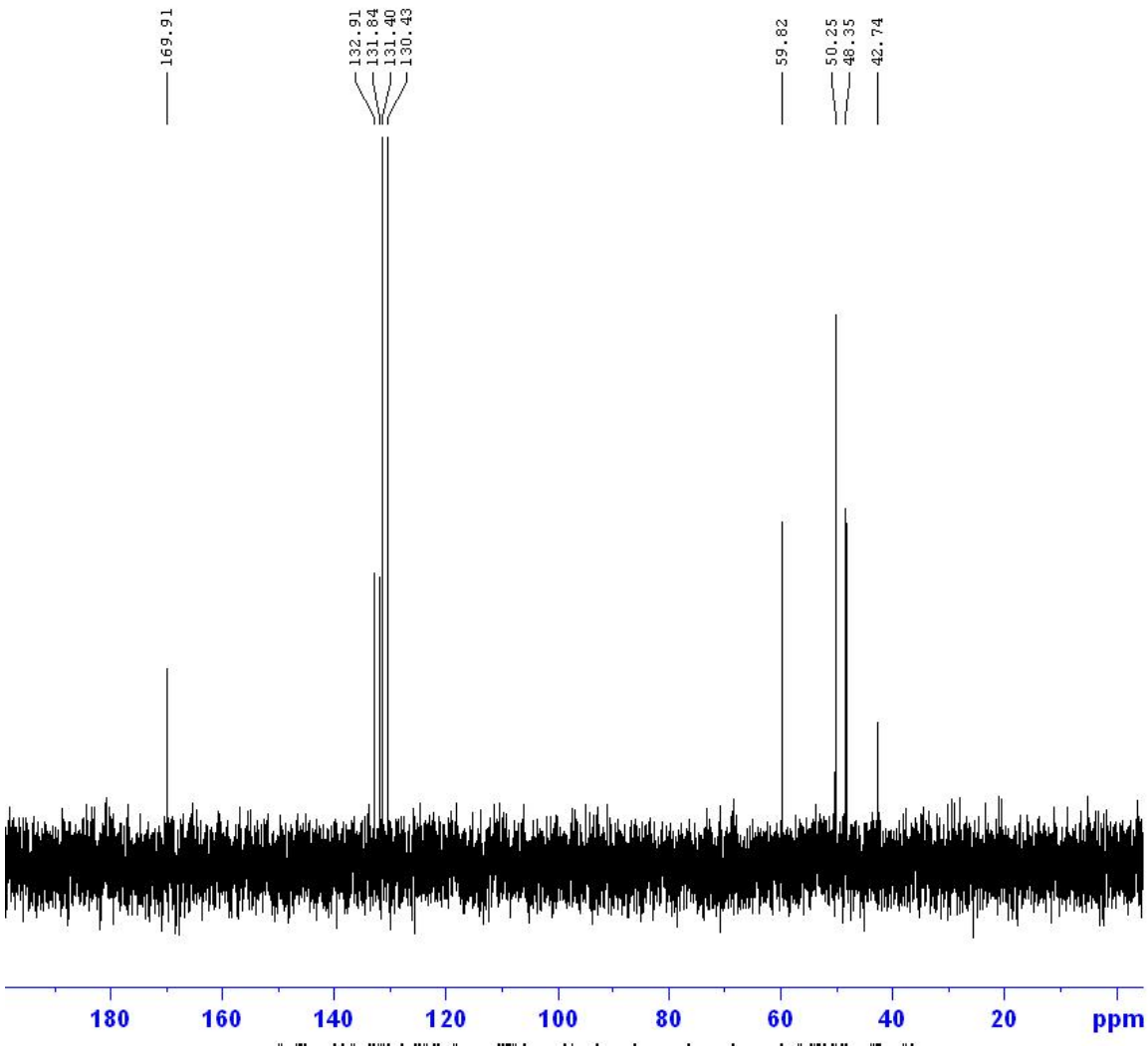

^{13}C-NMR Spectrum of 4-(4'-hydroxycarbonylbenzyl)-1-methylpiperazine (**9**, D_2O)

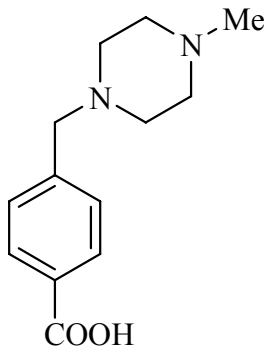

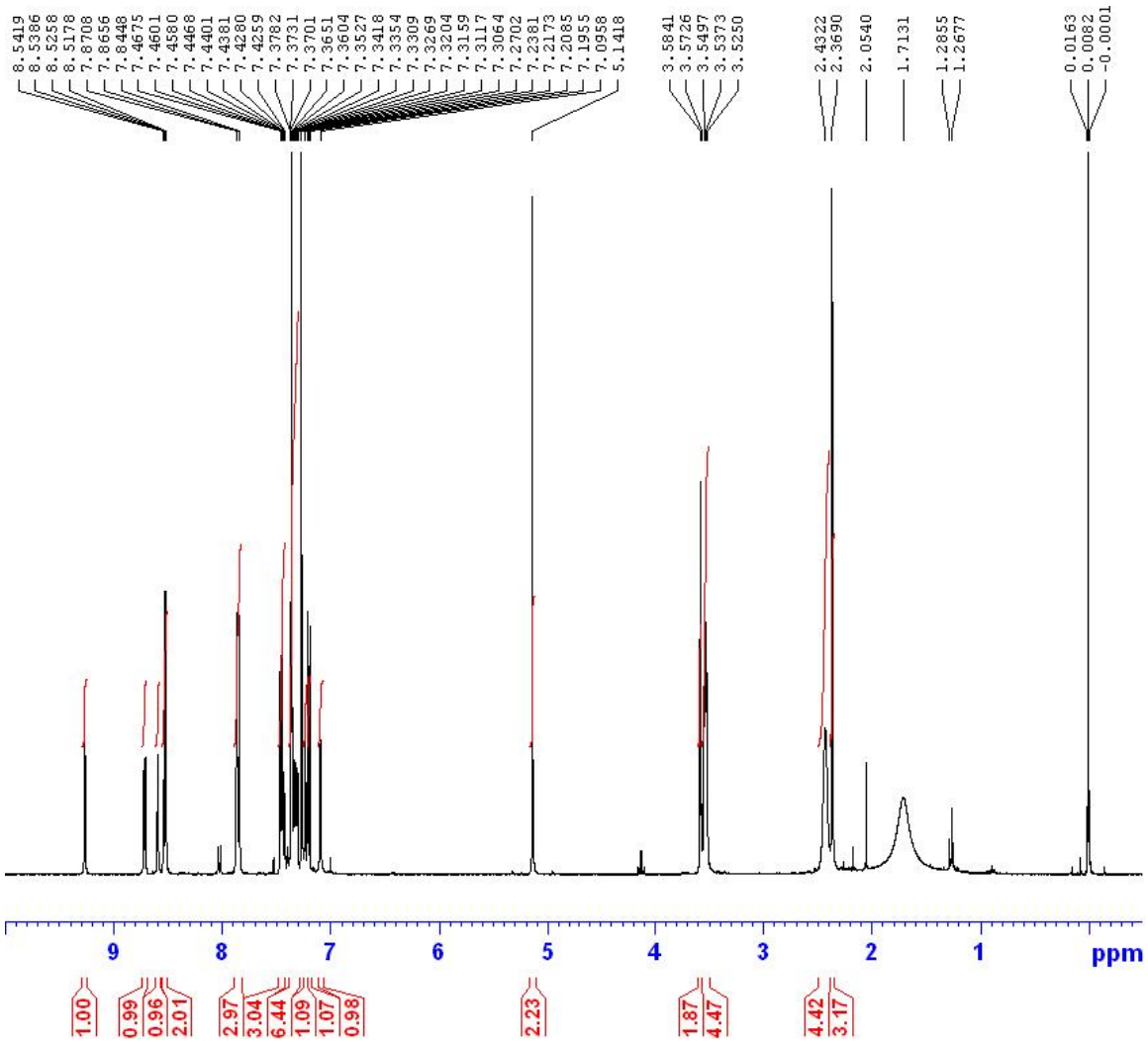

^{1}H-NMR Spectrum of 4-[(4-benzyloxycarbonyl-1-piperazinyl)methyl]-*N*-[4-methyl-3-[[4-(3-pyridyl)-2-pyrimidinyl]amino]phenylbenzamide (**10**)

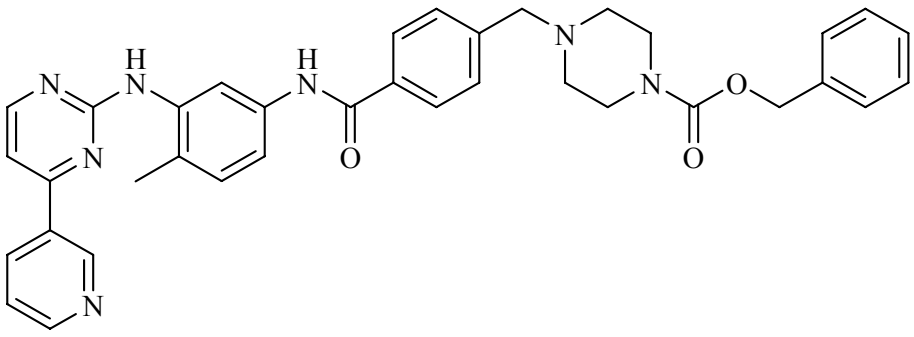

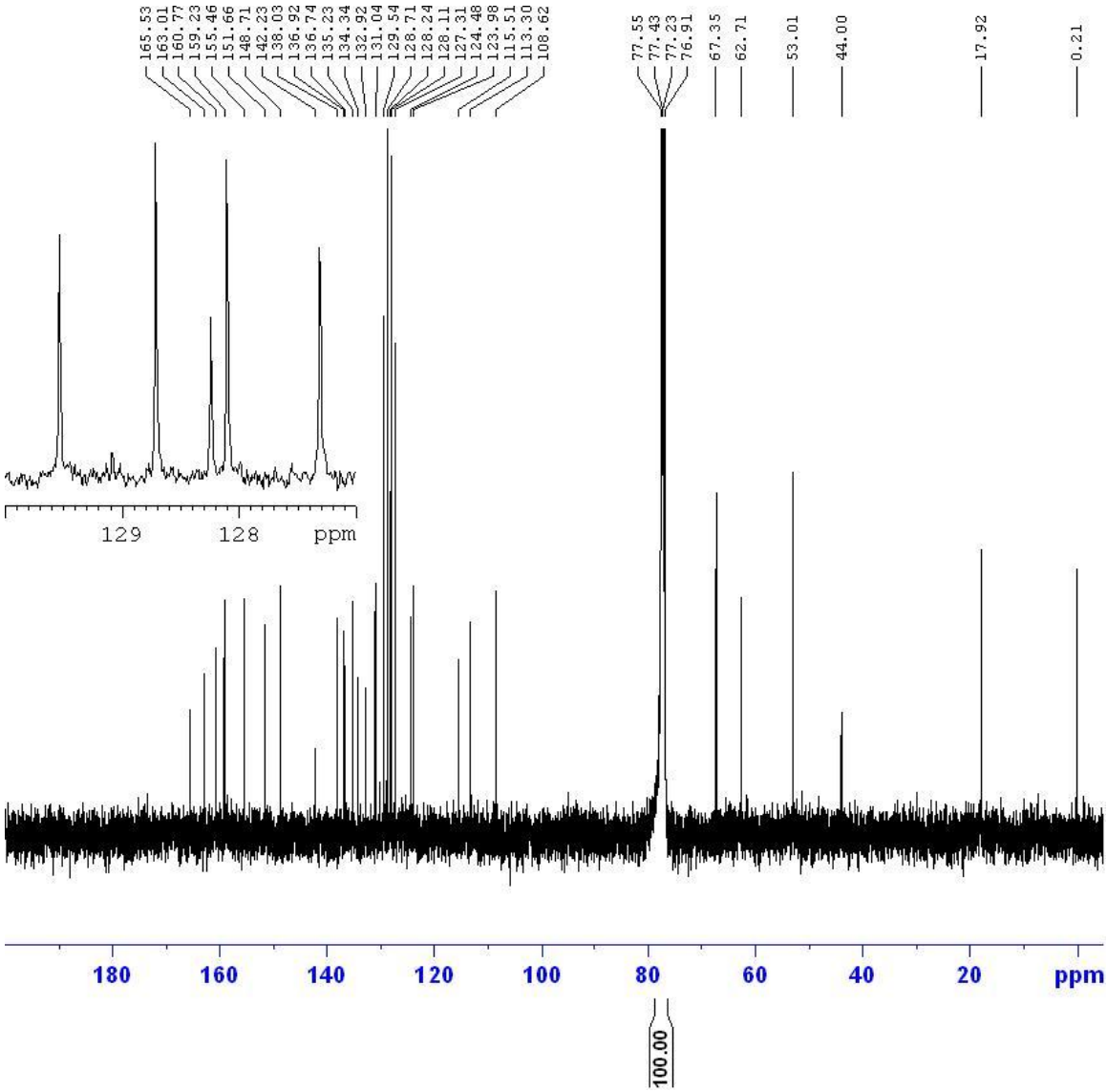

^{13}C-NMR Spectrum of 4-[(4-benzyloxycarbonyl-1-piperazinyl)methyl]-*N*-[4-methyl-3-[[4-(3-pyridyl)-2-pyrimidinyl]amino]phenylbenzamide (**10**)

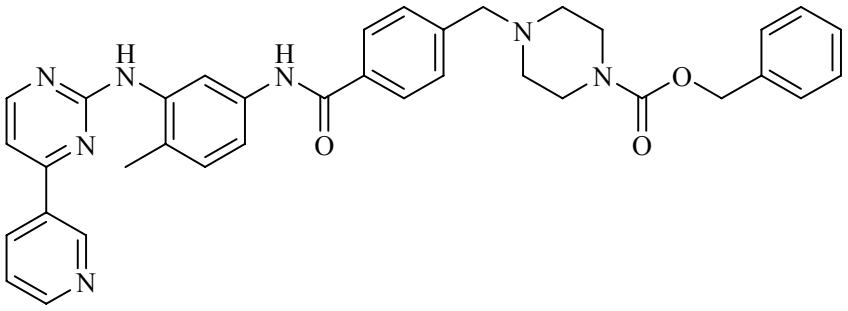

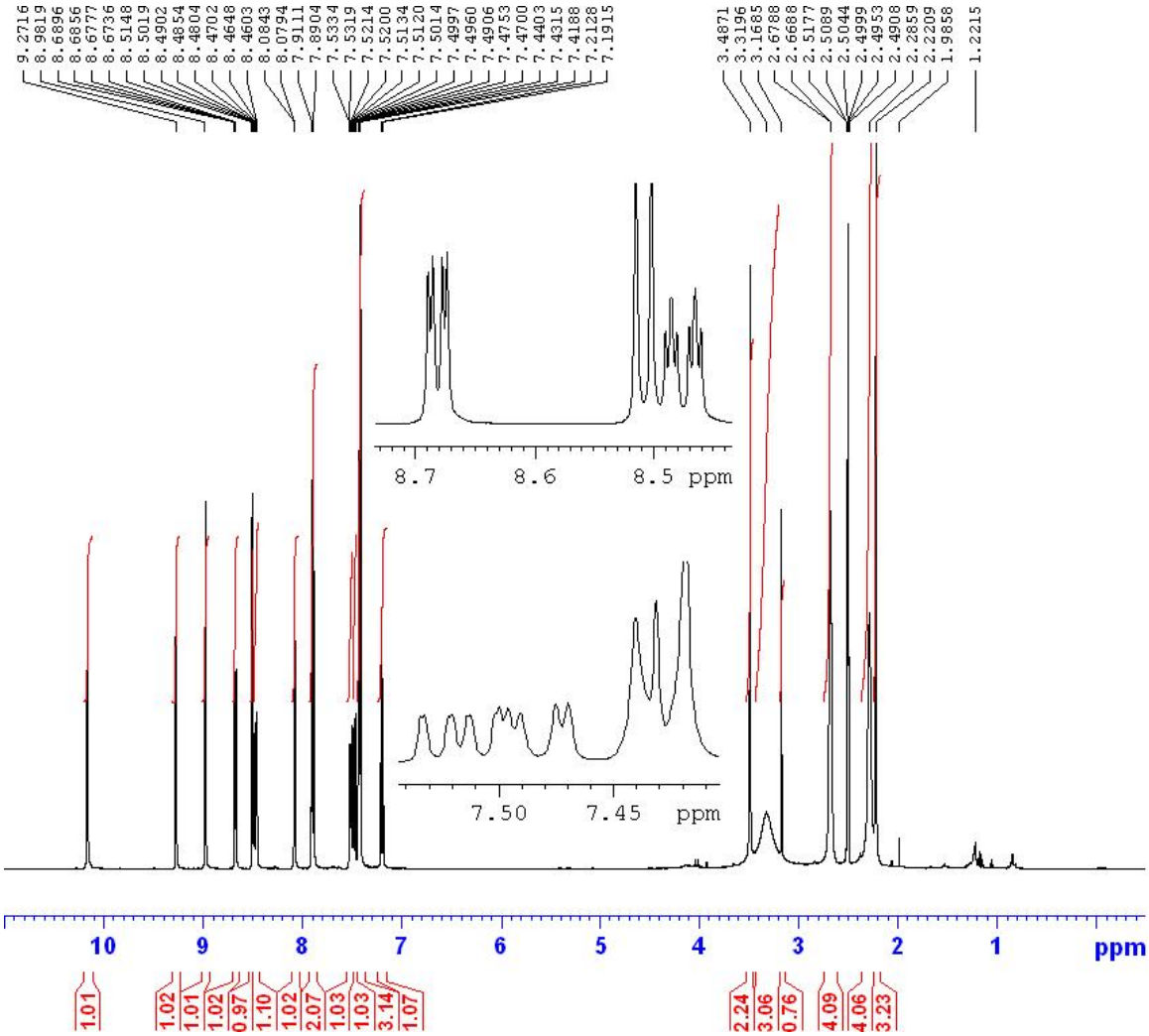

^{1}H-NMR Spectrum of 4-[(piperazinyl)methyl]-*N*-[4-methyl-3-[[4-(3-pyridyl)-2-pyrimidinyl]amino]phenylbenzamide (**2**, DMSO-d_6)

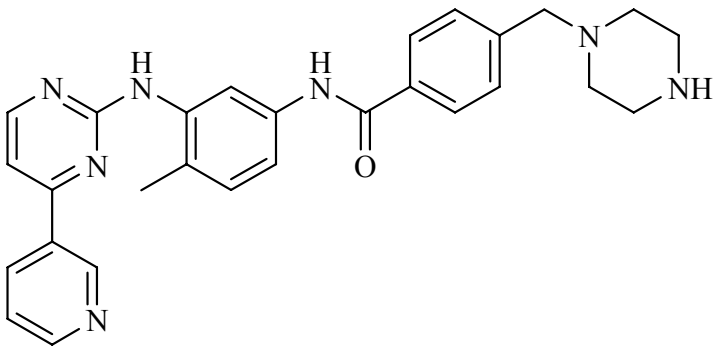

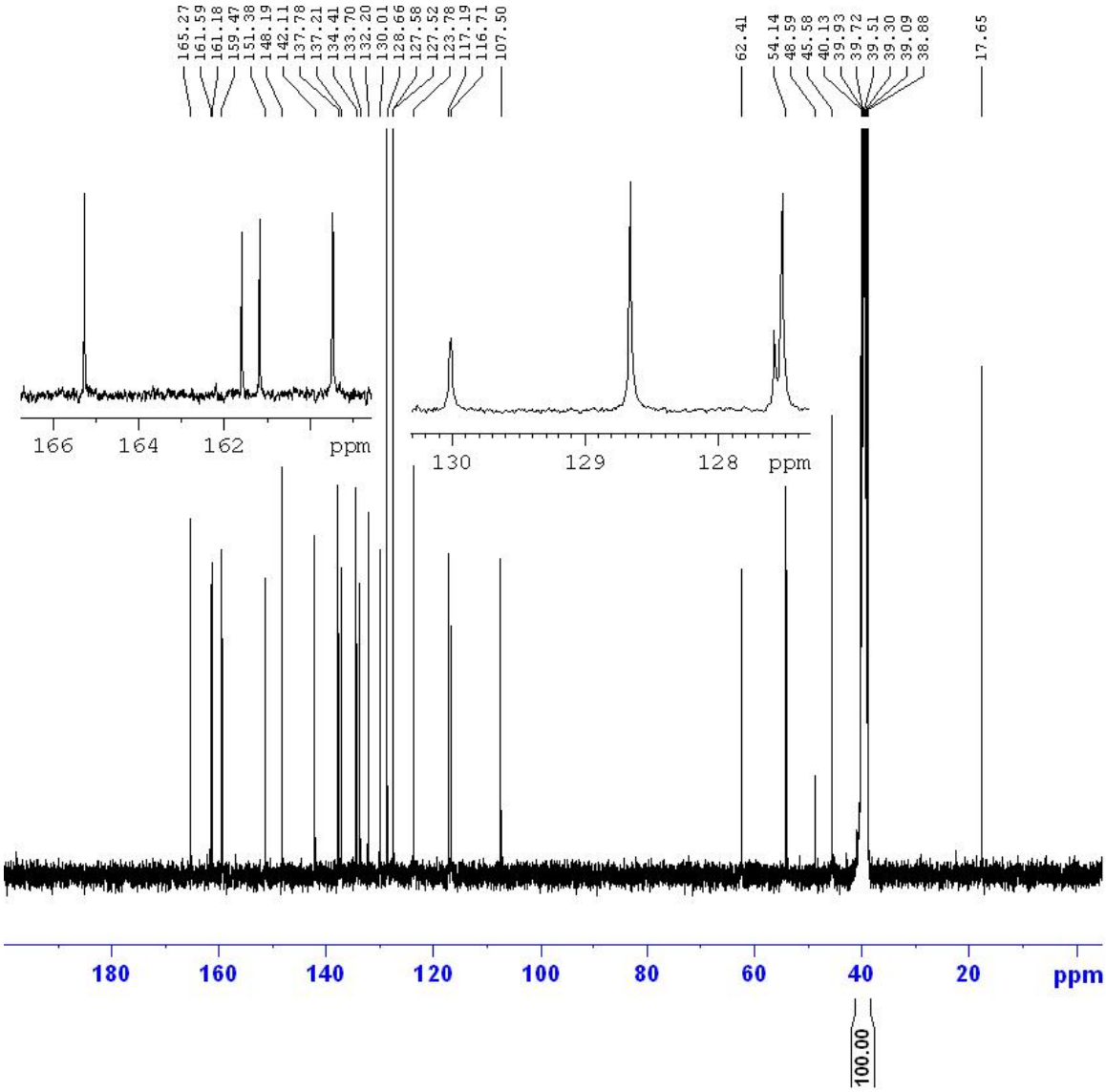

^{13}C-NMR Spectrum of 4-[(piperazinyl)methyl]-*N*-[4-methyl-3-[[4-(3-pyridyl)-2-pyrimidinyl]amino]phenylbenzamide (**2**, DMSO-d_6)

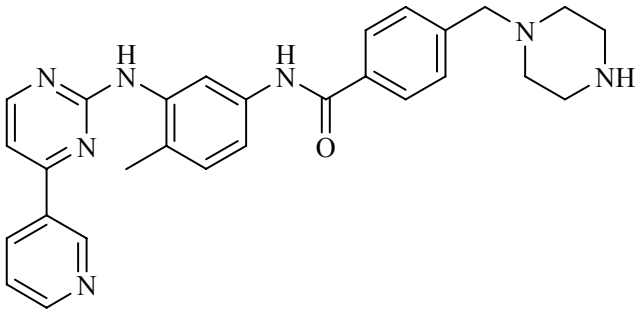

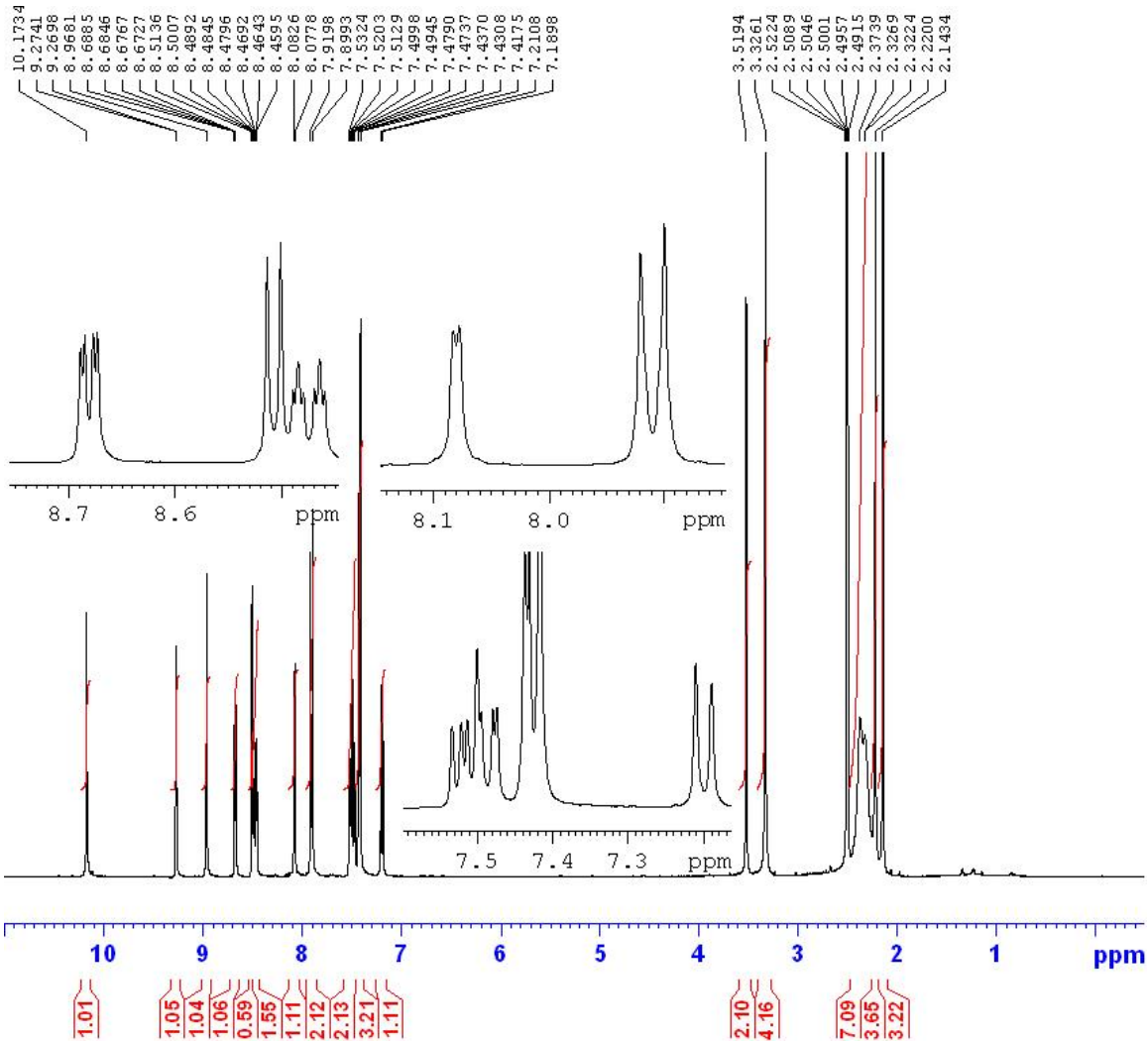

^{1}H-NMR Spectrum of [4-[(4-methyl-1-piperazinyl)methyl]-*N*-[4-methyl-3-[[4-(3-pyridyl)-2-pyrimidinyl]amino]phenyl]benzamide (Imatinib, **1**, DMSO-d_6)

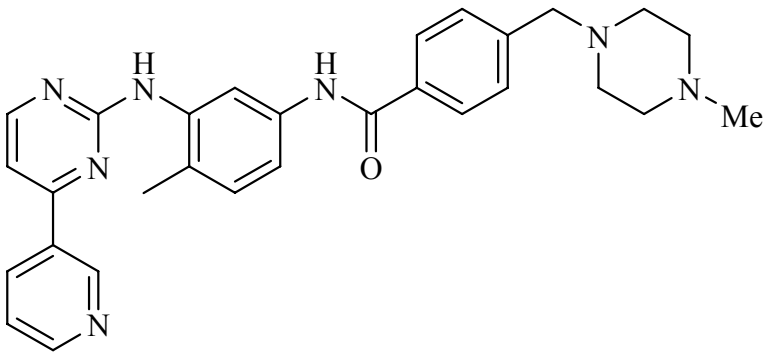

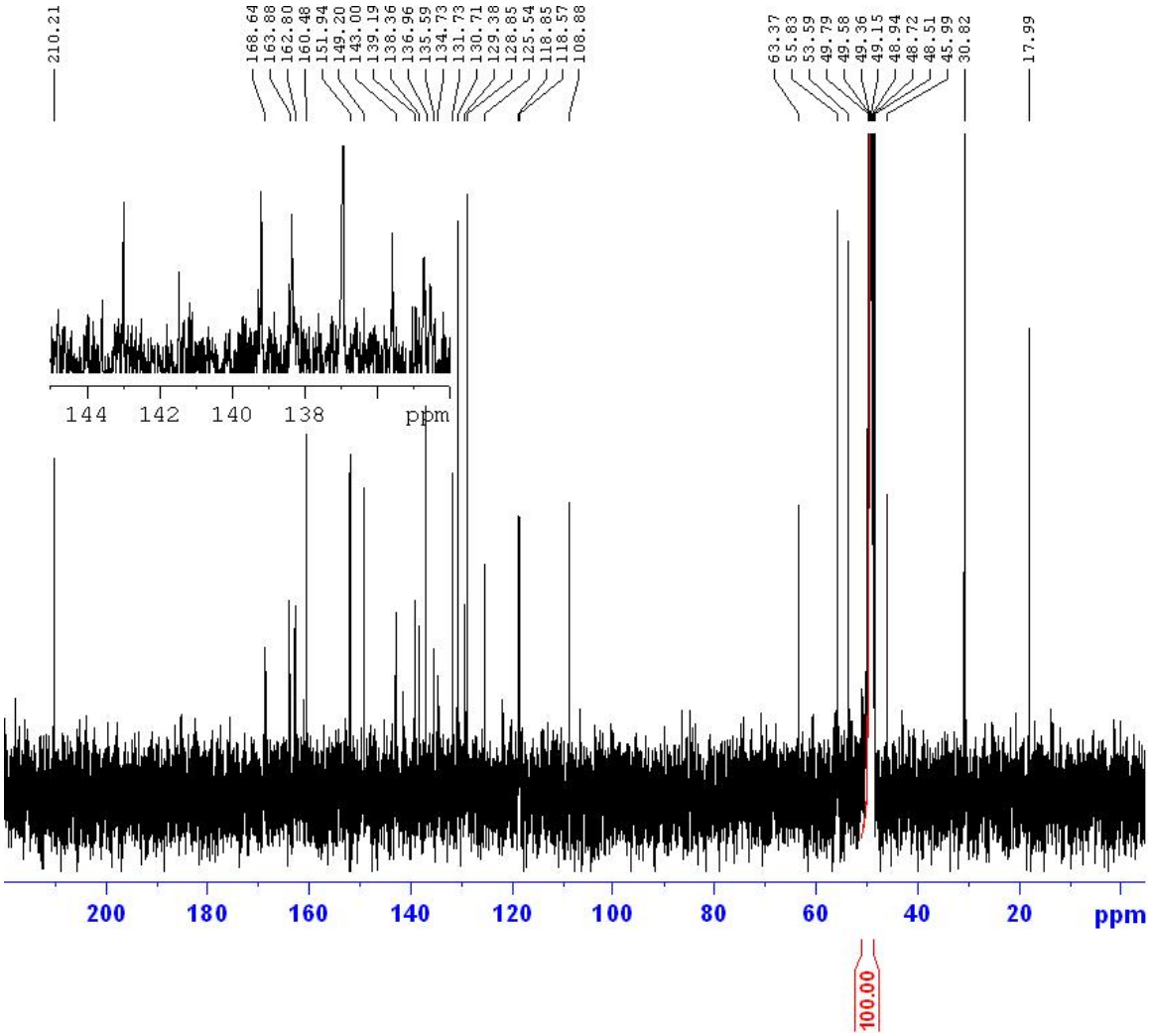

^{13}C-NMR Spectrum of [4-[(4-methyl-1-piperazinyl)methyl]-*N*-[4-methyl-3-[[4-(3-pyridyl)-2-pyrimidinyl]amino]phenyl]benzamide (Imatinib, **1**, DMSO-d_6)

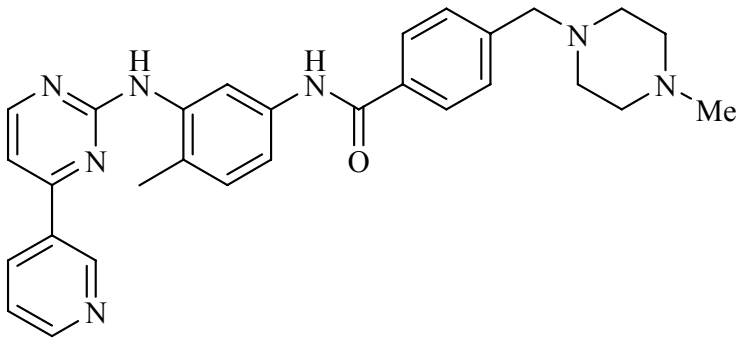

PART III

Title: Synthesis and PET studies of [^{11}C-cyano]letrozole (Femara®), an aromatase inhibitor drug.

Abstract

Introduction: Aromatase, a member of cytochrome P450 family, converts androgen into estrogen. Letrozole (1-[bis-(4-cyanophenyl)methyl]-1*H*-1,2,4-triazole, Femara®) is a high affinity aromatase inhibitor (K_i=11.5 nM) which has FDA approval for postmenopausal women with breast cancer treatment. Here we report the synthesis of carbon-11 labeled letrozole and the assessment of its utility as a radiotracer for brain aromatase in the baboon.

Methods: Letrozole and its precursor (4-[(4-bromophenyl)-1*H*-1,2,4-triazol-1-ylmethyl]benzonitrile) were prepared in two-step syntheses from 4-cyanobenzyl bromide and 4-bromobenzyl bromide, respectively. We introduced the [^{11}C]cyano group via the tetrakis(triphenylphosphine)palladium(0) catalyzed coupling of [^{11}C]cyanide with the bromo precursor. PET studies in the baboon brain were carried out to assess regional distribution and kinetics, reproducibility of repeated measures and saturability. We also measured free fraction of letrozole in the plasma, logD, and the [^{11}C-cyano]letrozole fraction in the arterial plasma.

Results: [^{11}C-cyano]letrozole was synthesized in 60 min with a radiochemical yield (RCY) of 79-80% with greater than 98% radiochemical purity and 4.16±2.21 Ci/μmol at the end of bombardment (n=4). PET studies in the baboon revealed initial rapid and high

uptake and initial rapid clearance followed by slow clearance of carbon-11 from the brain with no difference between brain regions. The brain kinetics was not affected by co-injection of unlabeled letrozole (0.1 mg/kg). The free fraction of letrozole in plasma was 48.9% and log D was 1.84.

Conclusion: [^{11}C-cyano]letrozole is unsuitable as a PET radiotracer for brain aromatase as revealed by the absence of retention in brain regions such as amygdale which are known to contain aromatase. However, it may be useful in measuring letrozole distribution and pharmacokinetics in brain and peripheral organs.

1. Introduction

The enzyme aromatase, a member of cytochrome P450 (CYP) protein superfamily, is the unique gene product of the CYP19 gene [136]. Aromatase regulates the last step of estrogen biosynthesis, aromatizing the A ring of androgens such as androstenedione and testosterone to estrone and estradiol, respectively (Figure 3-1).

Aromatase has become a target for controlling the generation and function of estrogen because its inhibition does not affect the biosynthesis of other steroids, such as glucocorticoids, mineralocorticoids, and androgens that share same pathway in the upstream of steroidogenesis.

Aromatase usually is expressed in gonadal tissues, such as the ovary [137]. Before menopause, the majority of estrogen was produced in gonadal tissue, but extragonadal estrogen is gaining more importance postmenopausal woman. Most of estrogen is synthesized in extragonadal tissues centrally and peripherally [138]. Peripheral estrogen

is generated in adipose cell [139], bone [140], placenta [141], and fetal liver [142]. The selective expression of aromatase in target tissue was controlled by tissue-specific promoters [143].

Aromatase is also expressed in brain tissues, viz., the preoptic nucleus and ventromedial nucleus in the hypothalamus, medial amygdala, and the bed nucleus of the stria terminalis where sexual preference of sexual behavior is determined especially in male [144, 145]. Rapid change of brain aromatase expression is observed in preoptic area after engaged in sexual behavior in quail [146]. Sexual behavior was suppressed by aromatase inhibitor (AI) in male mice, and it was stimulated by estrodiol in aromatase knockout mice [147]. As well as modulating sexual behavior, extragonadal estrogen acts as signal agent to mediate cell proliferation and growth both in central nervous system (CNS) regions and in peripheral regions. Estrogen stimulates an increase of the number of synapses in the hippocampus to regulate memory, cognition, and the plasticity of synapses, mechanisms of estrogen activity that were proved by treating animals with AIs [148, 149, 150, 151, 152]. Aromatase, estrogen receptors, and other steroidogenic enzymes were observed in hippocampus indicating that estrogen is locally synthesized in hippocampus, and a significant synaptic loss was observed in response to treatment of AI [149, 150]. Therefore, hippocampal estrogen maintained the plasticity of hippocampus. Aromatase knockout mice did not perform short term spatial memory test [152]. Another important role of estrogen is its neuroprotective role. Estrogen helps restore the density of synapses in the region of loss after injuries. Such increased estrogen activity in damaged brain areas was accompanied by extensive synaptic aromatase activity [153, 154, 155]. Many evidences also revealed that astrocytes are capable of expressing

aromatase after ischemic damage in the neuron and neuronal damage caused by stroke [153, 155, 156]. Treatment of AI slowed down recovery or expanded damaged region caused by ischemic and mechanical injury [153, 155]. Astrocytes derived from male culture are more susceptible to ischemic damage caused by oxygen-glucose deprivation than female astrocytes suggesting that female is more resistant to ischemic damage [157, 158].

AI are under investigation as treatment for breast cancer and also as scientific tools for studies of aromatase. They fall into two catagories: (1) steroidal AI's such as formestane and exemestane which bind irreversibly to the active site in aromatase [159] and (2) non-steroidal AI's such as aminogluthimide, fadrozole, anastrozole, letrozole, and vorozole whose binding mode is a competitive reversible one [159] (Figure 3-2). Anastrozole, letrozole and vorozole are more potent and more selective than aminogluthimide and fadrozole: that is, they inhibit the synthesis of estrogen, but do not interrupt the biosynthesis of other steroids such as glucocosteroids and mineralosteroids [160, 161, 162]. Among them, anastrozole, letrozole, and exemestane are considered as the new generation of FDA-approved AIs for treating breast cancer because of their potency and selectivity. Anastrozole, letrozole, and exemestane proved their selective blocking against aromatase up to 10 mg daily dose, up to 2.5 mg daily dose, and 25 mg daily dose, respectively [160, 161, 162]. Vorozole also demonstrated selectivity to estrogen, and no suppressive effect on corticosteroids generation up to 5 mg of daily dose [163]. However, despite this advantage, vorozole was not attempted further clinical studies because there was no critical improvement in the patient's overall response rate, and their survival rate, nor in the drug's efficacy compared with earlier drugs [164].

Among the AIs, only vorozole was developed as a PET radiotracer. Lidström and colleagues first synthesized [N-methyl-^{11}C]vorozole with [^{11}C]methyl iodide [165]. They checked the vorozole's inhibition constant and specificity using pig's organ tissue and human placental tissue. They also acquired in vivo PET images of torso of living female rhesus monkeys administered vorozole [165]. Scans of the brain of the animals revealed a high uptake of the drug in the amygdala region and hypothalamus [166]. Autoradiography of the brain of a male rat brain displayed specific binding in the medial amygdala, the bed nucleus of the stria terminalis, and the preoptic nucleus in hypothalamus [166]. The measured B_{max} of the rat's medial amygdala was 9.3±1.1 fmol/mg tissue [166]. They applied [^{11}C] vorozole to a male rat model of anabolic androgenic steroid abuse, and observed an increase in aromatase in the amygdala and the bed nucleus of the stria terminalis [167, 168]. This increase was mediated by androgen receptors [168]. Wang and colleagues also developed carbon-11 radiotracers for aromatase in human breast tumor cells based on NS-398, a dual inhibitor for aromatase and cyclooxygenase-2, and its derivatives [169].

Despite such recent progress in developing PET imaging agents for aromatase, none have yielded results suitable for applying them to PET studies. The brain study with [^{11}C]vorozole gave reliable results in the medial amygdala, but it did not produce reliable signal in the preoptic nucleus in hypothalamus of the rhesus monkeys [166]. Nonetheless, specific binding was noted in the autoradiography study with rats. Because aromatase has an important role in neuroprotection, neuroplasticity, reproduction behavior, and anabolic androgen steroid abuse, having sensitive radiotracers for PET would be invaluable for mapping brain aromatase in vivo. Among the three new selective AIs

including vorozole, we consider that letrozole might be a good candidate as an imaging agent because its drug properties are comparable to those of vorozole and the results of its clinical trials are better than those of vorozole. Moreover, letrozole can be labeled with [^{11}C]hydrogen cyanide by palladium catalyzed cyanide coupling reaction. The K_i value of letrozole and vorozole, respectively, was 11.5 nmol/l and 0.7 nmol/l on human placental aromatase [170, 171]. In vitro, letrozole and vorozole correspondingly are 200 times and 1029 times more potent for human placental aromatase than aminoglutethimide [171, 172]. However, letrozole is 10,000 times more potent in vivo than aminoglutethimide [172]. Because letrozole got good clinical result in human trial, it would be easily translated to human. Therefore, letrozole might be a better PET radiotracer for in vivo imaging.

Here we present our method of synthesizing [^{11}C-cyano]letrozole. We also synthesized its corresponding carbon-12 analogue and precursor by simple two-step reactions. While setting up the conditions for tetrakis(triphenylphosphine)palladium(0) catalyzed cyanide coupling, we also compared carbon-11 and carbon-12 cyanide chemistry in various solvents and amounts of palladium catalyst. We, then evaluated [^{11}C-cyano]letrozole as PET imaging agent for brain aromatase in vivo using one female baboon.

2. Material and Methods

2.1 General

All chemicals were purchased from Sigma-Aldrich Corp. (St. Louis, MO), and used directly without further chemical purification. ^{1}H-NMR and ^{13}C-NMR were obtained

from chloroform-*d* solution (unless specified) by Bruker Avance 400 MHz NMR spectrometer (400 MHz for ^{1}H and 100 MHz for ^{13}C) (Bruker Instruments Inc., Billerica, MA), and their peaks were measured in part per million downfield from tetramethylsilane. Melting point was measured using Fisher-Jones melting point apparatus (Fisher Scientific Co., Pittsburgh, PA). If necessary, Gas Chromatography (Agilent Technologies 6890N Network GC System, Santa Clara, CA) coupled with Mass spectroscopy (Agilent 5973 Network Mass Selective Detector) was used to identify the compound by molecular weight. Thin Layer Chromatography (TLC) method is used to monitor all organic reactions, and all reactions profiles were interpreted using Spectroline® Model ENF-240C 254 nm short wave UV lamp (Spectronics Corp., Westbury, NY). Especially, palladium catalyst mediated cyanide coupling reaction is monitored by high performance liquid chromatography (HPLC) on a Phenomenex Luna C18 (2) analytical column (250 mm×4.6 mm, 5 μm, Phenomenex Inc., Torrance, CA) with Knauer HPLC system (Sonntek Inc., Woodcliff Lake, NJ) equipped with model K-500 pump, a model 87 variable wavelength monitor (UV 254 nm), and a Hewlett-Packard 3390A integrator. TLC radioactivity was scanned by a Bioscan System 200 Imaging Scanner (Bioscan Inc., Washington DC).

2.2 Chemistry

*2.2.1 1-(4-cyanobenzyl)-1H-1,2,4-triazole (**1**) and 1-(4-bromobenzyl)-1H-1,2,4-triazole (**2**)*

Compounds **1** and **2** were prepared by an adaptation of the previous method [173]. A mixture solution of 4-cyanobenzyl bromide (1.00 mmol, 0.196 g) or 4-bromobenzyl

bromide (1.00 mmol, 0.250 g), potassium carbonate (1.50 mmol, 0.207 g), potassium iodide (0.059 mmol, 0.0098 g), and 1,2,4-triazole (1.50 mmol, 0.104 g) in acetone (12 ml) was refluxed overnight. Saturated sodium carbonate solution was added to the reaction mixture followed by extraction with ethyl acetate. The organic layers were dried by anhydrous magnesium sulfate, filtered, and evaporated. Column chromatography eluting with ethyl acetate afforded 0.146 g and 0.187 g of Compounds **1** and **2** (**1**, 0.146 g, 80%) and (**2**, 0.187 g, 79%). Both compounds were obtained as a white solid. mp 108-110^{o}C (lit: 77-79^{o}C [174], **1**), 83^{o}C (lit: 77-79^{o}C [175], **2**). GC-MS (**1**) Theoretical M^{+}: 184.07. Found M^{+}: 184. GC-MS (**2**) Theoretical M^{+}: 236.99. Found M^{+}: 237 and 239. NMR spectra of Compounds **1** and **2** were consistent with previous literatures [173, 175]. ^{1}H NMR (**1**): δ 5.46 (s, 2H), 7.35-7.37 (d, J=8.4 Hz, 2H), 7.64-7.67 (d, J=8.3 Hz, 2H), 8.01 (s, 1H), 8.26 (s, 1H), ^{13}C NMR (**1**): δ 152.37, 143.51, 140.01, 132.61, 128.24, 118.16, 112.20, 52.50. ^{1}H NMR (**2**): δ 5.30 (s, 2H), 7.12-7.15 (m, 2H), 7.48-7.51 (m, 2H), 7.97 (s, 1H), 8.08 (s, 1H). ^{13}C NMR (**2**): δ 152.12, 143.05, 133.62, 131.97, 129.46, 122.49, 52.57.

*2.2.2 4-[(4-bromophenyl)-1H-1,2,4-triazol-1-ylmethyl]benzonitrile (**3**)*

Compound **3** was prepared by an adaptation of the previous method [175]. To a slurry of potassium t-butoxide (30.241 mmol, 3.394 g) in 7 ml of anhydrous DMF at -55^{o}C was added 1-(4-bromobenzyl)-1*H*-[1,2,4]triazole (**2**, 5.040 mmol, 1.200 g) solution in 7 ml of anhydrous DMF drop by drop. A solution of 4-fluorobenzonitrile (7.560 mmol, 0.916 g) in 7 ml of DMF was added to the reaction mixture at -55^{o}C dropwise, and stirred for one hour. The reaction mixture was slowly heated to -30^{o}C and stirred for one hour.

The reaction mixture was quenched by 6 N HCl solution, and basified by saturated sodium bicarbonate solution. The aqueous solution was extracted with ethyl acetate. The organic solution was dried by anhydrous magnesium sulfate, filtered and evaporated. The residual DMF was further removed by high vacuum. The remaining residue was subjected to column chromatography (ethyl acetate:hexane=1:10, 1:5, 1:2, and then 2:1 co-solvent) to give Compound **3** (0.539 g, 32%) as a yellow solid. mp 98-99^{o}C. NMR spectrum was consistent with previous literature [175]. ^{1}H NMR: δ 6.90 (s, 1H), 7.12-7.14 (d, J=8.44 Hz, 2H), 7.29-7.31 (d, J=8.24 Hz, 2H), 7.50-7.52 (d, J=8.52 Hz, 2H), 7.64-7.66 (d, J=8.40 Hz, 2H), 8.03 (s, 1H), 8.21 (s, 1H). ^{13}C NMR: δ 153.06, 143.80, 142.97, 135.76, 132.99, 132.74, 130.26, 128.78, 123.89, 118.25, 113.06, 66.75. GC-MS (**3**) Theoretical M^{+}: 338.02. Found M^{+}: 338 and 340.

2.2.3 1-[Bis-(4-cyanophenyl)methyl]-1H-1,2,4-triazole (Letrozole)

Letrozole was prepared by an adaptation of previous method [173]. To a slurry solution of potassium t-butoxide (18 mmol, 2.0 g) in 30 ml of anhydrous DMF at room temperature was added **1** (2.0 mmol, 0.37 g) slowly in small portions, and stirred for 30 minutes at room temperature. To the resultant solution was added 4-fluorobenzonitrile (3.0 mmol, 0.37 g) slowly, and the mixture was stirred for one hour. The reaction mixture was diluted into methylene chloride/water (50 ml/50 ml), cooled to 0^{o}C, and neutralized with 6 N HCl. After separation of layers, the aqueous layer is extracted with methylene chloride (50 mL×2 times). The combined organic phases are washed with brine (50 ml), dried with anhydrous magnesium sulfate, and evaporated. The remaining crude mixture was purified by column chromatography eluting with hexane, ethyl

acetate:hexane=1:10, 1:5, 1:2, and then 2:1 co-solvent to afford crude product. The crude product was further purified by recrystallization from ethyl acetate-hexane co-solvent to give letrozole as a white powder after dryness *in vacuo* (0.27 g, 47%). mp 185-186^{o}C (lit: 182-185^{o}C [173]). NMR spectrum was consistent with previous literature [173]. ^{1}H NMR ($CDCl_3$): δ 6.81 (s, 1H), 7.28-7.30 (d, J=8.24 Hz, 4H), 7.70-7.72 (d, J=8.36 Hz, 4H), 8.07 (s, 1H), 8.09 (s, 1H). ^{13}C NMR: δ 153.06, 143.71, 141.75, 132.98, 128.94, 117.86, 113.37, 66.44.

*2.3 Model reaction for the synthesis of letrozole from 4-[(4-bromophenyl)-1H-1,2,4-triazol-1-ylmethyl]benzonitrile (**3**) and cyanide. (General)*

A mixture solution of potassium cyanide (8.85 μmol, 0.58 mg), 4-[(4-bromophenyl)-1*H*-1,2,4-triazol-1-ylmethyl]benzonitrile (**3**, 8.85 μmol, 3.0 mg), variable amounts of tetrakis(triphenylphosphine)palladium (0) (0.25 eq., 0.5 eq., or 0.75 eq.) and 4,7,13,16,21,24-hexaoxa-1,10-diazabicyclo[8,8,8]hexacosane (kryptofix222, 8.845 μmol, 3.33 mg) in 0.9 ml of solvent such as diglyme, toluene, DMSO, DMF, and THF was heated at 90^{o}C until reaction is complete (2 hours-3 days). The resulting solution was diluted with 3 ml of acetonitrile and injected into HPLC eluting with 37% acetonitrile:63% 0.1 M ammonium formate in Phenomenex® Luna C18 (2) analytical column equipped with model K-500 pump, a model 87 variable wavelength monitor (UV 254 nm), and Hewlett-Packard 3390A integrator. The yield of letrozole determined by HPLC were 67% from diglyme, and 21% from THF.

*2.3.1 4-(4'-bromobenzoyl)benzonitrile (**4**)*

Compound **4** was isolated from above general procedure as a major product under condition of 0.25 eq. of tetrakis(triphenylphosphine)palladium(0) in THF (59% yield), and 0.25 eq. and 0.50 eq. of the palladium catalyst in DMSO (37% yield) and DMF (71% yield). GC-MS Theoretical M^+ 284.98, 286.98. Found M^+: 285, 287. NMR spectrum was consistent with previous literature [176]. ^1H NMR ($CDCl_3$): δ 7.28 (s, 4H), 7.82-7.89 (dd, J=8.14 Hz, 12.84 Hz, 4H). ^{13}C NMR: δ 194.15, 140.98, 135.26, 132.49, 132.23, 131,69, 130.32, 128.84, 118.06, 116.18.

*2.3.2 4-(Phenyl-1H-1,2,4-triazol-1-ylmethyl)benzonitrile (**5**)*

Compound **5** was isolated as a side product (26% yield) when above general procedure was carried out in diglyme. GC-MS Theoretical M^+: 260.11. Found M^+: 260. ^1H NMR ($CDCl_3$): δ 6.80 (s, 1H), 7,20-7.24 (m, 4H), 7.43-7.45 (m, 3H), 7.69-7.70 (d, 2H), 7.99 (s, 1H), 8.07 (s, 1H). ^{13}C NMR: δ 152.92, 143.64, 136.65, 132.67, 129.40, 129.37, 128.56, 128.53, 118.38, 112.79, 67.29.

*2.3.3 4,4'-dicyanobenzophenone (**6**)*

Compound **6** was isolated as a major product (17% yield) when the above procedure was carried out in DMSO or DMF. GC-MS Theoretical M^+: 232.06 Found M^+: 232. NMR spectrum was consistent with previous literature [177]. ^1H NMR ($CDCl_3$): δ 7.82-7.89 (dd, J=18.7 Hz, 7.80 Hz, 8H). ^{13}C NMR: δ 193.64, 140.00, 132.70, 130.47, 117.88, 116.85.

2.4 Radiolabeling

[^{11}C-cyano]letrozole was prepared by palladium mediated cyanide coupling reaction modifying the method published by Andersson et. al. in 1994 [178]. Hydrogen [^{11}C]cyanide was produced by known procedure [4]. Carbon-11 was generated by proton bombardment with aluminum target containing trace of oxygen in nitrogen, and delivered to home-made [^{11}C]hydrogen cyanide production system as [^{11}C]carbon dioxide. [^{11}C]Carbon dioxide was reduced to [^{11}C]methane by hydrogen with a nickel catalyst at 390^{o}C for 5 minutes. [^{11}C]Methane was passed together with ammonia from nickel chamber, and passed through platinum furnace at 920^{o}C to convert into hydrogen [^{11}C]cyanide according to the original procedure [4]. Hydrogen [^{11}C]cyanide transferred into long neck V-shaped vessel containing 1.0 mg of **3** and 0.68 mg of tetrakis(triphenylphosphine)palladium(0) in 0.30 ml of dimethyl sulfoxide. When carbon-11 radioactivity peaked in the reaction vessel as determined by NaI detector, the reaction vessel was sealed, and heated at 110^{o}C for 5 minutes in an oil bath. The reaction mixture was diluted with 1 ml of water, and delivered to C18 Sep-Pak® (Waters Corp., Milford, MA) had been pretreated with methanol and water. The product was eluted with 5 ml of ether and removed by argon blowing in warm water bath for 3 minutes, and diluted with 1 ml of HPLC solvent before injection into HPLC system. The reaction mixture was eluted with 37% acetonitrile:63% 0.1 M ammonium formate co-solvent at a flow rate of 4.0 ml/min on a Phenomenex Luna C18 (2) semi-preparative column (250 mm×10 mm, 5 μm) with UV (254 nm) and radioactivity detector. [^{11}C-cyano]letrozole was eluted, and collected around 17.0-17.5 min. After [^{11}C-cyano]letrozole elusion, the system was eluted with 60% acetonitrile:40% 0.1 M ammonium formate to come out all

of side products with long retention time including bromo-precursor. The collected product solution was transferred to a rotary evaporator, and evaporated with acetonitrile until dryness. The residue dissolved in 4 ml of 5% ethyl alcohol solution in saline was transferred to sterile vial after passing through a 0.22 μm Millipore® filter (Millipore Corp., Billerica, MA) for PET study. Synthesis time was 60 minutes. Radiochemical yield (RCY) was 79-80% based on total hydrogen [^{11}C]cyanide activity determined by HPLC quality control (See Sec. 2.4). The specific activity was 4.16±2.21 Ci/μmol at the end of bombardment (n=4), and it was determined as the ratio of the total carbon-11 eluted with the product peak to the mass of letrozole determined by the area under the HPLC peak from a standard curve. HPLC profiles were shown in Figure 3-4.

2.5 Quality control and RCY determination of collected [^{11}C-cyano]letrozole

Both analytical HPLC system and TLC were used to determine the radiochemical purity of purified [^{11}C-cyano]letrozole. Quality control was conducted according to known method described in previous literature [179]. An aliquot of [^{11}C]product (10 μl) was injected into HPLC system equipped with UV and radioactivity detectors eluting with acetonitrile:0.1 M ammonium formate=1:1 co-solvent at a flow rate of 1.0 ml/min. The retention time was 10.82±1.5 min, and the radiochemical purity was >98%. When product aliquot (20 μl) was co-injected with unlabeled letrozole standard solution (5 μl), two compounds were recorded at the same time in UV detector and NaI radioactivity detector (Retention time: 10.82±1.5 min). Radiochemical purity was also checked by TLC co-spotted with unlabeled letrozole standard solution eluting with ethyl acetate as a developing solvent on Macherey-Nagel Polygram Sil G/UV254 plastic back TLC plate

with detection by UV detector. Radiochemical purity determined by TLC was also over >98% (n=4, R_f=0.42). The radioactivity was counted by Bioscan System 200 Imaging Scanner (Bioscan Inc., Washington DC). UV spot was confirmed by 254 nm short-wave UV lamp.

The RCY was determined by analytical HPLC comparing the amount of carbon-11 in the product peak relative to the amount of carbon-11 in the crude reaction mixture that was applied to the C18 Sep-Pak®.

2.6 Determination of log D of [^{11}C-cyano]letrozole.

The log D of [^{11}C-cyano]letrozole were measured by the method as described previously [179] (see Sec 2.5 in PART II). An aliquot (50 μl) of [^{11}C-cyano]letrozole was used, and six samples from octanol part (0.1 ml) and six samples from pH7.4 buffer solution part (1.0 ml) were prepared by same method. Log D was determined by the equation shown previously (see Sec 2.5 in PART II).

2.7 PET studies of [^{11}C-cyano]letrozole in baboon

Baboon study was approved by the Brookhaven National Laboratory Institutional Animal Care and Use Committee. A female baboon (Papio anubis) was prepared and anesthetized as described in the same procedure in PART II and previous literature [125] (see Sec. 2.6 in PART II). Two PET studies were performed one month apart with same baboon to assess the reproducibility and the effect of aromatase inhibition by letrozole. Before the [^{11}C-cyano]letrozole injection, transmission scan was conducted with ^{68}Ge rotating rod source. [^{11}C-cyano]letrozole was administered twice intravenously two

hours apart during each study. In first study, there was not intervention and in the second PET study, free letrozole (2 mg, 0.1 mg/kg) dissolved in 8% ethanol in water (10 ml) was co-injected with [^{11}C-cyano]letrozole. Injected doses of [^{11}C-cyano]letrozole ranged 2.6-4.2 mCi (n=4), and specific activity was 4.16±2.21 Ci/μmol at the end of bombardment (n=4). All studies were performed for 90 minutes with a high-resolution PET (Siemens HR+; 63 slices; 4.5×4.5×4.5 mm at the center of the field of view) in 3D mode with the following time frame (1×10 sec, 12×5 sec, 1×20 sec, 1×30 sec, 8×60 sec, 4×300 sec, and 8×600 sec). Arterial blood samples were collected and analyzed by same method described in PART II (see Sec. 2.6 in PART II).

2.8 HPLC determination of [^{11}C-cyano]letrozole fraction in blood plasma

The fraction of parent compound in plasma was determined according to the procedure described in PART II and previous literature [179] (see Sec. 2.7 in PART II). Plasma samples obtained at 1, 5, 10, 30, 60, and 90 minutes were performed by same treatment described in PART II. After the supernatant and precipitant were separated, and counted, the sample from supernatant was injected into HPLC system on a Phenomenex® Spherex C18 analytical column eluting with 35% acetonitrile:65% 50 mM ammonium formate co-solvent at a flow rate of 1.0 ml/min with UV detection. The retention time of [^{11}C-cyano]letrozole was 11 minute. The percent of [^{11}C-cyano]letrozole was obtained as the ratio of [^{11}C-cyano]letrozole isolated from HPLC to the carbon-11 in the supernatant.

2.9 Plasma protein binding (PPB) of [^{11}C-cyano]letrozole

The free fraction of [^{11}C-cyano]letrozole in plasma was obtained by the procedure described previously in PART II [179] (see Sec. 2.8 in PART II). An aliquot of [^{11}C]product (10 μl) was treated by the same method to prepare samples of total activity and activity of unbound sample. PPB was derived by following equation. % unbound = $A_{unbound} \times 100/A_T$, where $A_T = A_{bound} + A_{unbound}$.

2.10 Image and data analysis

All frames were summed over 90 minutes of scanning time and planes were summed in groups of two to select region of interest (ROI) on the brain. ROI's (cingular gyrus, striatum, thalamus, and amygdala) were chosen in the summed image, and then projected on to the dynamic frames to obtain time-activity curves (TAC's). The radioactivity (nCi/cc) was converted to percent injected dose per cc (%dose/cc) by dividing by the injected dose and multiplying by 100. Baseline time activity curves were compared to the repeated baseline and to the letrozole pretreatment scans for the two studies.

3 Results and discussion

3.1 Chemistry and Carbon-11 Labeling

Letrozole and its bromo-precursor (4-(4-bromophenyl)-1*H*-1,2,4-triazol-1-ylmethyl)benzonitrile, **3**) were prepared by the scheme shown in Scheme 3-1. Those two compounds were synthesized by two steps: triazole alkylation followed by nucleophilic

aromatic substitution reaction after carbanion generation. This was a modification of the patent and literature procedure described by Wood *et. al.* and Lang *et. al*. [173, 175].

Though this procedure was worked well for the synthesis of letrozole, the carbanion of **2** generated by treatment of potassium tert-butoxide was unstable at the temperature over 0^{o}C. After optimization of base amount and temperature, we could generate corresponding carbanion of **2** by treatment with 6 eq. of potassium tert-butoxide at -55^{o}C, and carrying out the reaction at -55^{o}C and -30^{o}C for one hour subsequently after the addition of 4-fluorobenzonitrile.

Cyanide labeling by transition metal catalyzed nucleophilic aromatic substitution was reported in several literatures. There are several examples of [^{11}C]cyanide labeling was been accomplished in the presence of tetrakis(triphenylphosphine)palladium(0), aryl tricarbonylchromium complex, or both catalysts [178, 180]. It has also been accomplished using a copper catalyst using the Rosenmund-von Brown reaction. [181] Sandell *et. al.* prepared [^{11}C]NAD-299 by labeling with [^{11}C]cyanide using Tris(dibenzylideneacetone)-dipalladium(0) ([$Pd_2(dba)_3$]), 1,1'-bis(diphenylphosphino)ferrocene (dppf), and N-methyl-2-pyrrolidinone (NMP). [182] We used [^{11}C]cyanide labeling method using tetrakis(triphenylphosphine)palladium(0) because this method had been shown to provide the best results with bromo- and iodo-substrates. [178] We attempted to optimize the conditions for the couping reaction with carbon-12 potassium cyanide, kryptofix222, and tetrakis(triphenylphosphine) palladium(0) as a model reaction shown in Scheme 3-2 before radiolabeling with [^{11}C]hydrogen cyanide.

The conditions described in scheme A, B, and C were tried. Letrozole was obtained as a major product in scheme A and B with THF as a solvent. However, scheme C, with a low amount of palladium catalyst did not work and ketone derivative (**4**) was generated as a major product instead. On the other hand, all ranges of palladium catalyst in diglyme produced letrozole and debrominated product (**5**) were produced in all range of palladium catalyst in diglyme as major and minor products respectively. When lower amount of palladium catalyst than scheme C was used in diglyme, small amount of letrozole was obtained. Most of substrate was unconverted up to three days (Data not shown). In DMF and DMSO, cyanide coupling product (**6**) from ketone derivative was observed at high amount of palladium catalyst along with letrozole as a minor product. Like in THF, cyanide coupling was not observed at low amount of tetrakis(triphenylphosphine) palladium(0) in DMF and DMSO. Only ketone derivative (**4**) was obtained as a major product. From the results, we speculated that each solvent might have its own threshold amount of catalyst to drive cyanide coupling.

Though the model reactions predicted that 0.25 eq. of palladium catalyst would not be effective and that diglyme would be best solvent for the reaction, when cyanide labeling was attempted with no-carrier-added hydrogen [^{11}C]cyanide, the use of 0.25 eq. of catalyst was sufficient and DMSO gave the best yield. The discrepancy between the model reaction and the carbon-11 labeling reaction probably related to the importance of the ratio of cyanide to catalyst. Because no-carrier-added [^{11}C]cyanide was significantly less than the amount of cyanide used in model reaction, 0.25 eq. of catalyst might be enough amount to give [^{11}C-cyano]letrozole in the labeling reaction.

As described in previous literature [178], [^{11}C]cyanide could be trapped in substrate and tetrakis(triphenylphospine)palladium(0) mixture solution at room temperature without any base, ammonia, hydrogen and other carrier gas did not interfere with reaction system. [^{11}C-cyano]letrozole was synthesized in DMSO at 110^{o}C for 5 minutes after which the crude reaction mixture was passed through C18 Sep-Pak® solid extraction column to remove palladium catalyst prior to HPLC injection. The resultant RCY was 79-80%. Total synthetic time was 60 minutes from EOB. The HPLC profile was shown in Figure 3-3. Most of carbon-11 species was [^{11}C-cyano]letrozole (R_t=17.04 min). A UV peak of UV sensitive letrozole (R_t=16.90 min) was also observed.

Specific activity was 4.16±2.21 Ci/μmol at the end of bombardment (n=4). Log D derived from equilibrium constant between octanol and pH 7.3 phosphate buffer solution was 1.84.

3.2 Evaluation of [^{11}C-cyano]letrozole with PET image in the baboon brain

[^{11}C-cyano]Letrozole was evaluated with reproducibility of repeated studies of the same day and for specificity in the anesthetized female baboon. In reproducibility study, two consecutive baseline scans were conducted two hours apart after injection of [^{11}C-cyano]letrozole. In specificity study, co-administration with [^{11}C-cyano]letrozole and unlabeled letrozole (0.1 mg/kg, [183, 184]) was performed after baseline scan was finished. In both sets of scans, TAC's for [^{11}C-cyano]letrozole in the arterial plasma were measured.

The TAC's of plasma from PET measures of reproducibility and binding specificity were compared each other in Figure 3-4(a) and 3-4(b). In both studies the peak time was slightly delayed and the integral over the time course of the study was slightly elevated. The effect was small, however and may relate to a different physiological state of the anaesthetized animal or slight differences in injection rate. The unbound fraction of [^{11}C-cyano]letrozole in plasma was 48.9% and the fraction of carbon-11 in the plasma in the chemical form of [^{11}C-cyano]letrozole was very high (99.2±0.3%, 99.0±0.3%, 98.2±0.3%. 96.9±1.1%, and 95.6±2.6% at 5, 10, 30, 60, and 90 minutes (n=4), respectively). Slow metabolism is consistent with a prior study on letrozole pharmacokinetics which reports on metabolites in plasma [184]. The major metabolite was secondary alcohol compound where the triazole ring is replaced with alcohol group [184]. Cytochrome P450 isoenzyme 3A4 and 2A6 are involved in the production of metabolites [185].

Representative PET images from baseline scan are shown in Figure 3-5. The summed image revealed high carbon-11 uptake in all brain regions such as thalamus, striatum, temporal cortex, and cerebellum. It is likely that the carbon-11 in the brain is in the form of [^{11}C-cyano]letrozole based on the absence of labeled metabolites in the plasma. Unfortunately, there was no enhanced uptake in the amygdala and hypothalamus both of which are rich in aromatase.

TAC's for different brain regions were similar to each other with rapid initial uptake peaking at ~5 minutes followed by an initial rapid clearance and a very slow clearance from 15-90 minutes. (Figure 3-6) There was no observed accumulation in the amygdala and the hypothalamus in any scans. In the studies of reproducibility, there were some

initial differences during first few minutes but the TAC's for different brain regions were generally similar with slight increase in clearance rate in the second scan on each day which could be accounted for by a difference in physiological state of the animal after prolonged anesthesia. (Figure 3-6 and Figure 3-7)

Co-administration of unlabeled letrozole produced global elevation in the TAC's for different brain regions with no distinctive change in the brain region (Figure 3-8). The changes in TAC from blocking scan after 40 minutes were attributed to a change of head position during the scan. Lack of accumulation of [^{11}C-cyano]letrozole in brain regions rich in aromatase and absence of regionally specific changes with co-administration of letrozole indicates that [^{11}C-cyano]letrozole will not be a useful tracer for brain aromatase. This contrasts with previous studies of [^{11}C]vorozole which reports that the amygdala and to a less extent the hypothalamus were visualized and blocked with aromatase inhibition [166]. This may reflect the higher affinity of vorozole than letrozole (0.7 nM vs 11.5 nM for human placental tissue, respectively) [170, 171].

4 Conclusions

We prepared [^{11}C-cyano]letrozole using [^{11}C]hydrogen cyanide by palladium-mediated cyanide coupling reaction. The yield was critically dependant on solvent. PET image study clearly showed that letrozole penetrated the blood-brain barrier. However, there was no accumulation of [^{11}C-cyano]letrozole in the brain regions with co-administration of letrozole limiting it utility for imaging and quantification of brain aromatase. Nonetheless, letrozole is approved for use for breast cancer treatment. Because personalized treatment is gaining a growing importance in modern medicine, the

radiotracers such as [^{11}C-cyano]letrozole may be useful in the future for planning treatment where distribution and pharmacokinetics and especially a knowledge of whether the drug targets the tumor may have value.

Figures and Schemes

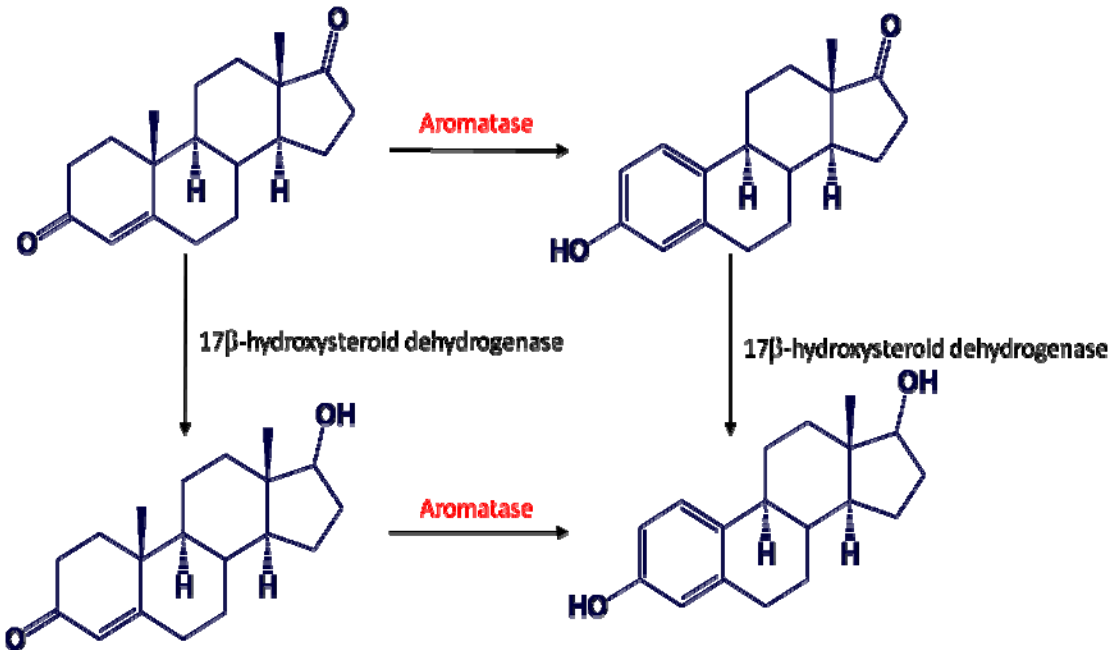

Figure 3-1. The function of aromatase

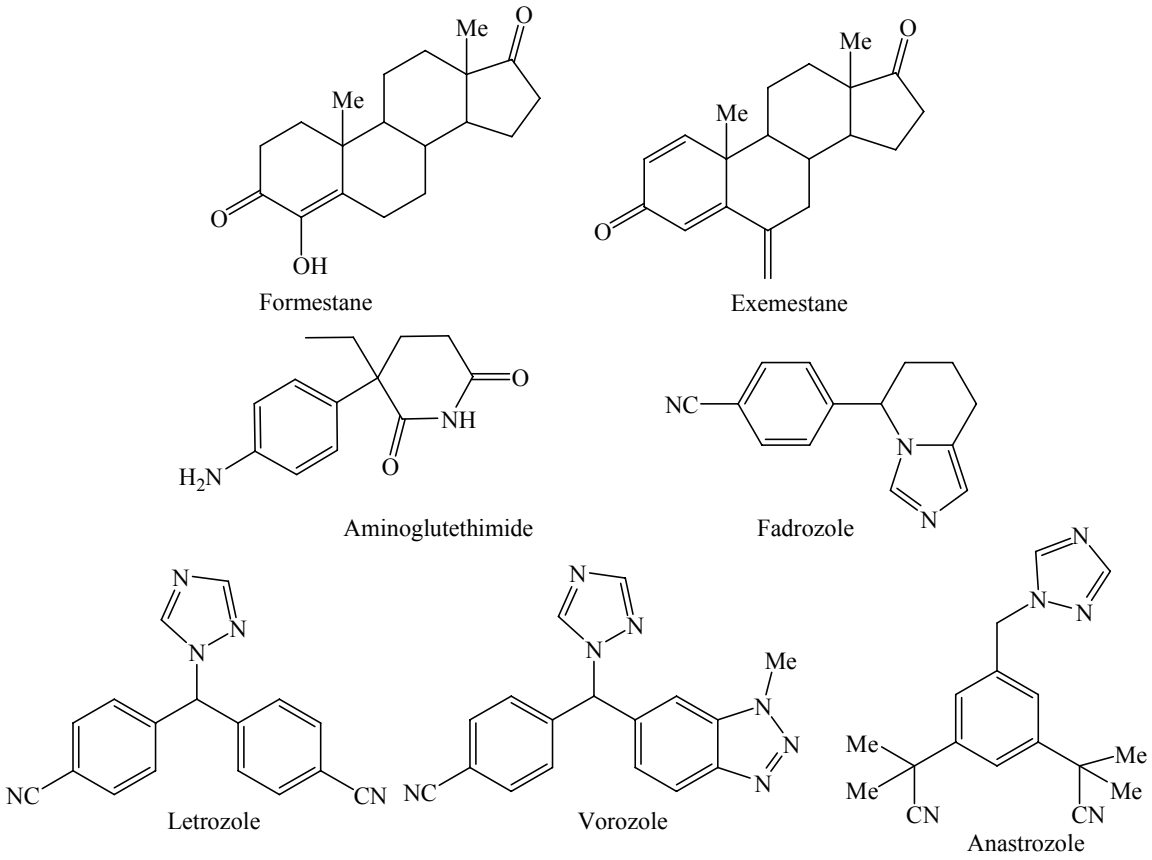

Figure 3-2. Representative aromatase inhibitors (AI)

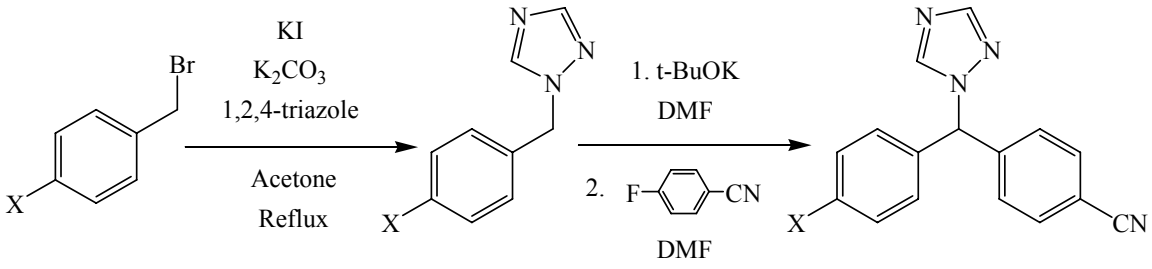

X=CN, 4-cyanobenzyl bromide X=CN, **1**, 80% X=CN, Letrozole, 47%

X=Br, 4-bromobenzyl bromide X=Br, **2**, 79% X=Br, **3**, 32%

Scheme 3-1. Synthesis of letrozole and bromo-precursor (**3**) for [^{11}C-cyano]letrozole

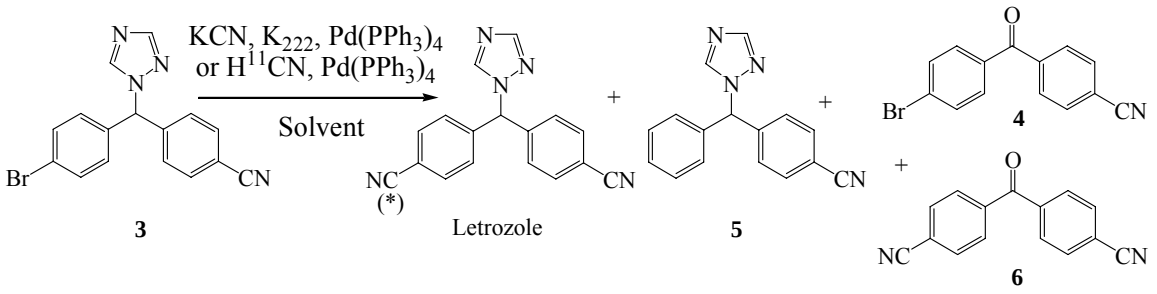

Model Reaction			Labeling Reaction
Scheme A	Scheme B	Scheme C	Scheme D
1.0 eq. KCN 1.0 eq. K_{222} 0.75 eq. $Pd(PPh_3)_4$ 90°C	1.0 eq. KCN 1.0 eq. K_{222} 0.50 eq. $Pd(PPh_3)_4$ 90°C	1.0 eq. KCN 1.0 eq. K_{222} 0.25 eq. $Pd(PPh_3)_4$ 90°C	$H^{11}CN$ 0.25 eq. $Pd(PPh_3)_4$ 110°C×5 min

Solvent	Model Reaction		Labeling Reaction	
	Scheme	Product	Scheme	Product
THF	A, B	Letrozole (up to 21%), but no **4**	D	[^{11}C-cyano]letrozole RCY: 29%
	C	**4** (59%) but no letrozole		
Diglyme	A, B, C	Letrozole (Up to 67%) + **5** (26%)	D	[^{11}C-cyano]letrozole RCY: 43%
DMF	A, B	**6** (Major) + Letrozole (3 ~ 7%)	D	[^{11}C-cyano]letrozole RCY: 58%
	C	**4** (Up to 71%)		
DMSO	A	**6** (17%) + Letrozole (trace)	D	[^{11}C-cyano]letrozole RCY: 80%
	B	**4** + **6** (Not determined)		
	C	**4** (37%)		

Scheme 3-2. Palladium catalyst mediated cyanide coupling reaction using potassium cyanide or [^{11}C]hydrogen cyanide in various solvents.

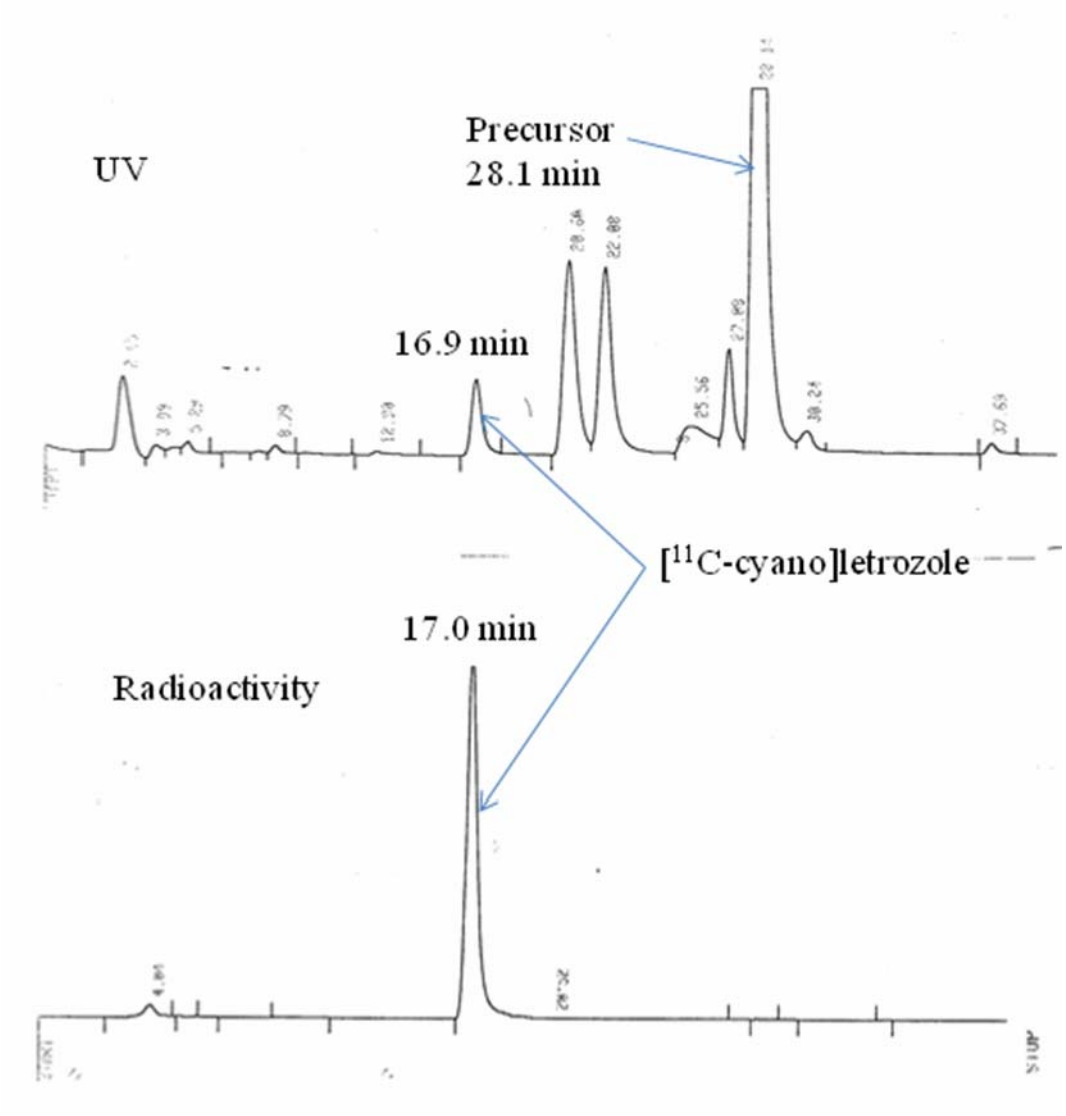

Figure 3-3. HPLC profile of [^{11}C-cyano]letrozole synthesis showing UV and radioactivity traces.

(a) (b)

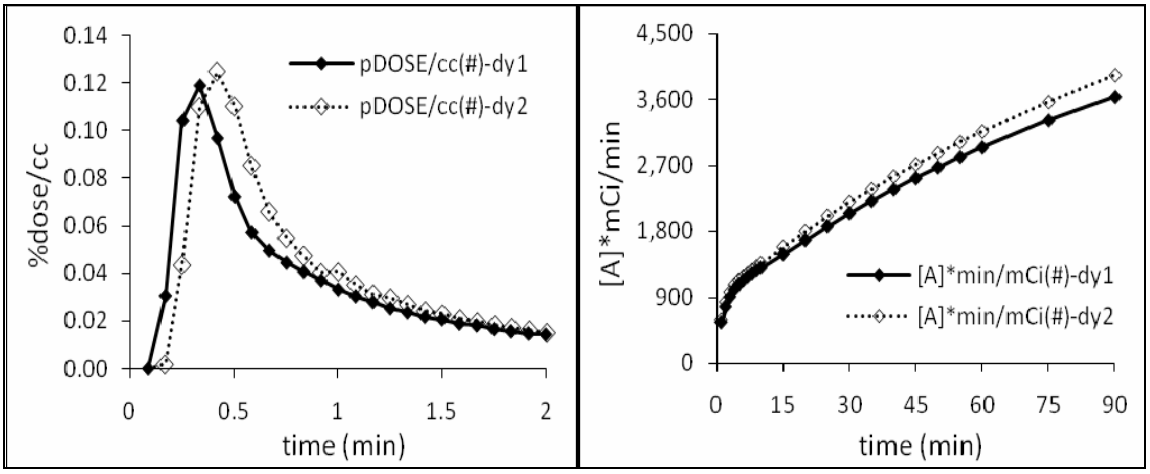

(c) (d)

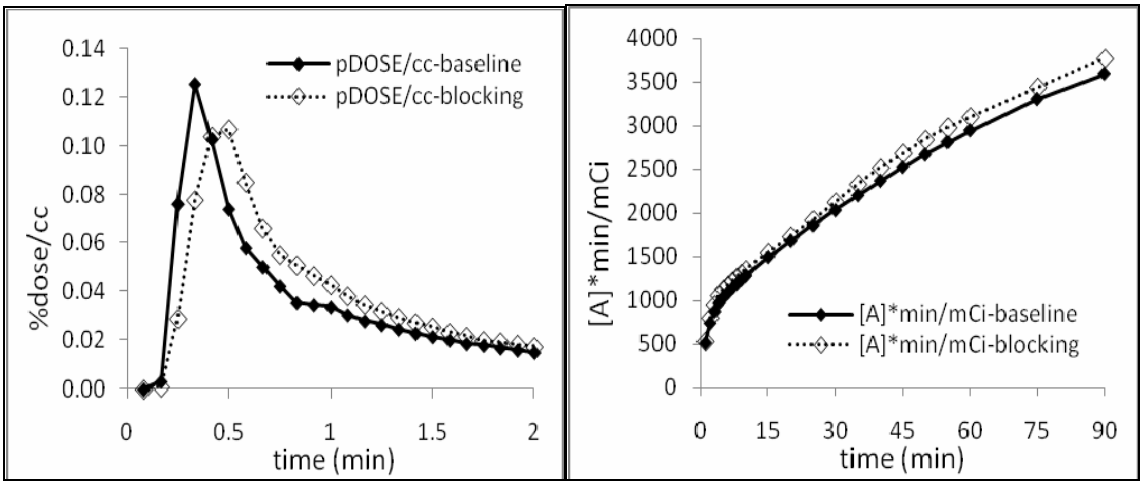

Figure 3-4. (a) TAC's of plasma from two baseline studies for the first two minutes. (b) Area under the curve (AUC) of [^{11}C-cyano]letrozole concentration in plasma over a 90 minute experiment for the two repeated baseline scans. (c) TAC's of plasma from baseline study and blocking study (0.1 mg/kg of unlabeled letrozole co-administration) for the first two minutes (d) AUC of [^{11}C-cyano]letrozole concentration in plasma over a 90 minute experiment at baseline and after letrozole treatment.

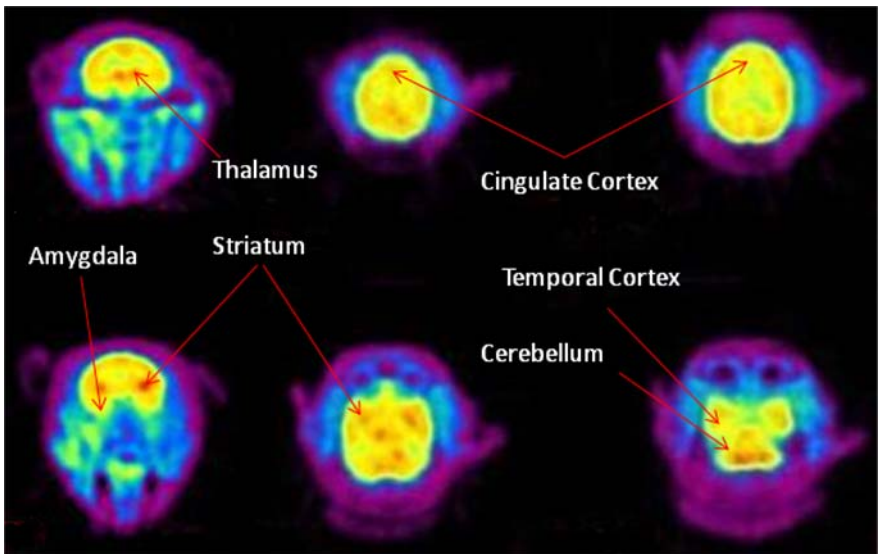

Figure 3-5. Summed frames PET images of baboon brain (0-90 min) from dynamic baseline scan. Carbon-11 uptake was observed in thalamus, striatum, temporal cortex, and cerebellum.

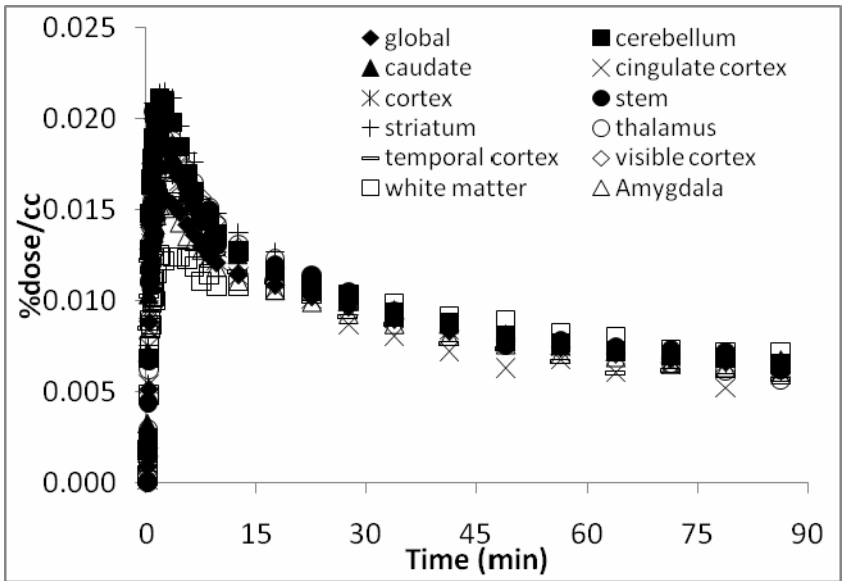

Figure 3-6. TAC's from baseline study showed that even if there are some differences in initial uptake depending on the region, the wash-out was fast for 10 minutes after peak time, but slowed down after 15 minutes.

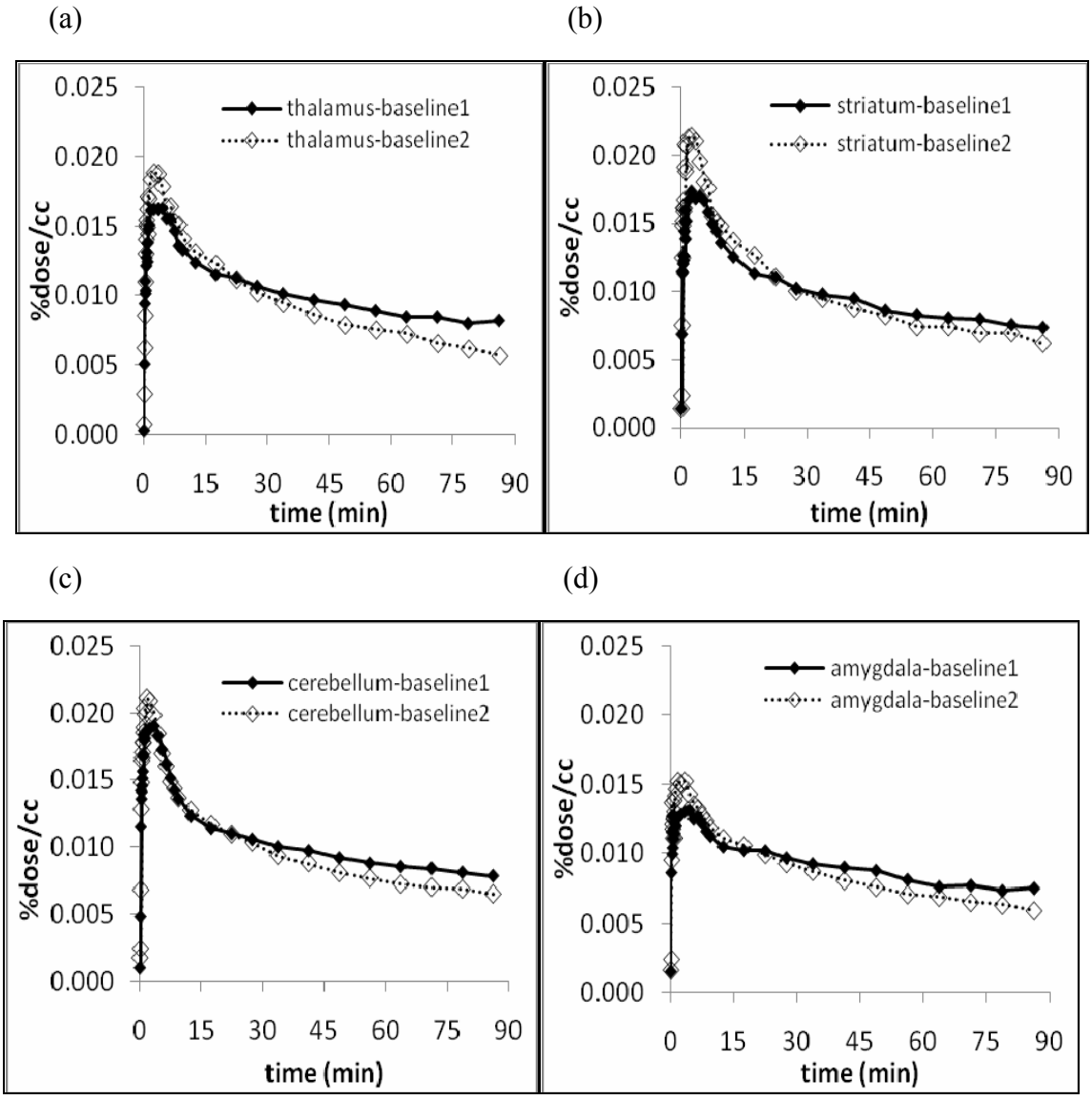

Figure 3-7. Comparison of first and second dynamic scan for reproducibility in various brain regions.

(a) Thalamus

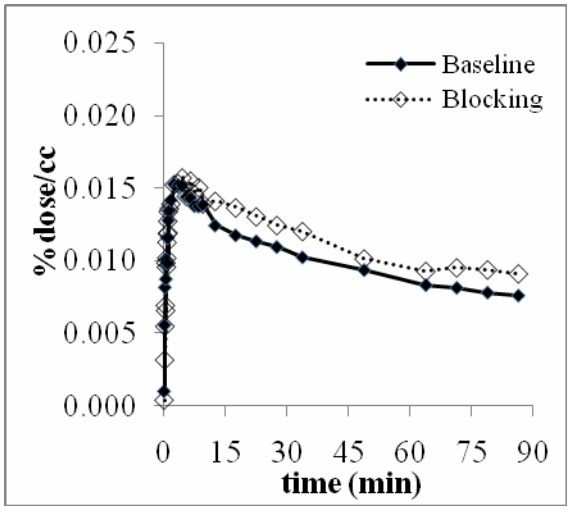

(b) Striatum

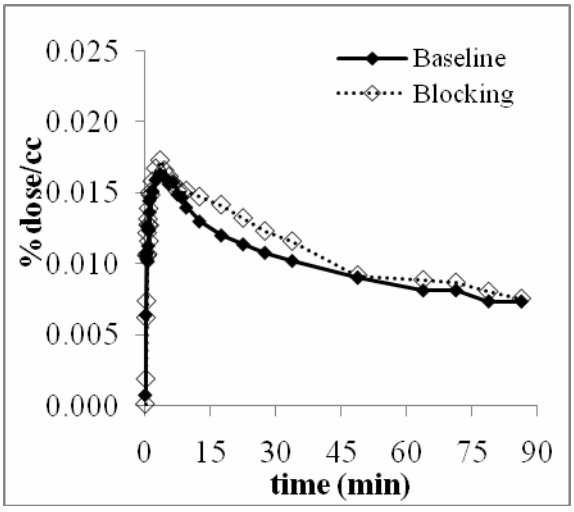

(c) Cerebellum

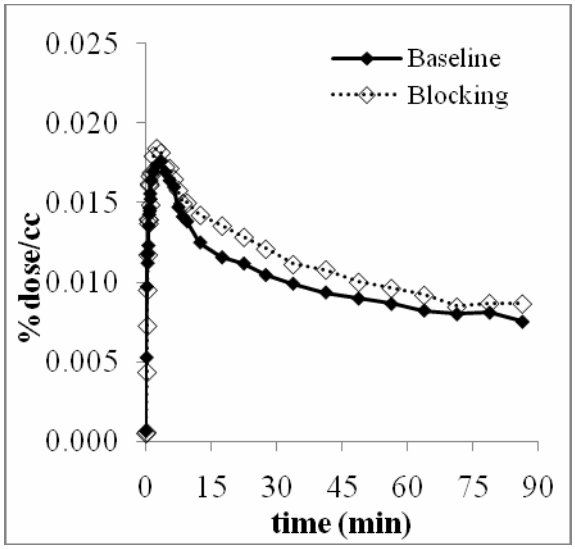

(d) Amygdala

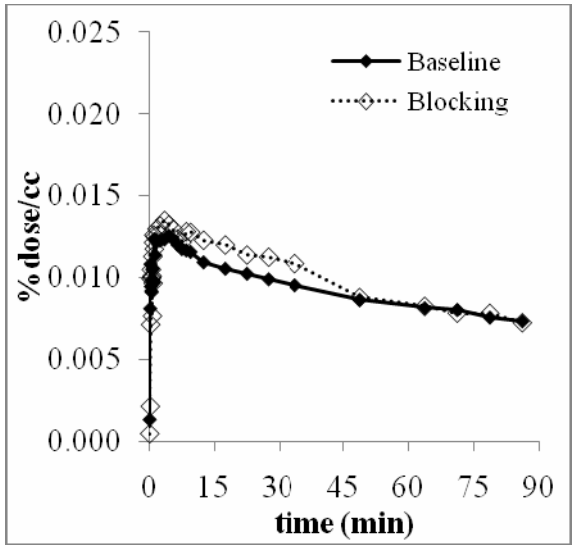

Figure 3-8. TAC's from baseline study and blocking studies for thalamus (a), striatum (b), cerebellum (c), and amygdala (d). There was some movement of the head during the period 35-60 min necessitating deletion of two time frames for the small ROI's (striatum, thalamus, and amygdala).

NMR Spectra

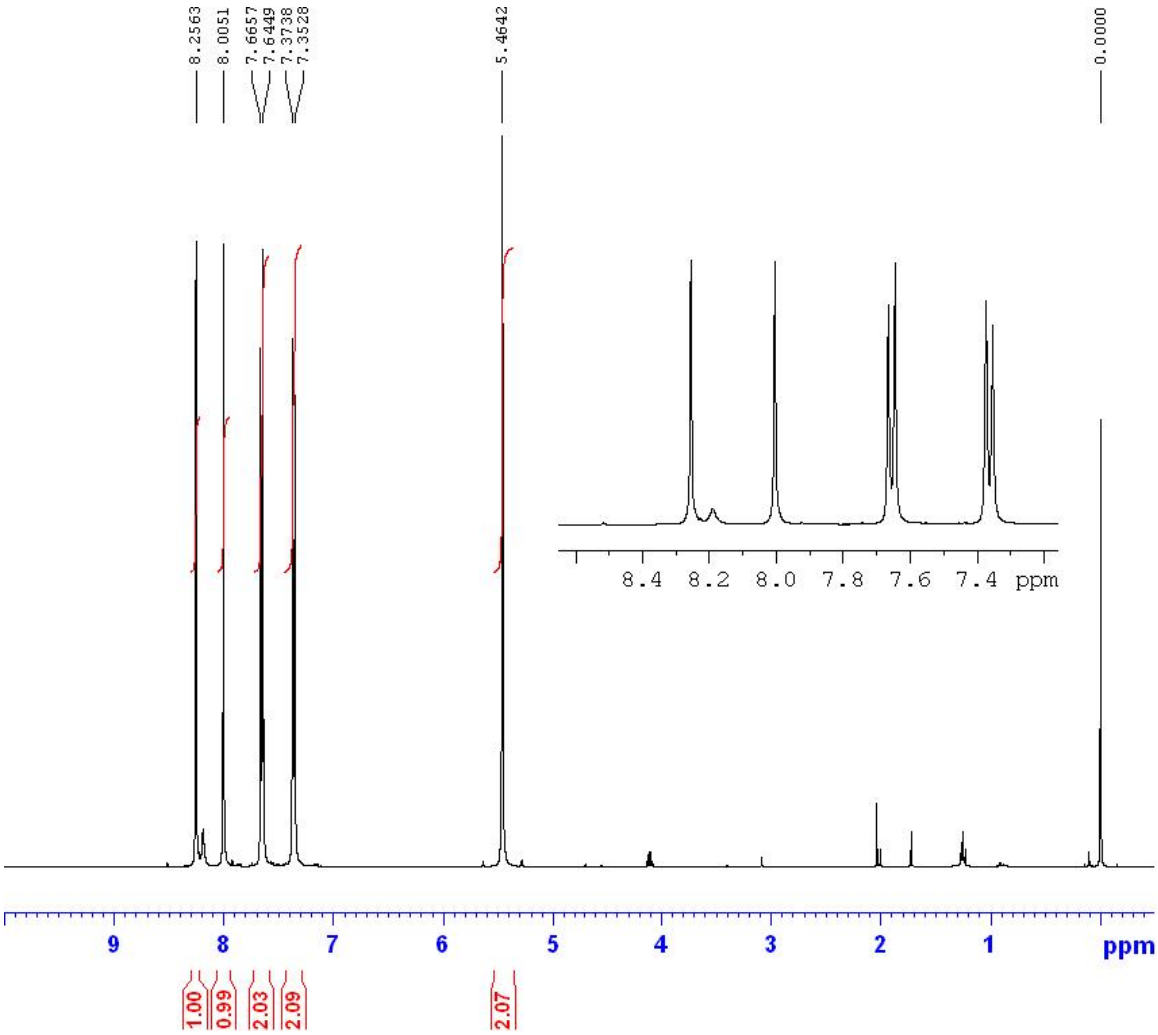

^{1}H-NMR Spectrum of 1-(4-cyanobenzyl)-1*H*-1,2,4-triazole (**1**)

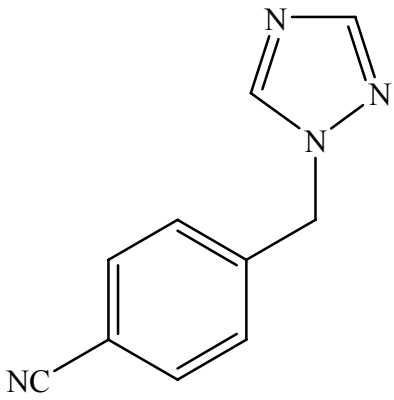

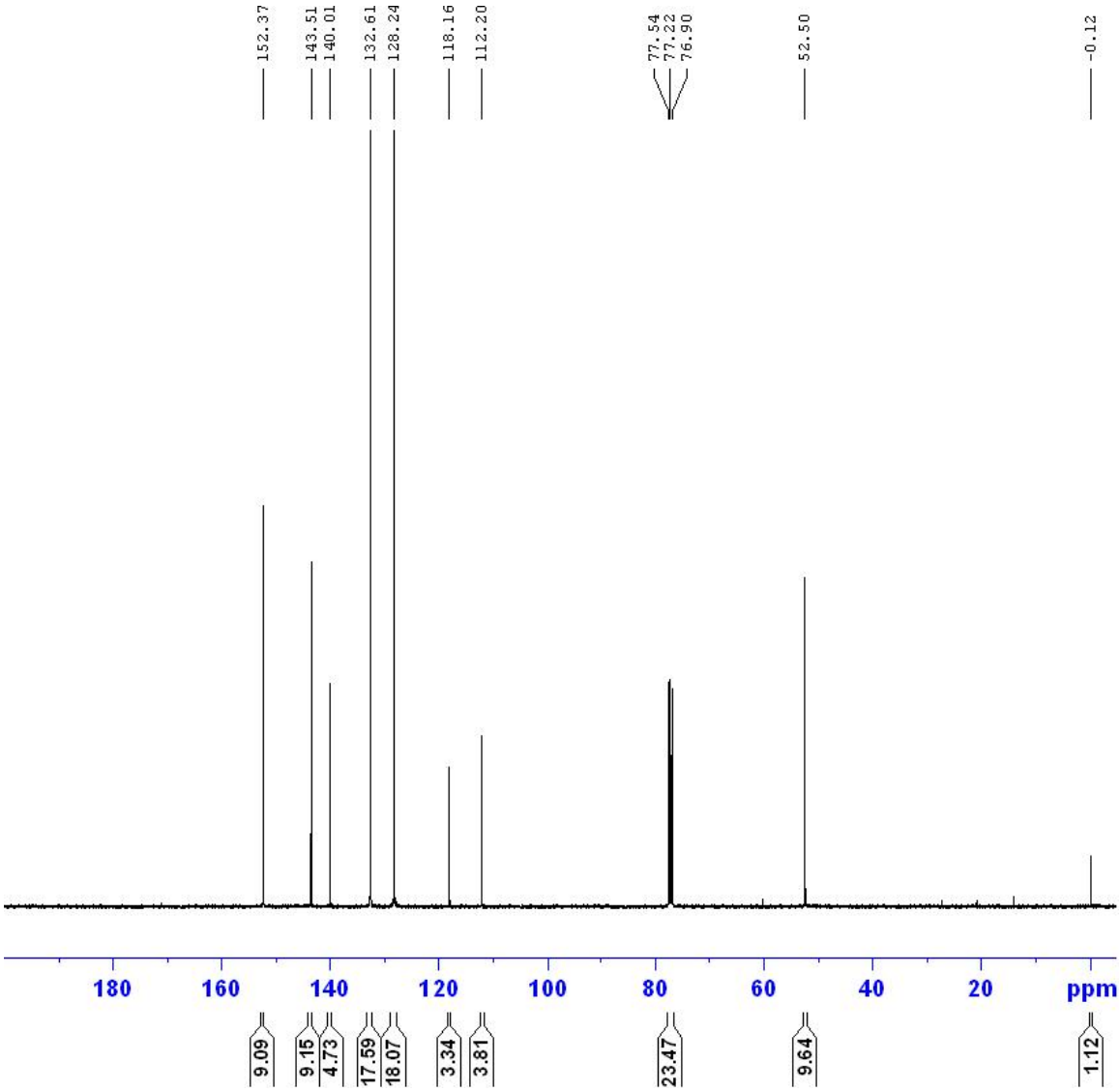

^{13}C-NMR Spectrum of 1-(4-cyanobenzyl)-1*H*-1,2,4-triazole (**1**)

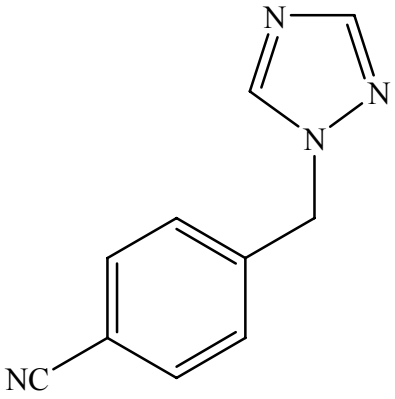

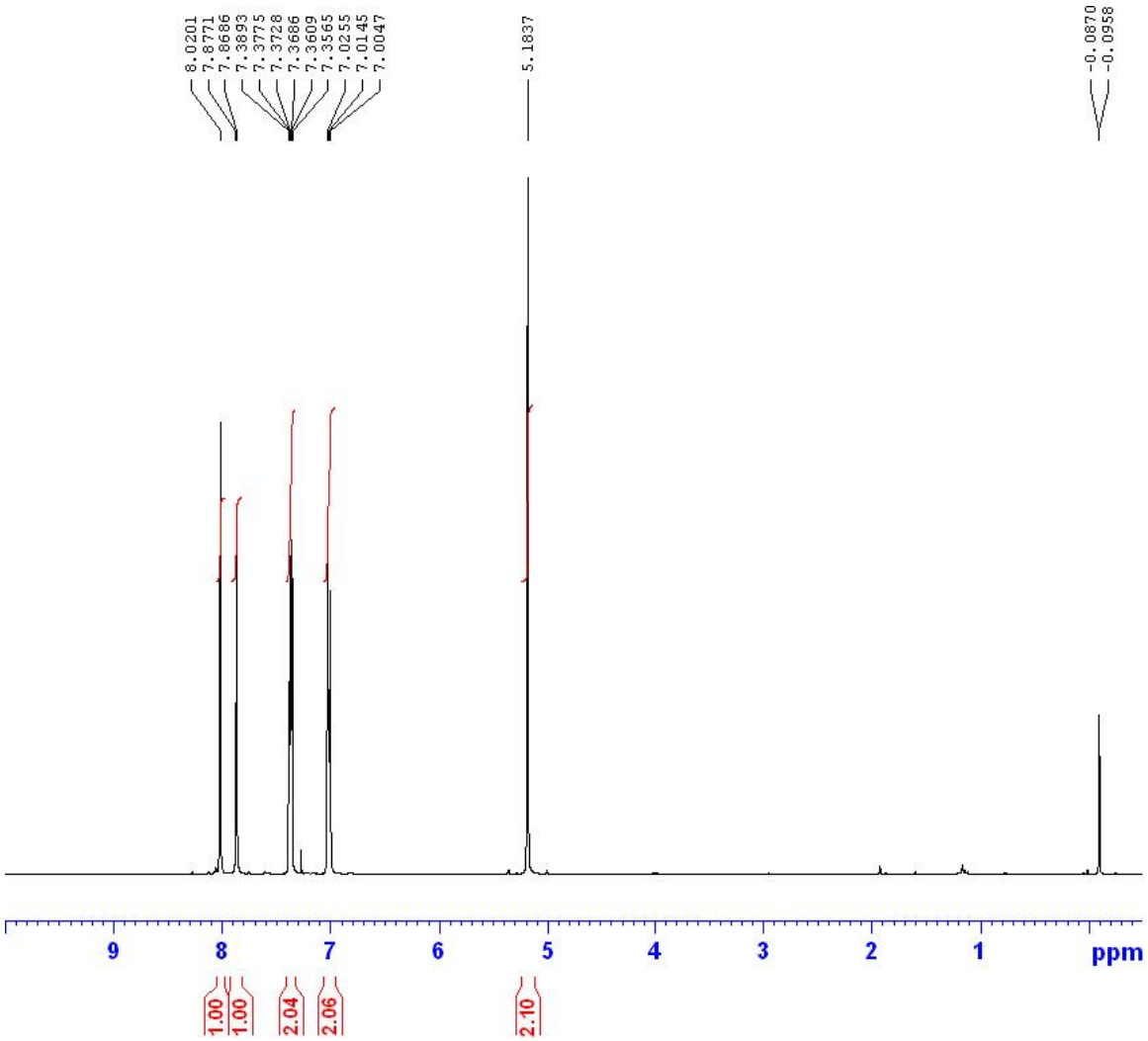

^{1}H-NMR Spectrum of 1-(4-bromobenzyl)-1*H*-1,2,4-triazole (**2**)

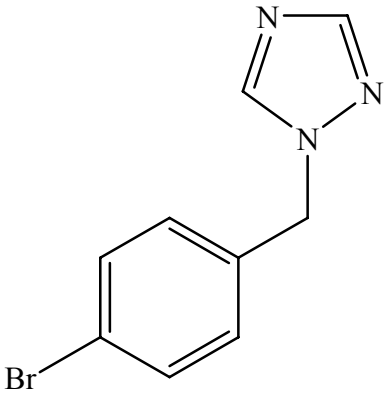

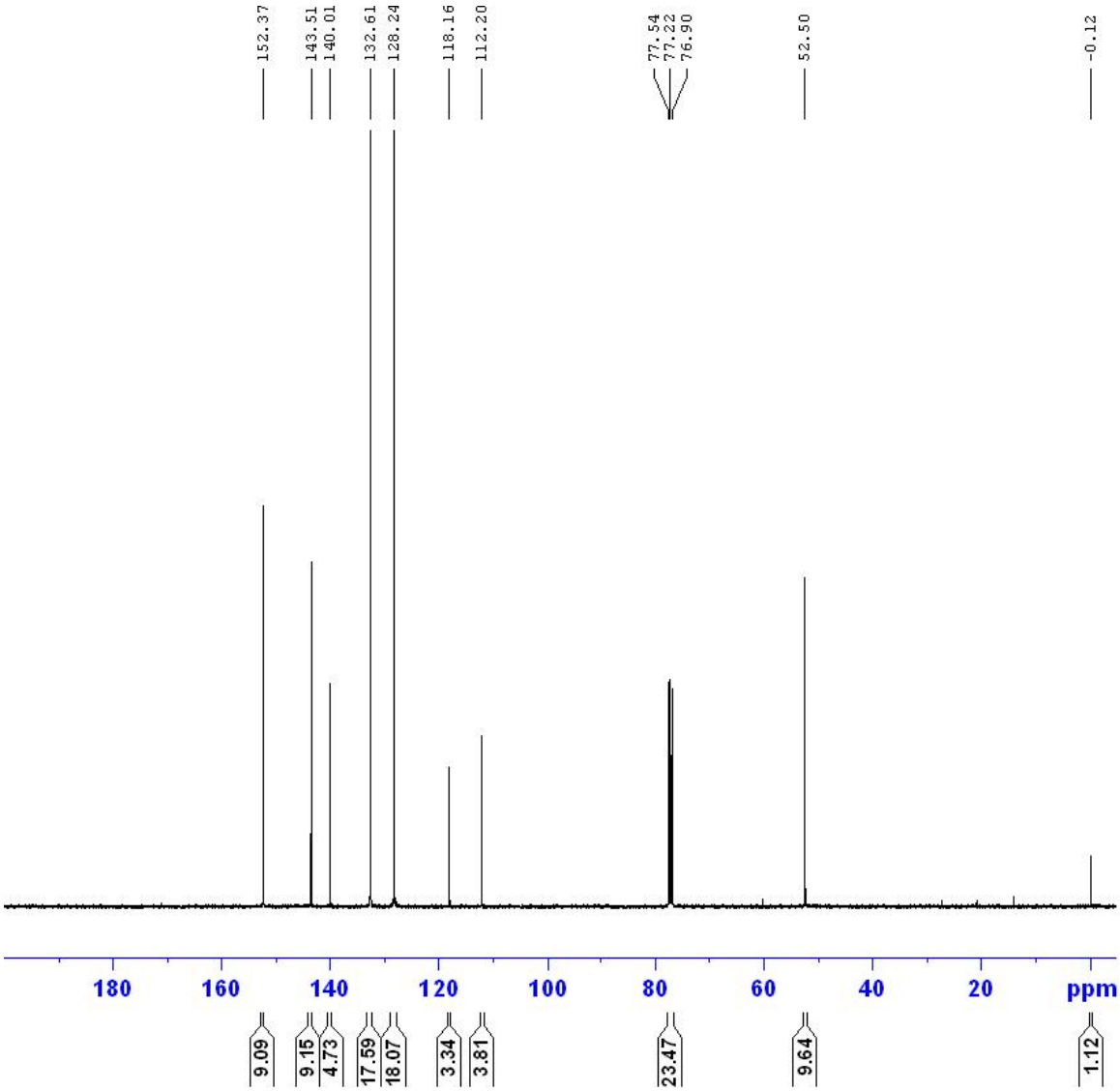

^{13}C-NMR Spectrum of 1-(4-bromobenzyl)-1*H*-1,2,4-triazole (**2**)

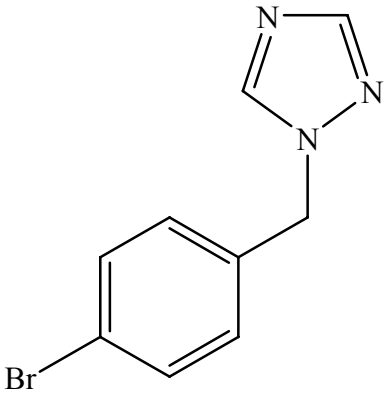

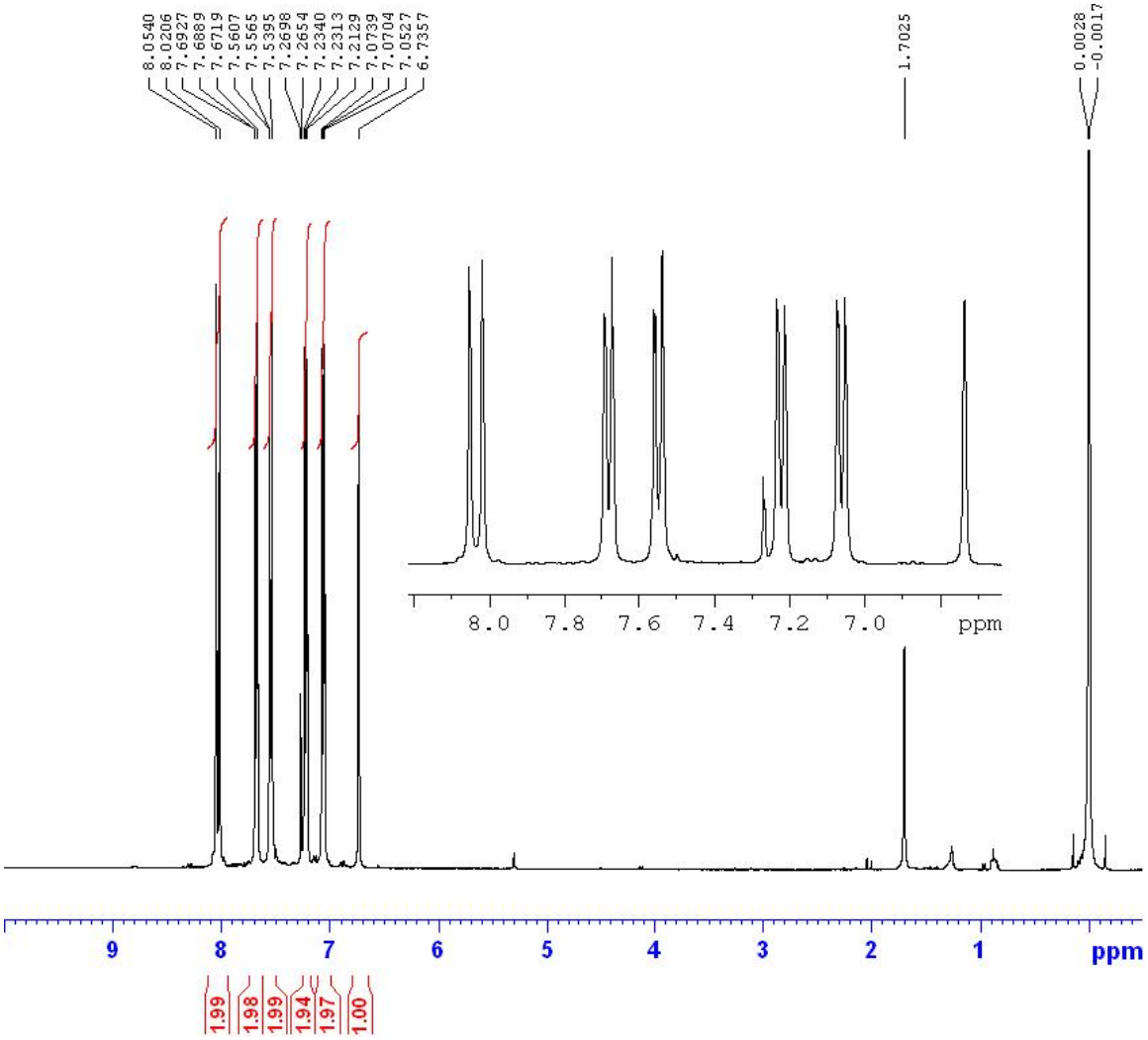

^{1}H-NMR Spectrum of 4-[(4-bromophenyl)-1*H*-1,2,4-triazol-1-ylmethyl]benzonitrile (**3**)

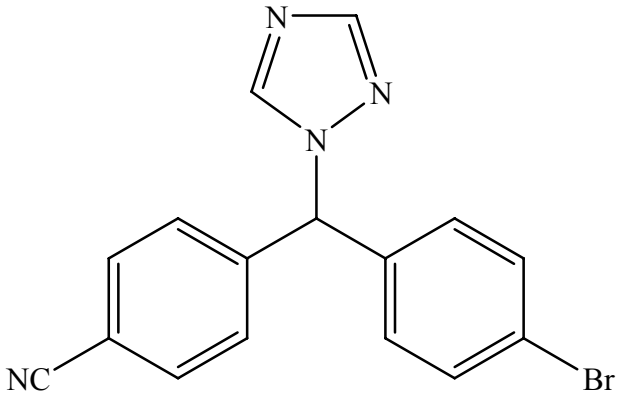

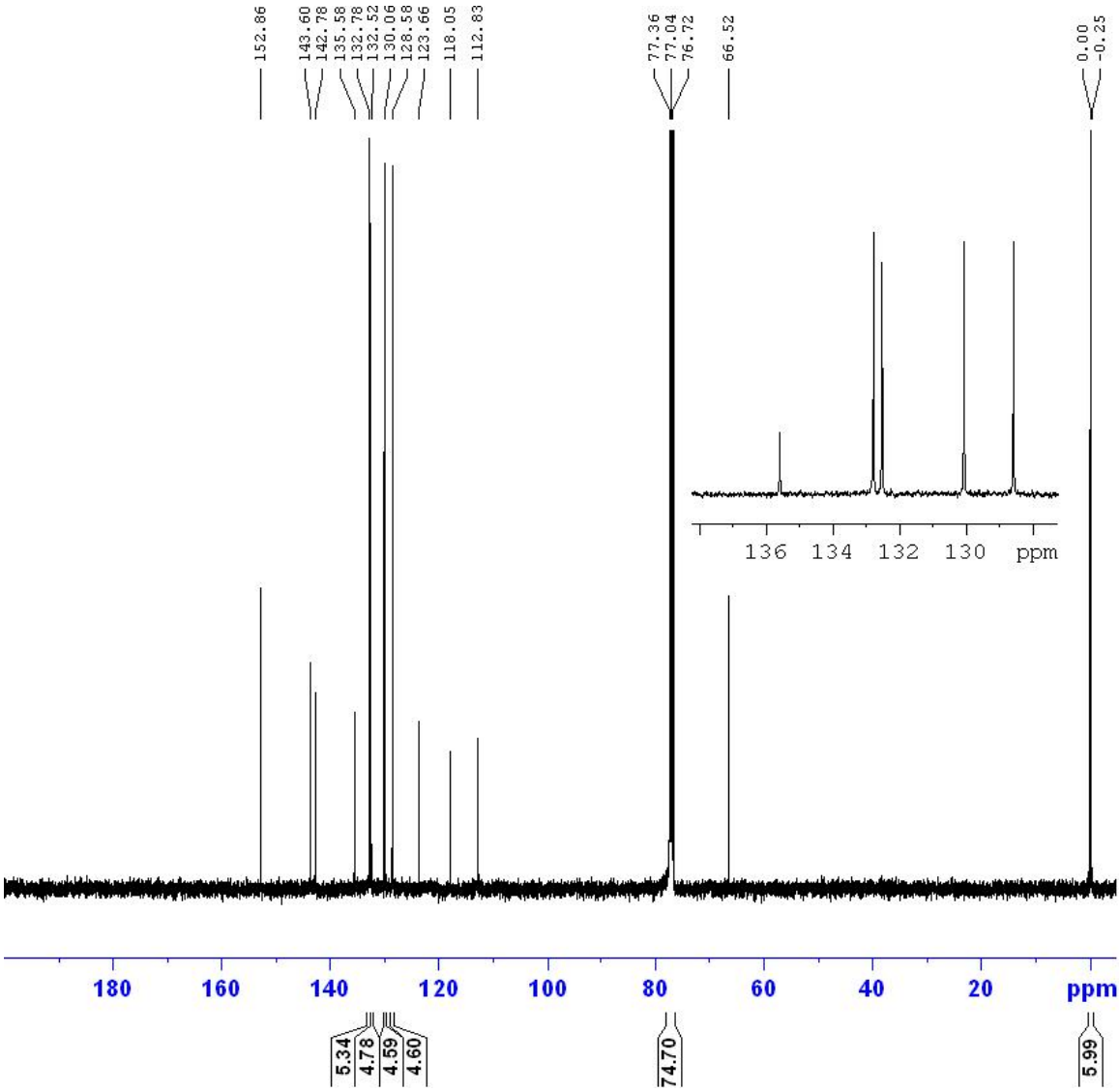

^{13}C-NMR Spectrum of 4-[(4-bromophenyl)-1*H*-1,2,4-triazol-1-ylmethyl]benzonitrile (**3**)

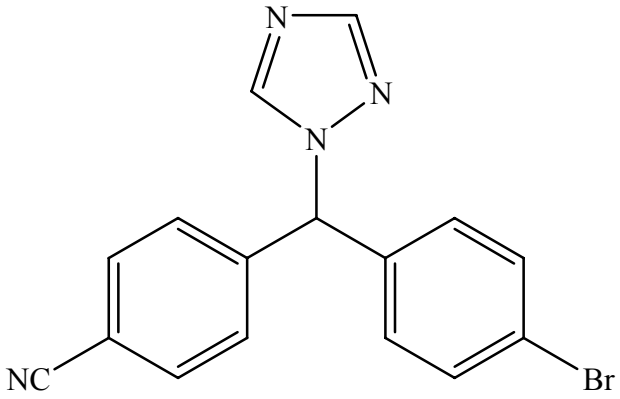

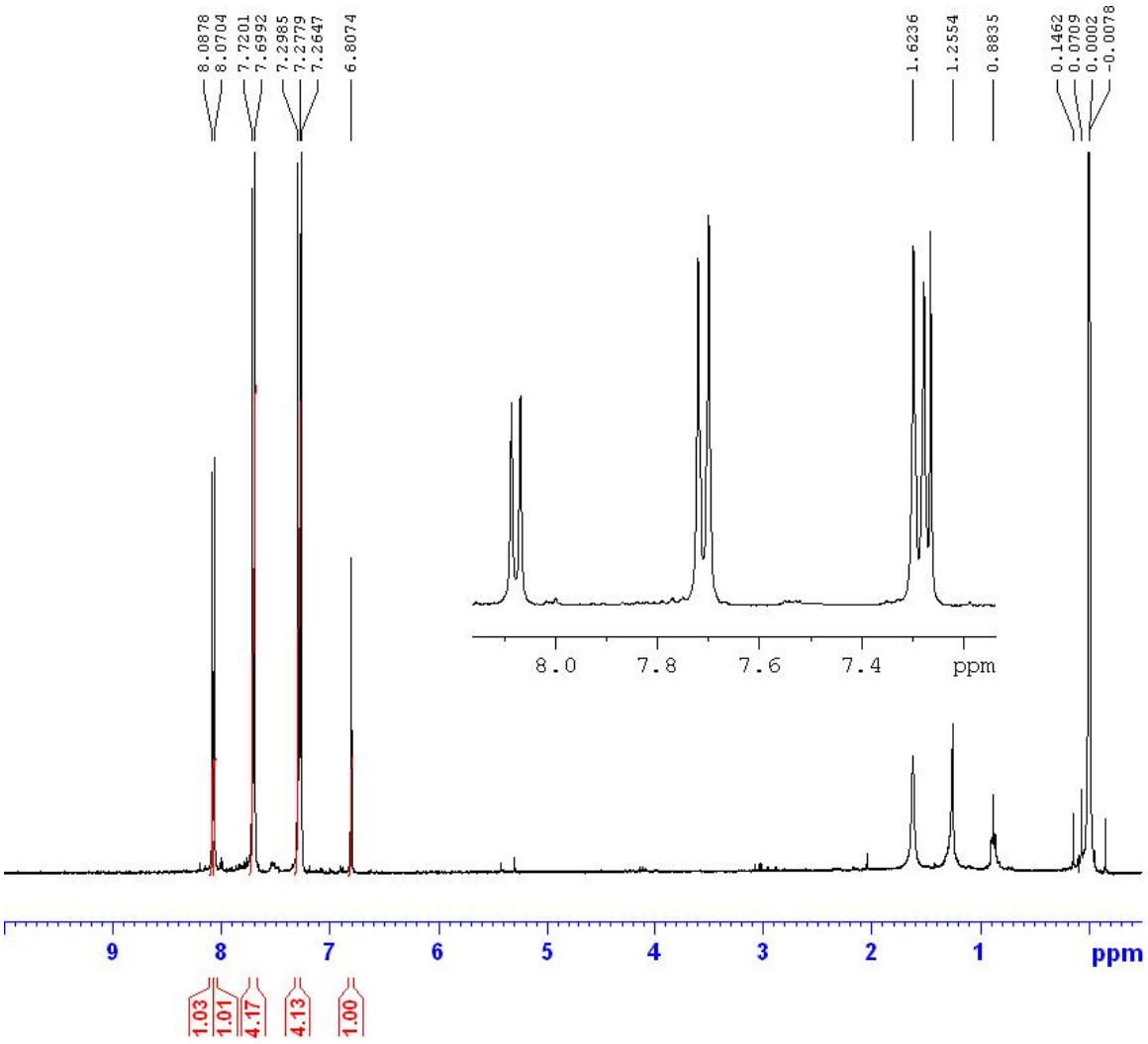

^{1}H-NMR Spectrum of 1-[Bis-(4-cyanophenyl)methyl]-1*H*-1,2,4-triazole (Letrozole)

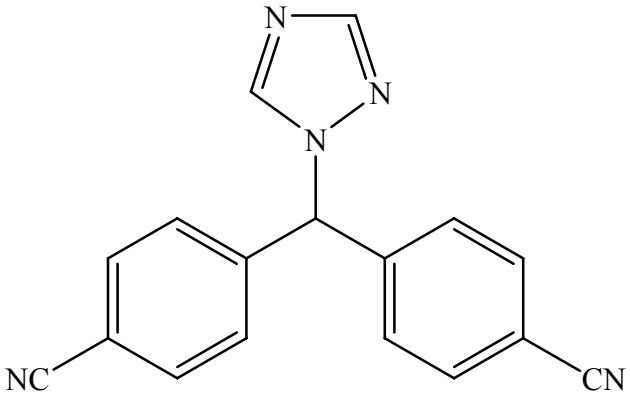

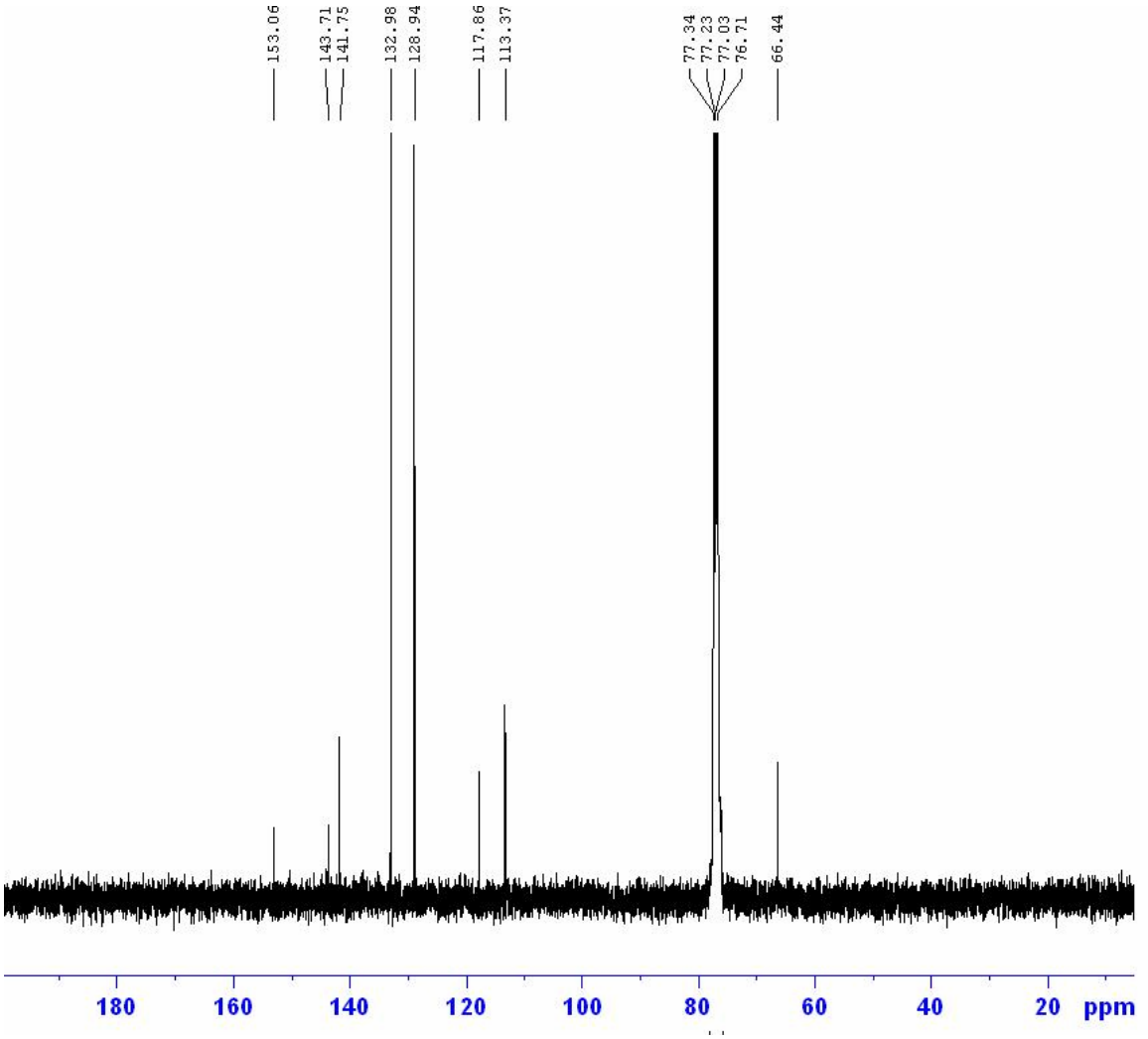

^{13}C-NMR Spectrum of 1-[Bis-(4-cyanophenyl)methyl]-1*H*-1,2,4-triazole (Letrozole)

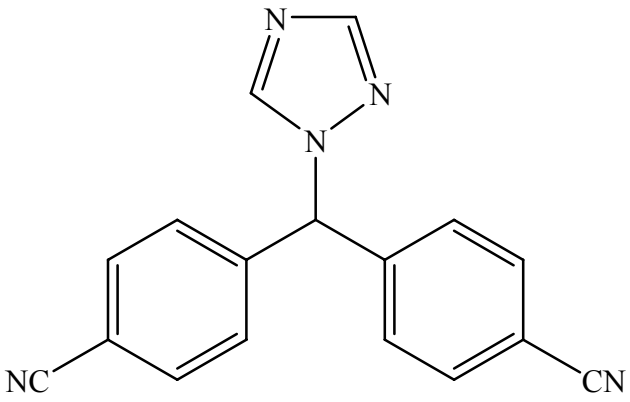

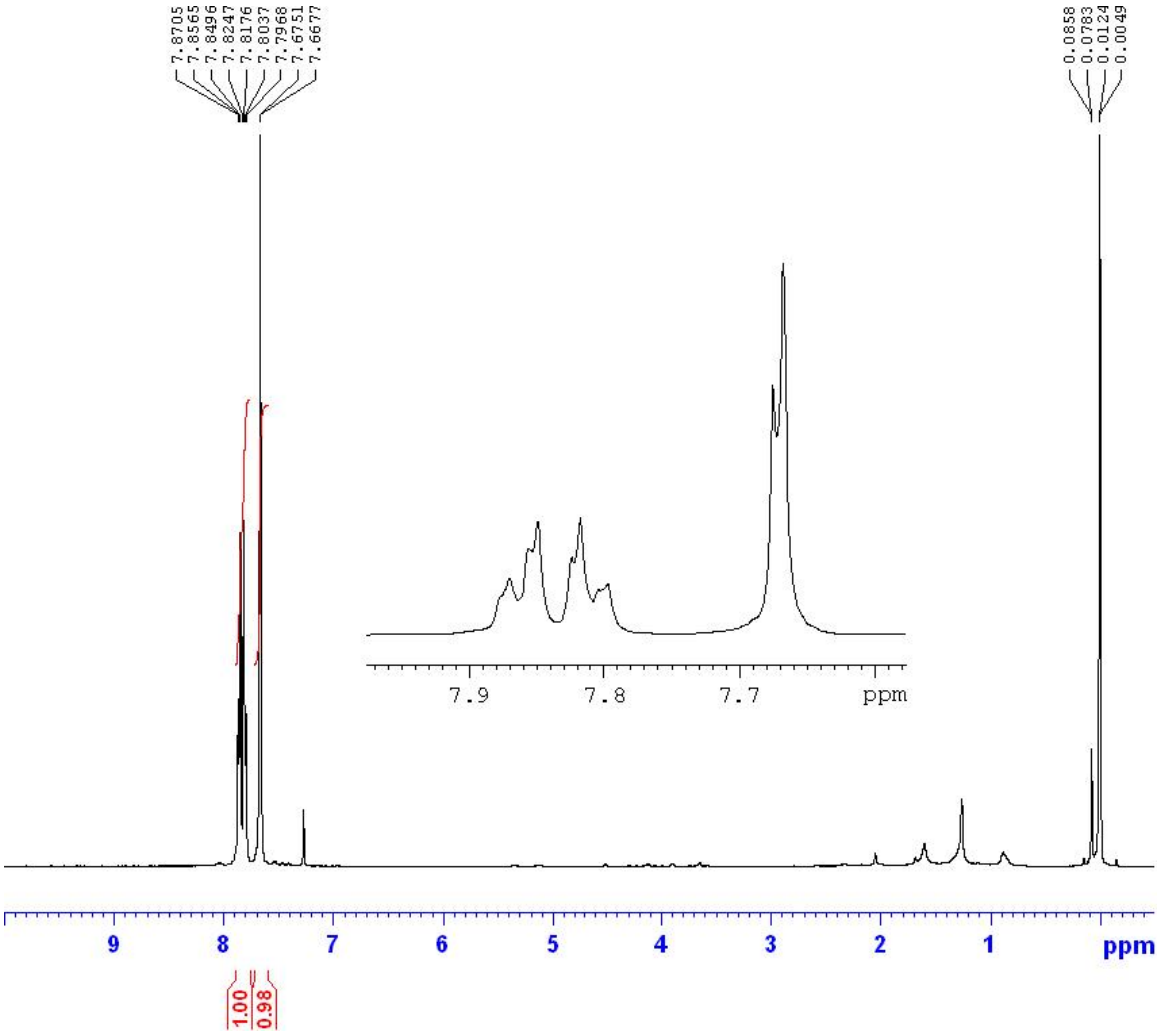

^{1}H-NMR Spectrum of 4-(4'-bromobenzoyl)benzonitrile (**4**)

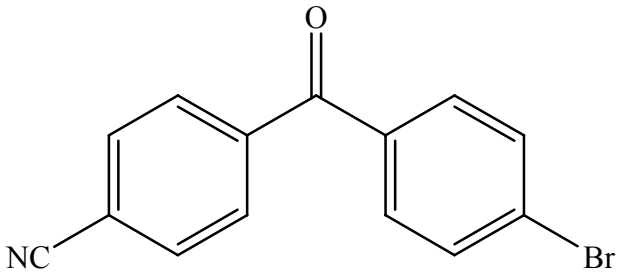

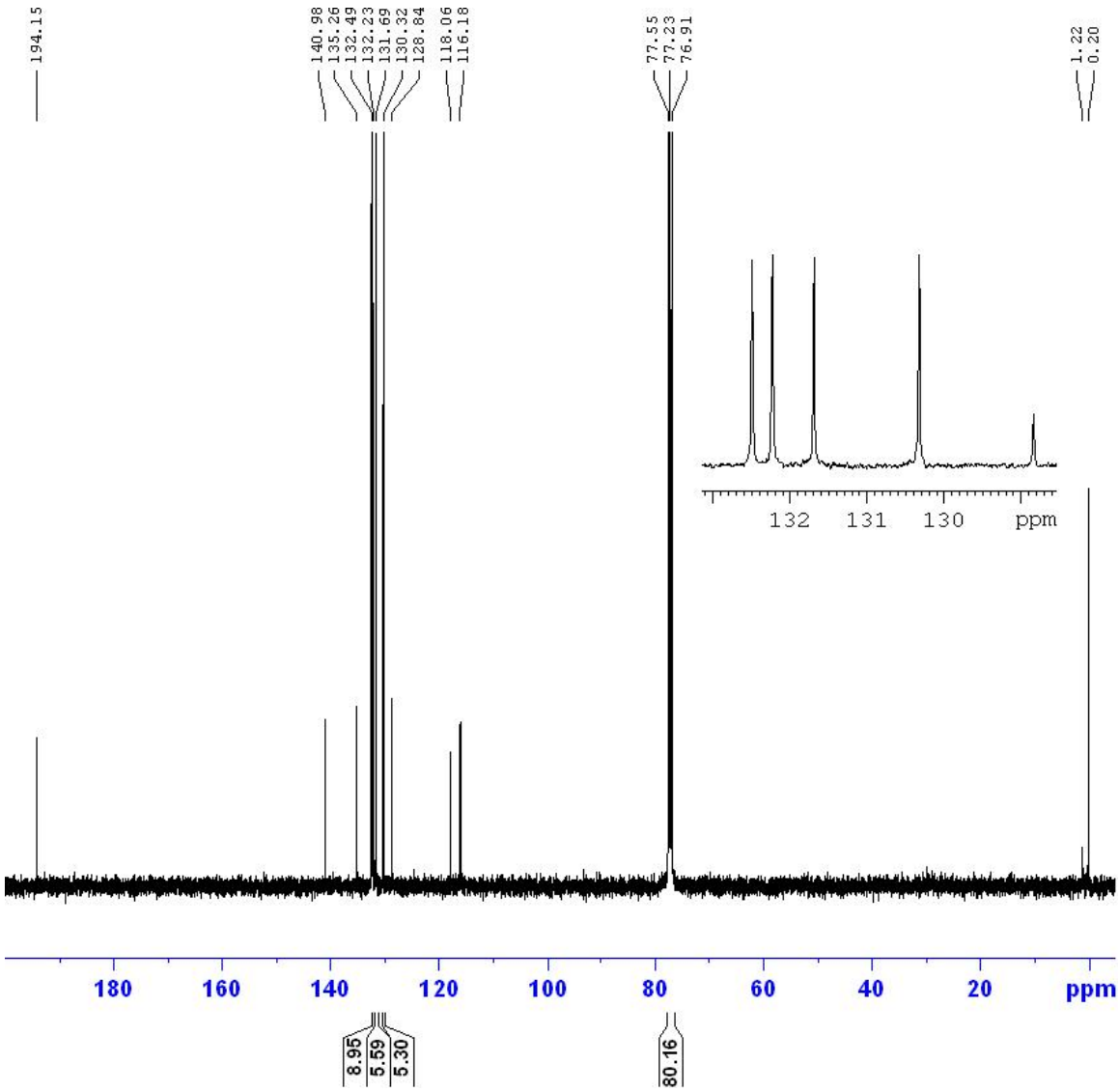

^{13}C-NMR Spectrum of 4-(4'-bromobenzoyl)benzonitrile (**4**)

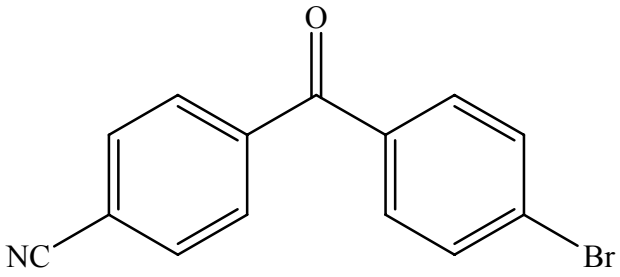

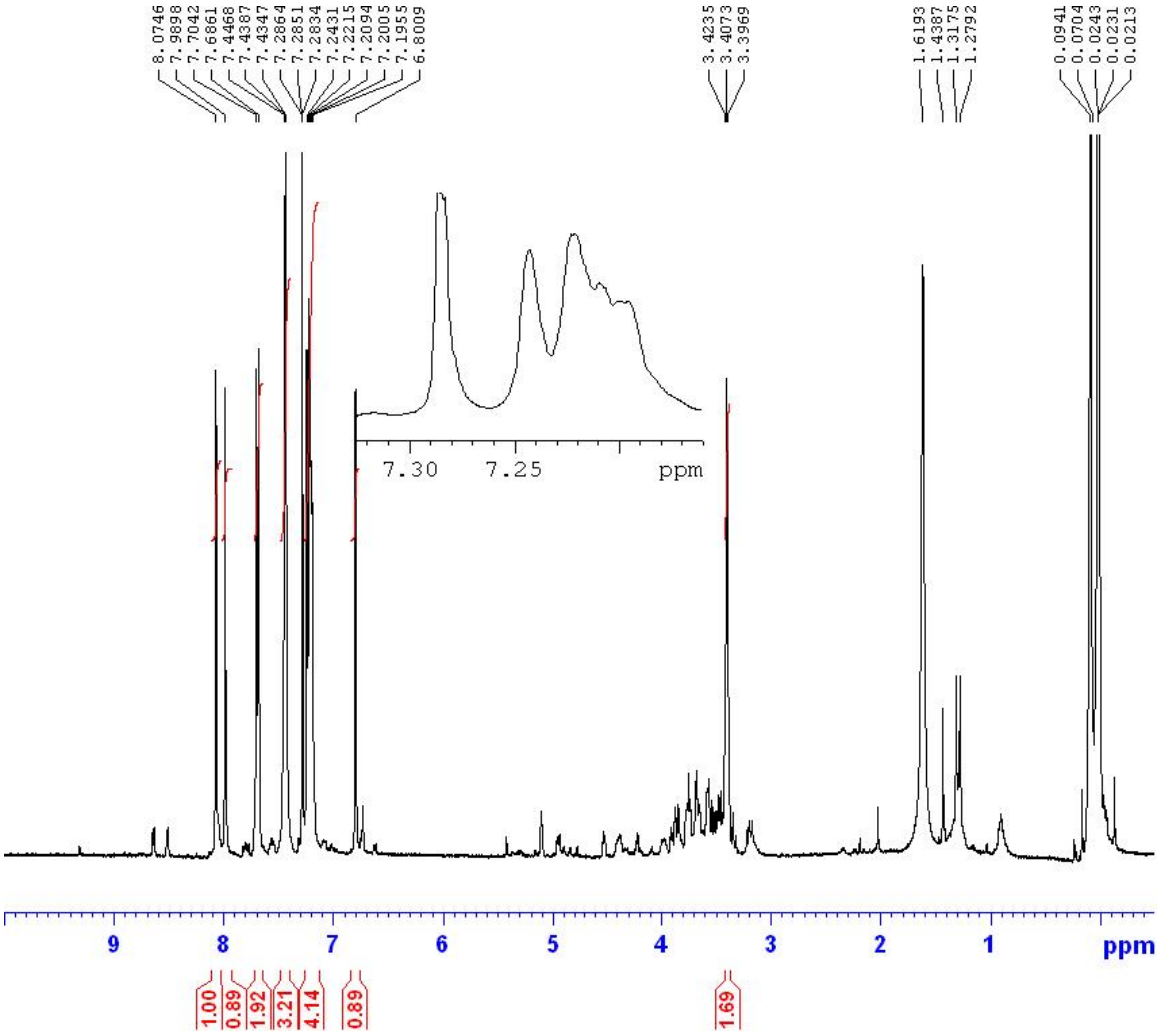

^{1}H-NMR Spectrum of 4-(Phenyl-1*H*-1,2,4-triazol-1-ylmethyl)benzonitrile (**5**)

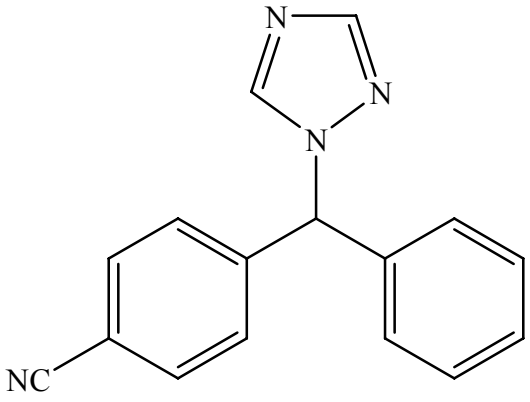

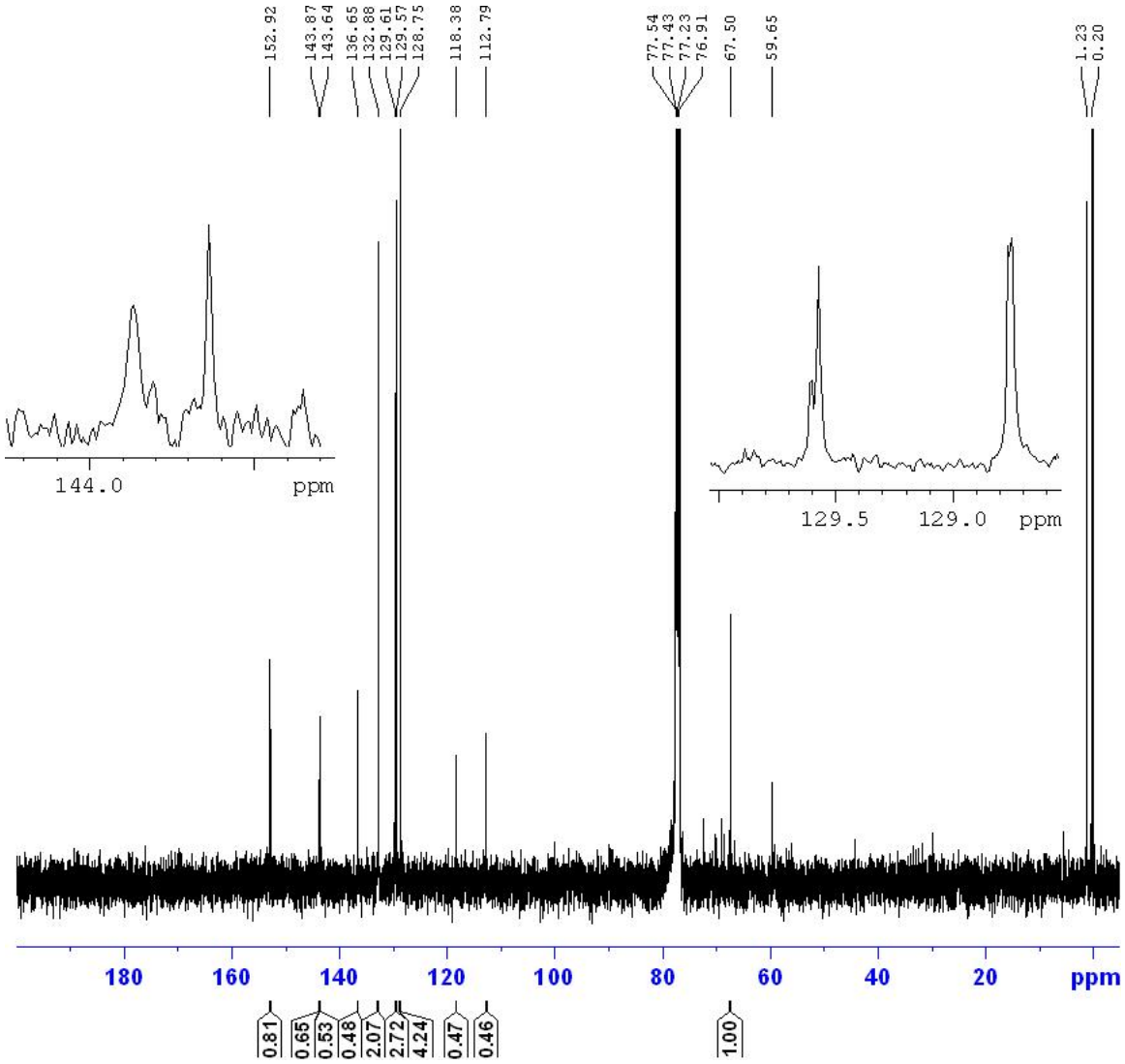

^{13}C-NMR Spectrum of 4-(Phenyl-1*H*-1,2,4-triazol-1-ylmethyl)benzonitrile (**5**)

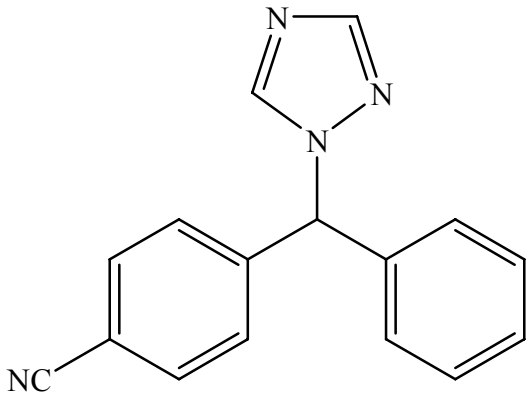

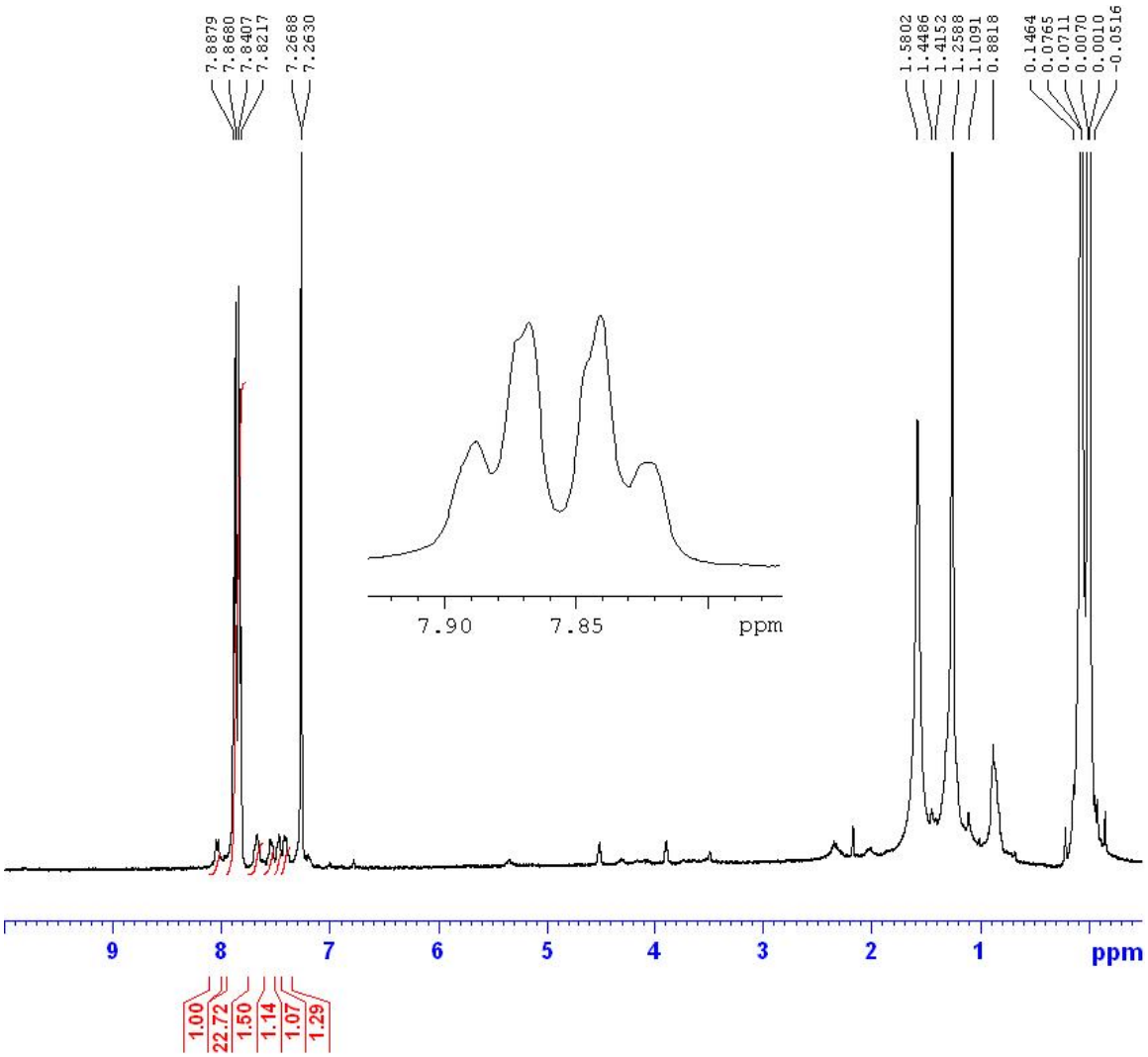

^{1}H-NMR Spectrum of 4,4'-dicyanobenzophenone (**6**)

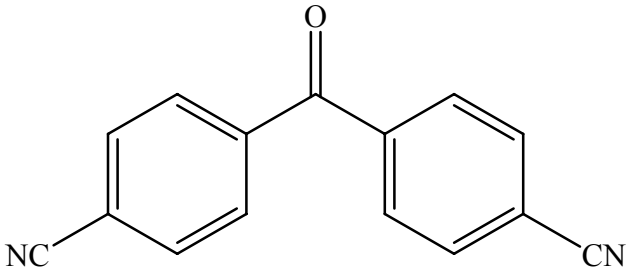

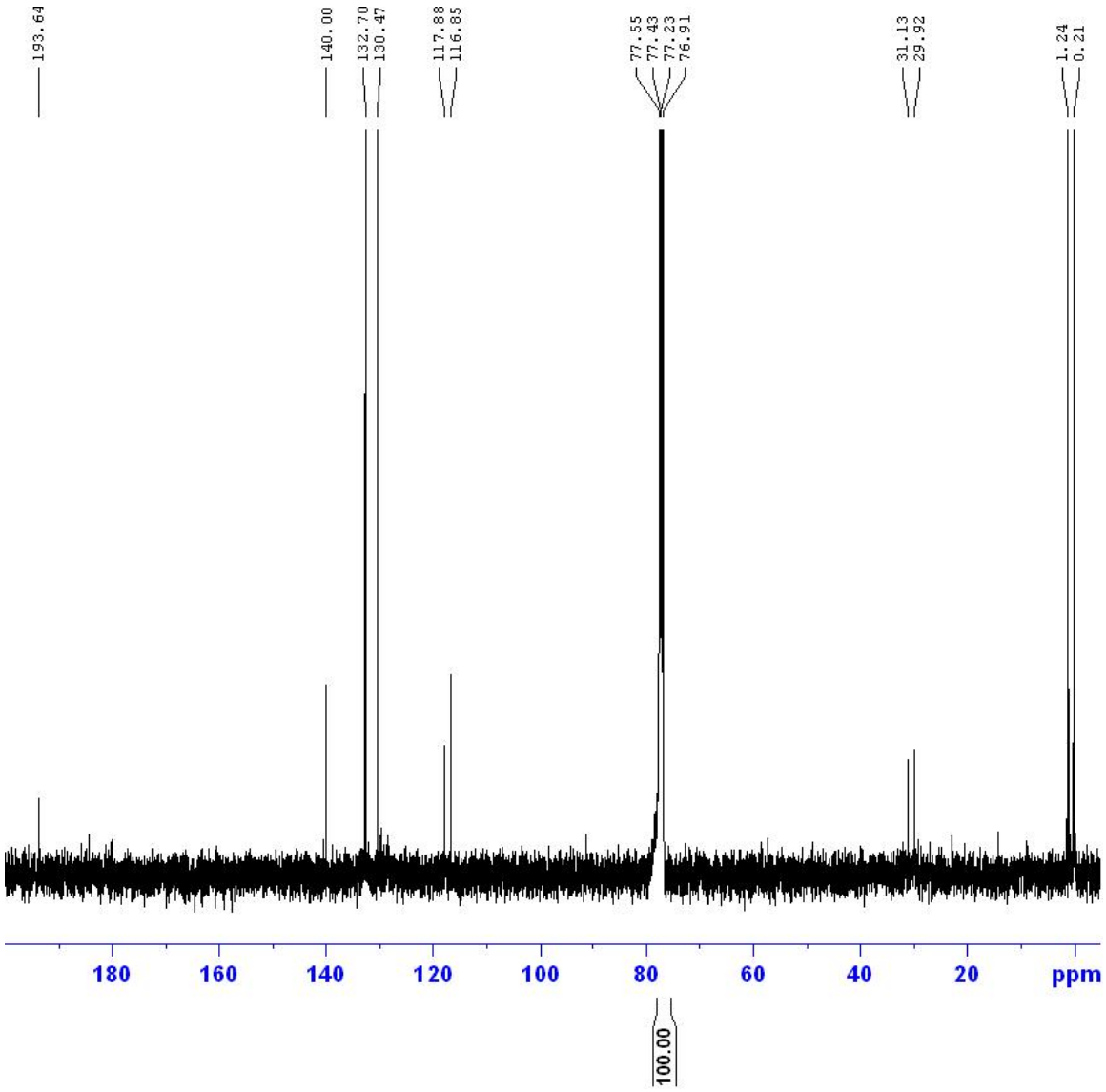

^{13}C-NMR Spectrum of 4,4'-dicyanobenzophenone (**6**)

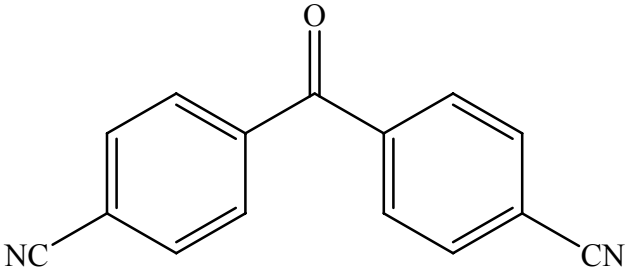

PART IV

Synthesis and Labeling of Monoamine Oxidase (MAO) Inhibitors

1. Introduction

Monoamine oxidase (MAO) oxidizes neurotransmitter amines such as dopamine, epinephrine, tryptamine, tyramine, and norepinephrine or xenobiotic amines to their correspondent aldehyde [186] (Figure 4-1). MAO has two different subtypes, monoamine oxidase (MAO A) and monoamine oxidase B (MAO B) which are different gene products with 70% primary sequence homology [187]. MAO A has 527 amino acids, and MAO B has 520 amino acids. MAO A usually breaks down norepinephrine [188] and serotonin and MAO B normally converts benzylamine and phenethylamine into their aldehyde analogues [189]. Both enzymes oxidize dopamine, tyramine, and octopamine [190]. (Figure 4-2)

MAO A and MAO B are localized in both the brain and peripheral organs. Human postmortem brain studies found that MAO A was abundant in cervical ganglion, paraventricular thalamus, locus coeruleus, interpeduncular nucleus, and ventiomedial hypothalamic nucleus. MAO B was mostly localized in serotoninergic raphe neurons, histaminergic hypothalamic neurons, and dentate gyrus granule cells [191, 192]. The two isoforms show different distribution in peripheral organs: MAO A is abundant in following order: liver>lung=kidney>thyroid>heart [191, 193]. MAO B is abundant in following order: kidney≥heart>lung=spleen [191, 194]. Moreover, their distributional difference depends on species. Whereas MAO A is predominant in the rat brain, MAO B is predominant in human brain [191, 192].

MAO regulates the concentrations of amines such as norepinephrine, serotonin and dopamine which are neurotransmitters often controlling or regulating mood. One of the first MAO inhibitors, iproniazide was used as a treatment for tuberculosis. When it was administered to the patients, their mood was elevated, a side effect of which was later used as a strategy to treat depressed patients [195]. Now, researchers appreciate that MAO inhibitor drugs are useful in the treatment of depression and Parkinson's disease and more recently for smoking cessation. In the beginning of MAO inhibitor therapy for depression, MAO inhibitors produced serious and sometimes fatal side effects due to hypertension because of the interaction between the drug and vasoactive amines such as tyramine normally contained in aged cheese, pickled meat, and red wine. MAO is protective in that it breaks down tyramine which causes elevations in blood pressure [196]. One way to address this problem is by developing subtype selective MAO inhibitors such as L-deprenyl and also by developing reversibly binding MAO inhibitors [189].

MAO B plays an important role in the metabolism of dopamine. L-deprenyl, an irreversible inhibitor of MAO B, and L-DOPA are sometimes prescribed together for treatment of Parkinson's disease, a disease in which the dopamine-producing cells in the substantia nigra die [197, 198]. L-DOPA is converted to dopamine in the brain. This dopamine is essential to transmit the signal of muscle movement from the substantia nigra to the corpus striatum. However, hydrogen peroxide which is a byproduct of MAO-catalyzed oxidation is a potential source of reactive oxygen species that is damaging to mitochodrial DNA and dopamine neuron. Thus, MAO inhibitors, such as L-deprenyl, have been proposed to have neuroprotective properties.

Many inhibitors of MAO have been developed as a treatment for psychiatric diseases like depression. Representative MAO inhibitors are shown below in Figure 4-3. MAO inhibitors can be categorized into two groups; selective or nonselective, and reversible or irreversible. At the beginning stage of MAO inhibitor development, nonselective inhibitors such as phenelzine, tranylcypromine, and pargyline were used to inhibit both MAO A and MAO B. Later, selective MAO inhibitor such as clorgyline, moclobemide, esuprone, L-deprenyl (also known as selegiline), and lazabemide (also known as Ro 19-6327) came to be used. Clorgyline, moclobemide, and, esuprone preferentially bind to MAO A. Selegiline, and lazabemide are selective inhibitors for MAO B.

These inhibitors are also divided into two groups depending on the mode of inhibition. Irreversible MAO inhibitors denature the enzyme by covalently binding to the active site in MAO [199]. Clorgyline, L-deprenyl, and pargyline are representative irreversible MAO inhibitors. Since they covalently bind to MAO, the efficacy of the drug will persist for several weeks after administration until the enzyme-inhibitor complex is replaced by new MAO [200]. After 10 mg/day administration for one week followed by drug withdrawal, the half-life of MAO B recovery was determined to be approximately 40 days [201]. On the other hand, after treatment with reversible inhibitors such as lazabemide and moclobemide, enzyme activity recovers rapidly [202]. When they were released from the enzyme, they no longer have an activity as an inhibitor because they changed to their corresponding aldehyde [203]. That is, the enzyme-inhibitor complex acts in a reversible mode. A PET study also proved that lazabemide is

selective for MAO B, and MAO B activity recovers in about a day after a 50 mg/dose [202].

Several MAO inhibitors have been labeled for PET studies by substituting the equivalent element with ^{11}C, ^{13}N or ^{18}F. These tracers are categorized into MAO A selective and MAO B selective tracers, and irreversible vs. reversible as shown in Figure 4-4. [^{11}C]Harmine, a selective MAO A inhibitor, is suitable for PET study in monkeys and humans, however, [^{11}C]brofaromine, [^{11}C]harmaline, and [^{11}C]clorgyline could not produce good images in monkeys [204, 205]. [^{11}C]Clorgyline shows species differences; whereas it is a good radiotracer in humans, it does not bind to MAO A in monkeys [206]. [^{11}C]Brofaromine has been used for depression studies. Labeling of the oxazolidinone ring can be achieved using [^{11}C]phosgene as labeling agent. [^{123}I]Ro 43-0463, a reversible MAO B radiotracer, has been used in single photon emission computed tomography (SPECT) [207]. [^{11}C]MD 230254 is another reversible radiotracer whose isotope source comes from [^{11}C]phosgene, and it was used to image MAO B in the brain of rats and baboons [208].

[^{11}C]Clorgyline and [^{11}C]deprenyl are irreversible inhibitors labeled with C-11 methyl group [209] via alkylation with [^{11}C]methyl iodide. They are suicide inhibitors which preferentially form a covalent bond with MAO A and MAO B respectively. They have provided information on the distribution of MAO in rat, baboon, and human [193, 194, 206, 210]. However, these suicide inhibitors bind rapidly to MAO and they are of limited utility in brain regions where MAO levels are high and blood flow is low. In this case the rate limiting step is delivery of the radiotracer to the brain and not MAO

oxidation. This problem is largely overcome by deuterium labeling in the propargyl group which reduces the rate of binding of radiotracer to MAO A but does not affect radiotracer delivery [206, 211, 212, 213]. Unlike unsubstituted [^{11}C]clorgyline, the cerebral binding of deuterated [^{11}C]clorgyline did not produce good contrast between regions with high MAO A activity and low MAO A activity due to non-specific binding in white matter which becomes more pronounced when binding to MAO A is reduced [211, 212].

MAO B activity is elevated in various brain diseases such as Alzheimer's disease, depression and epilepsy and also in normal aging. In Alzheimer's patients, MAO B is overexpressed in the brain region with senile plaque [214], and total uptake of deprenyl is increased in the brain of the patients. Increase in MAO B was also found in the brain of epilepsy patients [215] due to elevations in glia cells which occur in normal aging and in brain injury [216]. Postmortem study reported that MAO B started to increase in the brain after 50 or 60 [217]. We also have demonstrated that smoking affects the density of brain MAO A and B [218, 219]. However our PET study also showed that one cigarette does not reduce MAO density [220]. Even though long-term smoking diminished MAO, activity recovered after quitting smoking. MAO inhibition in smokers could help to understand the high rates smoking and mental disease such as depression and schizophrenia where it is speculated that smokers are self-medicating. MAO inhibition by cigarette smoke may also explain the reduced rate of Parkinson's disease in smokers [221, 222].

Because Ro 41-1049 and Ro 19-6327 are known as reversible inhibitors for MAO A and MAO B respectively, their carbon-11 radioligands are expected to be superior to

[^{11}C]clorgyline and [^{11}C]deprenyl. These radioligands will be important tools to elucidate the functions of MAO in depression, Parkinson's disease, Alzheimer's disease, schizophrenia, and smokers.

Here we present syntheses of Ro 41-1049, Ro 19-6327, and their precursors. We also described a two step labeling reaction with hydrogen [^{11}C]cyanide; nucleophilic substitution reaction followed by reduction of the resulting labeled nitrile with sodium borohydride in presence of Raney® nickel. The production of hydrogen [^{11}C]cyanide is also presented.

2. Chemistry

2.1 General

This section is similar to that of Sec. 2.1 in Part II. However, 2-Amino-1,3-thiazole-4-carboxamide, the staring material for Ro 41-1049, was purchased from Maybridge Chemicals (Morris Plain, NJ). 5-Chloro-2-cyanopyridine, the starting material for Ro 19-6327, was purchased from Matrix Scientific (Columbia, SC).

2.2 Experimental

2.2.1 Synthesis of Ro 41-1049

Ro 41-1049 and its precursors (**9**) were synthesized by following scheme 4-1.

2.2.1.1 Ethyl 2-amino-5-bromo-1,3-thiazole-4-carboxylate (2)

Compound **2** was prepared by the application of the reaction to synthesize ethyl 2-amino-5-chloro-1,3-thiazole-4-carboxylate (**3**) from ethyl 2-amino-1,3-thizole-4-carboxylate (**1**) [223]. To a solution of ethyl 2-amino-1,3-thiazole-4-carboxylate (**1**,

29.03 mmol, 5.00 g) in acetonitrile (116 ml) was added N-bromosuccimide (NBS, 31.94 mmol, 5.74 g), and the mixture refluxed for three hours. The reaction mixture was evaporated in vacuo, and ethyl acetate (116 ml) and charcoal (5 g) were added to the reaction residue. The mixture was gently heated for one hour. The reaction mixture was filtered through silica gel in a glass funnel. The filtrate was concentrated to give Compound **2** as a yellowish powder (6.02 g, 83%); mp 110-112^{o}C, *lit*. mp 115-117^{o}C [224]. NMR spectrum was consistent with previous literature [225]. ^{1}H-NMR ($CDCl_3$): δ 1.43-1.46 (t, J=7.2 Hz, 3H), 4.43-4.48 (q, J=7.1 Hz, 2H), 6.03 (s, 2H). ^{13}C NMR: δ 160.88, 150.43, 142.04, 135.87, 62.14, 14.63. GC-MS (**2**) m/z calcd for $C_6H_7N_2O_2SBr$ (M^+), 249.94; found (M^+) 250 and 252.

*2.2.1.2 Ethyl 2-amino-5-chloro-1,3-thiazole-4-carboxylate (**3**)*

Compound **3** was prepared by previous literature procedure [223]. N-Chlorosuccimide (NCS, 31.94 mmol, 4.27 g) was refluxed with Compound **1** in acetonitrile (116 ml) to give Compound **3** as a yellow solid (5.20 g, 87%). NMR was consistent with previous literature [223]. ^{1}H-NMR ($CDCl_3$): δ 1.33-1.37 (t, J=7.1 Hz, 3H), 4.34-4.39 (q, J=7.1 Hz, 2H), 6.04 (s, 2H). ^{13}C NMR: δ 164.27, 161.21, 137.19, 122.95, 61.91, 14.65.

*2.2.1.3 Ethyl 5-bromo-1,3-thiazole-4-carboxylate (**4**)*

This reaction was conducted according to previous procedure reported by Kanao et. al. [226]. To a tert-butyl nitrite (3.92 mmol, 0.52 ml) solution in *N*,*N*-dimethylformamide (DMF, 4.4 ml) at 50^{o}C was added ethyl 5-chloro-2-amine-1,3-

thiazole-4-carboxylate (**2**, 2.61 mmol, 0.656 g). The resulting solution was heated to 70^{o}C with stirring for an hour. The crude reaction mixture was purified by column chromatography on silica gel eluting with a mixture of ethyl acetate:hexane (25:75) co-solvent to give Compound **4** as a yellow powder (0.279 g, 45%); mp 81-82^{o}C, *lit.* mp 75-79^{o}C [224]. NMR spectrum was consistent with previous literature [225]. ^{1}H-NMR ($CDCl_3$): δ 1.40-1.44 (t, J=7.1 Hz, 3H), 4.41-4.46 (q, J=7.1 Hz, 2H), 8.66 (s, 1H). ^{13}C NMR: δ 160.88, 150.43, 142.04, 135.87, 62.14, 30.07, 14.63. GC-MS (**4**) m/z calcd for $C_6H_6NO_2SBr$ (M^+), 234.93; found (M^+) 235 and 237.

*2.2.1.4 Ethyl 5-chloro-1,3-thiazole-4-carboxylate (**5**)*

Compound **5** was synthesized by same method used for the preparation of Compound **4**. Compound **3** (5.0 g, 24.2 mmol) was stirred together with *t*-butyl nitrite (4.8 ml, 40.4 mmol) in DMF (40 ml) to give Compound **5** as a yellow powder (3.54 g, 76%); mp 90-92^{o}C. ^{1}H-NMR ($CDCl_3$): δ 1.40-1.44 (t, J=7.1 Hz, 3H), 4.41-4.46 (q, J=7.1 Hz, 2H), 8.66 (s, 1H). ^{13}C NMR: δ 160.88, 150.43, 142.04, 135.87, 62.14, 14.63. GC-MS (**5**) m/z calcd for $C_6H_6N_2O_2SCl$ (M^+), 190.98; found (M^+) 191.

*2.2.1.5 Ethyl 5-(3'-fluorophenyl)-1,3-thiazole-4-carboxylate (**6**)*

This reaction was carried out by the application of Suzuki coupling procedure published by Hodgett et. al. [227] and Thomson et. al. [228]. To a stirred mixture of tetrakis(triphenylphosphine) palladium (0) (1.5 mmol, 1.73 g) and either ethyl 5-bromo-1,3-thizole-4-carboxylate (**4**, 10.00 mmol, 2.36 g) or ethyl 5-chloro-1,3-thizole-4-carboxylate (**5**, 10.00 mmol, 2.22 g) in toluene (20 ml) at room temperature was added 2

M sodium carbonate solution (20.00 mmol, 10 ml) and 3-fluorophenyl boronic acid (12.00 mmol, 1.68 g). The vigorously stirred solution was then heated at 80^{o}C for 1.5 hours. The reaction mixture was cooled to room temperature and diluted with 2 M sodium carbonate solution (30 ml), then extracted with ethyl acetate (40 ml). The organic layer was dried using anhydrous magnesium sulfate, filtered, and evaporated in vacuo. Column chromatography of the organic residue eluting with ethyl acetate:hexane=33:67 co-solvent afforded Compound **6** as a yellow powder (2.09 g, 83% from Compound **4** and 1.73 g, 69% from Compound **5**). GC-MS (**6**) m/z calcd for $C_{12}H_{10}NO_2SF$ (M^+), 251.04; found (M^+) 251. ^{1}H-NMR ($CDCl_3$): δ 1.25-1.28 (t, J=7.1 Hz, 3H), 4.29-4.35 (q, J=7.1 Hz, 2H), 7.09-7.16 (m, 1H), 7.23-7.28 (m, 2H), 7.33-7.42 (m, 1H), 8.81 (s, 1H). ^{13}C NMR: δ 163.39, 161.68, 160.94, 151.71, 151.36, 144.81, 141.61, 132.07, 131.99, 130.01, 129.81, 129.72, 129.30, 128.18, 125.89, 125.86, 117.36, 117.13, 116.37, 116.16, 61.51, 14.04.

2.2.1.6 5-(3'-Fluorophenyl)-1,3-thiazole-4-carboxamide (7)

Compound **7** was prepared by adapting a literature procedure described by Oh et. al. [229]. To a solution of ethyl 5-(3-fluorophenyl)-1,3-thiazole-4-carboxylate (**6**, 5.178 mmol, 1.301 g) in methanol (52 ml) was added ammonium hydroxide solution (28% aqueous solution, 369 mmol, 52 ml), and reaction mixture stirred for 2 days at room temperature. The solution was diluted with 0.1% HCl solution, and extracted with ethyl acetate. The organic layer was dried using anhydrous magnesium sulfate, filtered, and evaporated to remove solvent. The residue was crystallized using hexane-ethyl acetate co-solvent to give Compound **7** as a white powder (1.022 g, 89%); mp 175-176^{o}C. ^{1}H-NMR (DMSO-d_6): δ 7.24-7.29 (td, J=8.2 Hz, 2.6 Hz, 1H), 7.37-7.39 (dd, J=7.6 Hz, 0.8

Hz, 1H), 7.44-7.48 (m, 2H), 7.58 (s, 1H), 7.83 (s, 1H), 9.15 (s, 1H). ^{13}C NMR (DMSO-d_6): δ 163.32, 162.72, 160.30, 152.90, 144.44, 139.56, 139.53, 132.63, 132.54, 130.11, 130.03, 126.03, 126.01, 116.83, 116.60, 115.61, 115.40. HRMS (**7**, DEI) m/z calcd for $C_{10}H_7FN_2OS$ (M^+), 222.0263; found ($M-H^+$) 221.0182.

*2.2.1.7 5-(3'-Fluorophenyl)-1,3-thiazole-4-(N-hydroxymethyl)carboxamide (**8**)*

To a 5-(3'-fluorophenyl)-1,3-thiazole-4-carboxamide (**7**, 2.084 mmol, 0.463 g) and potassium carbonate (0.2084 mmol, 0.0288 g) mixture in THF (3 ml) at room temperature was added formaldehyde (37% aqueous solution, 20.84 mmol, 1.56 ml), and the mixture heated to 50^{o}C until the mixture became clear. The resulting solution was stirred at room temperature for one day. The solution was diluted with ice water and extracted with ethyl acetate. The combined organic layers were dried using anhydrous magnesium sulfate, filtered, and evaporated in vacuo. The residue was purified by recrystallization using ethyl acetate-hexane co-solvent to give Compound **8** as a colorless solid (0.429 g, 82%); mp 124-125^{o}C. ^{1}H-NMR ($CDCl_3$): δ 3.65-3.69 (t, J=7.4 Hz, 1H), 4.88-4.91 (t, J=6.8 Hz, 1H), 7.10-7.15 (m, 1H), 7.32-7.39 (m, 3H), 8.42 (s, 1H), 8.70 (s, 1H). ^{13}C NMR ($CDCl_3$): δ 163.36, 162.42, 160.91, 150.99, 143.09, 142.44, 131.85, 131.77, 129.67, 129.58, 126.14, 126.11, 117.59, 117.36, 116.35, 116.14, 64.57. LC-MS (**8**) m/z calcd for $C_{11}H_9FN_2O_2S$ (M^+), 252.0369; found ($M+H^+$) 253.0

*2.2.1.8 5-(3'-Fluorophenyl)-1,3-thiazole-4-(N-acetoxymethyl)carboxamide (**9**)*

The procedure to prepare compound **9** was adopted from work published by Höfle et. al. [230]. To a stirred mixture of 5-(3-fluorophenyl)-1,3-thiazole-4-(*N*-

hydroxymethyl)carboxamide (**8**, 2.98 mmol, 0.751 g) and 4-(*N*,*N*-dimethyl) aminopyridine (DMAP, 4.46 mmol, 0.545 g) in anhydrous THF (60 ml) was added acetyl anhydride (4.46 mmol, 0.42 ml) dropwise, and the resulting solution was stirred for 30 minutes at room temperature. The solution was then diluted with ice water, and extracted with ether. The ether solution was dried using anhydrous magnesium sulfate, filtered, and evaporated. Recrystallization of the residue with ethyl acetate-hexane co-solvent afforded Compound **9** as a yellowish solid (0.769 g, 88%); mp 142-143^{o}C. ^{1}H-NMR ($CDCl_3$): δ 2.08 (s, 3H), 5.39-5.41 (d, J=7.5 Hz, 2H), 7.11-7.16 (m, 1H), 7.34-7.40 (m, 3H), 8.50 (s, 1H), 8.71 (s, 1H). ^{13}C NMR ($CDCl_3$): δ 171.83, 163.57, 161.57, 161.12, 151.08, 143.95, 143.93, 142.22, 131.87, 131.78, 129.87, 129.78, 126.40, 126.37, 117.86, 117.62, 116.61, 116.40, 64.21, 21.16. HRMS (**9**, NBA Matrix) m/z calcd for $C_{13}H_{11}FN_2O_3S$ (M^+), 294.0474; found ($M+Na^+$) 317.0372

*2.2.1.9 5-(3-Fluorophenyl)-1,3-thiazole-4-(N-cyanomethyl)carboxamide (**10**)*

A mixture of 5-(3-fluorophenyl)-1,3-thiazole-4-(*N*-acetoxymethyl)carboxamide (**9**, 0.680 mmol, 0.200g) and potassium cyanide (2.379 mmol, 0.155 g) in methyl sulfoxide (DMSO, 7.0 ml) was stirred for 2 hours at room temperature. The resulting solution was then diluted with 10 ml of water, and extracted with ether. The combined organic layers were dried using anhydrous magnesium sulfate, filtered, and evaporated in vacuo. The residue was purified by recrystallization using ethyl acetate-hexane co-solvent to give Compound **10** as a yellowish solid (0.133 g, 75%); mp 142-143^{o}C. ^{1}H-NMR (Methanol-d_4): δ 4.28 (s, 2H), 7.16-7.21 (m, 1H), 7.35-7.39 (m, 2H), 7.42-7.47 (m, 1H), 8.98 (s, 1H). ^{13}C NMR (Methanol-d_4): δ 165.06, 163.96, 162.62, 153.96, 144.18,

144.16, 143.66, 133.70, 133.62, 131.30, 131.22, 127.32, 127.29, 118.43, 118.20, 117.67, 117.26, 117.05, 28.16. HRMS (**10**, DEI) m/z calcd for $C_{12}H_8FN_3OS$ (M^+), 261.0372; found ($M+Na^+$) 261.1767

2.2.1.10 5-(3'-Fluorophenyl)-1,3-thiazole-4-(N-2'-aminoethyl)carboxamide (Ro 41-1049)

The procedure for reduction of the nitrile (**10**) was modified from previous literature method for nitrile reduction by Egli [231]. A mixture of 5-(3'-fluorophenyl)-1,3-thiazole-4-(cyanomethyl)carboxamide (**10**, 0.765 mmol, 0.200 g), sodium borohydride (7.65 mmol, 0.290 g), sodium carbonate monohydrate (7.65 mmol, 0.949 g), and Raney®-nickel (Raney® nickel 2800 suspension in water, 6 g) in methyl alcohol (60 ml) was stirred for one hour at room temperature. The resulting solution was passed through celite to remove nickel catalyst, and evaporated *in vacuo*. The residue was further separated by column chromatography eluting with ethyl aceate:hexane (2:1) co-solvent, ethyl acetate, and then with methanol:28% ammonia solution=100:1 to afford Ro 41-1049 as a free base (0.096 g, 42%, yellowish solid); mp 199-203°C, *lit.* mp 243-246°C for Ro 41-1049 HCl Salt [232]. LC-MS (Ro 41-1049) m/z calcd for $C_8H_{10}ClN_3O$ (M^+), 265.07; found (M^+) 266.1 ^{1}H-NMR (DMSO-d_6): δ 2.63-2.67 (t, J=6.4 Hz, 2H), 2.83 (broad s, 4H), 3.19-3.23 (q, J=6.2 Hz, 2H), 7.25-7.28 (m, 1H), 7.35-7.38 (m, 1H), 7.43-7.47 (m, 2H), 8.47 (s, 1H), 9.16 (s, 1H). ^{13}C NMR (Methanol-d_4): δ 162.69, 161.37, 160.27, 153.03, 144.20, 139.26, 139.24, 132.54, 132.45, 130.07, 129.99, 126.06, 126.04, 116.90, 116.67, 115.60, 115.40, 42.07, 41.03.

*2.2.1.11 5-(3'-Fluorophenyl)-1,3-thiazole-4-(N-2'-aminoethyl)carboxamide (Ro 41-1049) from Compound **6**.*

An ethyl 5-(3'-fluorophenyl)-1,3-thiazole-4-carboxylate (**6**, 1.99 mmol, 0.500 g) solution in ethylene diamine (10 ml) was stirred for 2.5 hours at 50^{o}C. The solvent was removed in vacuo over 2 hours. The residue was then purified with methanol:28% ammonia solution (200:1) co-solvent by column chromatography to give isolated product (0.459 g, 87%). NMR spectrum was consistent with previous NMR data.

2.2.2 Synthesis of Ro 19-6327 and its precursor

Ro 19-6327 and its precursor (**14**) were prepared according to the Scheme 4-2.

*2.2.2.1 5-Chloropyridine-2-carboxamide (**12**)*

Compound (**12**) was prepared by procedures adopted from literature. [233]. To a 5-chloro-2-cyanopyridine (**11**, 7.22 mmol, 1.00 g) in water (40 ml) was added hydrogen peroxide (35% aqueous solution, 36.09 mmol, 3.0 ml) and potassium hydroxide (10.104 mmol, 0.567 g). The reaction mixture was gently heated to 40^{o}C, and cooled to room temperature. After overnight stirring at room temperature, it was filtered, and washed with toluene. The residue was dried overnight dry to give Compound **12** as a white powder (1.047 g, 93%); mp 116-118^{o}C, *lit.* mp 200-201^{o}C [234]. ^{1}H-NMR ($CDCl_3$): δ 5.75 (s, 1H), 7.68 (s, 1H), 7.83-7.85 (dd, J=8.4 Hz, 2.4 Hz, 1H), 8.16-8.18 (d, J=8.3 Hz, 1H), 8.53-8.54 (d, J=2.2 Hz, 1H). ^{13}C NMR ($CDCl_3$): δ 165.74, 147.61, 147.35, 137.06, 135.40, 123.52. GC-MS (**12**) m/z calcd for $C_6H_5N_2OCl$ (M^+), 156.01; found (M^+) 156.

*2.2.2.2 5-Chloropyridine-2-(N-hydroxymethyl)carboxamide (**13**)*

Compound **13** was prepared as outlined for the synthesis of Compound **8**, but here the reaction was run overnight at room temperature. (See Sec. 2.2.1.7) Compound **12** (10.0 mmol, 1.57 g) in THF was treated with formaldehyde (37% aqueous solution, 100 mmol, 7.5 ml) in the presence of potassium carbonate (0.5 mmol, 0.069 g) to give Compound **13** as a white powder after recrystallization (1.98 g, 86.4%); mp 107-108^{o}C. ^{1}H-NMR ($CDCl_3$): δ 3.43 (s, 1H), 5.00-5.02 (d, J=6.7 Hz, 1H), 7.83-7.86 (dd, J=8.4 Hz, 2.3 Hz, 1H), 8.14-8.16 (d, J=8.3 Hz, 1H), 8.526-8.531 (d, J=2.0 Hz, 1H), 8.75 (s, 1H). ^{13}C NMR ($CDCl_3$): δ 165.11, 147.61, 147.48, 137.36, 135.77, 123.63, 64.99. LC-MS (**13**) m/z calcd for $C_7H_7ClN_2O_2$ (M^+), 186.0196; found (M^+) 186.8

*2.2.2.3 5-Chloropyridine-2-(N-acetoxymethyl)carboxamide (**14**)*

The procedure was similar to that used for the synthesis of Compound **9** except that the reaction was run for one hour at room temperature. (See Sec. 2.2.1.8) Compound **13** (5.627 mmol, 1.050 g) was treated with acetic anhydride (6.753 mmol, 0.64 ml) in the presence of DMAP (6.753 mmol, 0.823 g) in THF (100 ml) to afforded Compound **14** as a white powder after recrystallization (1.241 g, 96%); mp 128-131^{o}C. ^{1}H-NMR ($CDCl_3$): δ 2.09 (s, 3H), 5.47-5.49 (d, J=7.5 Hz, 2H), 7.84-7.86 (dd, J=8.4 Hz, 2.4 Hz, 1H), 8.17-8.19 (d, J=8.4 Hz, 1H), 8.53-8.54 (d, J=1.8 Hz, 1H), 8.85 (s, 1H). ^{13}C NMR ($CDCl_3$): δ 171.91, 164.43, 147.78, 147.39, 137.55, 136.08, 124.12, 64.45, 21.29. HRMS (**14**, NBA Matrix) m/z calcd for $C_9H_9ClN_2O_3$ (M^+), 228.0302; found ($M+Na^+$) 251.0205

*2.2.2.4 5-Chloropyridine-2-(N-cyanomethyl)carboxamide (**15**)*

The procedure was similar to that used for the synthesis of Compound **10** except here the reaction was run for one hour at room temperature and the product was purified by column chromatography by ethyl acetate:hexane=25:75 co-solvent instead of recrystallization. (See Sec. 2.2.1.9) Compound **14** (5.426 mmol, 1.241 g) was treated with potassium cyanide (18.99 mmol, 1.237 g) in DMSO (180 ml) at room temperature to give Compound **15** as a white powder after recrystallization (0.586 g, 55%); mp 129-131^{o}C. ^{1}H-NMR ($CDCl_3$): δ 4.41-4.43 (d, J=6.1 Hz, 2H), 7.86-7.89 (dd, J=8.4 Hz, 2.3 Hz, 1H), 8.16-8.18 (d, J=8.4 Hz), 8.24 (s, 1H), 8.54-8.55 (d, J=2.3 Hz, 1H). ^{13}C NMR ($CDCl_3$): δ 163.76, 147.69, 146.58, 137.57, 136.20, 123.83, 15.85, 27.73. HRMS (**15**, DEI) m/z calcd for $C_8H_6ClN_3O$ (M^+), 195.0199; found (M^+) 195.0198

2.2.2.5 5-Chloropyridine-2-(N-2-aminoethyl)carboxamide (Ro 19-6327)

The procedure was the same as outlined for the reaction for the synthesis of Ro 41-1049. (See Sec. 2.2.1.10) A mixture of Compound **15** (1.022 mmol, 0.200 g), sodium borohydride (10.22 mmol, 0.387 g), Raney® nickel (water suspension solution, 6 g), and sodium carbonate monohydrate (10.22 mmol, 1.268 g) in methanol (60 ml) was stirred for one hour at room temperature to give Ro 19-6327 as a white powder after purification by column chromatography (0.076 g, 37%); mp 175-177^{o}C. LC-MS (Ro 19-6327) m/z calcd for $C_{12}H_{12}FN_3OS$ (M^+), 199.05; found (M^+) 200.1 ^{1}H-NMR ($CDCl_3$): δ 1.63 (s, 3H), 2.95-2.97 (t, J=5.5 Hz, 2H), 3.51-3.55 (q, J=5.5 Hz, 2H), 7.81-7.83 (d, J=8.4 Hz, 1H), 8.14-8.16 (d, J=8.3 Hz, 1H), 8.22 (s, 1H), 8.50 (s, 1H). ^{13}C NMR ($CDCl_3$): δ 163.97, 148.23, 147.28, 137.24, 135.10, 123.41, 42.29, 41.71

2.3 Synthesis of [N-(2-^{11}C-2-aminoethyl)]Ro 41-1049

Hydrogen [^{11}C]cyanide was produced by known procedure described in Sec 2.5. A diagram of home-made hydrogen cyanide module is shown in Figure 4-5. A diagram of [*N*-(2-^{11}C-2-aminoethyl)]Ro 41-1049 synthesis system was shown in Figure 4-8. The generated hydrogen [^{11}C]cyanide and residual ammonia, hydrogen, [^{11}C]methane, and nitrogen were passed through a 4 g of citric acid monohydrate trap before they transfer to the reaction vessel. [^{11}C]Cyanide was trapped for 10 minutes in a mixture of potassium acetate (1.0 mg) and 4,7,13,16,21,24-hexaoxa-1,10-diazabicyclo[8,8,8]hexacosane (kryptofix222, 3.9 mg) in DMSO (0.2 ml) at room temperature until the radioactivity detected by NaI radioactivity detector reached maximum. After trapping, precursor (**9**, 1.0 mg) dissolved in 0.2 ml of DMSO was added to the resulting solution, and the mixture left at room temperature for 3 minutes. The solution was then diluted with 1.0 ml of water, and a small portion of solution was taken for analysis. The rest of solution was passed through C18 Sep-Pak® conditioned with methanol then water. The Sep-Pak® was first washed with 2 ml of water, and then with 3 ml of ether. The ether eluent was passed through 1 g of anhydrous sodium sulfate, and collected in second reaction vessel. The ether was then evaporated in a warm water bath, and the remaining residue diluted with 0.3 ml of Raney® nickel solution in methanol made by diluting 1 g of Raney® nickel slurry with 20 ml of methanol. A sodium carbonate(4.1 mg) and sodium borohydride (0.7 mg) mixture solution in water (0.05 ml) was then added, and the resulting mixture stirred for 5 minutes at room temperature. The solution was diluted with 1 mL of an acetonitrile/0.1 M ammonium formate (25%:75%) solution, and passed through an Alltech® HPLC syringe filter (0.22 μm, Deerfield, IL) to remove nickel catalyst prior to

HPLC injection. The reaction mixture was eluted with 25% acetonitrile:75% 0.1 M ammonium formate co-solvent at a flow rate of 4.0 mL/min on a Phenomenex Luna C18 (2) semi-preparative column (250 mm×10 mm, 5 μm) with UV (254 nm) and radioactivity detector until 10 minutes. After 10 minutes, and the solution was charged to 50% acetonitrile:50% 0.1 M ammonium formate solution. [*N*-(2-^{11}C-2-aminoethyl)]Ro 41-1049 eluted around 9.2-9.8 min. The HPLC solvent containing [^{11}C]product was then removed by a rotary evaporation with the aid of acetonitrile to azeotropically remove water. The residue was dissolved in 1 mL of sterile water, and was passed through a 0.22 μm Millipore® filter (Millipore Corp., Billerica, MA) into a sterile vial. The total synthesis time was 60 minutes. Radiochemical yield as determined by HPLC was 71.5±3.1% (n=4) for first step and 26.8±5.2% (n=5) for second step.

*2.4. 5-Chloropyridine-2-(N-^{11}C-cyanomethyl)carboxamide ([^{11}C]**15**)*

Hydrogen [^{11}C]cyanide generated by cyanide module was delivered and trapped in a solution of kryptofix222 (4.9 mg) and potassium acetate (1.3 mg) in 0.2 ml of DMSO at room temperature. Compound **14** in DMSO (0.2 ml) was then added to the reaction vessel, and the mixture was heated for 3 minutes at 40^{o}C. The reaction mixture was diluted with 1 ml of water, and a 20 μl of aliquot removed for analysis by HPLC analytical system which is consisted with Phenomenex C18 (2) Luna analytical column, and UV and radioactivity detectors eluting with 30% acetonitrile and 70% 0.1 M ammonium formate HPLC solvent at a rate of 1.0 ml/min. [^{11}C]**15** eluted at 12-13.5 min.

2.5. Hydrogen [^{11}C]cyanide synthesis

Figure 4-5 shows the detailed diagram of the hydrogen [^{11}C]cyanide module which produces hydrogen [^{11}C]cyanide from [^{11}C]carbon dioxide according to the following scheme.

$$[^{11}C]CO_2 \xrightarrow[390^oC]{H_2,\ Ni} [^{11}C]CH_4 \xrightarrow[920^oC]{NH_3,\ Pt} [^{11}C]HCN$$

[^{11}C]Carbon dioxide was transferred from the target through valve #8 and trapped in a nickel furnace filled with 0.24 g of molecular sieve 4Å (Alltech Associates Inc., Deerfield, IL) and 0.19 g of nickel powder (Shimalite-Ni® (Reduced), Shimadzu Inc., Kyoto, Japan). After trapping, any untrapped waste is passed through valve #7 for disposal. Valve #4 is then closed, and start to fill with hydrogen gas through #1 valve. The nickel furnace is heated from room temperature to 390^{o}C over 3-4 minutes, and maintained at 390^{o}C for another 1-2 minutes to synthesize [^{11}C]methane after valve #3 is closed. After [^{11}C]methane synthesis, valve #2 and valve #5 were opened to feed ammonia and nitrogen+5% hydrogen carrier gas, and valve #6 was opened to transfer hydrogen [^{11}C]cyanide to reaction vessel. Valve #3 and valve #4 were also opened to release [^{11}C]methane which was then mixed with carrier gas and ammonia. Valve #7 and valve #8 were closed from target and waste, so all gas mixtures were passed through soda lime and platinum furnace which was maintained at 920^{o}C to convert [^{11}C]methane into hydrogen [^{11}C]cyanide. Unconverted [^{11}C]carbon dioxide was trapped in soda lime before it was passed through platinum furnace. Unconverted [^{11}C]methane moved faster than hydrogen [^{11}C]cyanide and passed through trapping solution and soda lime trap after

reaction vessel. We noted that when the transfer line was getting basified by ammonia, the transfer of hydrogen [^{11}C]cyanide was decreased because of retention in the line. To prevent this phenomenon, the line was passivated with 2 N hydrogen chloride in ether followed by drying before running hydrogen cyanide module. Ammonia and carrier gas were fed for 5 minutes during transfer, and then additional transfer by carrier gas was conducted by 2.25 minutes. The cyanide module was flushed with hydrogen gas for one minute, then most of hydrogen [^{11}C]cyanide was transferred during this process. After that, #5 and #6 valves were closed, and the module was reconditioned for the next run by flushing nickel furnace with hydrogen and cooling down with compressed air.

This [^{11}C]cyanide module requires considerable care in maintenance and setup in order to work reliably. Thus, it is important to take the following steps. (1) Make sure all tank valves and feed valves are open and furnaces are working. (2) Check that the platinum and nickel furnace is the controlling desired range of temperature. (3) Recondition the cyanide module before first run. (4) Acidify the transfer line by treating with 2 N hydrogen chloride in diethyl ether followed by drying with argon before each run. (5) Make sure all lines are not clogged, and all valves in the cyanide module and reaction module are in the right position. (6) Make sure that platinum wire is in the furnace as its position can be displaced from the heated zone with high gas flows preventing the conversion of [^{11}C]methane into hydrogen [^{11}C]cyanide. (7) Nickel catalyst should be regularly checked for best activity as it loses its activity after repeated runs possible due to exposure to ammonia. In such case, [^{11}C]carbon dioxide is not converted into [^{11}C]methane and the unconverted [^{11}C]carbon dioxide is retained by molecular sieve or soda lime. Nickel catalyst can be changed according to the manual of

[^{11}C]methyl iodide module. The new nickel catalyst should be activated by baking above 350^{o}C over 15 minutes in a high hydrogen flow. (8) The gas flow of nitrogen and ammonia should be checked before each run. The ideal gas balance between ammonia and carrier (nitrogen) gas was a flow of 12.5 ml/min and 25 ml/min respectively. Ammonia is a corrosive gas, therefore it causes uneven feeding from the flow control valve. Improper balance of the ammonia and carrier gas feed produces not only a low yield of hydrogen [^{11}C]cyanide, but it also causes the flow back to the nickel furnace resulting in poisoning of the nickel catalyst by ammonia. Since gas flow is changed after the run, ammonia and carrier gas flow should be realigned before each run for best performance.

3. Results and Discussion

Ro 41-1049 was synthesized from ethyl 2-amino-1,3-thiazole-4-carboxamide (**1**) in four steps, and its precursor (**9**) was synthesized in six steps (Scheme 4-1). Briefly, halogenation of Compound **1** at the 5-position of the thiazole by NBS or NCS afforded bromothiazole (Compound **2**) or chlorothiazole (Compound **3**), respectively. The amine at the 2-position of the thiazole ring for each compound was removed using tert-butyl nitrite affording Compounds **4** and **5**, which were subsequently coupled with 3-fluorophenyl boronic acid via Suzuki coupling to produce phenylthiazole (Compound **6**) in high yields [228, 235]. The ester group of Compound **6** was converted into the corresponding amide (**7**) using ammonium hydroxide. The hydroxymethyl group was then added to the amide using an excess of formaldehyde under basic conditions to produce Compound **8**, and the hydroxyl group was further acetylated by acetic anhydride

in the presence of DMAP to give precursor **9** at good yield. Alternatively, Ro 41-1049 could be obtained from Compound **6** by using excess amount of ethylene diamine as a neat reagent in as high as 87% yield. The reaction of Compound **6** with ethylene diamine proved to be a more efficient way to synthesize Ro 41-1049.

The method shown above could be compared with previous literature method shown in Scheme 4-3 [236, 237]. Both the literature method and our method took four steps to synthesize Ro 41-1049. Whereas our method took three steps to synthesize Compound **6** from starting compound, literature procedure took two steps to synthesize Compound **6**. However, our method seems to be more efficient to synthesize Ro 41-1049 because overall yield to synthesize Ro 41-1049 was 40% and 27% via chlorination and bromination respectively. Although the patent literature [236] did not report the yield the each step from Compound **16** to Ro 41-1049, the reference literature showed that overall yield from iodo-derivatives of Compound **16** to iodo-derivatives of Ro 41-1049 was 11% [237]. Therefore, our method might give an overall better yield of Ro 41-1049 than the literature procedure in spite of an additional step.

To verify that the precursor could be converted to Ro 41-1049 under conditions for carbon-11 labeling, we carried out a model reaction with non-isotopically enriched cyanide. The acetate group of Compound **9** was displaced to a cyanide group using an excess amount of potassium cyanide (3.5 eq.) at room temperature for 2 hour while stirring (76% yield). The addition of kryptofix222 (a common potassium macrochelate) increased the yield and rate of the substitution reaction (82% in 30 min at room temperature). We also screened conditions to determine the ideal solvent. The reaction

was inefficient in THF, which is likely due to the poor solubility of the potassium cyanide. Reactions in DMF were plagued by the formation of several side-products that were minimized by the use of DMSO.

When the analogous reaction using DMSO was applied to carbon-11 reactions, an additional problem was encountered. The process producing hydrogen [^{11}C]cyanide uses a stream of ammonia gas, which we found would react with precursor compound (**9**) thus destroying the compound before carbon-11 incorporation could occur. Moreover, we found that this decomposition was a general phenomenon and even heterogenous bases such as carbonate suspended in low quantities in DMSO would cause nearly complete precursor degradation. By HPLC we also determined that the precursor substrate (**9**) was even partially decomposed by kryptofix222 in DMSO. In order to address this, we screened bases to determine the most appropriate additives for the carbon-11 labeling reaction. Eventually, we settled on potassium acetate as a weak base. We found that some of Compound **9** survived in up to 4.5 eq. of potassium acetate after 10 minutes at room temperature. In parallel, we determined that a potassium acetate, kryptofix222 solution of DMSO was basic enough to efficiently trap [^{11}C]cyanide at room temperature.

To remove the residual ammonia in the gas stream used to produce hydrogen [^{11}C]cyanide so that it would not consume the precursor, we tried a number of different materials. Initially, we envisioned a simple by-pass line to allow ammonia to flow past the reaction solution as we streamed nitrogen, which we would divert through the reaction solution when hydrogen [^{11}C]cyanide which moves slowly through the system was eluting. Unfortunately, this simple solution was inadequate. Often greater than 60%

of the radioactivity (hydrogen [^{11}C]cyanide) was lost to the bypass as it eluted in the ammonia stream. Next we attempted to separate hydrogen [^{11}C]cyanide from ammonia by cold trapping (bp: hydrogen cyanide=26^{o}C, ammonia=-33^{o}C). A cold trap was installed in transfer line to collect hydrogen [^{11}C]cyanide at 0^{o}C. However, this method was not efficient either, in terms of time required for trap and release as well as overall hydrogen [^{11}C]cyanide recovery. Only one third of the radioactivity from the trap could be recovered after warming to room temperature under a constant flow of gas.

Finally, we turned to solid-phase media to scrub the residual ammonia from the gas phase as hydrogen [^{11}C]cyanide was released. A variety of ion exchange resins, silica gel, sicapent®, molecular sieve, and citric acid monohydrate were packed into in-line flow columns and used between the hydrogen [^{11}C]cyanide outlet and the reaction vessel. To detect residual ammonia penetration after passing through the trapping column, the gas was bubbled through 2 N hydrogen chloride in ether which results in a precipitate if ammonia is present. Flow was then directed through a 1 N sodium hydroxide solution to assess hydrogen [^{11}C]cyanide production. (Figure 4-6) Gas flow was checked to make sure that the trapping material (2-5 g) did not interfere with the gas flow in the system. A blank test was also attempted to calculate penetration of ammonia by running cyanide module without a trap. We found that two kinds of cation exchange resin (Dowex® 50W-X4 and Amberlite® CG-50 Type 2) trapped ammonia effectively, but also trapped the hydrogen [^{11}C]cyanide. Silica gel and molecular sieve 5Å trapped all of the ammonia and most of the hydrogen [^{11}C]cyanide (Only 7-9% of hydrogen [^{11}C]cyanide passed through to the sodium hydroxide trap). Sicapent® trapped 36% of ammonia, and it also allowed to pass 35% of hydrogen [^{11}C]cyanide. However, citric acid monohydrate (4 g)

completely removed ammonia, allowing 80% of hydrogen [^{11}C]cyanide to pass through to the hydroxide trap. Moreover, no ammonium chloride precipitate was observed in ether/HCl when using citric acid monohydrate (Table 4-1). The citric acid trap containing 4 g of citric acid monohydrate completely removed ammonia for up to two cycles of hydrogen [^{11}C]cyanide production runs.

In the substitution reaction, citric acid monohydrate (4 g) was used as trapping agent for ammonia and potassium acetate (1.0 mg) and kryptofix222 (3.9 mg) in DMSO (0.2 ml) were used to trap hydrogen [^{11}C]cyanide at room temperature in reaction vessel. After [^{11}C]cyanide trapping, the Compound **9** was loaded in 0.2 ml of DMSO, and added to the solution. After the substitution reaction for three minutes at room temperature, an aliquot was removed for analysis by HPLC (Phenomenex® Luna C18 (2) analytical column) eluting with 37% acetonitrile and 63% 0.1 M ammonium formate solution with UV and NaI radioactivity detectors. The radiochemical yield of first step was found to be 71.5±3.1% (n=4). The profile of first step reaction was shown in Figure 4-7.

Content with this set-up, we proceeded forward to the reduction of [^{11}C]**10** to form [^{11}C]Ro 41-1049. Again we modeled the reaction with "cold" (i.e. carbon-12) chemistry. The final reduction of the nitrile was attempted using various conditions including palladium on activated charcoal [238] and sodium borohydride with cobalt (II) chloride, which was a promising lead from the literature [239]. Attempts with palladium on charcoal were met with limited success so we explored other metal catalysts. After several trials of different reduction or hydrogenation conditions, hydrogenation of nitrile group in the presence of Raney® nickel gave a promising result (70% for Ro 41-1049)

[240]. The carbon-12 reaction was completed in one hour, but reaction did not appear to proceed at all within the first 10 minutes which would be required for the carbon-11 reaction. Nonetheless, we attempted the carbon-11 analogue and as predicted observed no reduction within 10 minutes. We surmised that reaction initiation might simply depend on solubility of hydrogen in the reaction medium, and looked to soluble hydrogen equivalents. We adopted a modified procedure in the previous literature using Raney® nickel with sodium borohydride, and found that the model reaction gave Ro 41-1049 in 42% of yield [231]. This reaction was also completed in one hour like hydrogenation with Raney® nickel using hydrogen, however product formation was observed within of the first 10 minutes. Our best result in 10 minutes as determined by HPLC showed 70% conversion of Compound **9** affording 41% yield of the desired product (with one major byproduct).

With suitable conditions in hand, the procedure was applied to the carbon-11 reaction. After the initial [^{11}C]cyanide displacement reaction as detailed above, the entire reaction solution was diluted with 1 ml of water and passed through C18 Sep-Pak®, and washed with additional 2 ml of water, then eluted with 3 ml of ether. The ether solution was dried by flowing through a sodium sulfate column, and transferred to second reaction vessel for the reduction step. (Figure 4-8)

The ether was evaporated from the second reaction vessel, and a solution of Raney® nickel in methanol (0.3 ml, 1 g of Raney® nickel slurry diluted with 20 ml of methanol) was added to the resulting residue. Sodium borohydride and sodium carbonate dissolved in minimum amount of water (0.05-0.1 ml) were added to the reaction mixture.

Since the second step was not water sensitive, a small amount of water was allowed in the reaction system. However, we found that too much of water deteriorated the reaction. Therefore, we kept the volume of water added as low as possible. After reaction for 5 minutes at room temperature, the radiochemical yield for [*N*-(2-^{11}C-2-aminoethyl)]Ro 41-1049 was 26.8±5.2% (n=5) based on total radioactivity after C18 Sep-Pak® treatment. The HPLC profile for second reaction step was shown in Figure 4-9.

Usually, it took 20 minutes to trap [^{11}C]cyanide in the reaction vessel. Ten more minutes were required to run first step, and transfer to second step. Another five minutes were needed to evaporate ether, and add reagents for the second step. It took another ~10 minutes to run the second step and filter the resulting solution. HPLC purification and evaporation followed by formulation required ~15 minutes. Total synthesis time was 60 minutes. Therefore, when we consider decay of carbon-11 and ~70% recovery of total radioactivity during C18 Sep-Pak® treatment, total 1.5% (decay uncorrected) of total radioactivity at the end of bombardment was acquired after 60 minutes of labeling synthesis.

Ro 19-6327 and its precursor (**14**) were synthesized by same methodology used in Ro 41-1049 except for the first step. Hydrolysis of cyanide group in 5-chloro-2-cyanopyridine (**11**) at basic condition was carried out successfully to convert into amide (**12)** at room temperature. The methodologies to prepare the rest of Compounds **13**, **14**, **15**, and Ro 19-6327 were same as the ones to prepare Compounds **8, 9, 10,** and Ro 41-1049 respectively in Ro 41-1049 synthesis. Each step in the synthesis gave good yield except cyanide substitution step (55%). However, the substitution reaction was

accelerated by the addition of kryptofix222 at 40°C (74% yield at 40°C×30 minutes determined by HPLC). When the same procedure was applied to carbon-11 chemistry like in [*N*-(2-^{11}C-2-aminoethyl)]Ro 41-1049, [^{11}C]**15** was produced at 40°C in 3 minutes with 70% radiochemical yield. The HPLC profile is shown in Figure 4-10. The UV side product peak at 12.08 minutes will not be a problem because [^{11}C]**15** will convert into final product, [*N*-(2-^{11}C-2-aminoethyl)]Ro 19-6327 which will have different retention time. The second step, reduction of [^{11}C]**15** to [*N*-(2-^{11}C-2-aminoethyl)]Ro 19-6327, is underway.

4. Conclusion and Future Work

The syntheses of Ro 41-1049, Ro 19-6327, and their precursors (**9** and **14**) were accomplished. Ro 41-1049 was synthesized by four steps, the same number of steps as the previous literature. [236, 237] The precursor (**9**) of Ro 41-1049 was synthesized by six steps, and the synthesis of Ro 41-1049 via precursor (**9**) was also accomplished in eight steps. Each step of Ro 41-1049 synthesis gave a good yield. The precursor (**14**) of Ro 19-6327 was synthesized in three steps, and Ro 19-6327 was synthesized in five steps via precursor (**14**) as a model reaction. We found that the rate of substitution reaction was increased by the addition of kryptofix222. After several trials of the final nitrile reduction step, the model reaction revealed that sodium borohydride reduction in presence of Raney nickel gave fast reduction during first 10 minutes. In the carbon-11 reaction, after optimization of base and removal of ammonia, [^{11}C]cyanide substitution of Compounds **9** and **14** occurred in 71.5±3.1% (n=4) and 70% radiochemical yield at room temperature and at 40°C respectively. [*N*-(2-^{11}C-2-aminoethyl)]Ro 41-1049 was

successfully synthesized by the same scheme in model reaction and gave up to 35% of radiochemical yield. In the future, [*N*-(2-^{11}C-2-aminoethyl)]Ro 19-6327 will be synthesized by the same scheme of [*N*-(2-^{11}C-2-aminoethyl)]Ro 41-1049 synthesis. Two radioactive compounds will be evaluated by in vitro study such as log D, plasma protein binding, and blood metabolite study. The two compounds will be used as a radiotracer to produce PET images of baboon or rat brain. Those two radiotracers are evaluated by assessing reproducibility and specificity of binding. If they successfully display specific binding in the region, the images from [*N*-(2-^{11}C-2-aminoethyl)]Ro 41-1049 and [*N*-(2-^{11}C-2-aminoethyl)]Ro 19-6327 will be compared with those from [^{11}C]clorgyline and [^{11}C]deprenyl respectively. If necessary, the kinetic parameters, B_{max}, K_d (Dissociation constant of ligand), binding potential (BP), and distribution volume (DV) will be derived and compared to each other to evaluate the properties of new radiotracers and previous ones. This will reveal whether there are advantages of the reversible MAO radiotracers over the irreversible radiotracers.

Figures, Schemes, and Table

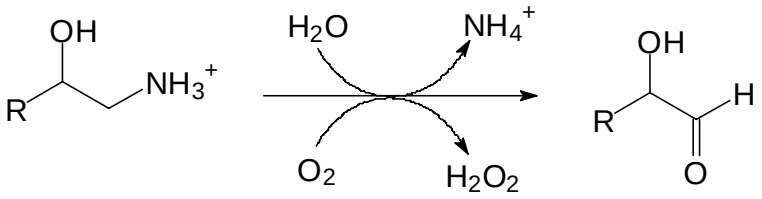

Figure 4-2. An example of monoamine oxidation by monoamine oxidase (MAO)

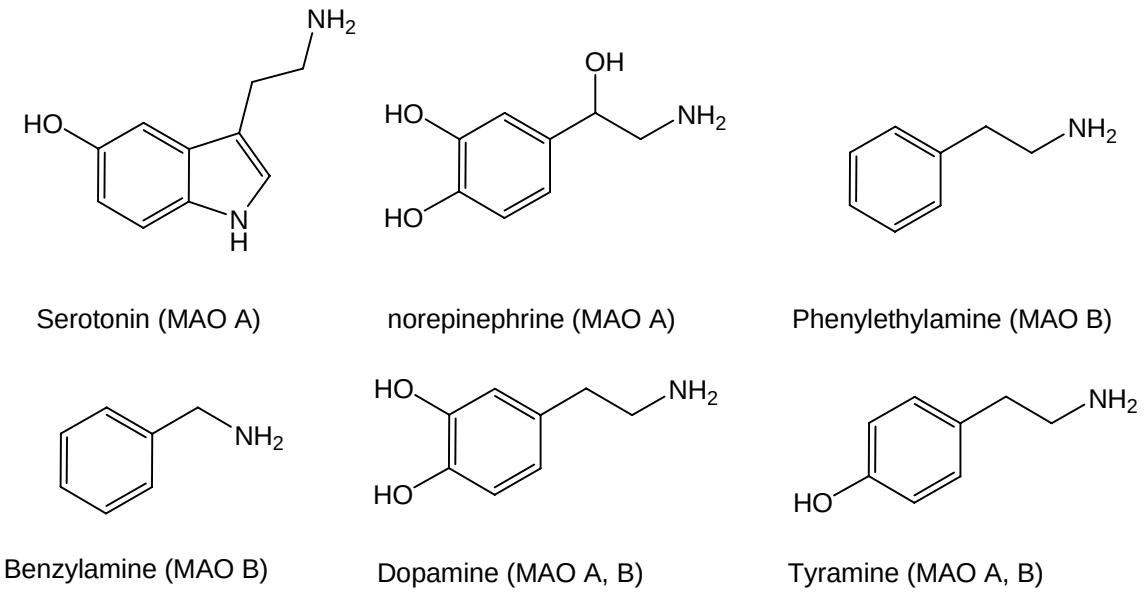

Figure 4-3. Representative substrates for MAO A and MAO B

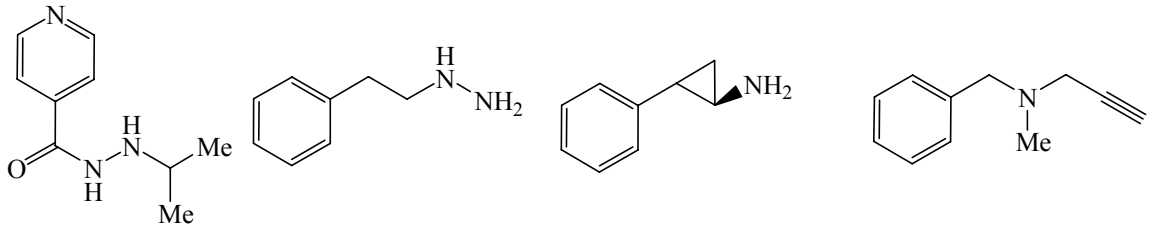

Iproniazide Phenelzine Tranylcypromine Pargyline

MAO A / MAO B Inhibitors

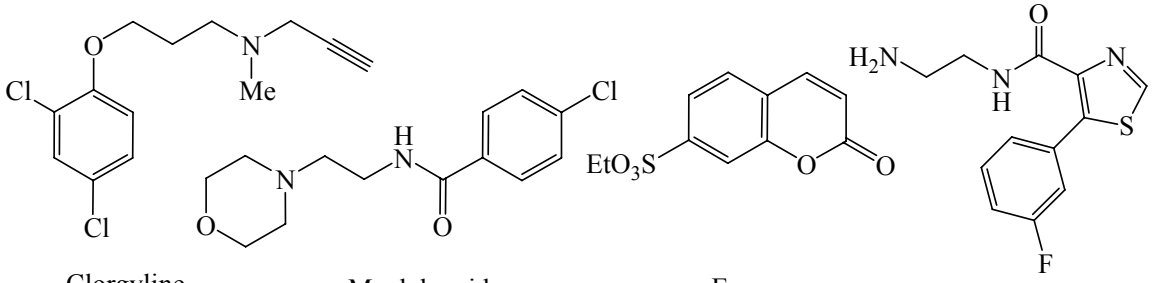

Clorgyline Moclobemide Esuprone Ro 41-1049

MAO A Specific Inhibitors

(L)-Deprenyl Lazabemide (Ro 19-6327)

MAO B Specific Inhibitors

Figure 4-4 Representative MAO inhibitors

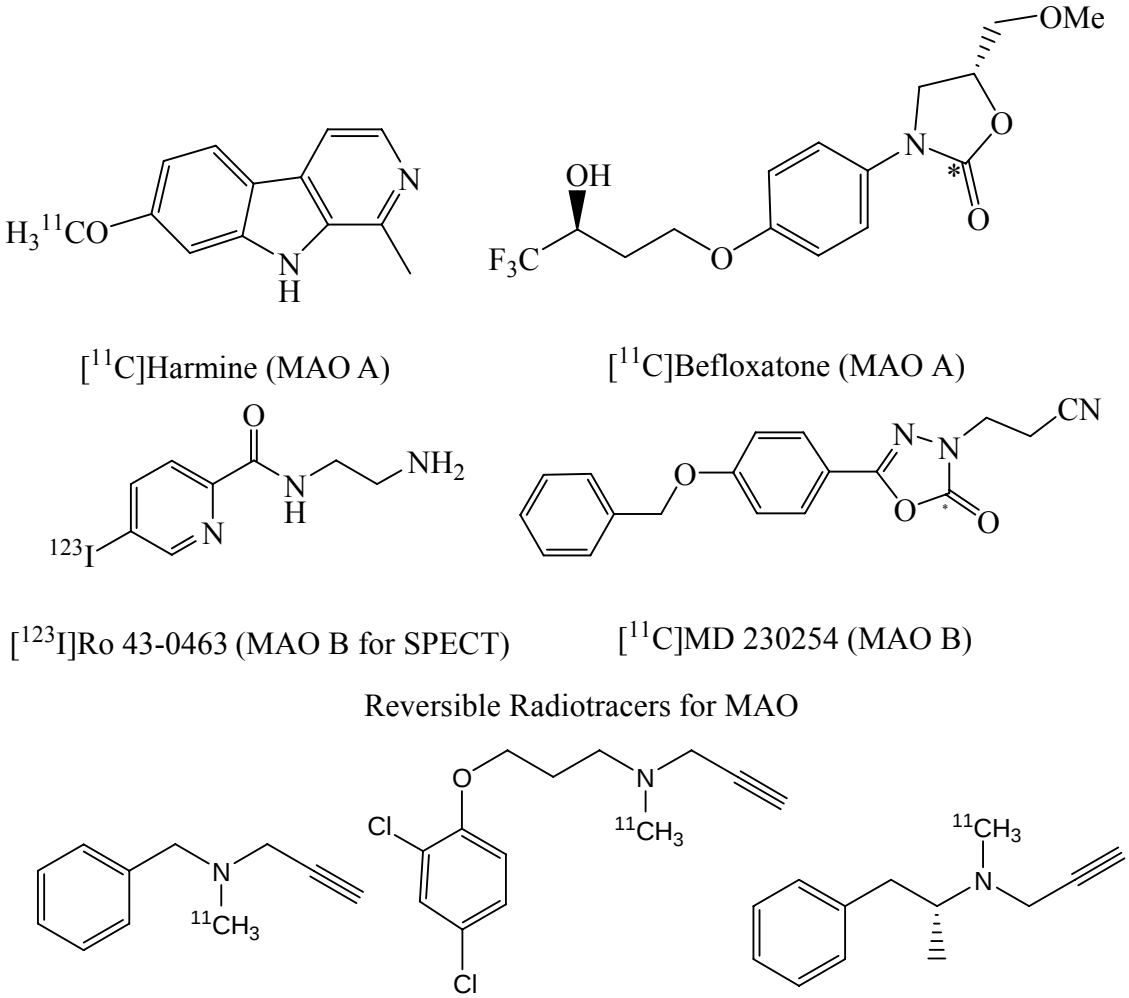

Figure 4-5. Representative PET radiotracers for MAO

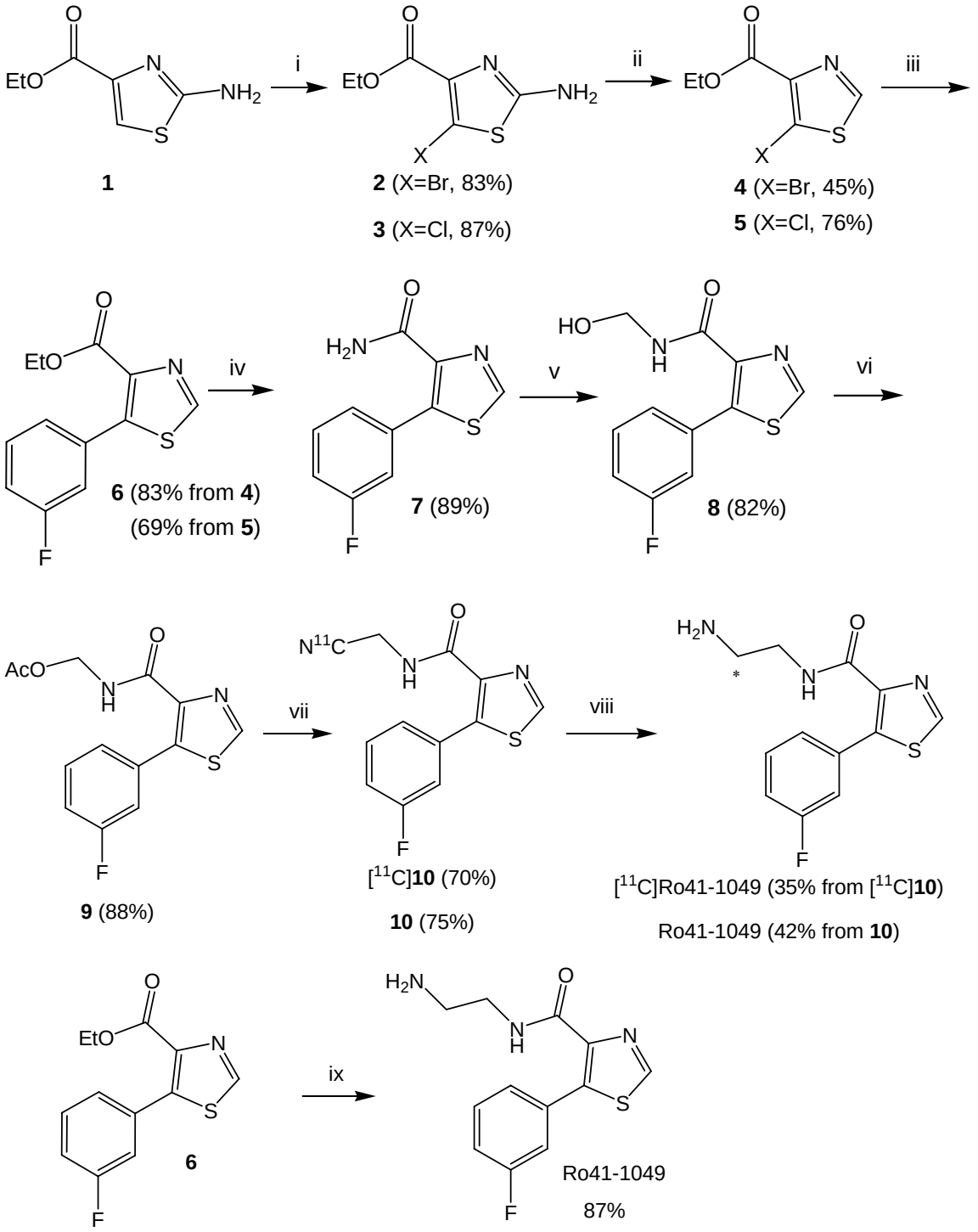

i: NBS or NCS, CH_3CN, reflux ii: t-$BuNO_2$, DMF, 50°C → 70°C iii: $Pd(PPh_3)_4$, Na_2CO_3, 3-fluorophenylboronic acid, toluene, 80°C iv: NH_4OH, MeOH, rt v: HCHO, THF, 50°C → rt, vi: Ac_2O, DMAP. THF, rt vii: KCN, DMSO, rt or KOAc, $H^{11}CN$, Kryptofix222, DMSO, rt viii: Raney®Ni, $NaBH_4$, Na_2CO_3, MeOH, rt ix: $NH_2CH_2CH_2NH_2$, 50°C

Scheme 4-1. Synthesis of Ro 41-1049, [^{11}C]Ro 41-1049 and its acetate precursor (**9**)

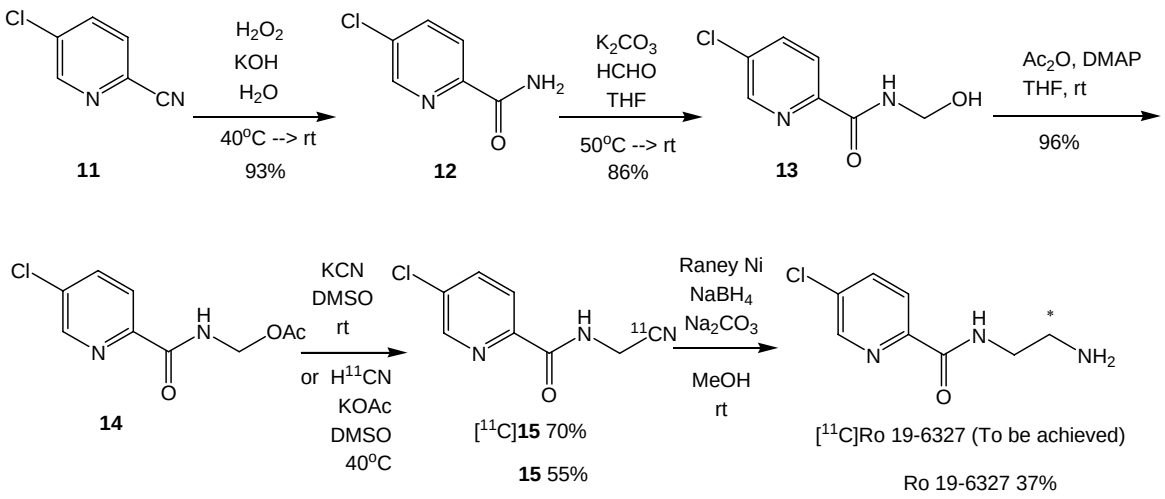

Scheme 4-2. Synthesis of [*N*-(2-[^{11}C]-2-aminoethyl)]Ro 19-6327 and its precursor (**14**)

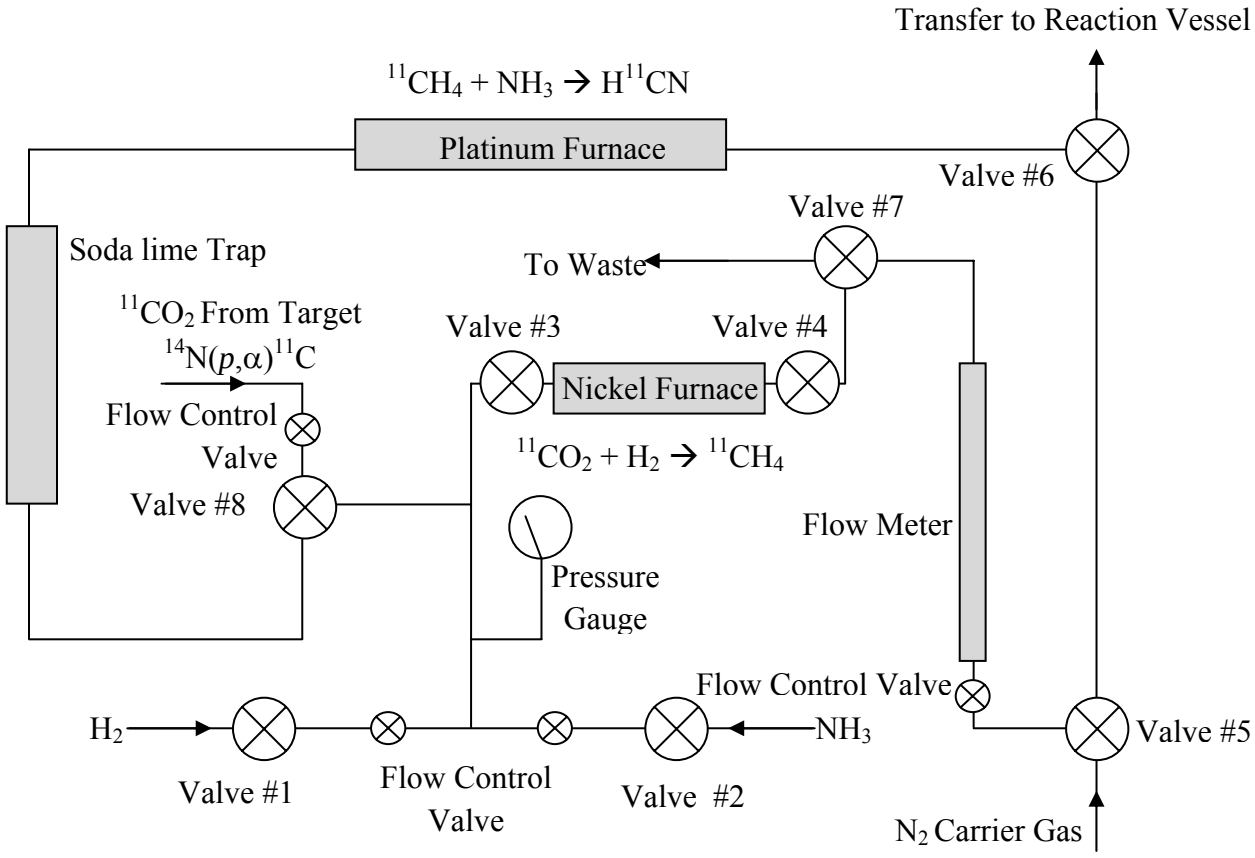

Figure 4-5. Diagram of [^{11}C]Hydrogen Cyanide Module

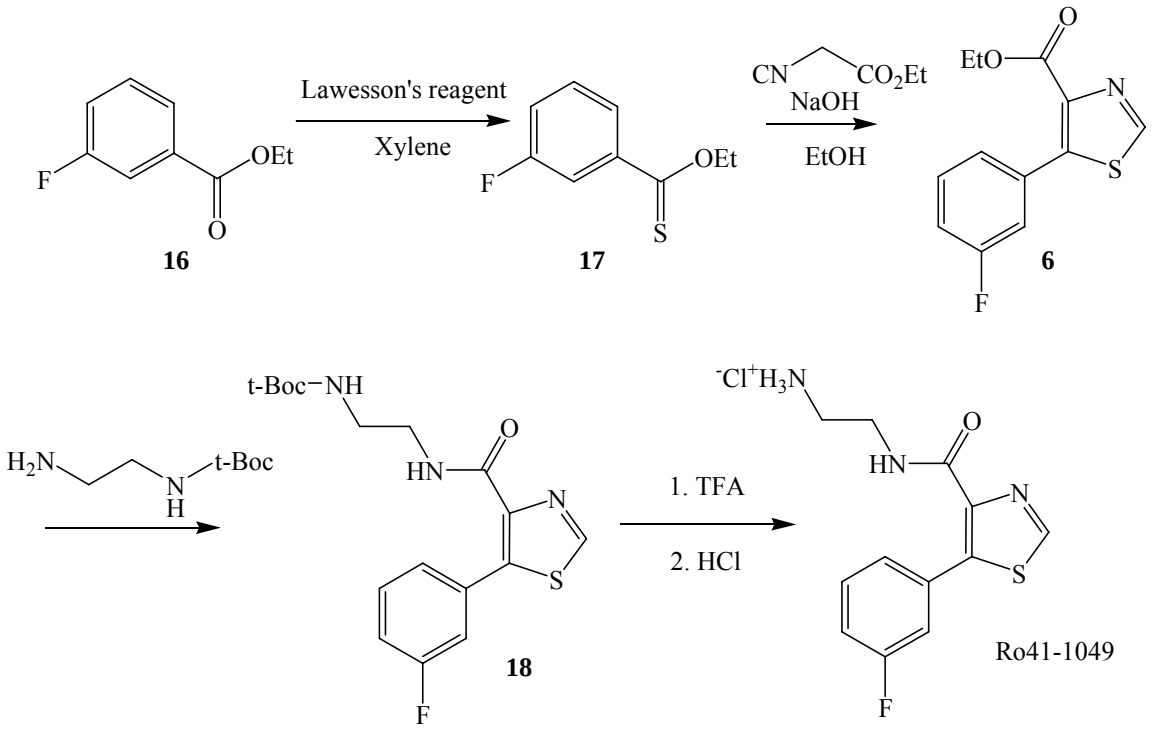

Scheme 4-3. Literature method to synthesize Ro 41-1049 [236, 237].

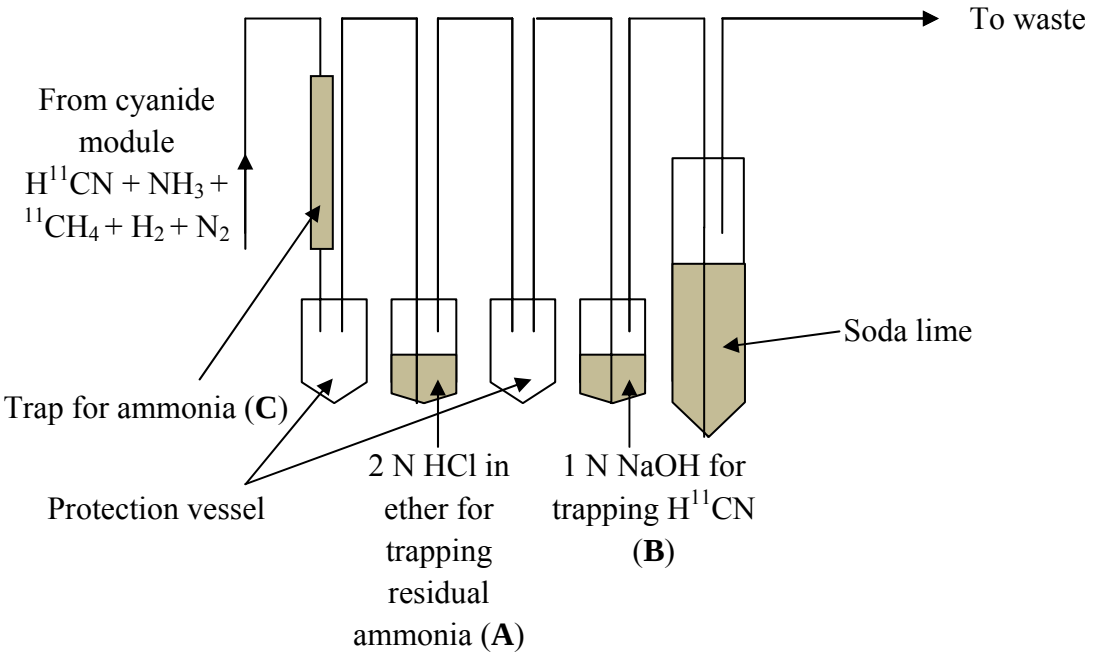

Figure 4-6. Diagram of ammonia removal test

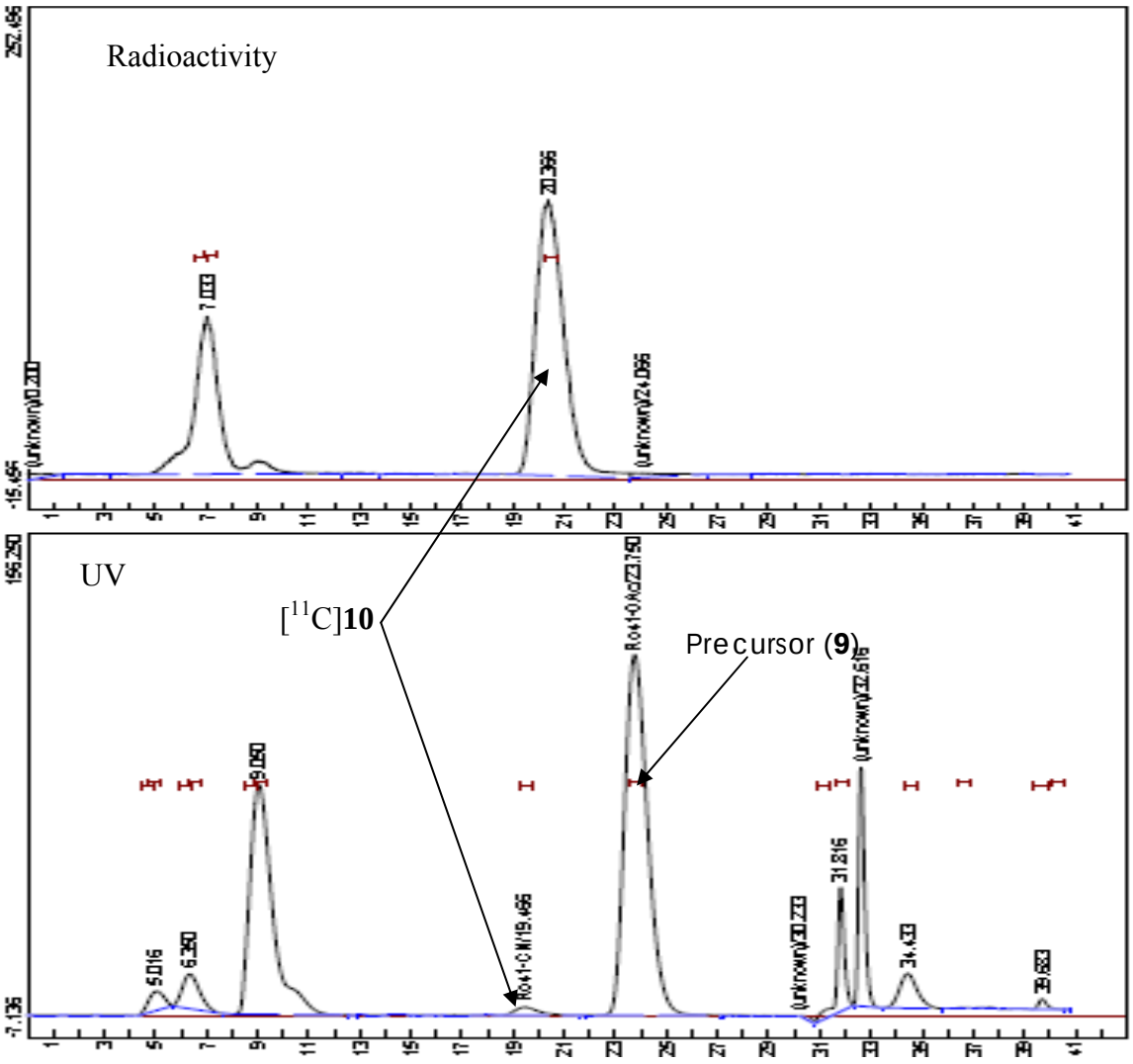

Figure 4-7. HPLC profile of substitution step to give [^{11}C]**10**.

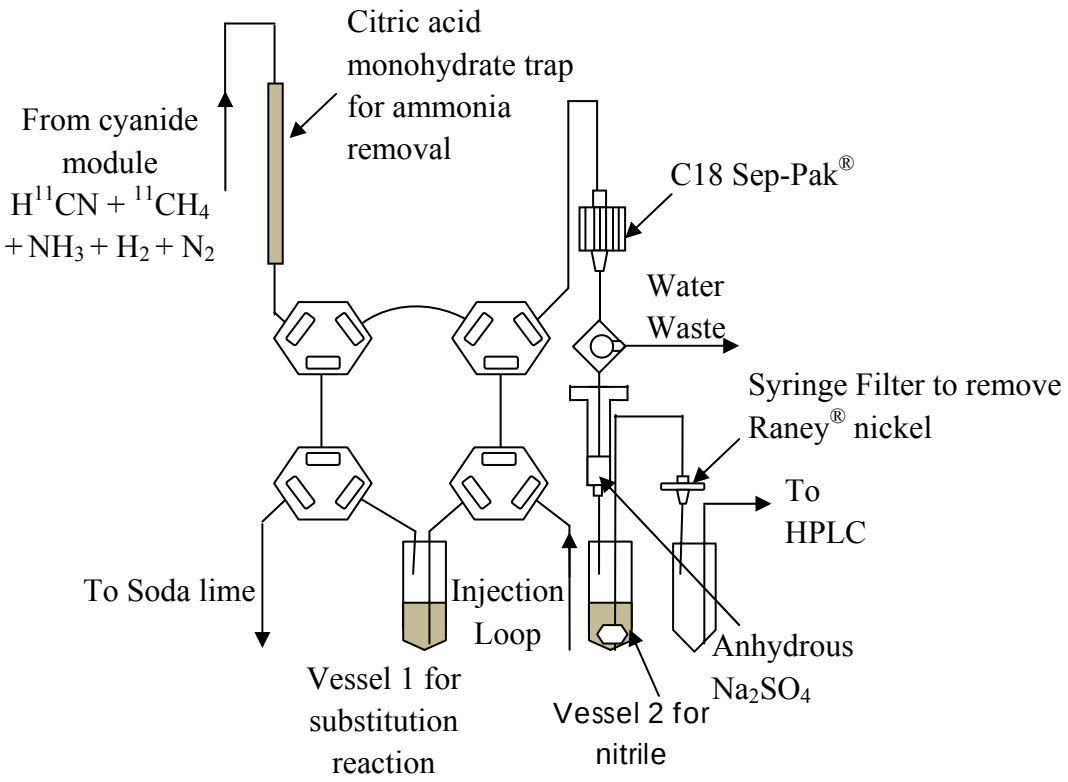

Figure 4-8. Diagram of Synthesis for [*N*-(2-[^{11}C]-2-aminoethyl)]Ro 41-1049.

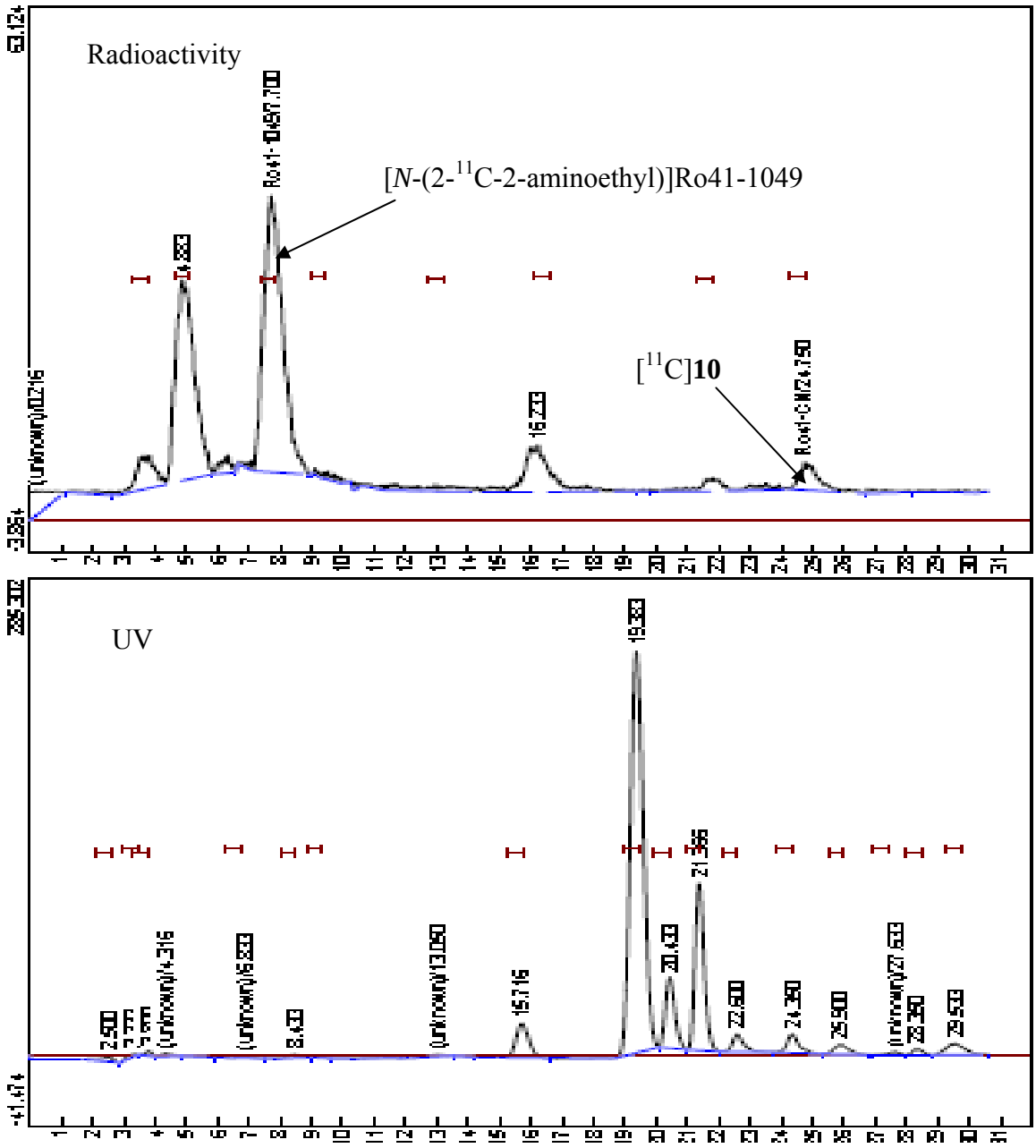

Figure 4-9. HPLC profile of [*N*-(2-^{11}C-2-aminoethyl)]Ro 41-1049 synthesis: Cyanide reduction eluting with 25% acetonitrile + 75% 0.1 M ammonium formate until 10 minutes and 50% acetonitrile + 50% 0.1 M ammonium formate after 10 minutes.

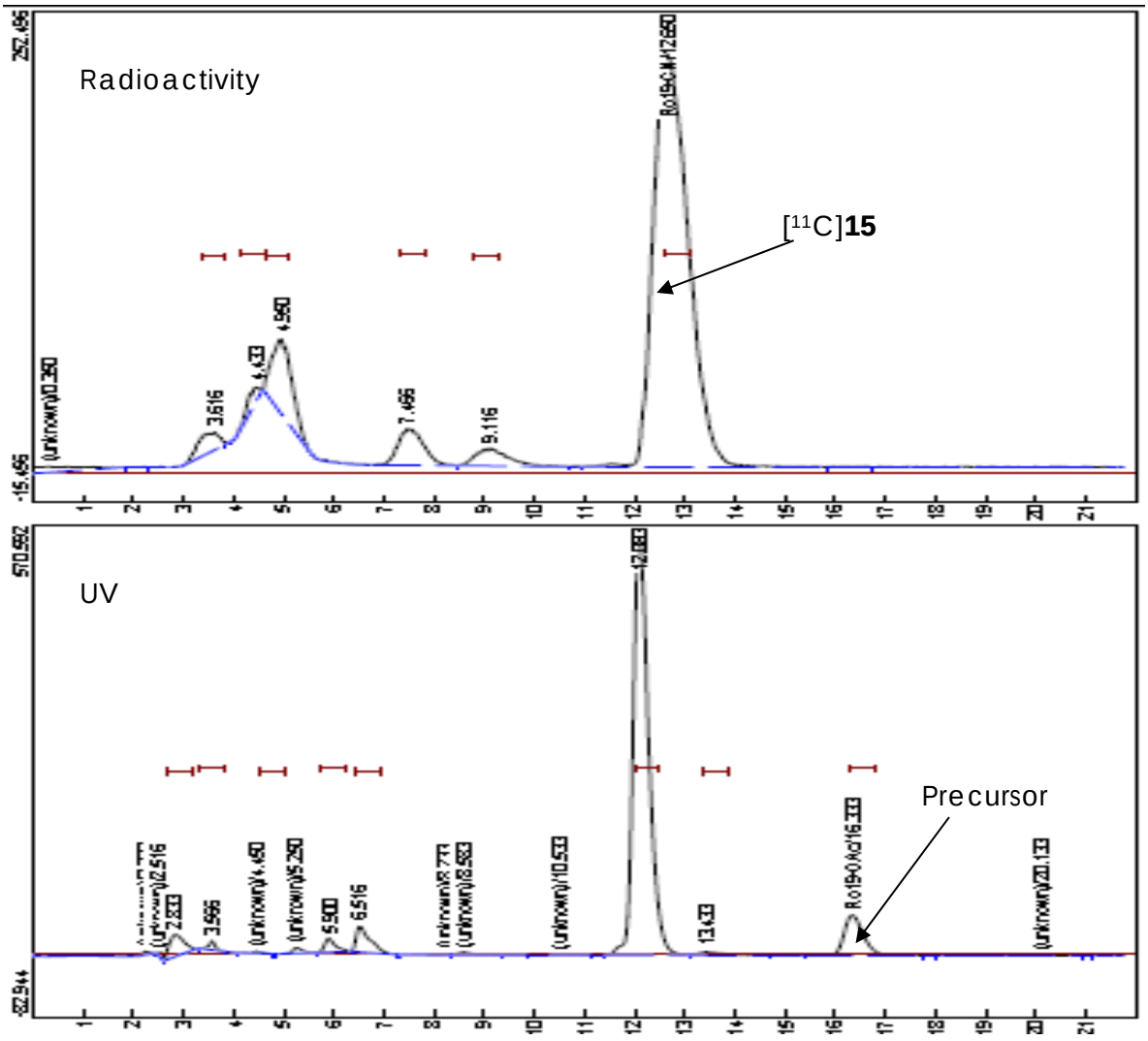

Figure 4-10. HPLC profile to synthesize 5-chloropyridine-2-(*N*-^{11}C-cyanomethyl) carboxamide ([^{11}C]**15**) eluting with 30% acetonitrile + 70% 0.1 M ammonium formate.

Trapping material for ammonia	2 N Hydrogen Chloride in ether to trap residual ammonia (**A**)	1 N Sodium Hydroxide Solution to trap $H^{11}CN$ (**B**)	Trap to remove ammonia (**C**)	Comment
Blank	0.14 mCi 2.8 mg of NH_4Cl	3.22 mCi	-	$H^{11}CN$ Penetrability(%) =(**A**+**B**)*100/(**A**+**B**+**C**)
Sicapent® 2 g	2.08 mCi 1.8 mg of NH_4Cl	0.32 mCi	4.41 mCi	• 35% $H^{11}CN$ passed through Sicapent® trap • 36% ammonia trapped
Silica Gel 3 g	0.418 mCi No NH_4Cl	0.03 mCi	4.44 mCi	• 9% of $H^{11}CN$ passed through silica gel trap • No ammonium chloride precipitant
Molecular Sieve 5Å 4 g	1.01 mCi No NH_4Cl	0 mCi	13.2 mCi	• 7% of $H^{11}CN$ passed through silica gel trap • No ammonium chloride precipitant
Dowex® 50W-X4 5 g	0 mCi No NH_4Cl	0 mCi	10.0 mCi	• No $H^{11}CN$ passed through the cation exchange resin trap • No ammonium chloride precipitant
Amberlite® CG-50 Type 2 4 g	0 mCi No NH_4Cl	0 mCi	4.9 mCi	• No $H^{11}CN$ passed through the cation exchange resin trap • No ammonium chloride precipitant
Citric acid monohydrate 4 g	4.39 mCi No NH_4Cl	1.33 mCi	1.41 mCi	• 80 % of $H^{11}CN$ passed through citric acid trap. • No ammonium chloride precipitant

Table 4-1. Ammonia removal test with various trapping material.

NMR Spectra

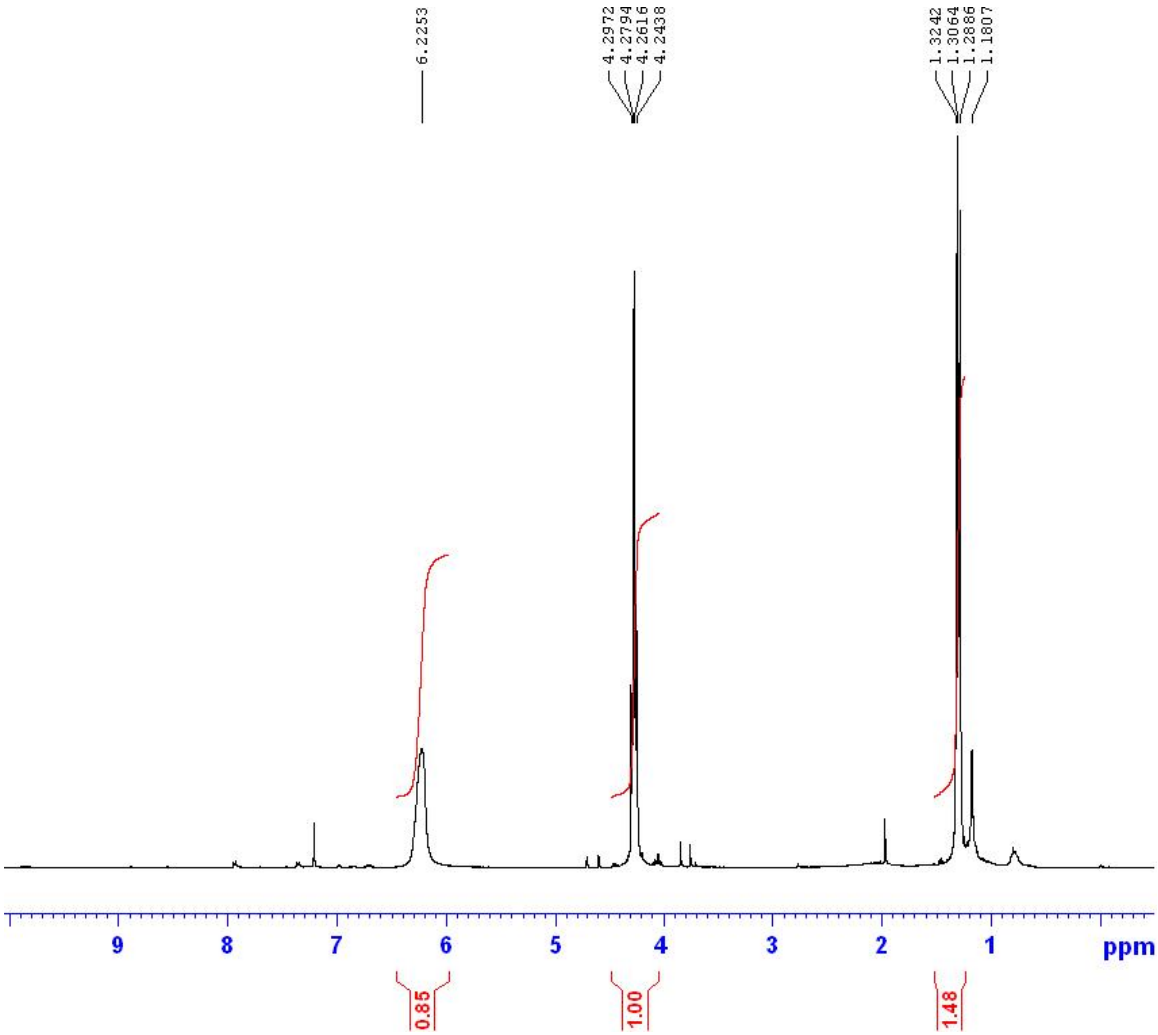

^{1}H-NMR Spectrum of ethyl 2-amino-5-bromo-1,3-thiazole-4-carboxylate (**2**)

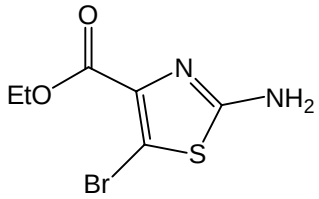

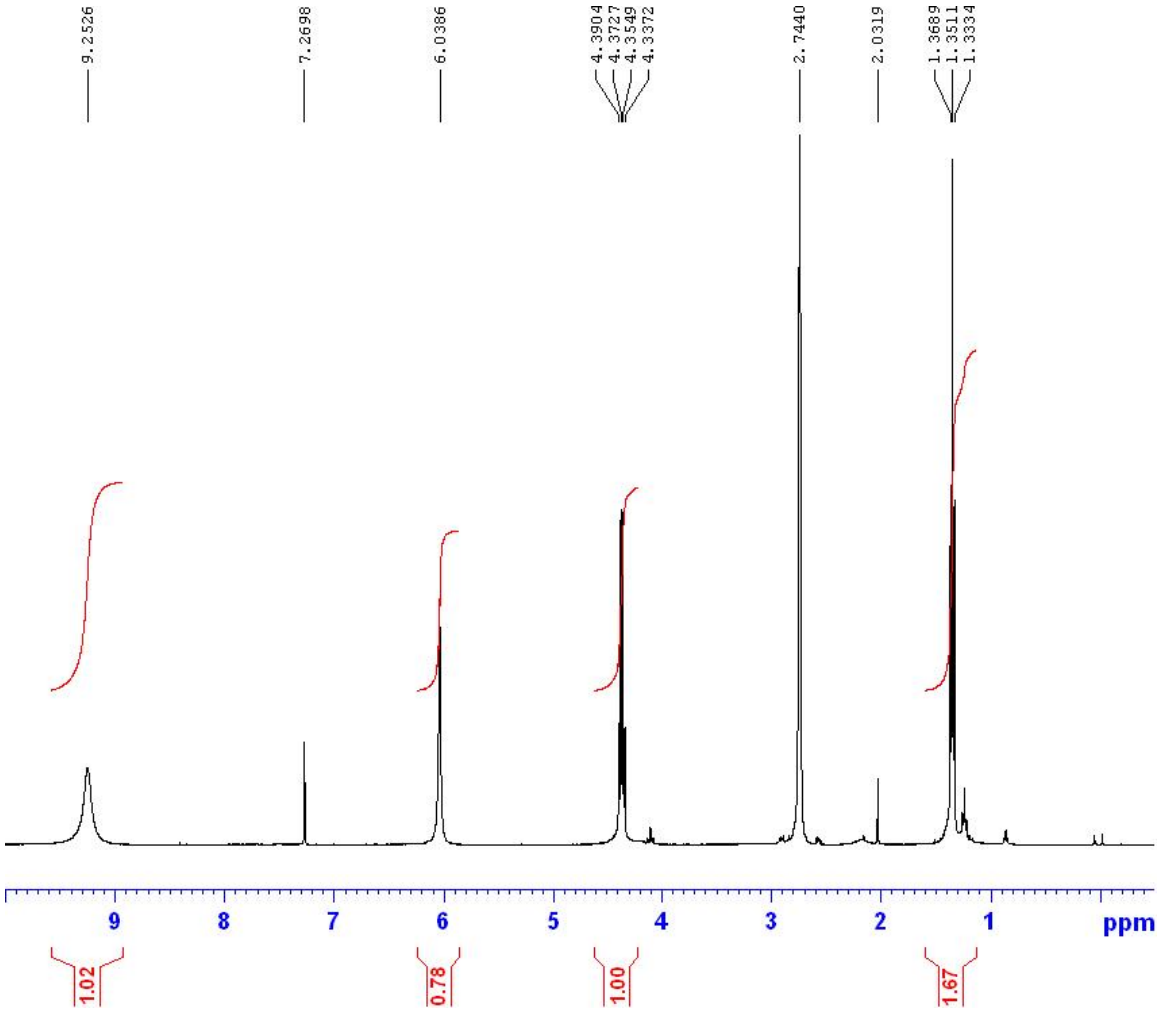

^{1}H-NMR Spectrum of ethyl 2-amino-5-chloro-1,3-thiazole-4-carboxylate (**3**)

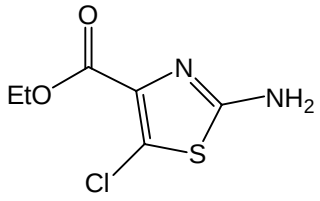

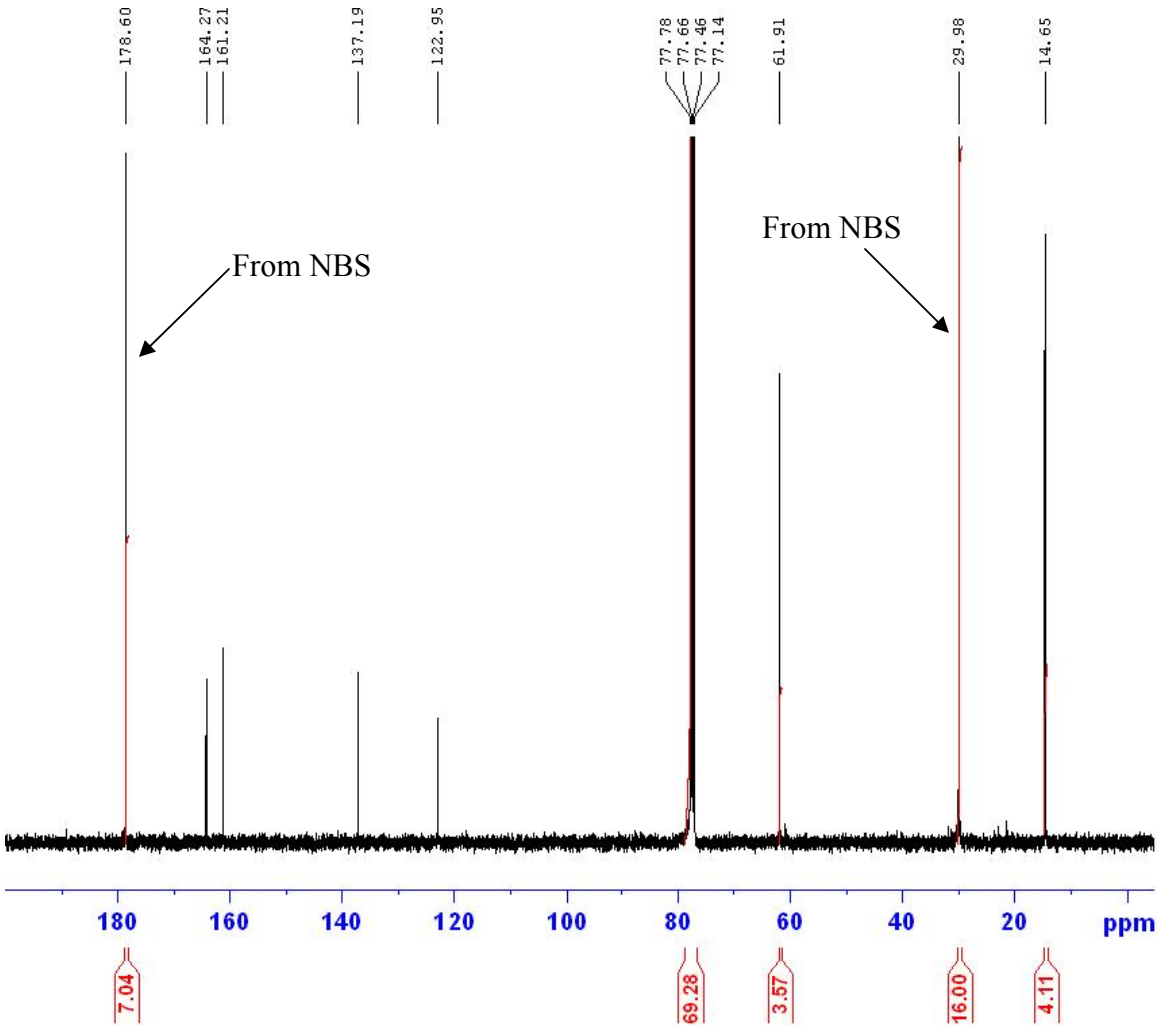

^{13}C-NMR Spectrum of ethyl 2-amino-5-chloro-1,3-thiazole-4-carboxylate (**3**)

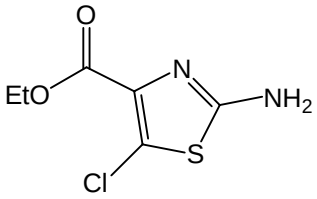

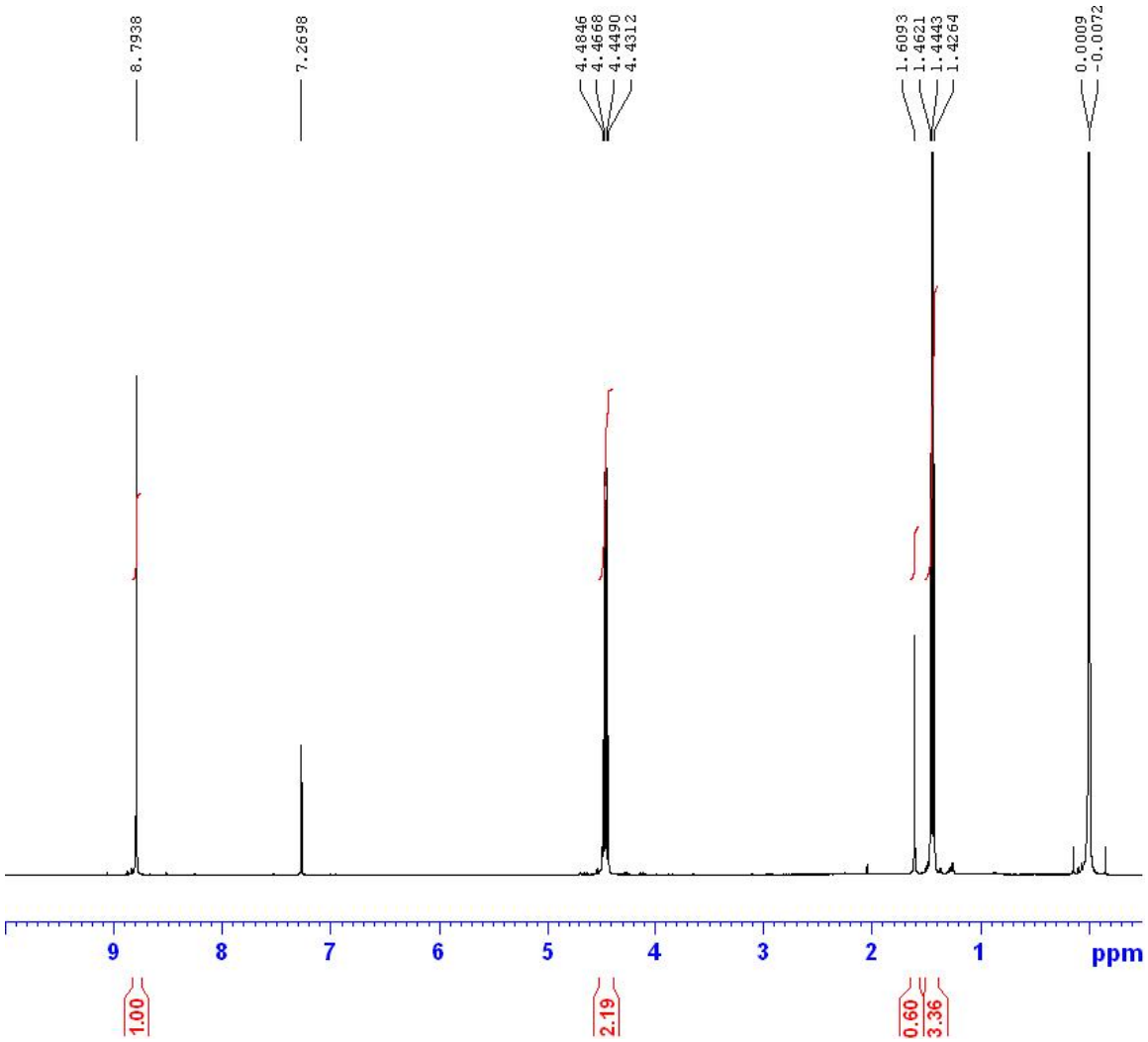

^{1}H-NMR Spectrum of ethyl 5-bromo-1,3-thiazole-4-carboxylate (**4**)

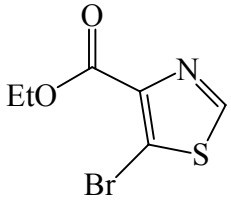

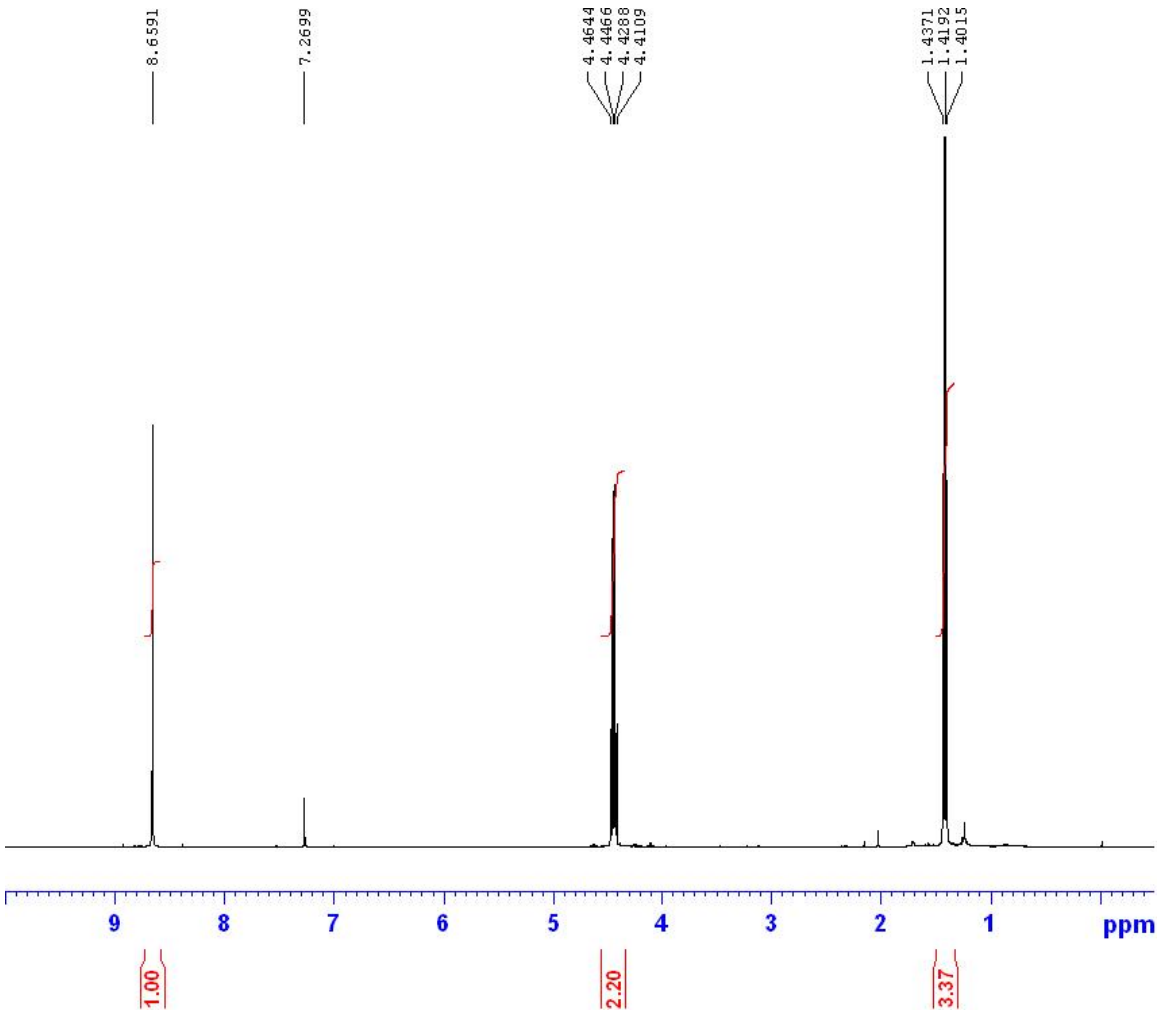

^{1}H-NMR Spectrum of ethyl 5-chloro-1,3-thiazole-4-carboxylate (**5**)

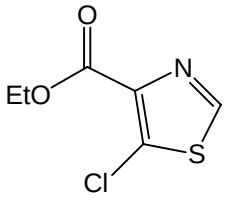

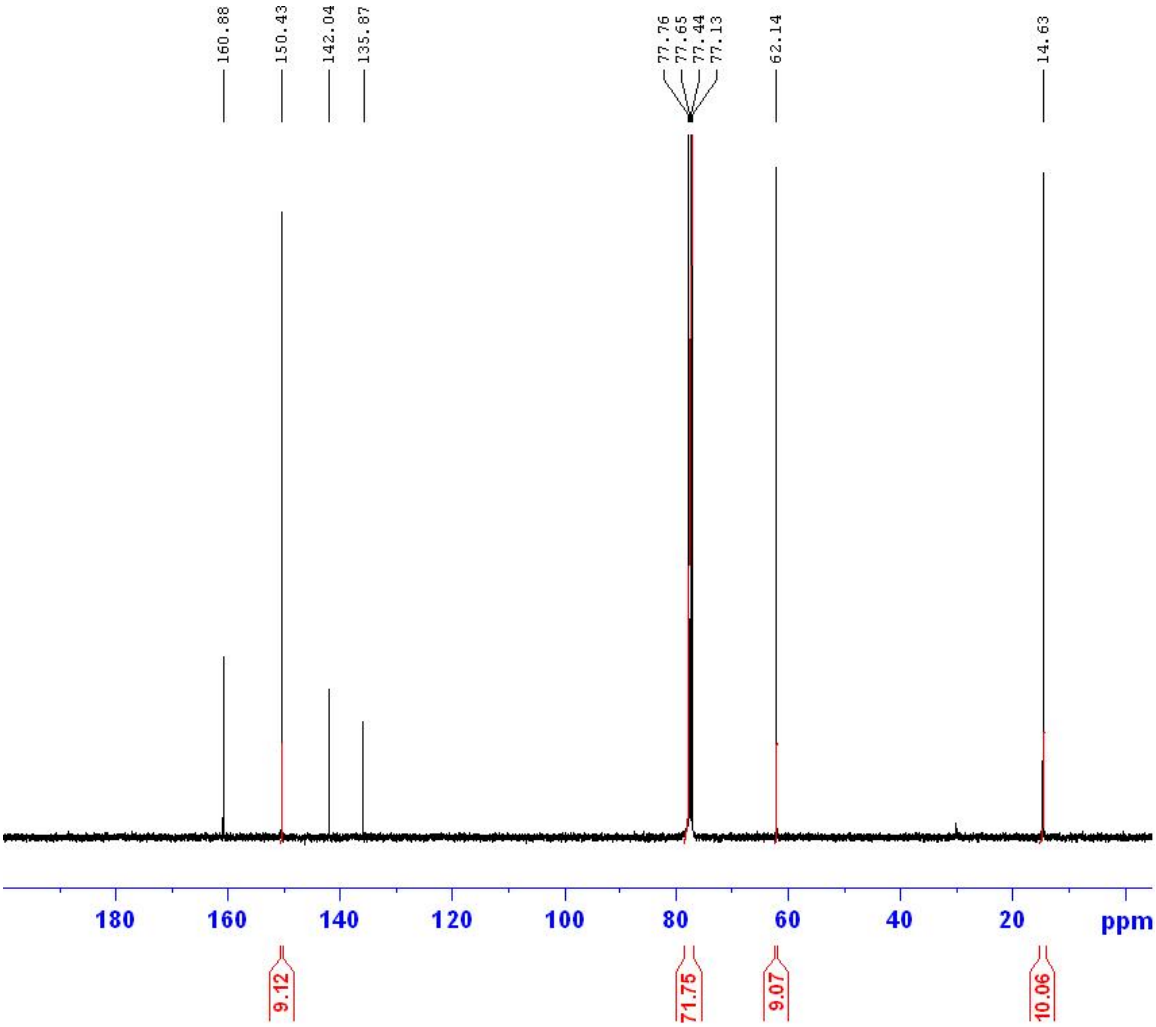

^{13}C-NMR Spectrum of ethyl 5-chloro-1,3-thiazole-4-carboxylate (**5**)

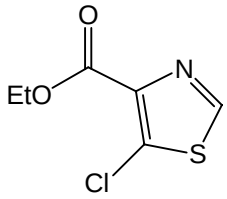

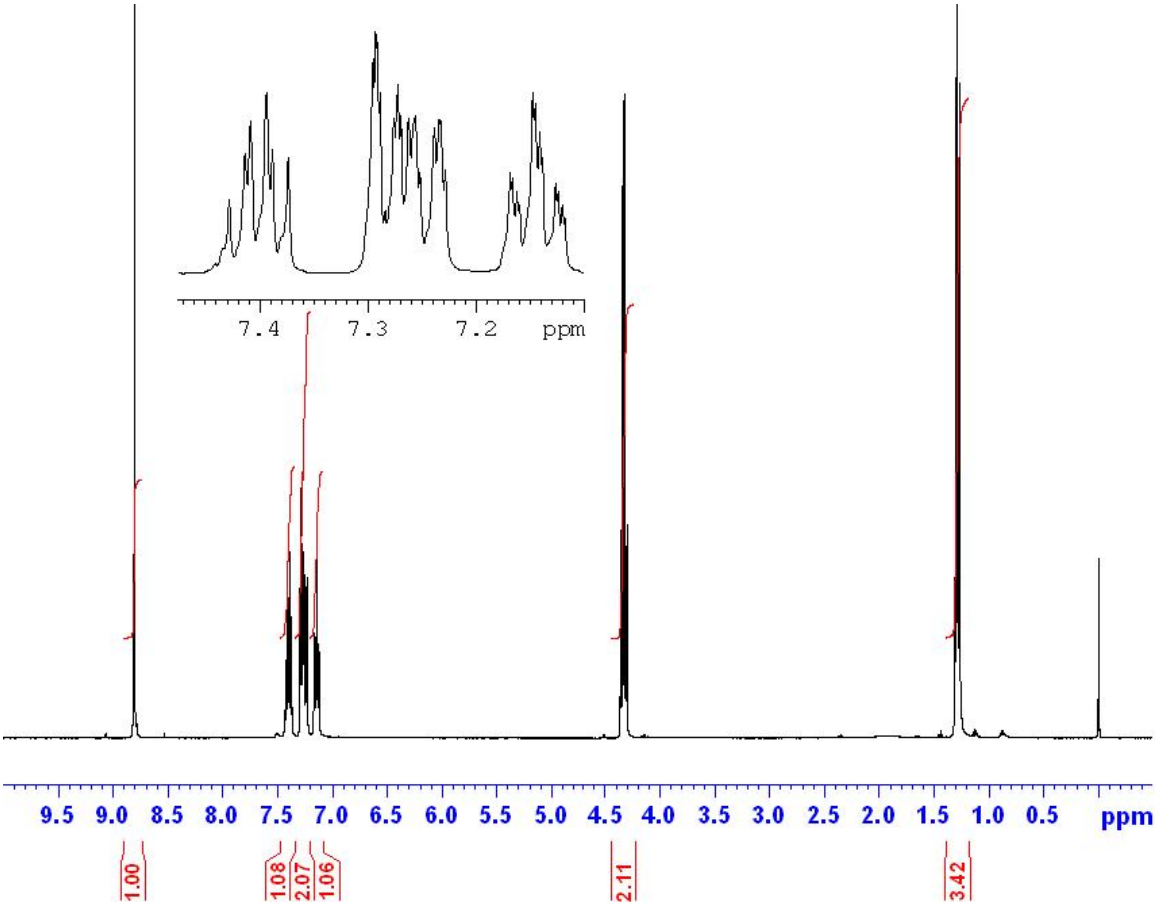

^{1}H-NMR Spectrum of ethyl 5-(3'-fluorophenyl)-1,3-thiazole-4-carboxylate (**6**)

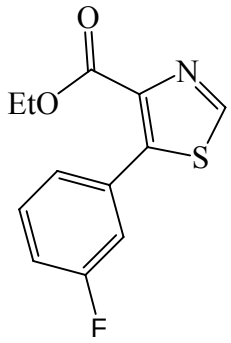

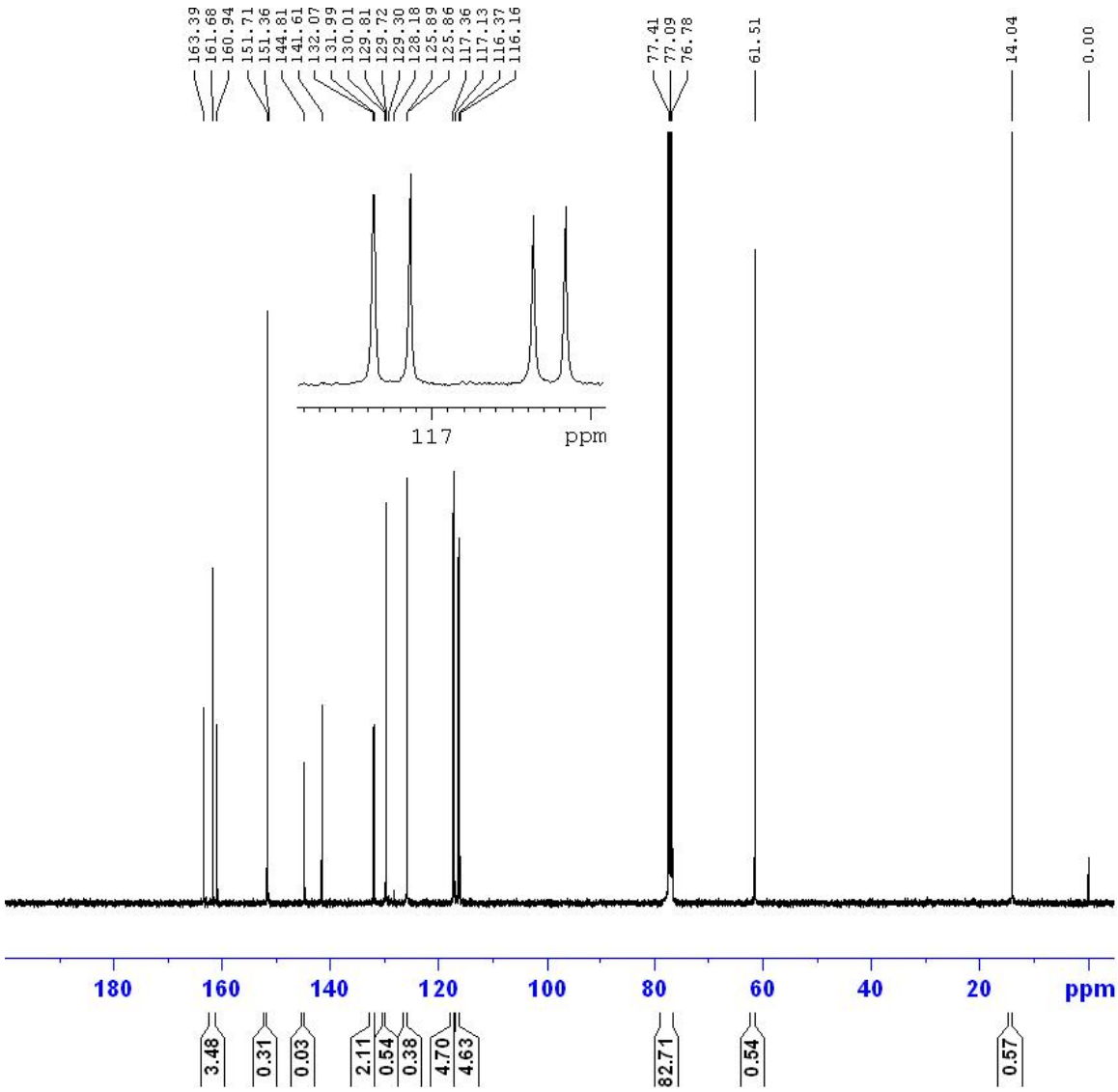

^{13}C-NMR Spectrum of ethyl 5-(3'-fluorophenyl)-1,3-thiazole-4-carboxylate (**6**)

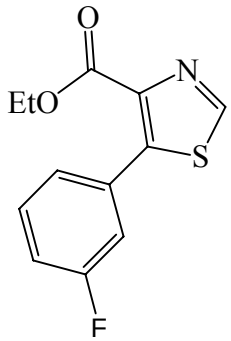

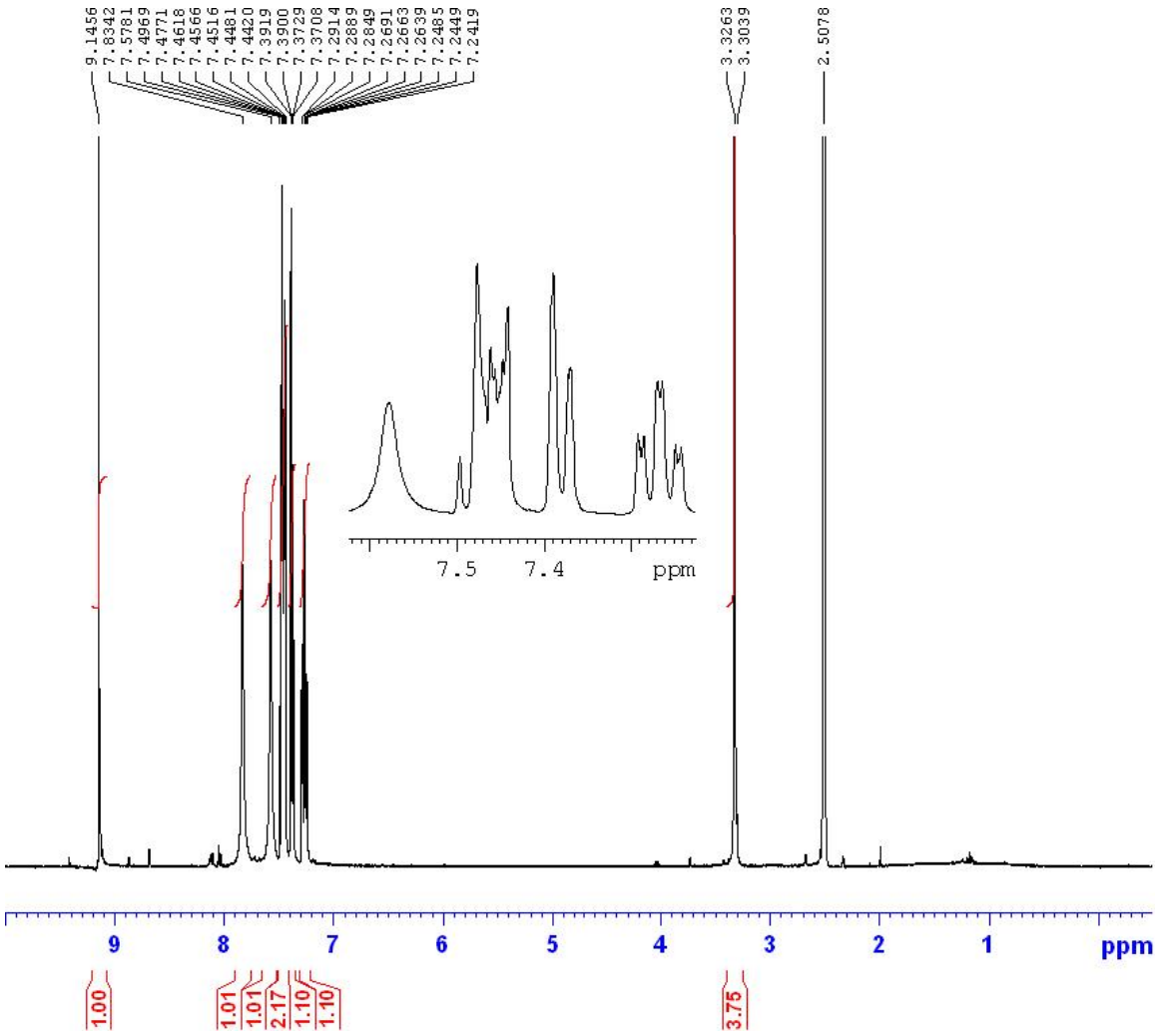

^{1}H-NMR Spectrum of 5-(3'-fluorophenyl)-1,3-thiazole-4-carboxamide (**7**, DMSO-d_6)

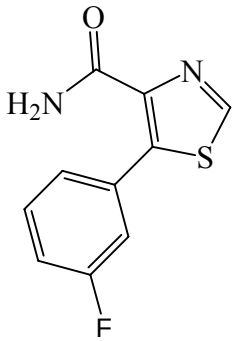

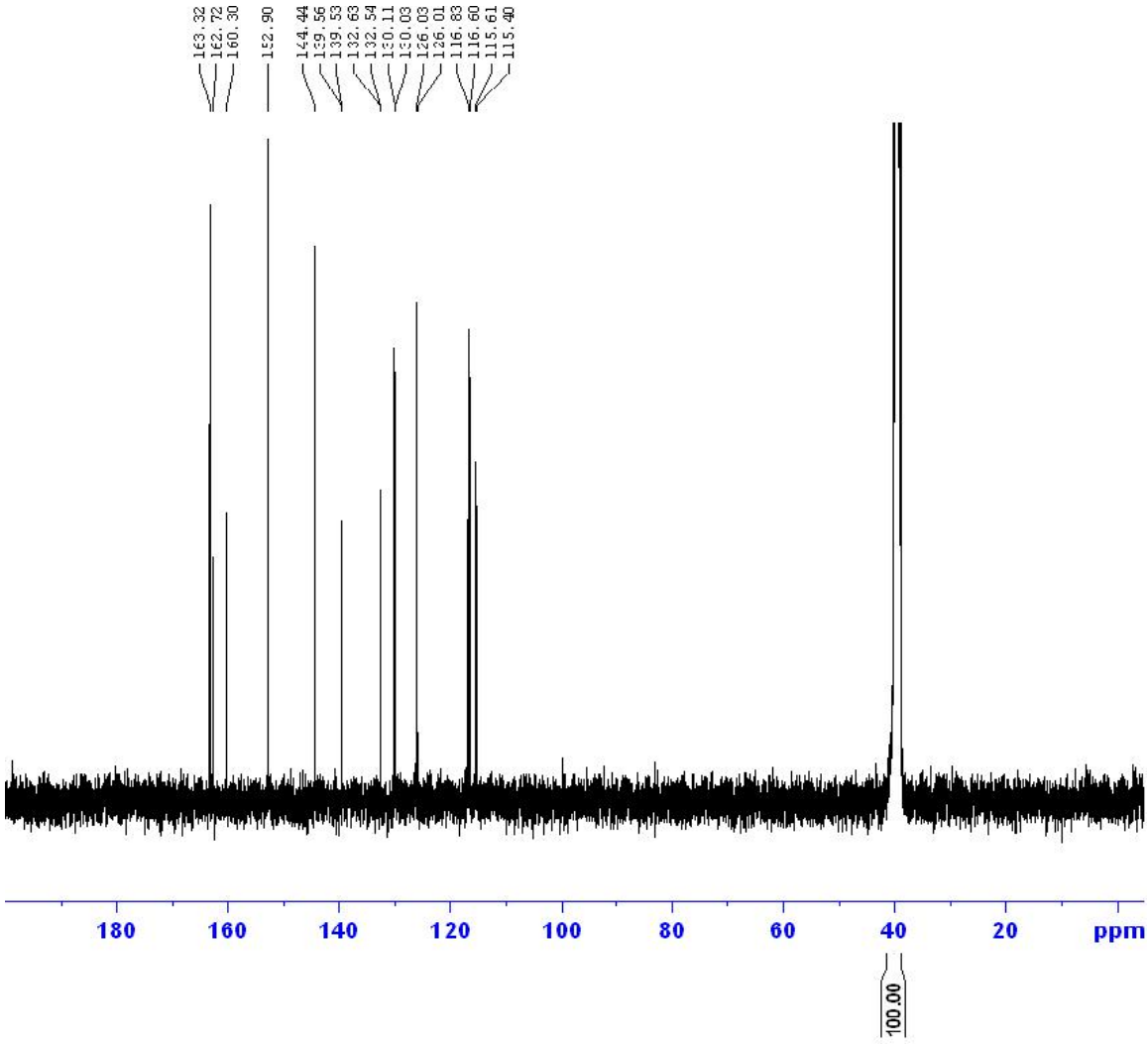

^{13}C-NMR Spectrum of 5-(3'-fluorophenyl)-1,3-thiazole-4-carboxamide (**7**, DMSO-d_6)

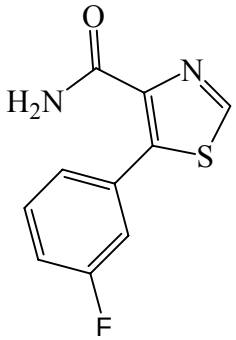

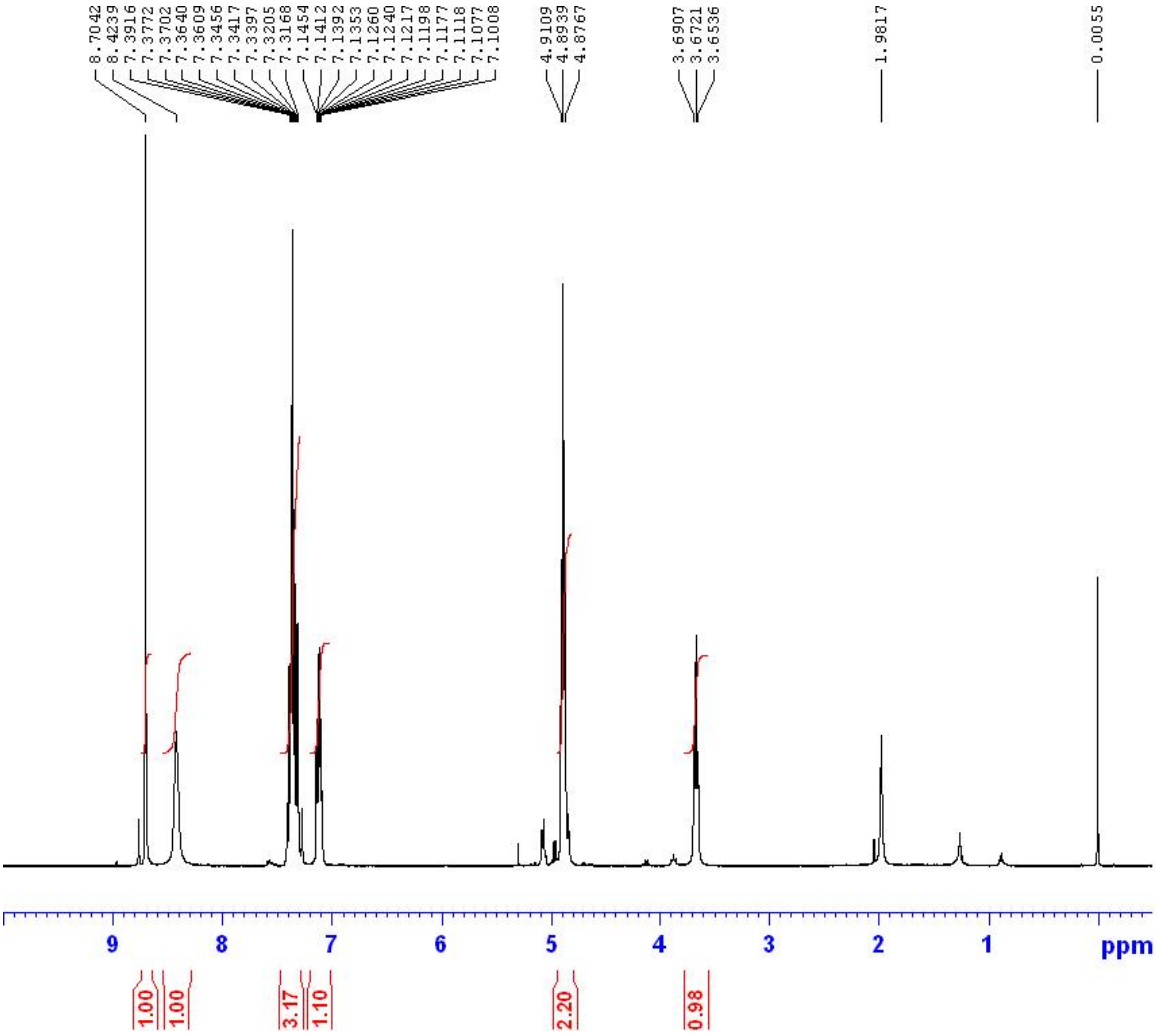

^{1}H-NMR Spectrum of 5-(3'-fluorophenyl)-1,3-thiazole-4-(*N*-hydroxymethyl) carboxamide (**8**)

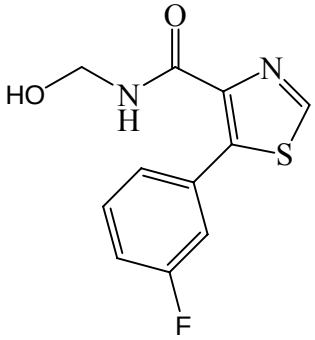

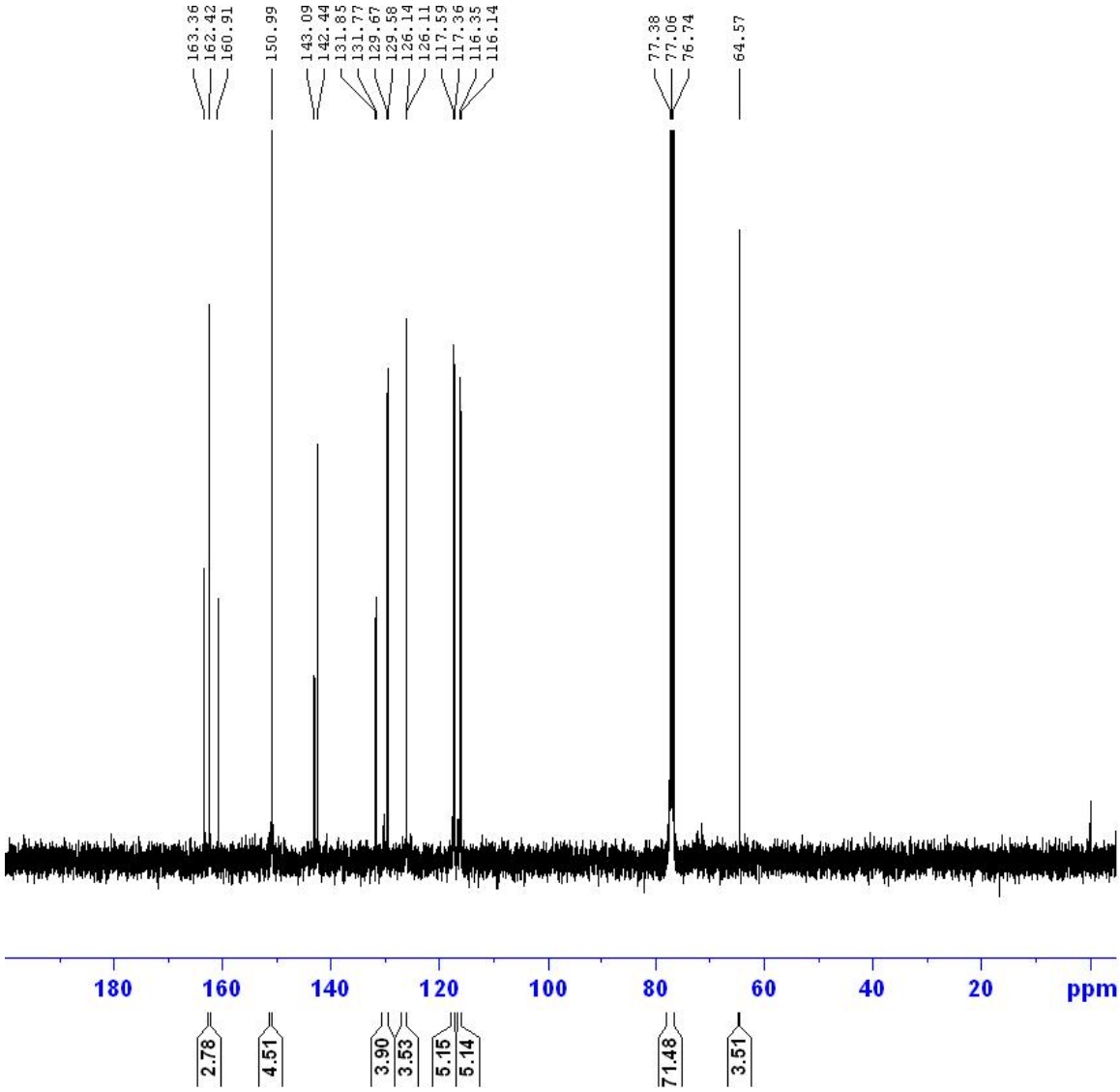

^{13}C-NMR Spectrum of 5-(3'-fluorophenyl)-1,3-thiazole-4-(*N*-hydroxymethyl) carboxamide (**8**)

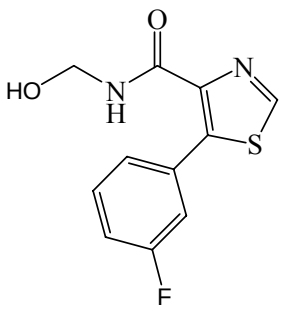

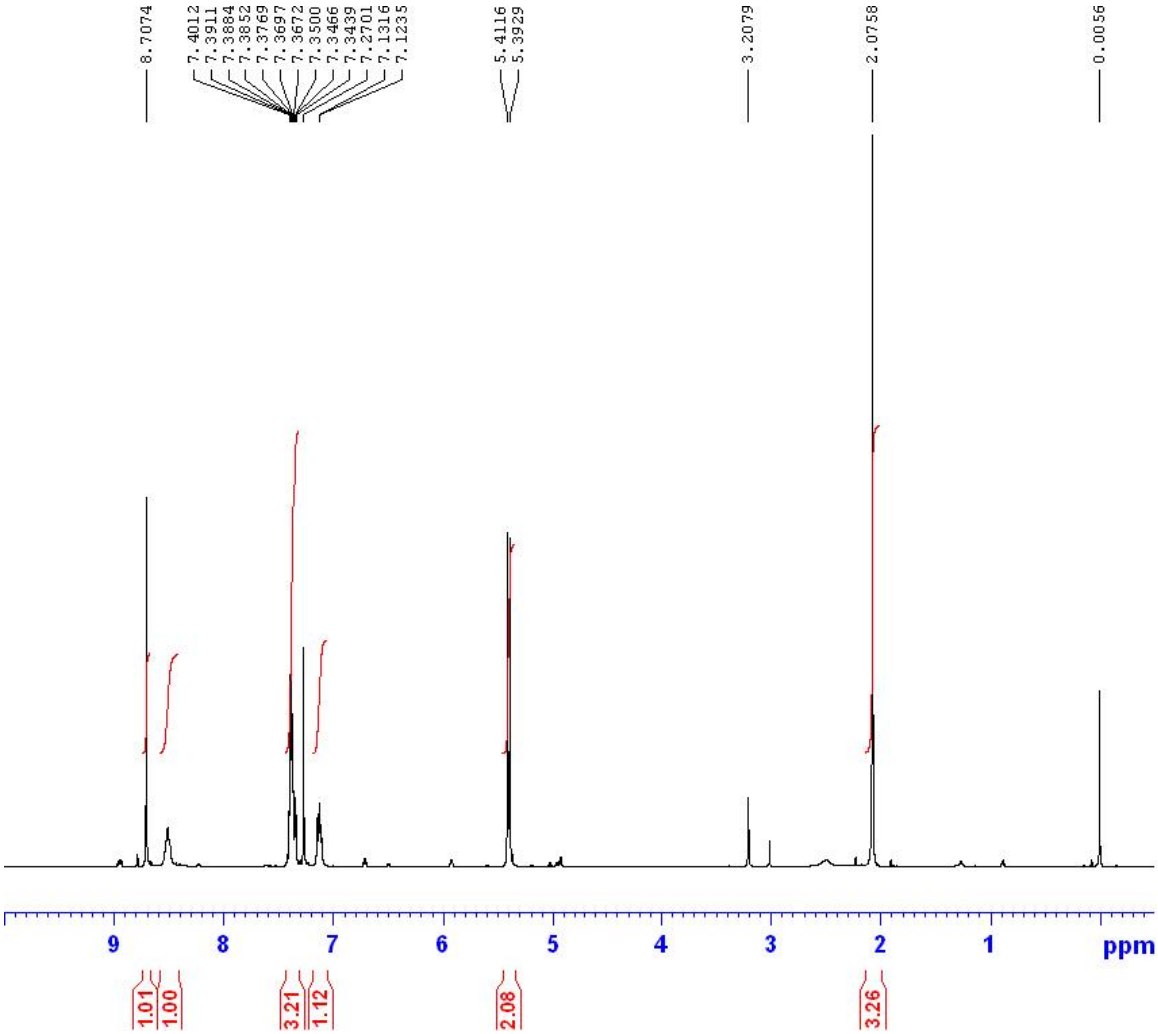

^{1}H-NMR Spectrum of 5-(3'-fluorophenyl)-1,3-thiazole-4-(*N*-acetoxymethyl) carboxamide (**9**)

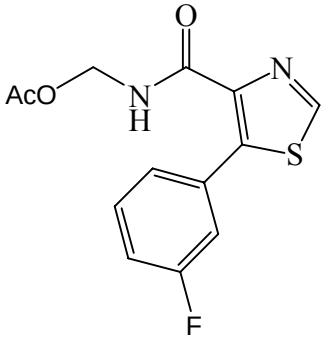

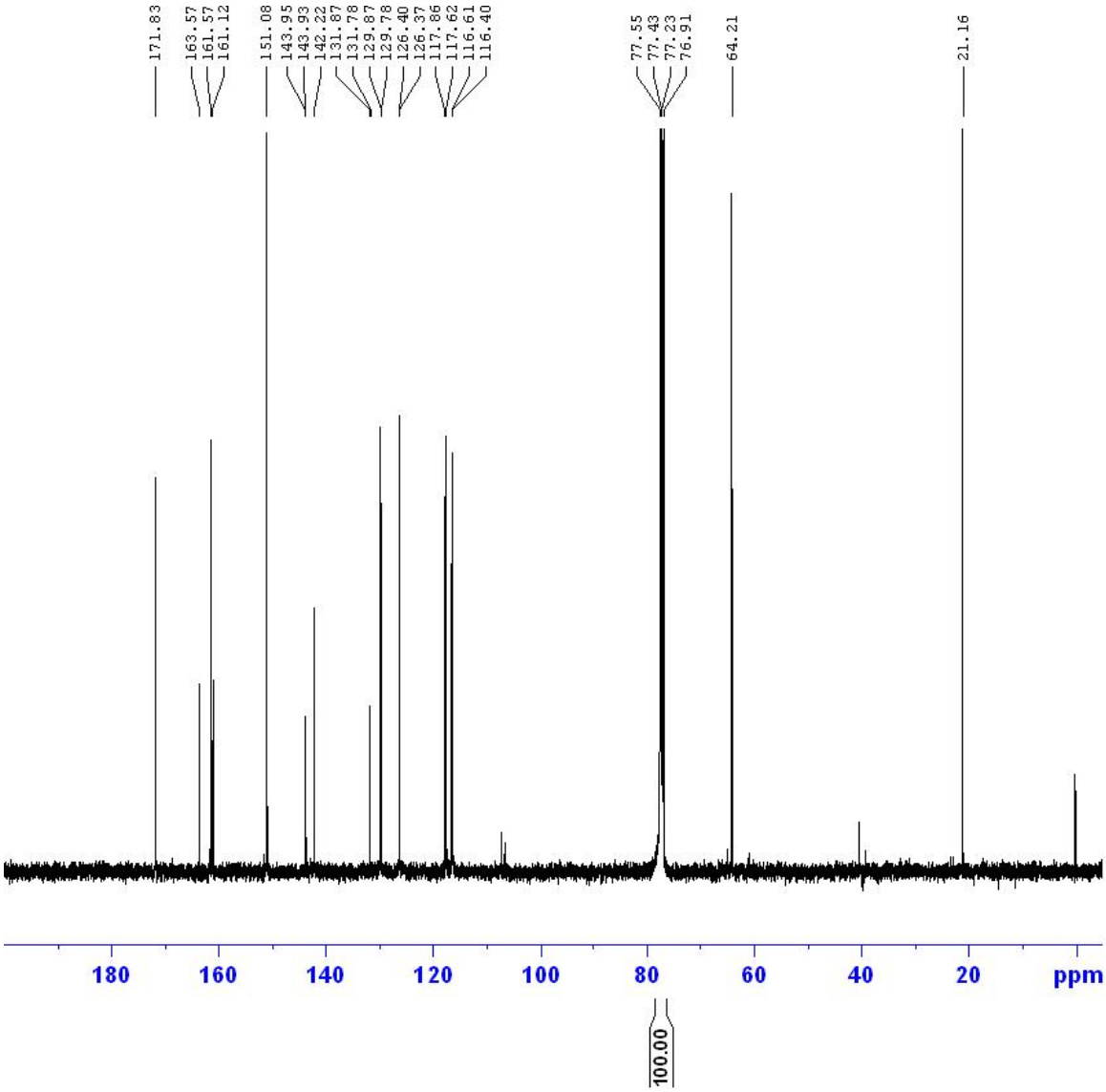

^{13}C-NMR Spectrum of 5-(3'-fluorophenyl)-1,3-thiazole-4-(*N*-acetoxymethyl) carboxamide (**9**)

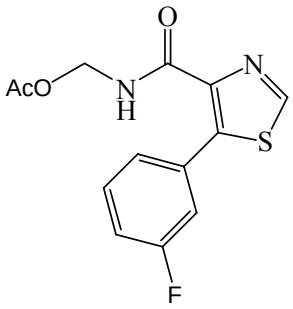

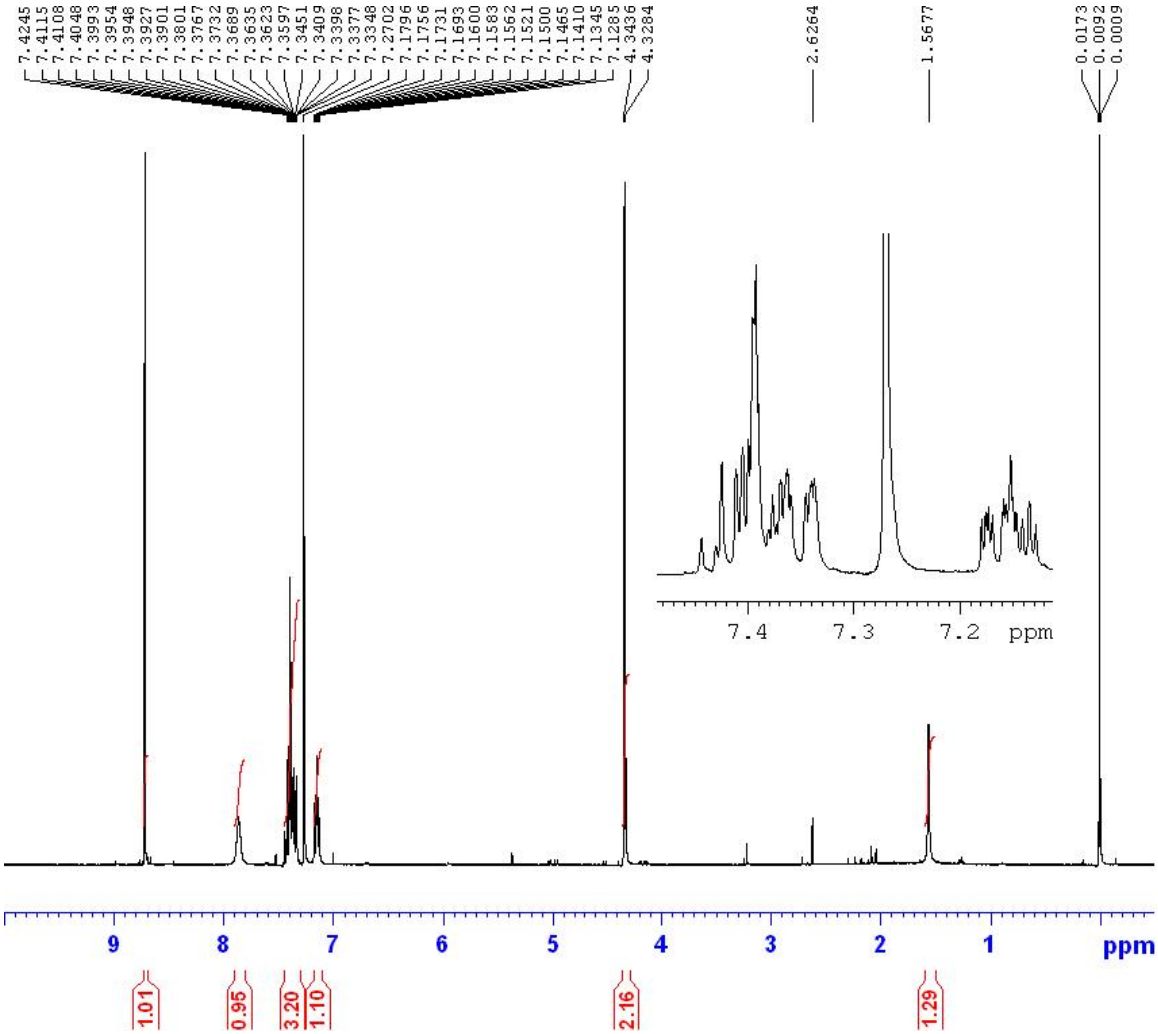

^{1}H-NMR Spectrum of 5-(3'-fluorophenyl)-1,3-thiazole-4-(*N*-cyanomethyl)carboxamide (**10**, DMSO-d_6)

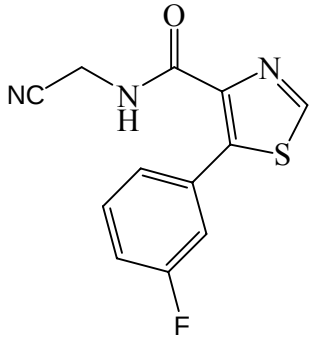

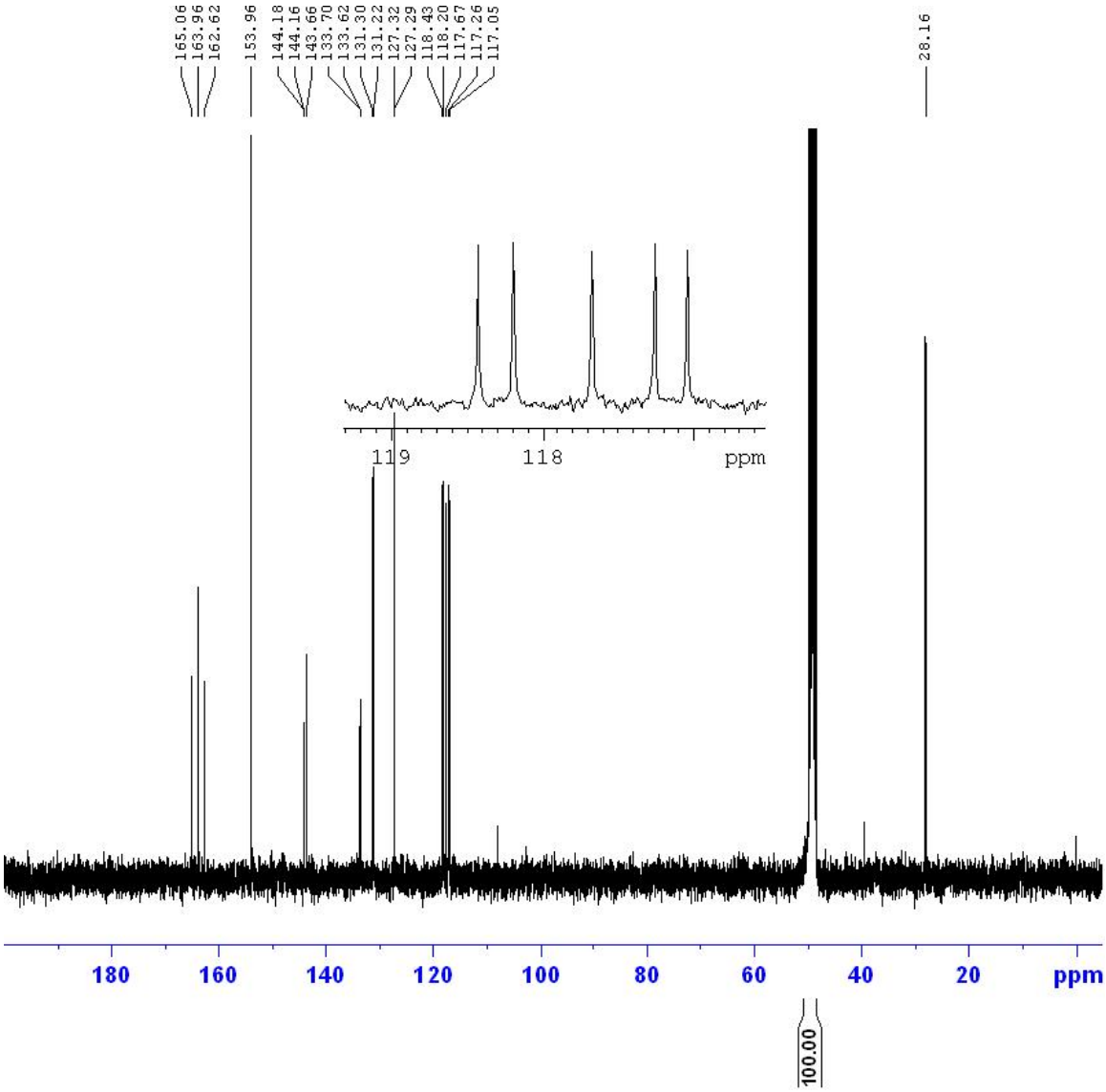

^{13}C-NMR Spectrum of 5-(3'-fluorophenyl)-1,3-thiazole-4-(*N*-cyanomethyl)carboxamide (**10**, DMSO-d_6)

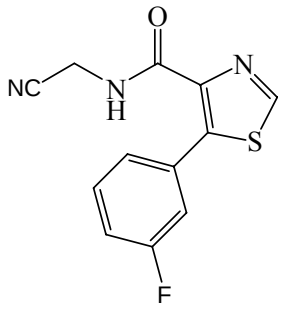

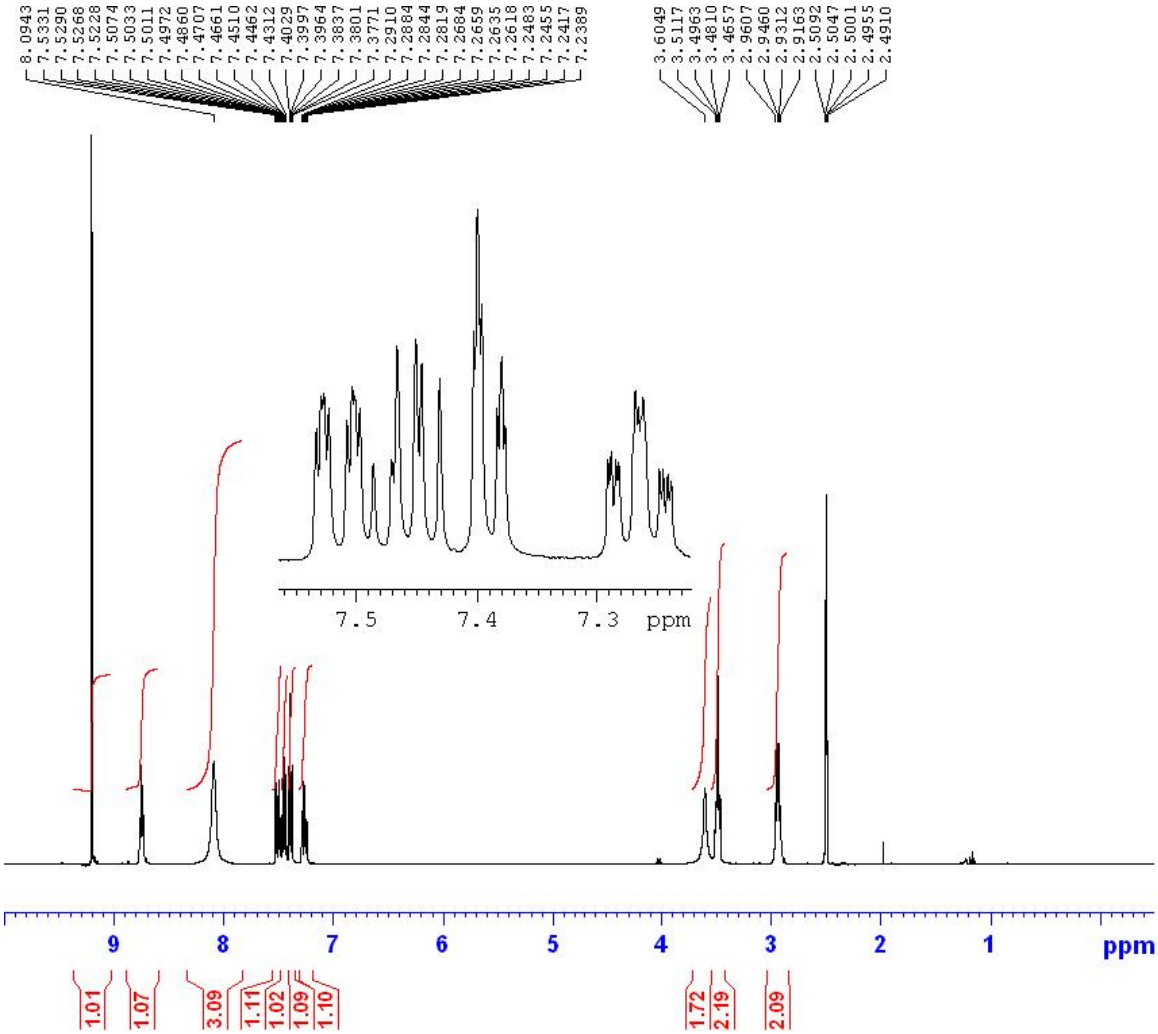

^{1}H-NMR Spectrum of 5-(3'-fluorophenyl)-1,3-thiazole-4-(*N*-2-aminoethyl)carboxamide (Ro 41-1049, DMSO-d_6)

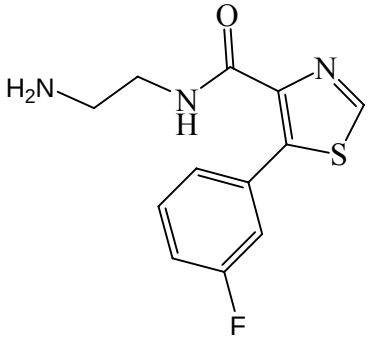

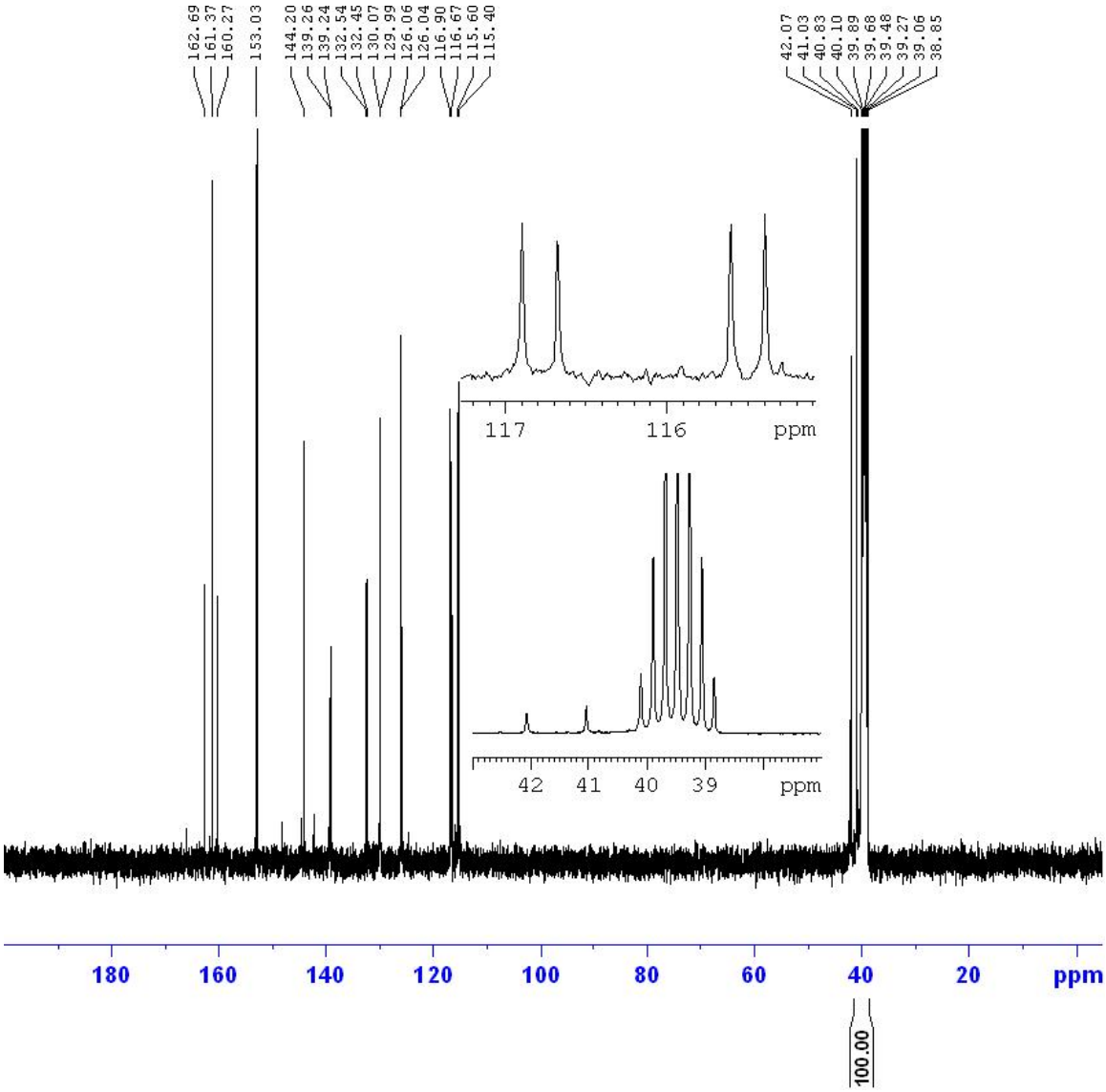

^{13}C-NMR Spectrum of 5-(3'-fluorophenyl)-1,3-thiazole-4-(*N*-2-aminoethyl)carboxamide (Ro 41-1049, DMSO-d_6)

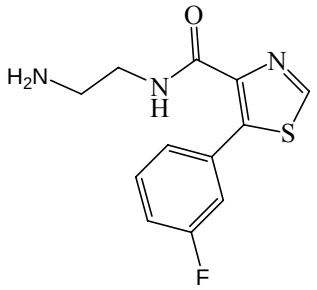

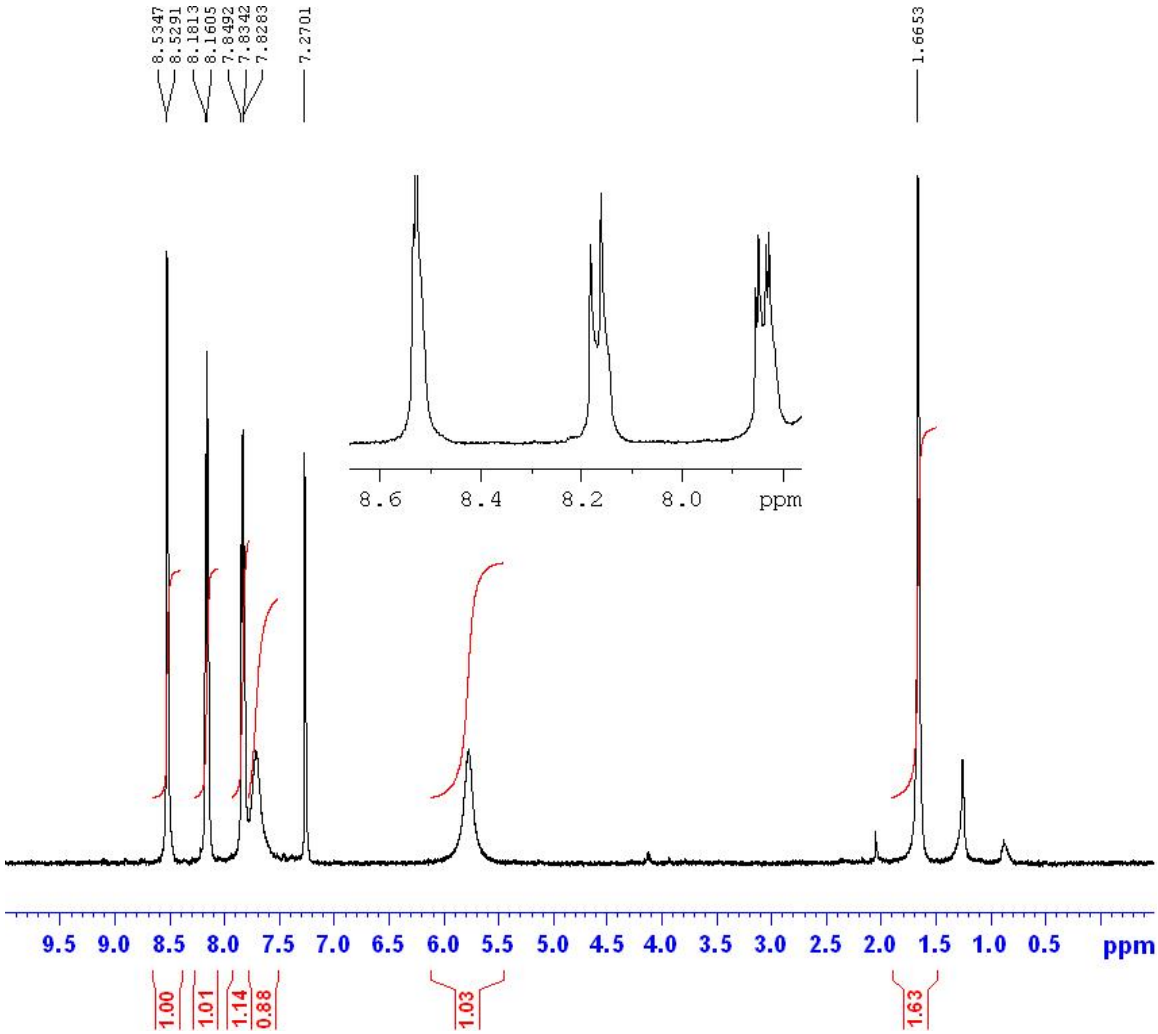

^{1}H-NMR Spectrum of 5-chloropyridine-2-carboxamide (**12**)

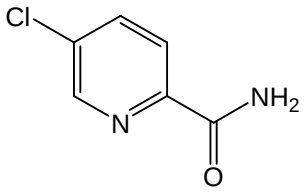

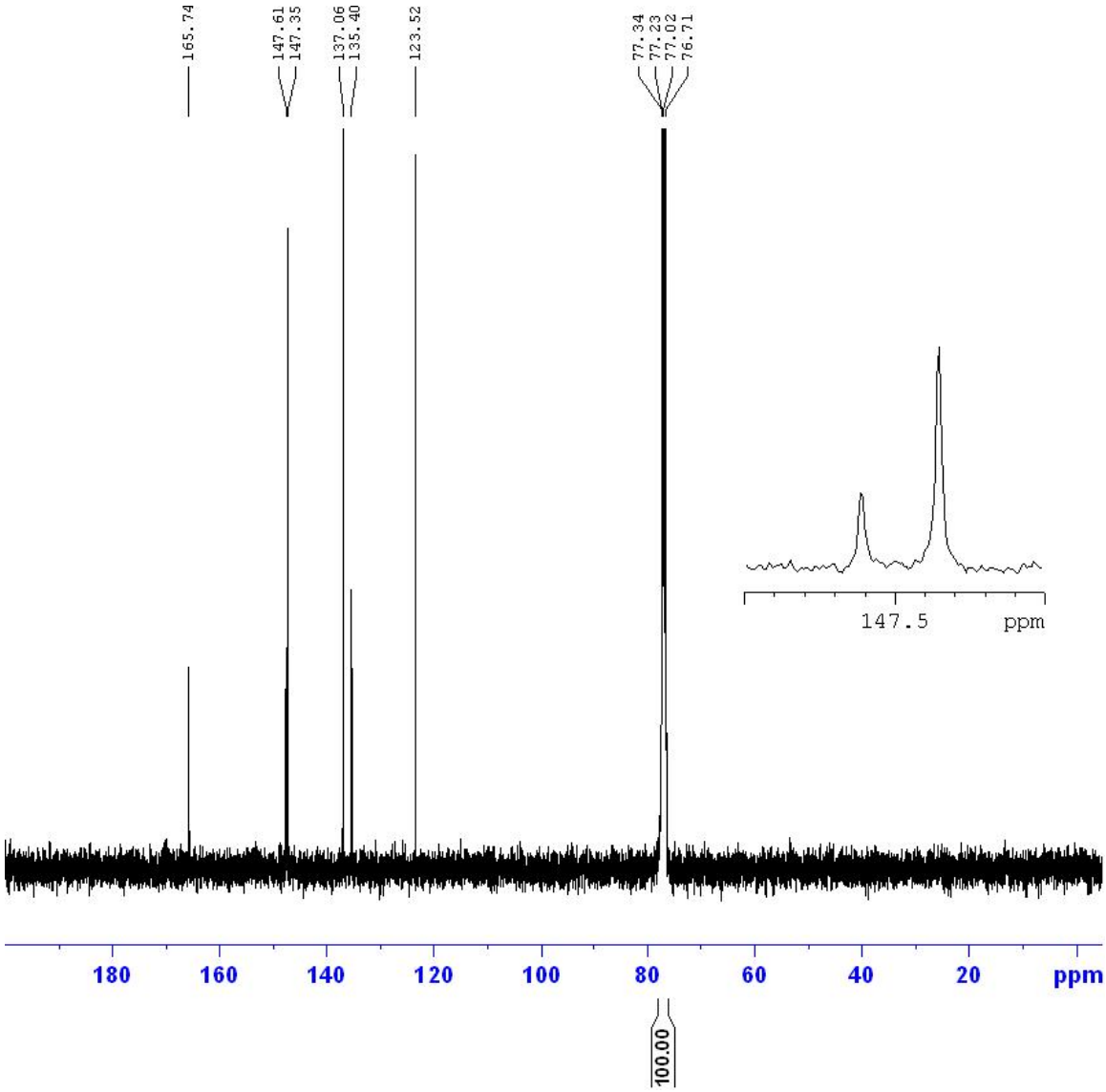

^{13}C-NMR Spectrum of 5-chloropyridine-2-carboxamide (**12**)

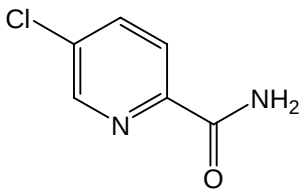

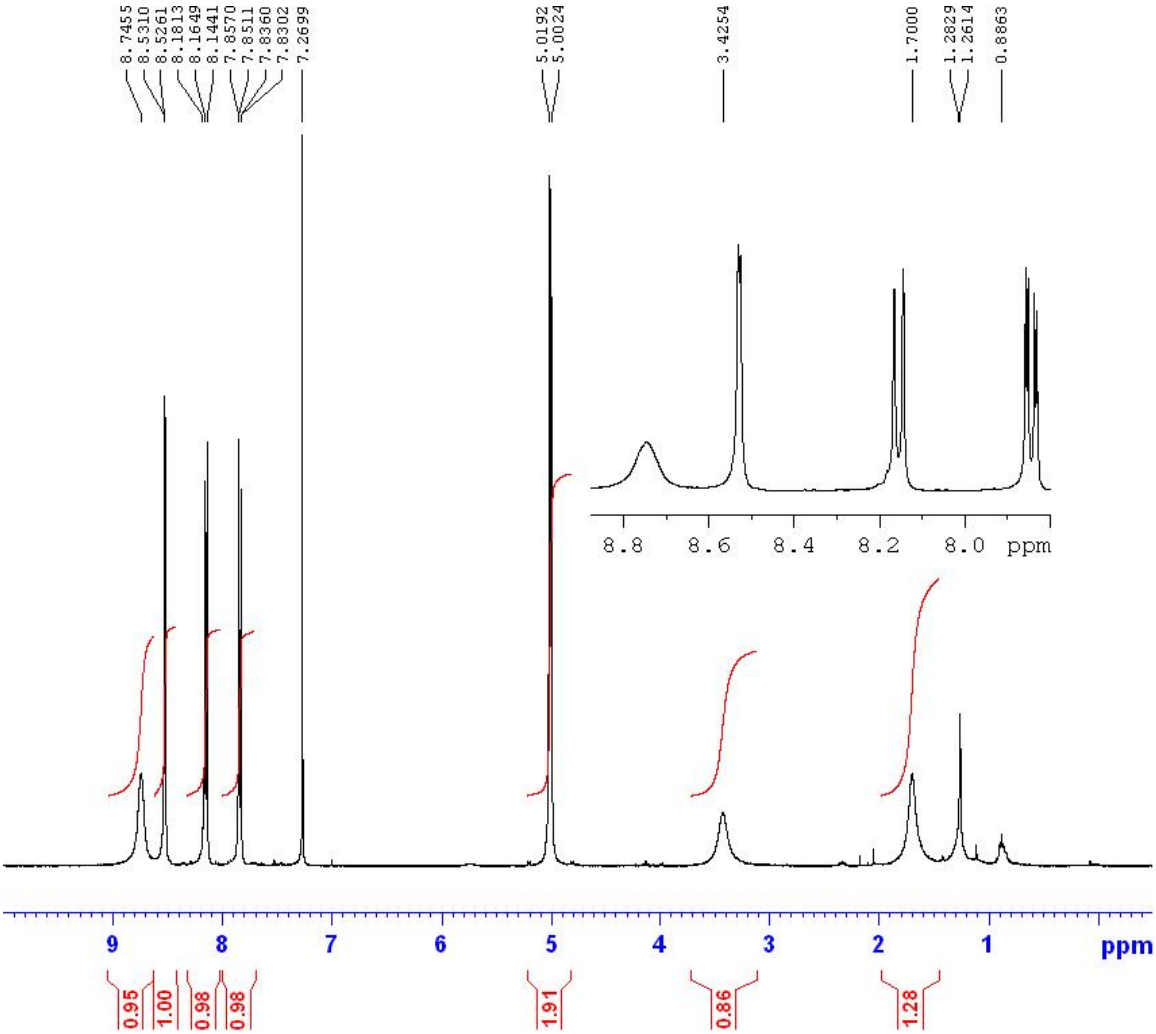

^{1}H-NMR Spectrum of 5-chloropyridine-2-(*N*-hydroxymethyl)carboxamide (**13**)

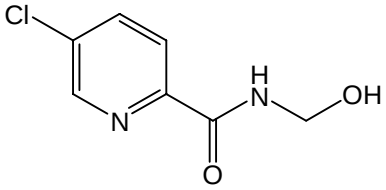

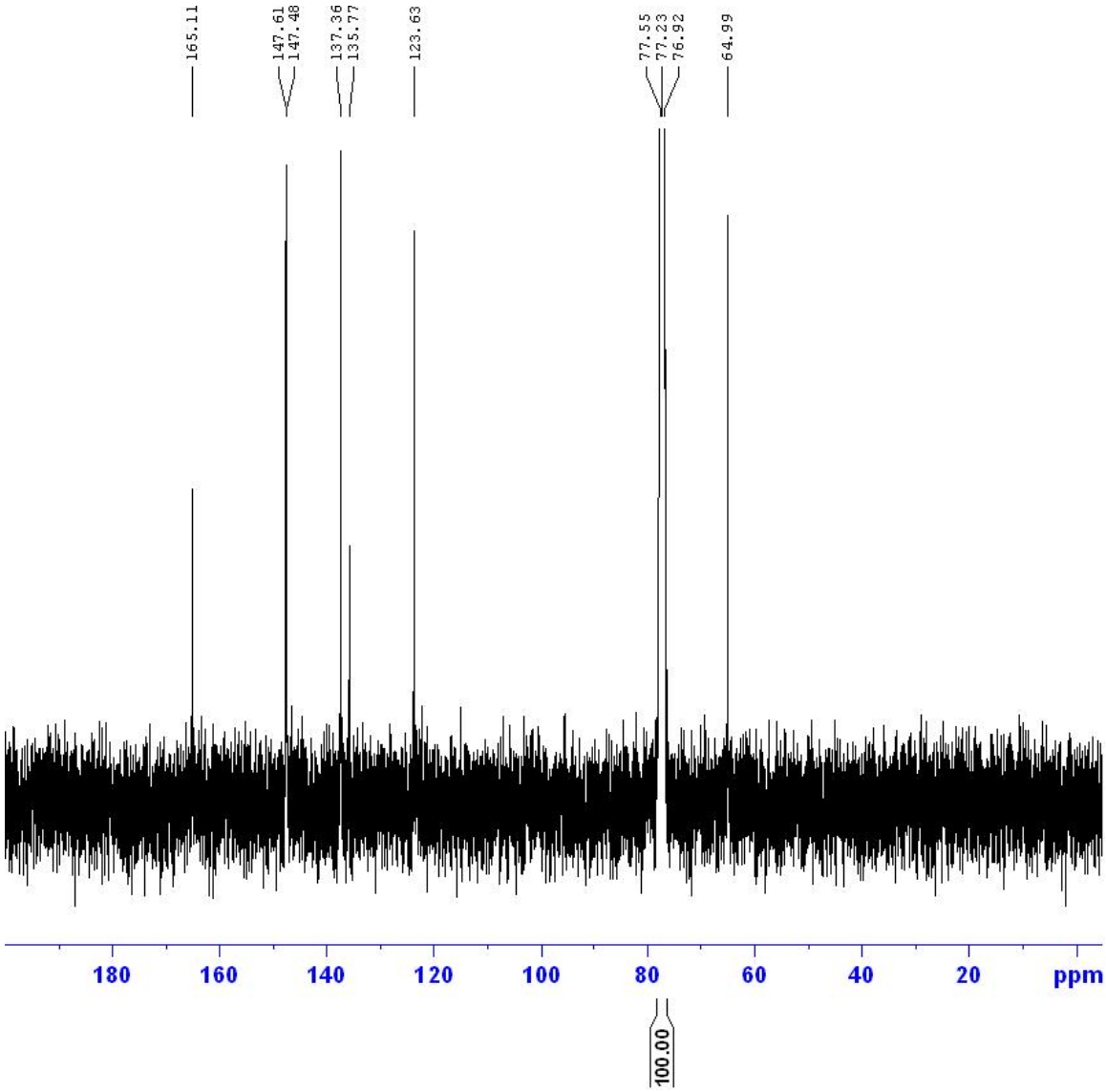

^{13}C-NMR Spectrum of 5-chloropyridine-2-(*N*-hydroxymethyl)carboxamide (**13**)

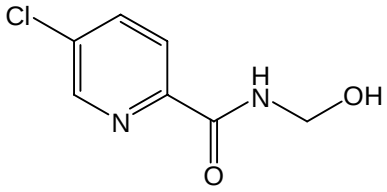

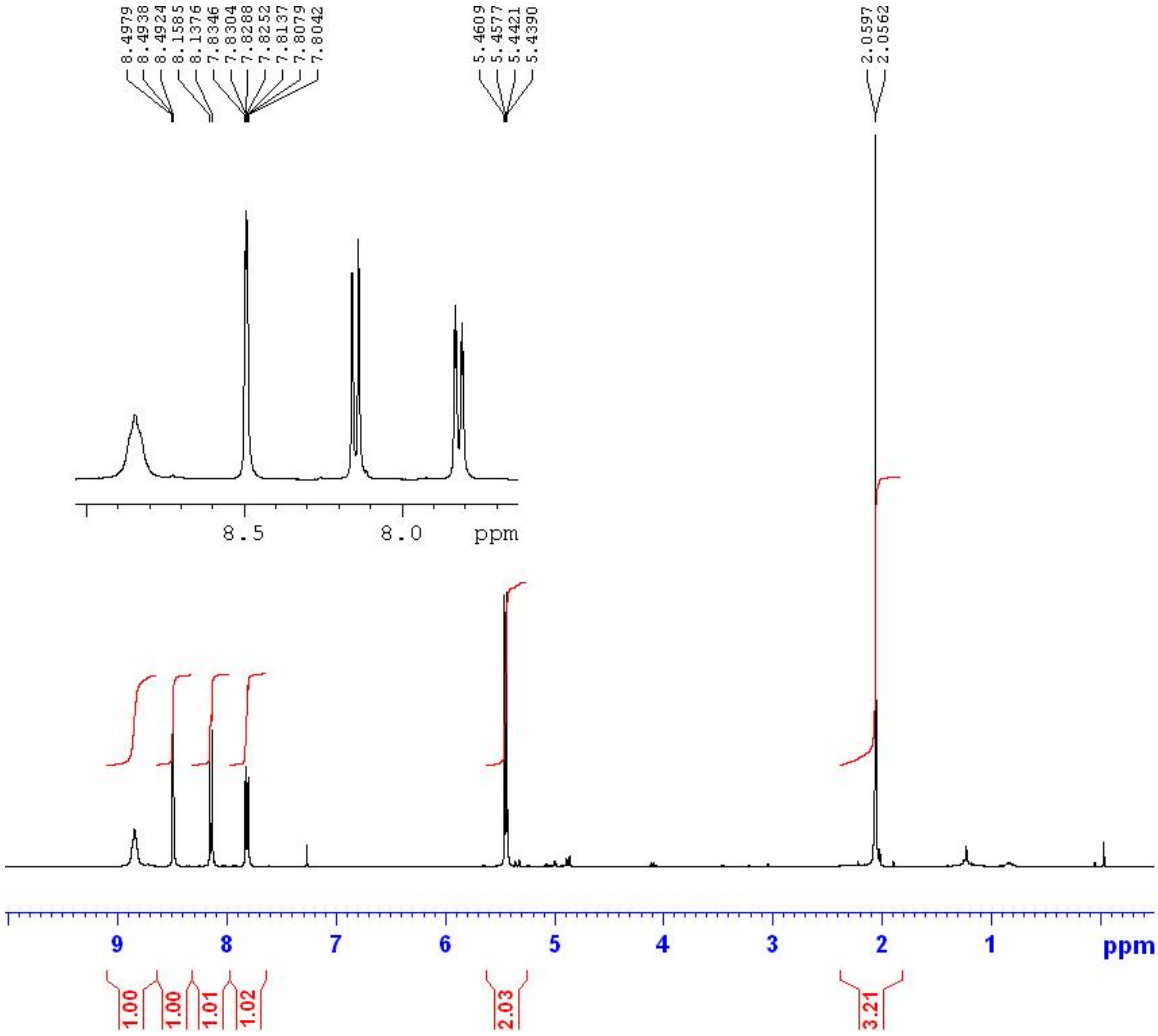

^{1}H-NMR Spectrum of 5-chloropyridine-2-(*N*-acetoxymethyl)carboxamide (**14**)

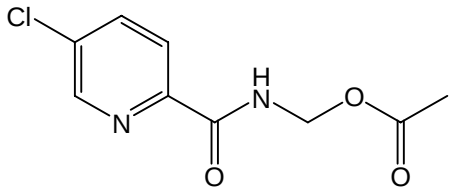

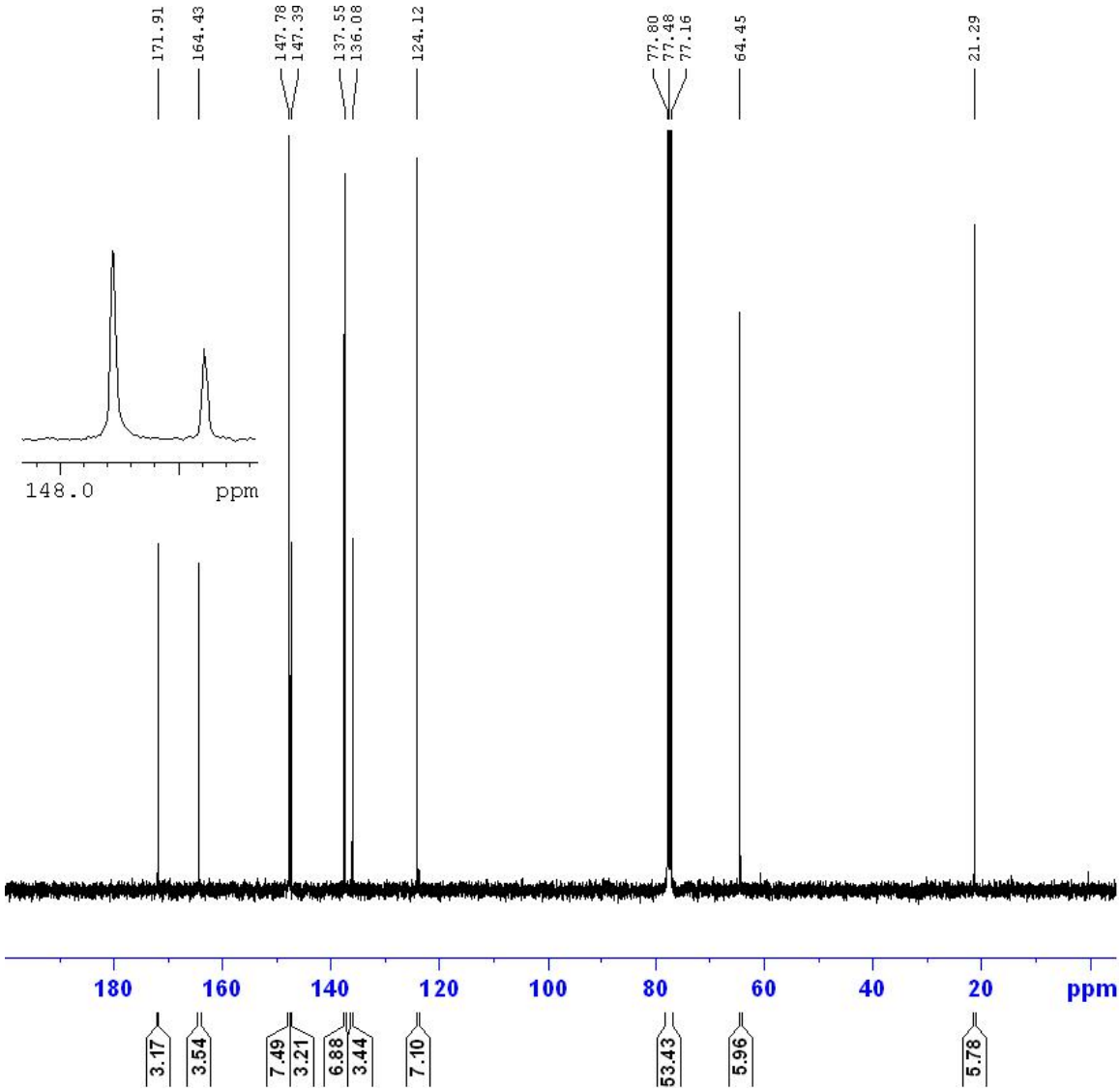

^{13}C-NMR Spectrum of 5-chloropyridine-2-(*N*-acetoxymethyl)carboxamide (**14**)

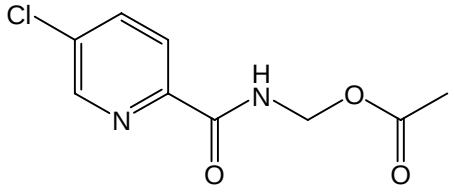

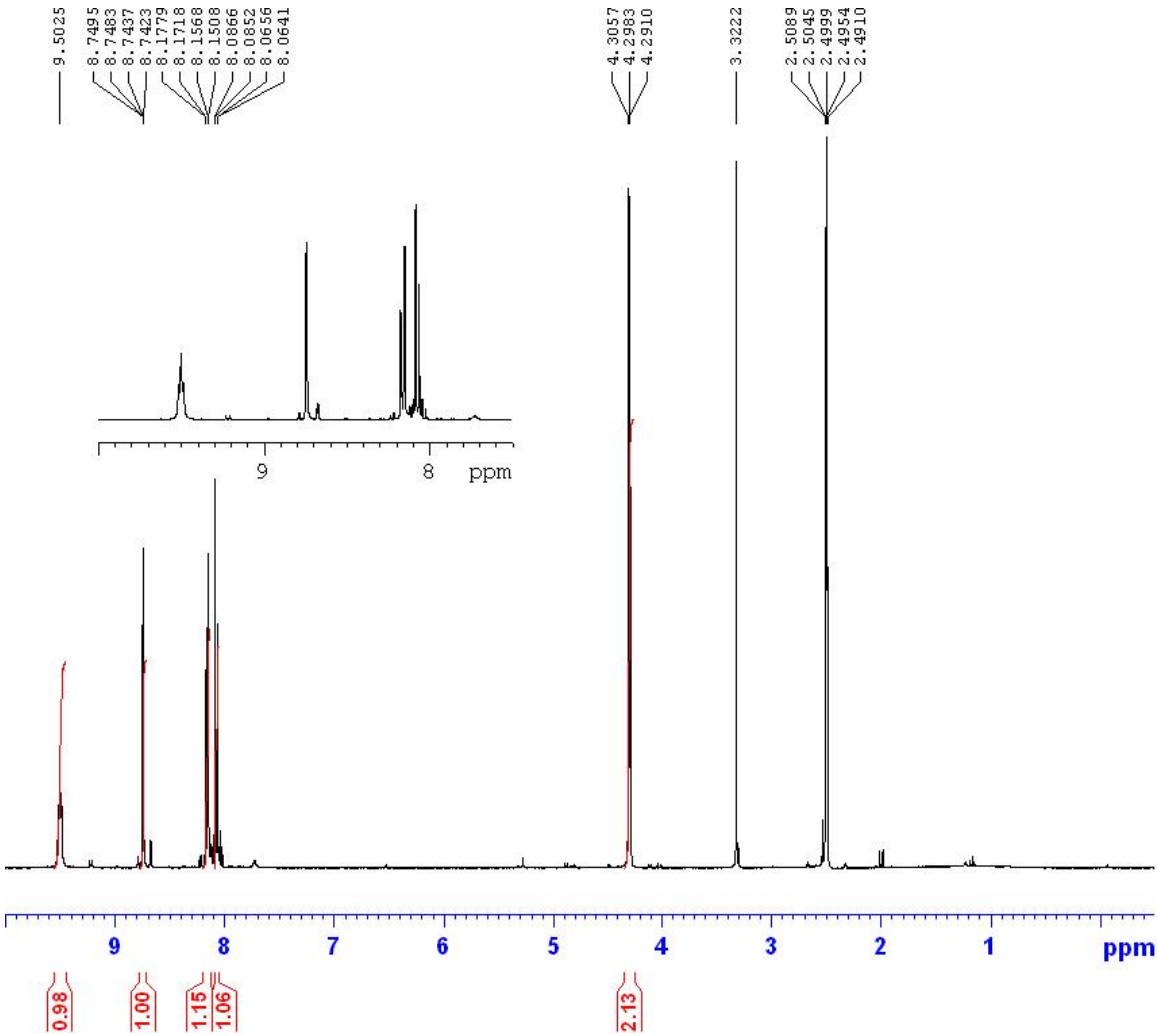

^{1}H-NMR Spectrum of 5-chloropyridine-2-(*N*-cyanomethyl)carboxamide (**15**, DMSO-d_6)

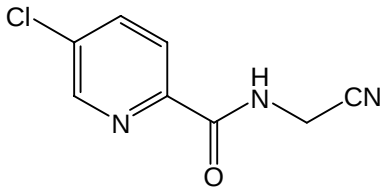

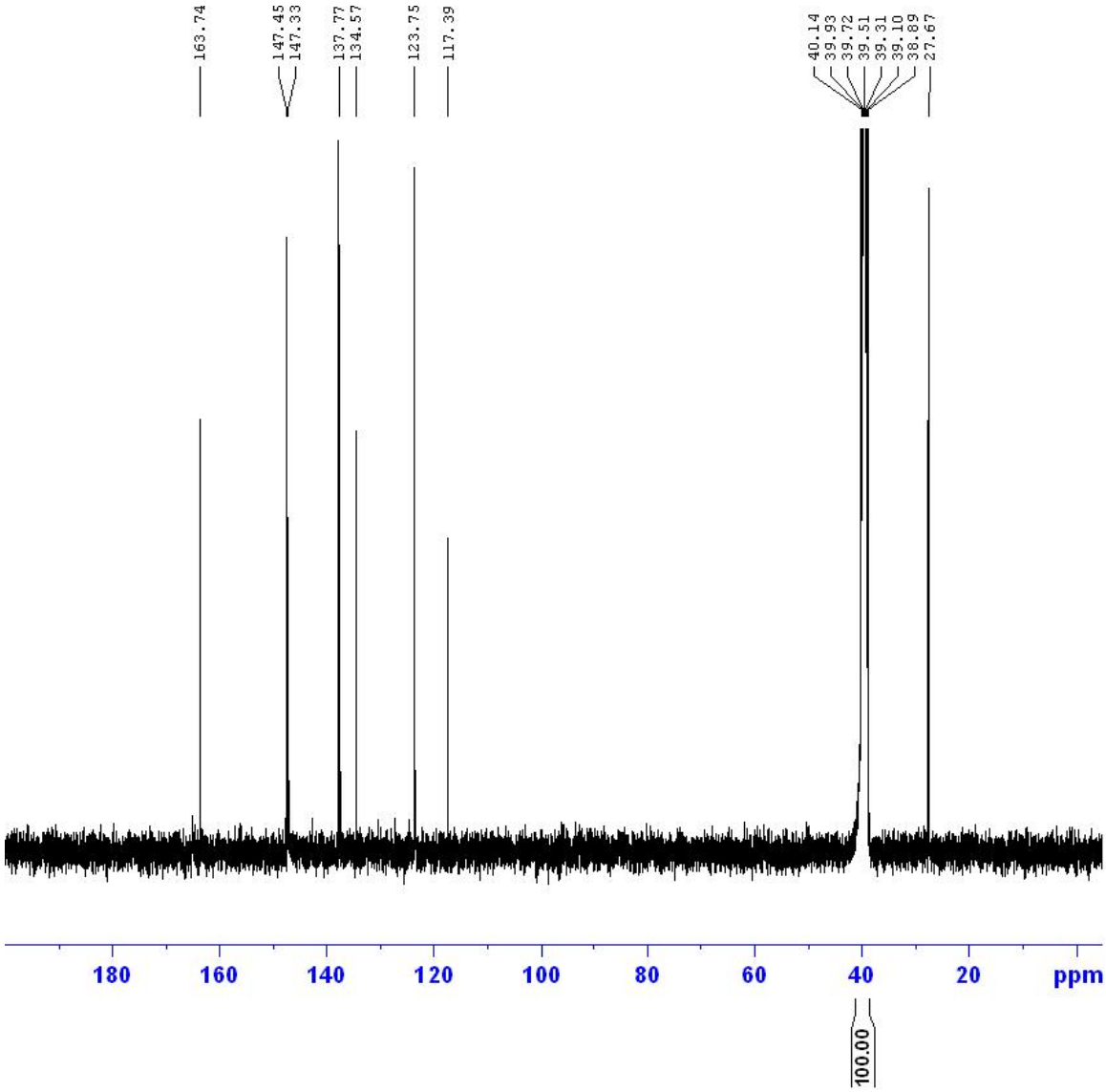

^{13}C-NMR Spectrum of 5-chloropyridine-2-(*N*-cyanomethyl)carboxamide (**15**, DMSO-d_6)

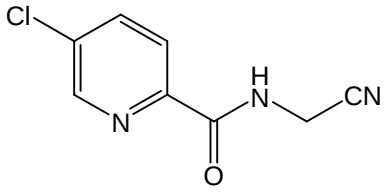

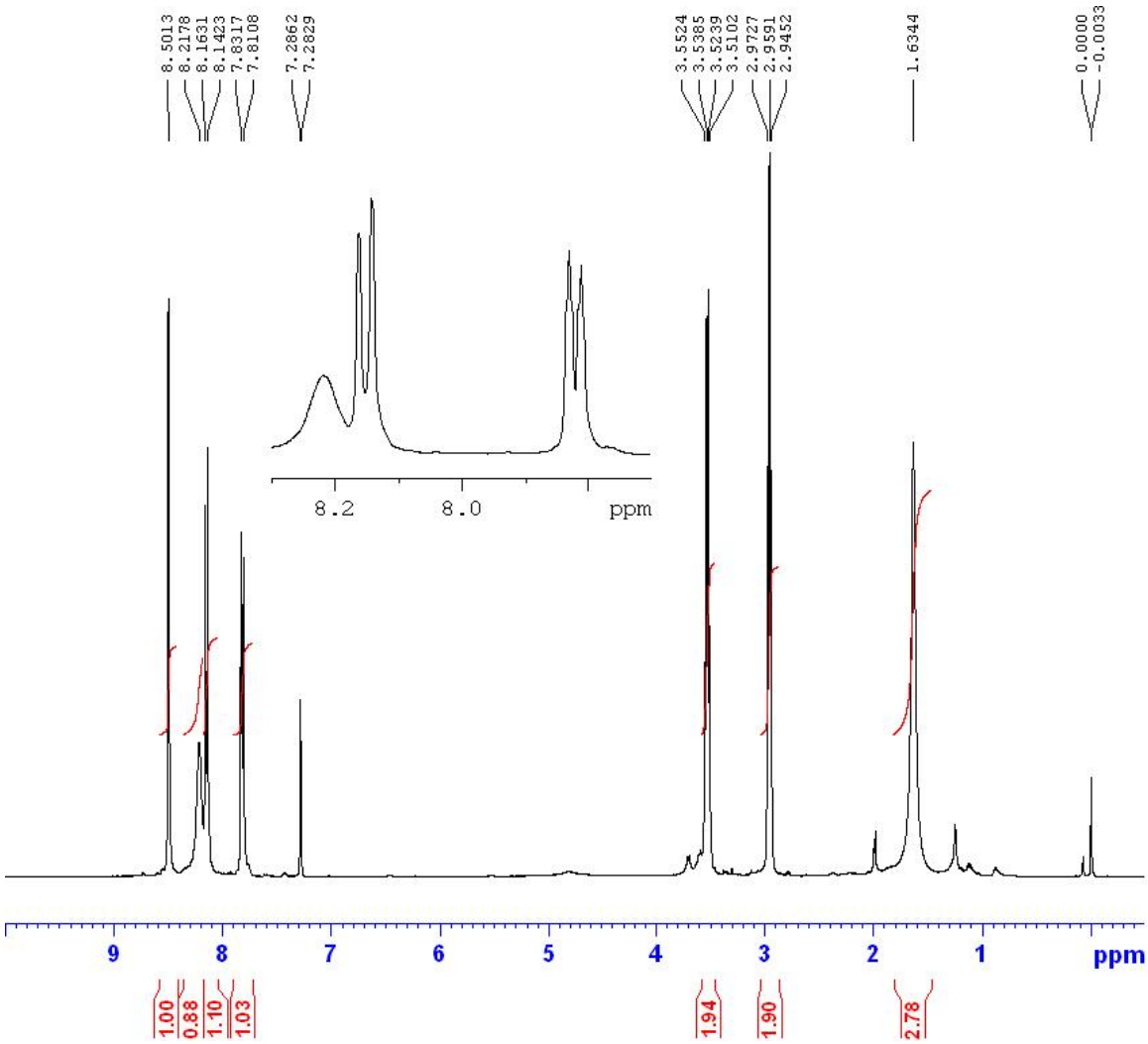

^{1}H-NMR Spectrum of 5-chloropyridine-2-(*N*-2'-aminoethyl)carboxamide (Ro 19-6327)

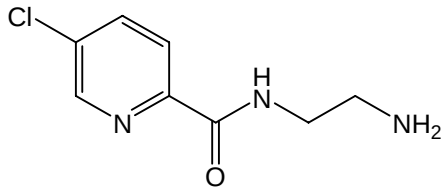

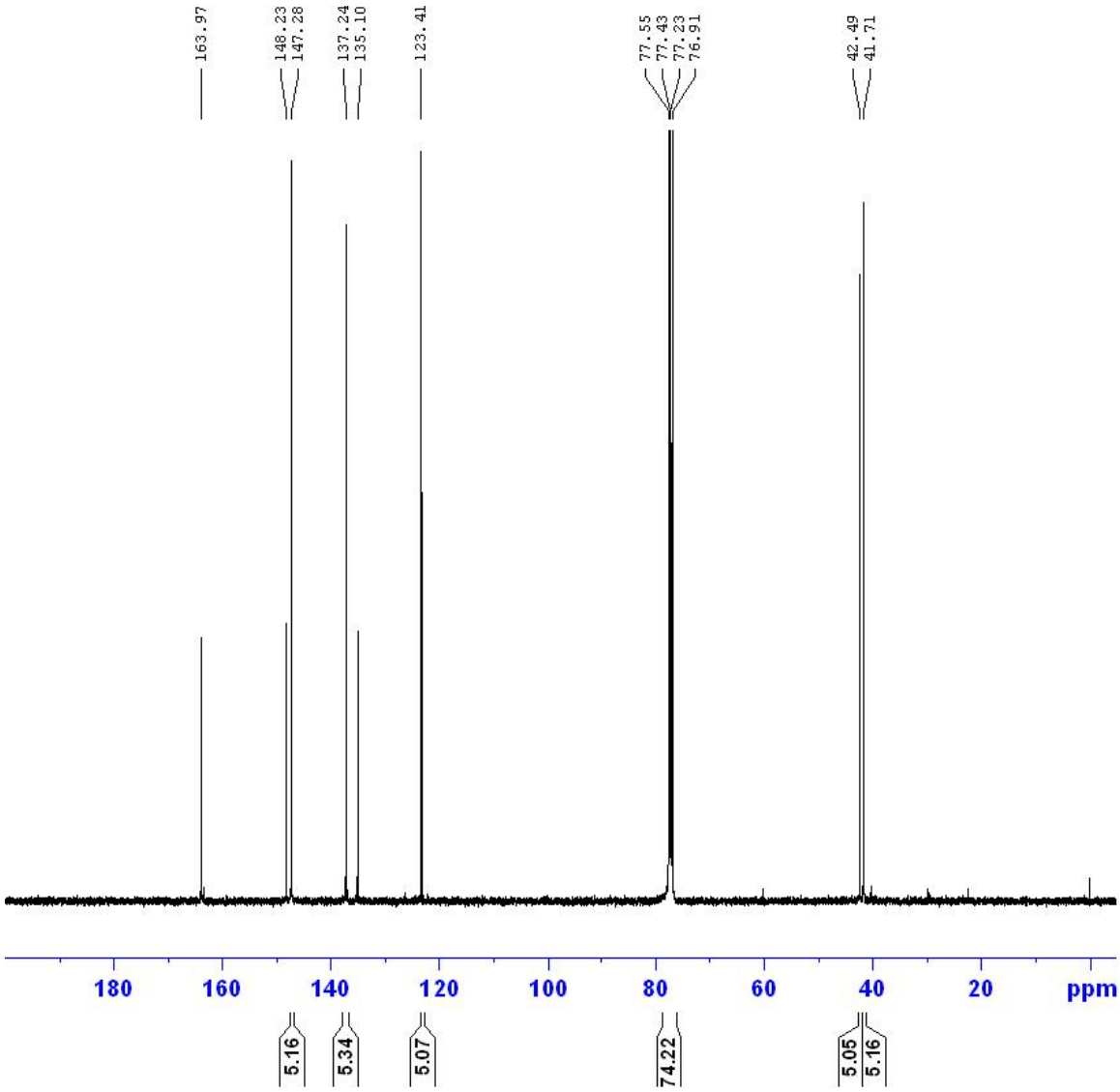

^{13}C-NMR Spectrum of 5-chloropyridine-2-(*N*-2'-aminoethyl)carboxamide (Ro 19-6327)

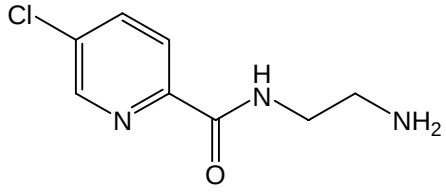

Reference

[1] Reivich M, Kuhl D, Wolf AP, Greenberg J, Phelps M, Ido T, Casella V, Fowler JS, Hoffman E, Alavi A, Som P, Sokoloff L. The [^{18}F]fluorodeoxyglucose method for the measurement of local cerebral glucose utilization in man. Circ Res 1979; 44: 127-37.

[2] Farde L, Ehrin E, Eriksson L, Greitz T, Hall H, Hedström CG, Litton JE, Sedvall G. Substituted benzamides as ligands for visualization of dopamine receptor binding in the human brain by positron emission tomography. Proc Natl Acad Sci USA 1985; 82: 3863-7.

[3] Fowler JS, Wolf AP. Working against time. Rapid radiotracer synthesis and imaging the human brain. Acc Chem Res 1997; 30: 181-8.

[4] Christman DR, Finn RD, Karlstrom KI, Wolf AP. The production of ultra-high activity ^{11}C-labelled hydrogen cyanide, carbon dioxide, carbon monoxide and methane via the ^{14}N(p,α)^{11}C reaction. Int J Appl Radiat Isot 1975; 26: 435-42.

[5] Schlyer DJ, Bastos MA, Alexoff D, Wolf AP. Separation of [^{18}F]fluoride from [O-18]water using anion exchange resin. Int J Appl Radiat Isot [A] 1990; 41: 531-3.

[6] Hamacher K, Coenen HH, Stocklin G. Effective stereospecific synthesis of no-carrier-added 2-[^{18}F]fluoro-2-deoxy-D-glucose using amino-polyether supported nucleophilic substitution. J Nucl Med 1986; 27: 235-8.

[7] Kiesewetter DO, Eckelman WC, Cohen RM, Finn RD, Larson SM. Syntheses and D_2 receptor affinities of derivatives of spiperone containing aliphatic halogens. Int J Appl Radiat Isot [A] 1986; 37: 1181-8.

[8] Ferrieri RA, Schlyer DJ, Wieland BW, Wolf AP. On-line production of ^{13}N-nitrogen gas from a solid enriched ^{13}C-target and its application to ^{13}N-ammonia synthesis using microwave radiation. Int J Appl Radiat Isot 1983; 34: 897-900.

[9] Bida G, Wieland BW, Ruth TJ, Schmidt DG, Hendry GO, Keen RE. An economical target for nitrogen-13 production by proton bombardment of a slurry of C-13 powder on ^{16}O water. J Labelled Compds Radiopharm 1986; 23: 1217-8.

[10] Dence CS, Welch MJ, Hughey BJ, Shefer RE, Klinkowstein RE. Production of [^{13}N]ammonia applicable to low energy accelerators. Nucl Med Biol 1994; 21: 987-96.

[11] Vaalburg W, Kamphuis JA, Beerling-van der Molen HD, Rijskamp A, Woldring MG. An improved method for the cyclotron production of ^{13}N-labeled ammonia. Int J Appl Radiat Isot 1975; 26: 316-8.

[12] Vera-Ruiz H, Wolf AP. Direct synthesis of oxygen-15 labeled water of high specific activity. J Labelled Compds Radiopharm 1978; 15: 186-9.

[13] Iwata R, Ido T, and Saji H. A remote controlled synthesis of ^{11}C-iodomethane for the practical preparation of ^{11}C-labeled radiopharmaceuticals. Int J Appl Radiat Isot 1979; 30: 194-6.

[14] Marazano C, Maziere M, Berger G, Comar D. Synthesis of methyl iodide-^{11}C and formaldehyde-^{11}C. Int J Appl Radiat Isot 1977; 28: 49-54.

[15] Hooker JM, Schönberger M, Schieferstein H, Fowler JS. A simple, rapid method for the preparation of [^{11}C]formaldehyde. Angew Chem Int Ed 2008; 47: 5989-92.

[16] Roeda D, Crouzel C, Van Zanten B. Synthesis of ^{11}C-urea for medical use. Radiochem Radioanalytical Lett 1978; 33: 175-6

[17] Steel CJ, Brady F, Luthra SK, Brown G, Khan I, Poole KG, Sergis A, Jones T, Price PM. An automated radiosynthesis of 2-[^{11}C]thymidine using anhydrous [^{11}C]urea derived from [^{11}C]phosgene. Appl Radiat Isot 1999; 51: 377-88.

[18] Emran AM, Boothe TE, Finn RD, Vora MM, Kothari PJ, Wooten JT. Optimized production of high specific activity [^{11}C]urea. Int J Appl Radiat Isot 1985; 36: 739-40.

[19] Visser TJ, van der Wouden EA, van Waarde A, Doze P, Elsinga PH, Vaalburg W. Synthesis and biodistribution of [^{11}C]procaterol a β_2-adenoceptor agonist for positron emission tomography. Appl Radiat Isot 2000; 52: 857-63.

[20] Långström B, Itsenko O, Rahman O. [^{11}C]Carbon monoxide, a versatile and useful precursor in labelling chemistry for PET-ligand development. J Label Compd Radiopharm 2007; 50: 794-810.

[21] Larsen P, Ulin J, Dalhstrom K, and Jensen M. Synthesis of [^{11}C]iodomethane by iodination of [^{11}C]methane. Appl Radiat Isot 1997; 48: 153-7.

[22] Jewett DM. A simple synthesis of [^{11}C]methyl triflate. Appl Radiat Isot 1992; 43: 1383-5.

[23] Reiffers S, Vaalburg W, Wiegman T, Wijnburg H, Woldring MG. Carbon-11 labelled methyl lithium as a methyl donating agent: the addition to 17-keto steroids. Int J Appl Radiat Isot 1980; 31: 535-9.

[24] McCarran JA, Pike VW. Synthesis of no-carrier-added [^{11}C]methanesulfonyl chloride as a new labeling agent for PET radiopharmaceutical development. J Labelled Compd Radiopharm. 2003; 46: 1127-40.

[25] Brown GD, Luthra SK, Brock CS, Stevens MFG, Price PM, Brady F. Antitumor imidazotetrazines 40. ^{1}Radiosyntheses of [4-^{11}C-c*arbonyl*]- and [3-*N*-^{11}C-*methyl*]-8-carbamoyl-3-methylimidazo[5,1-*d*]-1,2,3,5-tetrazin-4(3*H*)-one (temozolomide) for positron emission tomography (PET) studies. J Med Chem 2002; 45: 5448-57.

[26] Schoeps K-O, Stone-Elander S, Halldin C. On-line synthesis of [^{11}C]nitroalkanes. Appl Radiat Isot 1989; 40: 261-2.

[27] Westerberg G, Långström B. On-line production of [^{11}C]cyanogen bromide. Appl Radiat Isot 1997; 48: 459-61.

[28] Crouzel C, Amano R, Fournier D. Synthesis of carbon-11 labelled diazomethane. Appl Radiat Isot 1987; 38: 669-70.

[29] Ehrin E, Gawell L, Hogberg T, de Paulis T, Ström P. Synthesis of [methoxy-^{3}H]- and [methoxy-^{11}C]-labelled raclopride. Specific dopamine-D_2 receptor ligands. J Labelled Compd Radiopharm 1987; 24: 931-40.

[30] Wilson AA, Ginovart N, Schmidt M, Meyer JH, Threlkeld PG, Houle S. Novel radiotracers for imaging the serotonin transporter by positron emission tomography: synthesis, radiosynthesis, and in vitro and ex vivo evaluation of ^{11}C-labeled 2-(phenylthio)araalkylamines. J Med Chem 2000; 43: 3103-10.

[31] Samuelsson L, Långström B. Synthesis of 1-(2'-deoxy-2'-fluoro-β-rabinofuranosyl)-[methyl-^{11}C]thymine ([^{11}C]FMAU) via a Stille cross-coupling reaction with [^{11}C]methyl iodide. J Labeled Compd Radiopharm 2003; 46: 263-72.

[32] McCarron JA, Turton DR, Pike VW, Poole KG. Remotely-controlled production of the 5-HT_{1A} receptor radioligand, [carbonyl-^{11}C]WAY-100635, via ^{11}C-carboxylation of an immobilized Grignard reagent. J Labelled Compd Radiopharm 1996; 38: 941-53.

[33] Kihlberg T, Karimi F, Långström B. [^{11}C]Carbon monoxide in selenium-mediated synthesis of ^{11}C-carbamoyl compounds. J Org Chem 2001; 67: 3687-92.

[34] Dolle F, Valette H, Bramoulle Y, Guenther I, Fuseau C, Coulon C, Lartizien C, Jegham S, George P, Curet O, Pinquier J-L, Bottlaender M. Synthesis and in vivo imaging properties of [^{11}C]befloxatone: A novel highly potent positron emission tomography ligand for mono-amine oxidase-A. Bioorg Med Chem Lett 2003; 13: 1771-5.

[35] Mathews WB, Nakamoto Y, Abraham EH, Scheffel U, Hilton J, Ravert HT, Tatsumi M, Rauseo PA, Traughber BJ, Salikhova AY, Dannals RF, Wahl RL. Synthesis and biodistribution of [^{11}C]adenosine 5'-monophosphate ([^{11}C]AMP). Mol Imaging Biol 2005; 7: 203-8.

[36] Dollé F, Hinnen F, Valette H, Fuseau C, Duval R, Péglion J-L, Crouzel C. Synthesis of two optically active calcium channel antagonists labeled with carbon-11 for in vivo cardiac PET imaging. Bioorg Med Chem 1997; 5: 749-64.

[37] Wilson AA, Garcia A, Chestakova A, Kung H, Houle S. A rapid one-step radiosynthesis of the β-amyloid imaging radiotracer N-methyl-[^{11}C]2-(4'-methylaminophenyl)-6-hydroxybenzothiazole ([^{11}C]-6-OH-BTA-1). J Labelled Compd Radiopharm. 2004; 47: 679-82.

[38] Lidström P, Neu H, Långström B. Synthesis of [21-^{11}C] and (21-^{13}C)progesterone. J Labelled Compd Radiopharm 1997; 39: 695-704.

[39] Soloviev DV, Matarrese M, Moresco RM, Todde S, Bonasera TA, Sudati F, Simonelli P, Magni F, Colombo D, Carpinelli A, Kienle MG, Ferruccio Fazio F. Asymmetric synthesis and preliminary evaluation of (R)- and (S)-[^{11}C]bisoprolol, a putative β_1-selective adrenoceptor radioligand. Neurochem Int 2001; 38: 169-80.

[40] Prenant C, Sastre J, Crouzel C, Syrota A. Synthesis of ^{11}C-pindolol. J Labelled Compd Radiopharm 1987; 24: 227-32.

[41] Någren K, Schoeps K-O, Halldin C, Swahn C-G, Farde L. Selective synthesis of racemic 1-^{11}C-labelled norepinephrine, octopamine, norphenylephrine and phenylethanolamine using [^{11}C]nitromethane. Appl Radiat Isot 1994; 45: 515-21.

[42] Westerberg G, Långström B. Labelling of proteins with ^{11}C in high specific radioactivity: [^{11}C]albumin and [^{11}C]transferrin. Appl Radiat Isot 1994; 45: 773-82.

[43] Müller K, Faeh C, Diederich F. Fluorine in pharmaceuticals: Looking beyond intuition. Science 2007; 317: 1881-6.

[44] Zhao K, Lim DS, Funaki T, Welch JT. Inhibition of dipeptidyl peptidase IV (DPP IV) by 2-(2-amino-1-fluoro-propylidene)-cyclopentanecarbonitrile, a fluoroolefin containing peptidomimetic. Bioorg Med Chem 2003; 11: 207-15.

[45] Casella V, Ido T, Wolf AP, Fowler JS, MacGegor RR, Ruth TJ. Anhydrous F-18 labeled elemental fluorine for radiopharmaceutical preparation. J Nucl Med 1980; 21: 750-7.

[46] Bergman J, Solin O. Fluorine-18-labeled fluorine gas for synthesis of tracer molecules. Nucl Med Biol 1997; 24: 677-83.

[47] Nickles RJ, Hichwa RD, Daube ME, Hutchins GD, Congdon DD. An $^{18}O_2$-target for the high yield production of ^{18}F-fluoride. Int J Appl Radiat Isot 1983; 34: 625-9.

[48] Ido T, Wan C-N, Casella V, Fowler JS, Wolf AP, Reivich M, Kuhl DE. Labeled 2-deoxy-D-glucose analogs, ^{18}F-labeled 2-deoxy-2-fluoro-D-glucose, 2-deoxy-2-fluoro-D-mannose and ^{14}C-2-deoxy-2-fluoro-glucose. J Labelled Compd Radiopharm 1978; 14: 171-83.

[49] Murakami M, Takahashi K, Kondo Y, Mizusawa S, Nakamichi H, Sasaki H, Hagami E, Iida H, Kanno I, Miura S, Uemura K. The comparative synthesis of ^{18}F-fluorophenylalanines by electrophilic substitution with ^{18}F-F_2 and ^{18}F-AcOF. J Labelled Compd Radiopharm 1988; 25: 573-8.

[50] Sood S, Fimau G, Garnett ES. Radiofluorination with xenon difluoride. Int J Appl Radiot Isot 1983; 34: 743-5.

[51] Oberdorfer F, Hofmann E, Maier-Borst W. Preparation of a new ^{18}F-labelled precursor: 1-[^{18}F]fluoro-2-pyridone. Appl Radiat Isot 1988; 39: 685-8.

[52] Oberdorfer F, Hofmann E, Maier-Borst W. Preparation of ^{18}F-labelled N-fluoropyridinium triflate. J Labeled Compd Radiopharm 1988; 25: 999-1005.

[53] Ehrenkaufer RE, MacGregor RR. Synthesis of [^{18}F]perchloryl fluoride and its reactions with functionalized aryl lithiums. Int J Appl Radiat Isot. 1983; 34: 613-5.

[54] Satyamurthy N, Bida GT, Phelps ME, Barrio JR. N-[^{18}F]fluoro-N-alkylsulfonamides: Novel reagents for mild and regioselective radiofluorination. Appl Radiat Isot 1990; 41: 733-8.

[55] Namavari M, Bishop A, Satyamurthy N, Bida G, Barrio JR. Regioselective radiofluorodestannylation with [^{18}F]F_2 and [^{18}F]CH_3COOF: a high yield synthesis of 6-[^{18}F]fluoro-l-dopa. Appl Radiat Isot 1992; 43: 989-96.

[56] Hamacher K, Coenen HH, Stöcklin G. Efficient stereospecific synthesis of no-carrier-added 2-[^{18}F]-fluoro-2-deoxy-D-glucose using aminopolyether supported nucleophilic substitution. J Nucl Med 1986; 27: 235-8.

[57] Ding Y-S, Liang F, Fowler JS, Kuhar MJ, Carroll FI. Synthesis of [^{18}F]norchlorofluoroepibatidine and its N-methyl derivative: new PET ligands for mapping nicotinic acetylcholine receptors. J labelled Compd Radiopharm 1997; 39: 827-32.

[58] Forngren T, Andersson Y, Lamm B, Långström B. Synthesis of [4-^{18}F]-1-bromo-4-fluorobenzene and its use in palladium-promoted cross coupling reactions with organostannanes. Acta Chem Scand 1998; 52: 475-9.

[59] Satyamurthy N, Bida GT, Barrio JR, Luxen A, Mazziotta JC, Huang S-C, Phelps ME. No-carrier-added 3-(2'-[^{18}F]fluoroethyl)spiperone, a new dopamine receptor-binding tracer for positron emission tomography. Nucl Med Biol 1986; 13: 617-24.

[60] Mercer JR. Molecular imaging agents for clinical positron emission tomography in oncology other than fluorodeoxyglucose (FDG): applications, limitations, and potential. J Pharm Pharmaceut Sci 2007; 10: 180-202.

[61] United States Pharmacopeia. The United States Pharmacopeia. 27th ed., and The National Formulary, 22nd ed. Rockville, MD: United States Pharmacopeial Convention, Inc.; 2004.

[62] Yu S. Review of ^{18}F-FDG synthesis and quality control. Biomed Imaging Interv J 2006; 2: e57-67.

[63] Zeng Z, Chen T-B, Miller PJ, Dean D, Tang YS, Sur C, Williams DL Jr. The serotonin transporter in rhesus monkey brain: comparison of DASB and citalopram binding sites. Nucl Med Biol 2006; 33: 555-63.

[64] Abeles RH, Maycock AL. Suicide Enzyme Inactivators. Acc Chem Res 1976; 9: 313-9.

[65] Maycock AL, Abeles RH, Salach JI, Singer TP. The structure of the covalent adduct formed by the interaction of 3-dimethylamino-1-propyne and the flavine of mitochondrial amine oxidase. Biochem 1976; 15: 115-25.

[66] Fowler JS, Wang G-J, Logan J, Xie S, Volkow ND, MacGregor RR, Schlyer DJ, Pappas N, Alexoff DL, Patlak C, Wolf AP. Selective reduction of radiotracer trapping by deuterium substitution: comparison of carbon-11-L-deprenyl and carbon-11-deprenyl-D_2 for MAO B mapping. J Nucl Med 1995; 36: 1255-62.

[67] Ding Y-S, Fowler JS. New-generation radiotracers for nAChR and NET. Nucl Med Biol 2005; 32: 707-18.

[68] Lipinski CA, Lombardo F, Dominy BW, Feeney PJ. Experimental and computational approaches to estimate solubility and permeability in drug discovery and development settings. Adv Drug Del Rev 1997; 23: 3-25.

[69] Elsinga PH. Radiopharmaceutical chemistry for positron emission tomography. Methods 2002; 27: 208-17.

[70] Huang Y, Hwang D-R, Narendran R, Sudo Y, Chatterjee R, Bae S-A, Mawlawi O, Kegeles LS, Wilson AA, Kung HF, Laruelle M. Comparative evaluation in nonhuman primates of five PET radiotracers for imaging the serotonin transporters: [^{11}C]McN 5652, [^{11}C]ADAM, [^{11}C]DASB, [^{11}C]DAPA, and [^{11}C]AFM.

[71] Logan J, Fowler JS, Volkow ND, Wolf AP, Dewey SL, David SJ, MacGregor RR, Hitzemann R, Bendriem B, Gatley SJ, Christman DR. Graphical analysis of reversible radioligand binding from time-activity measurements applied to [N-^{11}C-

methyl]-(-)-cocaine PET studies in human subjects. J Cereb Blood Flow Metab 1990; 10: 740-7.

[72] Logan J. A review of graphical methods for tracer studies and strategies to reduce bias. Nucl Med Biol 2003; 30: 833-44.

[73] Bessell EM, Courtenay VD, Foster AB, Jones M, Westwood JH. Some in vivo and in vitro antitumor effect of the deoxyfluoro-D-glucopyranoses. Eur J Cancer 1973; 9: 463-70.

[74] Matheny CJ, Lamb MW, Brouwer KLR, Pollack GM. Pharmacokinetic and pharmacodynamic implications of P-glycoprotein modulation. Pharmacotherapy 2001; 21: 778-96.

[75] Hendrikse NH, Franssen EJF, van der Graaf WTA, Vaalburg W, de Vries EGE. Visualization of multidrug resistance in vivo. Eur J Nucl Med 1999; 26: 283-93.

[76] Passchier J, van Waarde A, Doze P, Elsinga PH, Vaalburg W. Influence of P-glycoprotein on brain uptake of [^{18}F]MPPF in rats. Eur J Pharmacol 2000; 407: 273-80.

[77] Houle S, Ginovart N, Hussey D, Meyer JH, Wilson AA. Imaging of serotonin transporter with positron emission tomography: initial human studies with [^{11}C]DAPP and [^{11}C]DASB. Eur J Nucl Med 2000; 27: 1719-22.

[78] Rudd JHF, Warburton EA, Fryer TD, Jones HA, Clark JC, Antoun N, Johnström P, Davenport AP, Kirkpatrick PJ, Arch BN, Pickard JD, Weissberg PL. Imaging atherosclerotic plaque inflammation with [^{18}F]-fluorodeoxyglucose positron emission tomography. Circulation 2002; 105: 2708-11.

[79] Collins JM, Klecker RW Jr., Anderson LW. Imaging of drug accumulation as a guide to antitumor therapy. US Patent 20030198594A1; 2003

[80] Fowler JS, Volkow ND, Wang G-J, Ding Y-S, Dewey SL. PET and drug research and development. J Nucl Med. 1999; 40: 1154-63

[81] Collins JM. PET and drug development. In: Wahl RL, Buchanan JW, editors. Principles and practice of positron emission tomography. Lippincott Williams & Wilkins; 2002, p.411-9

[82] Saglo G, Morotti A, Mattioli G, Messa E, Giugliano E, Volpe G, Rege-Cambrin G, Cilloni D. Rational approaches to the design of therapeutics targeting molecular markers: The case of chronic myeloid leukemia. Ann N Y Acad Sci. 2004; 1028; 423-31

[83] Cohen P. Protein Kinase-the major drug targets of the twenty-first century? Nat Rev Drug Discov. 2002; 1; 309-15

[84] Joensuu H. Treatment of inoperable gastrointestinal stromal tumor (GIST) with Imatinib (Glivec, Gleevec). Med Klin (Munich). 2002; 97: S1 28-30

[85] Zaknun JJ, Kendler D, Moncayo R, zur Nedden D, Virgolini I. F-18 FDG PET for assessing tyrosine kinase-related signal transduction inhibition in a GIST c-kit-positive tumor patient by imatinib. Clin Nucl Med. 2005; 30: 749-51

[86] For recent review, see Deininger M, Buchdunger E, Druker BJ. The development of imatinib as a therapeutic agent for chronic myeloid leukemia. Blood 2005; 105: 2640-53

[87] Nowell P, Hungerford D. A minute chromosome in human chronic granulocytic leukemia. Science 1960; 132: 1497

[88] Rowley JD. A new consistent chromosomal abnormality in chronic myeloid leukemia identified by quinacrine fluorescence and Giemsa staining. Nature 1973; 243: 290-3

[89] Druker BJ, Tamura S, Buchdunger E, Ohno S, Segal GM, Fanning S, Zimmermann J, Lydon NB. Effects of a selective inhibitor of the abl tyrosine kinase on the growth of bcr-abl positive cells. Nat Med. 1996; 2: 561-6

[90] Deininger M, Goldman GM, Lydon NB, Melo JV. The tyrosine kinase inhibitor CGP57148B selectively inhibits the growth of bcr-abl positive cells. Blood 1997; 90: 3691-8

[91] Nagar B, Bornmann WG, Pellicena P, Schindler T, Veach DR, Miller WT, Clarkson B, Kuriyan J. Crystal structure of the kinase domain of c-abl in complex with the small molecule inhibitors PD173955 and imatinib (STI-571). Cancer Res. 2002; 62: 4236-43

[92] La Rosee P, Corbin AS, Stoffregen EP, Deininger MW, Druker BJ. Activity of the bcr-abl kinase inhibitor PD180970 against clinically relevant bcr-abl isoforms that cause resistance to imatinib mesylate (Gleevec, STI571). Cancer Res. 2002; 62: 7149-53

[93] Cowan-Jacob SW, Guez V, Fendrich G, Griffin JD, Fabbro D, Furet P, Liebetanz J, Mestan J, Manley PW. Imatinib (STI571) resistance in chronic myelogenous leukemia: molecular basis of the underlying mechanisms and potential strategies for treatment. Mini Rev Med Chem. 2004; 4: 285-99

[94] Buchdunger E, Cioffi CL, Law N, Stover D, Ohno-Jones S, Druker BJ, Lydon NB. Abl protein-tyrosine kinase inhibitor STI571 inhibits in vitro signal transduction mediated by c-kit and platelet-derived growth factor receptors. J Pharmacol Exp Ther. 2000; 295: 139-45

[95] Tuveson DA, Willis NA, Jacks T, Griffin JD, Singer S, Fletcher CD, Fletcher JA, Demetri GD. STI571 inactivation of the gastrointestinal stromal tumor c-kit oncoprotein: biological and clinical implications Oncogene 2001; 20: 5048-58

[96] Kindblom LG, Remotti HE, Aldenborg F, Meis-Kindblom JM. Gastrointestinal pacemaker cell tumor (GIPACT): gastrointestinal stromal tumors show phenotype characteristics of the intestinal cells of Cajal. Am J Pathol. 1998; 152: 1259-69

[97] Hirota S, Isozaki K, Moritama Y, Hashimoto K, Nishida T, Ishiguro S, Kawano K, Hanada M, Kurata A, Takeda M, Tunio GM, Matsuzawa Y, Kanakura Y, Shinomura Y, Kitamura Y. Gain-of-function mutations of c-kit in human gastrointestinal stromal tumors. Science 1998; 279: 577-80

[98] Antonescu CR, Sommer G, Sarran L, Tschernyavsky SJ, Riedel E, Woodruff JM, Robson M, Maki R, Brennan MF, Ladanyi M, DeMatteo RP, Besmer P. Association of kit exon9 mutations with nongastric primary site and aggressive behavior: kit mutation analysis and clinical correlates of 120 gastrointestinal stromal tumors. Clin Cancer Res. 2003; 9: 3329-37

[99] Lux ML, Rubin BP, Biase TL, Chen C-J, Maclure T, Demetri G, Xiao S, Singer S, Fletcher CD, Fletcher JA. Kit extracellular and kinase domain mutations in gastrointestinal stromal tumors. Am J Pathol. 2000; 156: 791-5

[100] Verweij J, Casali PG, Zalcberg J, LeCesne A, Reichardt P, Blay J-Y, Issels R, van Oosterom A, Hogendoorn PCW, Glabbeke MV, Bertulli R, Judson I. Progression-free survival in gastrointestinal stromal tumors with high-dose imatinib: randomized trial. Lancet 2004; 364: 1127-34

[101] Netzer WJ, Dou F, Cai D, Veach D, Jean S, Li Y, Bornmann WG, Clarkson B, Xu H, Greengard P. Gleevec inhibits β-amyloid production but not notch cleavage. Proc Natl Acad Sci U S A. 2003; 100: 12444-9

[102] Takayama N, Sato N, O'Brien SG, Ikeda Y, Okamoto S-I. Imatinib mesylate has limited activity against the central nervous system involvement of Philadelphia chromosome-positive acute lymphoblastic leukaemia due to poor penetration into cerebrospinal fluid. Br J Haematol. 2002; 119: 106-8

[103] Ramadori G, Füzesi L, Grabbe E, Pieler T, Armbrust T. Successful treatment of hepatocellular carcinoma with the tyrosine kinase inhibitor imatinib in a patient with liver cirrhosis. Anti-Cancer Drugs 2004; 15: 405-9

[104] Eckel F, von Delius S, Mayr M, Dobritz M, Fend F, Hosius C, Schleyer E, Schulte-Frohlinde E, Schimid RM, Lersch C. Pharmacokinetic and clinical phase II trial of imatinib in patients with impaired liver function and advanced hepatocellular carcinoma. Oncology 2005; 69: 363-71

[105] Yoshiji H, Noguchi R, Kuriyama S, Ikenaka Y, Yoshii J, Yanase K, Namisaki T, Kitade M, Masaki T, Fukui H. Imatinib mesylate (STI-571) attenuates liver fibrosis development in rats. Am J Physiol Gastrointest Liver Physiol 2005; 288: G907-13

[106] Neef M, Ledermann M, Saegesser H, Schneider V, Widmer N, Decosterd LA, Rochat B, Reichen J. Oral imatinib treatment reduces early fibrogenesis but does not prevent progression in the long term. J Hepatol 2006; 44: 167-75

[107] Abdollahi A, Li M, Ping G, Plathow C, Domhan S, Kiessling F, Lee LB, McMahon G, Grone H-J, Lipson KE, Huber PE. Inhibition of platelet-derived growth factor signaling attenuates pulmonary fibrosis. J Exp Med 2005; 201: 925-35

[108] Aono Y, Nishioka Y, Inayama M, Ugai M, Kishi J, Uehara H, Izumi K, Sone S. Imatinib as a novel antifibrotic agent in bleomycin-induced pulmonary fibrosis in mice. Am J Respir Crit Care Med 2005; 171: 1279-85

[109] Zimmermann J, Burger HM. Crystal modification of a N-phenyl-2-pyrimidineamine derivative, process for its manufacture and its use. WO 9903854; 1999

[110] Zimmerman J, Buchdunger E, Mett H, Meyer T, Lydon NB. Potent and selective inhibitors of the *abl*-kinase: Phenylamino-pyrimidine (PAP) derivatives. Bioorg Med Chem Lett. 1997; 7: 187-92

[111] Szczepek W, Luniewski W, Kaczmarek L, Zagrodzki B, Samson-Lazinska D, Szelejewski W, Skarzynski M. A process for preparation of imatinib base. WO 2006071130 A2; 2006

[112] Mary A, Renko DZ, Guillou C, Thai C. Selective N-demethylation of galanthamine to norgalanthamine via a non classical Polonovski reaction. Tetrahedron Lett. 1997; 38: 5151-2

[113] Jameson DL, Guise LE. An improved, two-step synthesis of 2,2':6',2"-terpyridine. Tetrahedron Lett. 1991; 32: 1999-2002

[114] Liu Y-F, Wang C-L, Bai Y-J, Han N, Jiao J-P, Qi X-L. A facile total synthesis of imatinib base and its analogues. Org Process Res Dev. 2008; 12: 490-5

[115] Son J-K, Zhao L-X, Basnet A, Thapa P, Karki R, Na Y, Jahng Y, Jeong TC, Jeong B-S, Lee C-S, Lee E-S. Synthesis of 2,6-diaryl-substituted pyridines and their antitumor activities. Eur J Med Chem. 2008; 43: 675-82.

[116] Zimmerman J. Pyrimidine derivatives and processes for the preparation thereof. US Patent 5,521,184: 1994

[117] Kompella A, Rao B, Chowdary V. Process for preparation of the anti-cancer drug imatinib and its analogue. WO 2004108699 A1; 2004

[118] Zimmerman J, Buchdunger E, Mett H, Meyer T, Lydon NB, Traxler P. Phenylamino-pyrimidine (PAP) – derivatives: a new class of potent and highly selective PDGF-receptor autophosphorylation inhibitors. Bioorganic & Med Chem Lett. 1996; 6: 1221-6

[119] Satoh T, Suzuki S, Suzuki Y, Miyaji Y, Imai Z. Reduction of organic compounds with sodium borohydride-transition metal salt system (1): Reduction of organic nitrile, nitro and amide compounds to primary amines. Tetrahedron Lett. 1969; 52: 4555-8

[120] Metcalf CA III, Shakespeare WC, Sawyer TK, Wang Y, Bohacek R. Preparation of phosphorus-substituted pyridopyrimidimines as therapeutic agents. WO 2003000011; 2003

[121] Sairam P, Puranik R, Kelkar AS, Sasikiran S, Veerender M, Parvathi A. The ester and amide derivatives of 4-(4-methyl piperazinomethyl)benzoic acid. Syn Comm. 2003; 33: 3597-605

[122] Lee CK, Yu JS, Ji YR. Determination of aromaticity indices of thiophene and furan by nuclear magnetic resonance spectroscopic analysis of their anilides. J Heterocyclic Chem. 2002; 39: 1219-27

[123] Barker PL, Gendler PL, Rapoport H. Acylation of dibasic compounds containing amino amidine and aminoguanidine functions. J Org Chem. 1981; 46: 2455-65

[124] Del Rosario RB, Jung Y-W, Baidoo KE, Lever SZ, Wieland DM. Synthesis and *in vivo* evaluation of a $^{99m/99}$Tc-DADT-benzovesamicol: a potential marker for cholinergic neurons. Nucl Med Biol. 1994; 21: 197-203

[125] Ding Y-S, Fowler JS, Volkow ND, Logan J, Gatley SJ, Sugano Y. Carbon-11-*d-threo*-methylphenidate binding to dopamine transportor in baboon brain. J Nucl Med. 1995; 36: 2298-305

[126] Peng B, Dutreix C, Mehring G, Hayes MJ, Ben-Am M, Seiberling M, Pokorny R, Capdeville R, Lloyd P. Absolute bioavailability of imatinib (Glivec®) orally versus intravenous infusion. J Clin Pharmacol. 2004; 44: 158-62

[127] Ding Y-S, Lin K-S, Logan J, Benveniste H, Carter P. Comparative evaluation of positron emission tomography radiotracers for imaging the norepinephrine transporter: (S,S) and (R,R) enantiomers of reboxetine analogs ([^{11}C] methylreboxetine, 3-Cl-[^{11}C] methylreboxetine and [^{18}F] fluororeboxetine), (R)-[^{11}C] nisoxitine, [^{11}C] oxaprotiline and [^{11}C] lortalamine. J Neurochem. 2005; 94: 337-51

[128] Lipinski CA, Lombardo F, Dominy BW, Feeney PJ. Experimental and computational approaches to estimate solubility and permeability in drug discovery and development settings. Adv Drug Del Rev. 1997; 23; 3-25

[129] Dai HQ, Marbach P, Lemaire M, Hayes M, Elquist WF. Distribution of STI-571 to the brain is limited by p-glycoprotein-mediated efflux. J Pharmacol Exp Ther. 2003; 304: 1085-92

[130] Breedveld P, Pluim D, Cipriani G, Wielinga P, van Tellingen O, Schinkel AH, Schellen JH. The effect of bcrp1 (abcg2) on the in vivo pharmacokinetics and brain penetration of imatinib mesylate (Gleevec): Implication for the use of breast cancer resistance protein and p-glycoprotein inhibitors to enable the brain penetration of imatinib in patients. Cancer Res. 2005; 65: 2577-82

[131] Mahon FX, Deininger MW, Schultheis B, Chabrol J, Reiffers Jgoldman JM, Melo JV. Selection and characterization of bcr-abl positive cell lines with differential sensitivity to the tyrosine kinase inhibitor STI571: diverse mechanism of resistance. Blood. 2000; 96: 1070-9

[132] Novartis Pharma Stein AG. Gleevec® (imatinib mesylate): prescribing information [online]. Available from

URL: http://www.us.gleevec.com/hcp/page/hcp_prescribing_info [Accessed Oct 24, 2006]

[133] Cohen MH, Williams G, Johnson JR, Duan J, Gobburu J, Rahman A, Benson K, Leighton J, Kim SK, Wood R, Rothmann M, Chen G, Maung UK, Staten AM, Pazdur R. Approval summary for imatinib mesylate capsules in the treatment of chronic myelogenous leukemia. Clin Cancer Res 2000; 8: 935-42

[134] Deinger MW, Druker BJ. Specific targeted therapy of chronic myelogenous leukemia with imatinib. Pharmacol Rev. 2003; 55: 401-23

[135] Kerkela R, Grazette L, Yacobi R, Iliescu C, Patten R, Beahm C, Walters B, Shevtsov S, Pesant S, Clubb FJ, Rosenzweig A, Salomon RN, van Etten RA, Alroy J, Durand J-B, Force T. Cardiotoxicity of the cancer therapeutic agent imatinib mesylate. Nat Med. 2006; 12: 908-16

[136] Danielson PB. The cytochrome P450 superfamily: Biochemistry, evolution and drug metabolism in humans. Curr Drug Metab. 2002; 3: 561-97.

[137] Kragie L. Aromatase in primate pregnancy: a review. Endocr Res. 2002; 28: 121-8.

[138] Simpson ER, Clyne C, Rubin G, Boon WC, Robertson K, Britt K, Speed C, Jones M. Aromatase-A brief overview. Annu Rev Physiol. 2002; 64: 93-127.

[139] Price T, O'Brien S, Dunaif A, Simpson ER. Comparison of aromatase P450 mRNA levels in adipose tissue from the abdomen and buttock using competitive polymerase chain reaction amplification. Proc Soc Gynecol Invest. 1992; 1: 179

[140] Sasano H, Uzuki M, Sawai T, Nagura H, Matsunaga G, Kashimoto O, Harada N. Aromatase in human bone tissue. J Bone Miner Res. 1997; 12: 1416-23.

[141] Mahendroo MS, Means GD, Mendelson CR, Simpson ER. Tissue-specific expression of human P450arom: the promoter responsible for expression in adipose is different from that utilized in placenta. J Biol Chem. 1991; 266: 11276-81.

[142] Lanoux MJ, Cleland WH, Mendelson CR, Carr BR, Simpson ER. Factors affecting the conversion of androstenedione to estrogens by human fetal hepatocytes in monolayer culture. Endocrinology 1985; 117: 361-7.

[143] Simpson ER, Mahendroo MS, Means GD, Kilgore MW, Hinshelwood MM, Graham-Lorence S, Amarneh B, Ito Y, Fisher CR, Michael MD, Mendelson CR, Bulun SE. Aromatase cytochrome P450, the enzyme responsible for estrogen biosynthesis. Endocr Rev. 1994; 15: 342-55.

[144] Roselli CE, Klosterman S, Resko JA. Anatomic relationships between aromatase and androgen receptor mRNA expression in the hypothalamus and amygdala of adult male cynomolgus monkeys. J Comp Neurol. 2001; 439: 208-23.

[145] Sachs BD, Meisel RL. The physiology of male sexual behavior. In: Knobil E, Neil J, editors. The physiology of reproduction. New York: Raven Press; 1994, p 3-105.

[146] Cornil CA, Dalla C, Papadopoulou-Daifoti Z, Baillien M, Dejace C, Ball GF, Balthazart J. Rapid decreases in preoptic aromatic activity and brain monoamine concentrations after engaging in male sexual behavior. Endocrinology 2005; 146: 3809-20.

[147] Taziaux M, Keller M, Bakker J, Balthazart J. Sexual behavior activity tracks rapid changes in brain estrogen concentrations. J Neurosci. 2007; 27: 6563-72

[148] Hojo Y, Hattori T-A, Enami T, Furukawa A, Suzuki K, Ishii H-T, Mukai H, Morrison JH, Janssen WGM, Kominami S, Harada N, Kimoto T, Kawato S. Adult male rat hippocampus synthesizes estradiol from pregnenolone by cytochromes P45017a and P450 aromatase localized in neurons. Proc Natl Acad Sci USA 2004; 101: 865-70.

[149] Kretz O, Fester L, Wehrenberg U, Zhou L, Brauckmann S, Zhao S, Prange-Kiel J, Naumann T, Jarry H, Frotscher M, Rune GM. Hippocampal synapses depend on hippocampal estrogen synthesis. J Neurosci. 2004; 24: 5913-21.

[150] Rune GM, Frotscher M. Neurosteroid synthesis in the hippocampus: role in synaptic plasticity. Neurosci. 2005; 136: 833-42.

[151] Fester L, Ribeiro-Gouveia V, Prange-Kiel J, von Schassen C, Böttner M, Jarry H, Rune GM. Proliferation and apoptosis of hippocampal granule cells require local oestrogen synthesis. J Neurochem. 2006; 97: 1136-44.

[152] Martin S, Jones M, Simpson E, van den Buuse M. Impaired spatial reference memory in aromatase-deficient (ArKO) mice. Neuroreport 2003; 14: 1979-82.

[153] Garcia-Segura LM, Veiga S, Sierra A, Melcangi RC, Azcoitia I. Aromatase: a neuroprotective enzyme. Prog Neurobiol. 2003; 71: 31-41.

[154] Zhou L, Lehan N, Wehrenberg U, Disteldorf E, von Lossow R, Mares U, Jarry H, Rune GM. Neuroprotection by estradiol: a role of aromatase against spine synapse loss after blockade of $GABA_A$ receptors. Exp Neurol. 2007; 203: 72-81.

[155] McCullough LD, Blizzard K, Simpson ER, Öz OK, Hurn PD. Aromatase cytochrome P450 and extragonadal estrogen play a role in ischemic neuroprotection. J Neurosci. 2003; 23: 8701-5.

[156] Carswell HVO, Dominiczak AF, Garcia-Segura LM, Harada N, Hutchison JB, Macrae IM. Brain aromatase expression after experimental stroke: topography and time course. J Steroid Biochem Mol Biol. 2005; 96: 89-96.

[157] Giffard RG, Swanson RA. Ischemia-induced programmed cell death in astrocytes. Glia 2005; 50: 299-306.

[158] Hurn PD, Vannucci SJ, Hagberg H. Adult or perinatal brain injury: does sex matter? Stroke 2005; 36: 193-5.

[159] Budzar A, Howell A. Advances in aromatase inhibition: Clinical efficacy and tolerability in the treatment of breast cancer. Clin Cancer Res. 2001; 7: 2620-35.

[160] Plourde PV, Dyroff M, Dukes M. Arimidex. A potent and selective fourth-generation aromatase inhibitor. Breast Cancer Res treat. 1994; 30: 103-11.

[161] Iveson TJ, Smith IE, Ahern J, Smithers DA, Trunet PF, Dowsett M. Phase I study of the oral nonsteroidal aromatase inhibitor CGS 20267 in healthy postmenopausal women. J Clin Endocrinol Metab. 1993; 77: 324-31.

[162] di Salle E, Giudici D, Briatico G, Ornati G. Novel irreversible aromatase inhibitors. Ann NY Acad Sci. 1990; 595: 357-67.

[163] Goss PE, Clark RM, Ambus U. Phase II study of vorozole (R83842), a new aromatase inhibitor, in postmenopausal women with advanced breast cancer in progression of tamoxifen. Clin Cancer Res. 1995; 1: 287-94.

[164] Goss PE, Winer EP, Tannock IF, Schwartz LH. Randomized phase III trial comparing the new potent and selective third-generation aromatase inhibitor vorozole with megestrol acetate in postmenopausal advanced breast cancer patients. J Clin Oncol. 1999; 17: 52-63.

[165] Lidström P, Bonasera TA, Kirilovas D, Lindblom B, Lu L, Bergström E, Bergström M, Westlin J-E, Långström B. Synthesis, in vivo rheus monkey biodistribution and in vitro evaluation of a ^{11}C-labelled potent aromatase inhibitor: [N-methyl-^{11}C]vorozole. Nucl Med Biol. 1998; 25: 497-501.

[166] Takahashi K, Bergström M, Frändberg P, Vesström E-L, Watanabe Y, Långström B. Imaging of aromatase distribution in rat and rhesus monkey brains with [^{11}C]vorozole. Nucl Med Biol. 2006; 33: 599-605.

[167] Takahashi K, Hallberg M, Magnusson K, Nyberg F, Watanabe Y, Långström B, Bergström M. Increase in [^{11}C]vorozole binding to aromatase in the hypothalamus in rats treated with anabolic adrogenic steroids. Neororeport 2007; 18: 171-4.

[168] Takahashi K, Tamura Y, Watanabe Y, Långström B, Bergström M. Alteration in [^{11}C]vorozole binding to aromatase in neuronal cells of rat brain induced by anaboli androgenic steroids and flutamide. Neuroreport 2008; 19: 431-5.

[169] Wang M, Lacy G, Gao M, Miller KD, Sledge GW, Zheng Q-H. Synthesis of carbon-11 labeled sulfoanilide analogues as new potential PET agents for imaging of aromatase in breast cancer. Bioorg Med Chem Lett. 2007; 17: 332-6.

[170] Bhatnagar AS, Häusler A, Schieweck K, Lang M, Bowman R. highly selective inhibition of estrogen biosynthesis by CGS 20267, a new non-steroidal aromatase inhibitor. J Steroid Biochem Mol Biol. 1990; 37: 1021-7.

[171] Vanden Bossche H, Willemsens G, Roels I, Bellens D, Moereels H, Coene M-C, Le Jeune L, Lauwers W, Janssen PAJ. R76713 and enantiomers: selective

nonsteroidal inhibitors of the cytochrome P450-dependent oestrogen synthesis. Biochem Pharmacol. 1990; 40: 1707-18.

[172] Bhatnagar AS, Häusler A, Schieweck K. Inhibition of aromatase in vitro and in vivo by aromatase inhibitors. J Enzyme Inhib Med Chem. 1990; 4: 179-86.

[173] Wood PM, Woo LWL, Humphreys A, Chander SK, Purohit A, Reed MJ, Potter BVL. A letrozole-based dual aromatase-sulphatase inhibitor with in vivo activity. J Steroid Biochem Mol Biol. 2005; 94: 123-30.

[174] Bowman RM, Steele RE, Browne L. Alpha-heterocyclic substituted tolunitriles. 1990 US 4,978,672.

[175] Lang M, Differding E, Stanek J. α-fluoro-α-tetrazolyl-phenylmethyl derivatives useful as aromatase inhibitors. 1993 US 5,227,393.

[176] Wang D, Kuang L, Li Z, Ding K. L-Proline-promoted Rosenmund-von Braun reaction. Synlett 2008; 1: 69-72.

[177] Enquist P-A, Nilsson P, Larhed M. Ultrafast chemistry: Cobalt carbonyl-mediated synthesis of Diaryl ketones under microwave irradiation. Org Lett 2003; 5: 4875-8.

[178] Andersson Y, Långström B. Transition metal-mediated reactions using [^{11}C]cyanide in synthesis of ^{11}C-labelled aromatic compounds. J Chem Soc Perkin Trans I 1994; 1395-400.

[179] Kil K-E, Ding Y-S, Lin K-S, Alexoff D, Kim SW, Shea C, Xu Y, Muench L, Fowler JS. Synthesis and positron emission tomography studies of carbon-11-labeled imatinib (Gleevec®). Nucl Med Biol. 2007; 34: 153-63.

[180] Balatoni JA, Adam MJ, Hall LD. Synthesis of ^{11}C-labeled aromatics using aryl chromium tricarbonyl intermediates. J Labelled Compd Radiopharm. 1999; 26: 159-64.

[181] Ponchant M, Hinnen F, Demphel S, Crouzel C. [^{11}C]Copper(I) cyanide: a new radioactive precursor for ^{11}C-cyanization and functionalization of haloarenes. Appl Radiat Isot. 1997; 48: 755-62.

[182] Sandell J, Halldin C, Hall A, Thorberg S-O, Werner T, Sohn D, Sedvall G, Farde L. Radiosynthesis and autoradiographic evaluation of [^{11}C]NAD-299, a radioligand for visualization of 5-HT$_{1A}$ receptor. Nucl Med Biol. 1999; 26: 159-64.

[183] Sioufi A, Sandrenan N, Godbillon J, Trunet P, Czendlik C, Howald H, Pfister CH, Ezzet F. Comparative bioavailability of letrozole under fed and fasting conditions in 12 healthy subjects after a 2.5 mg single oral administration. Biopharm Drug Dispos. 1997; 18: 489-97.

[184] Sioufi A, Gauducheau N, Pineau V, Marfil F, Jaouen A, Cardot JM, Godbillon J, Czendlik C, Howald H, Pfister CH, Vreeland F. Absolute bioavailability of letrozole in healthy postmenopausal women. Biopharm Drug Dispos. 1997; 18: 779-89.

[185] Pfister CU, Martoni A, Zamagni C, Lelli G, De Braud F, Souppart C, Duval M, Hornberger U. Effect of age and single versus multiple dose pharmacokinetics of letrozole (Femara®) in breast cancer patients. Biopharm Drug Dispos. 2001; 22: 191-7.

[186] Richards JG, Saura J, Luque JM. Monoamine oxidases: from brain maps to physiology and transgenics to pathophysiology. J Neural Transm 1998; 52 (Suppl): 173-87.

[187] Bach AWJ, Lan NC, Johnson DL, Abell CW, Bembenek ME, Kwan SW, Seeburg PH, Shih JC. cDNA cloning of human liver monoamine oxidase A and B: molecular basis of differences in enzymatic properties. Proc Natl Acad Sci USA 1988; 85: 4934-8.

[188] Johnson JP. Some observations upon a new inhibitor of monoamine oxidase in brain tissue. Biochem Pharmacol 1968; 17: 1285-97.

[189] Knoll J, Magyar K. Some puzzling pharmacological effects on monoamine oxidase inhibitors. Adv Biochem Psychopharmacol 1972; 5: 393-408.

[190] Youdim MB, Riederer J. Dopamine metabolism and neurotransmission in primate brain in relationship to monoamine oxidase A and B inhibition. J Neural Transm Gen Sect 1993; 91: 181-95.

[191] Saura J, Kettler R, Da Prada M, Richards JG. Quantitative enzyme autoradiography with ^{3}H-Ro 41-1049 and ^{3}H-Ro 19-6327 in vitro: localization and abundance of MAO-A and MAO-B in rat CNS, peripheral organs, and human brain. J Neurosci 1992; 12: 1977-99.

[192] Saura J, Bleuel Z, Ulrich J, Mendelowitsch A, Chen K, Shih JC, Malherbe P, Da Prada M, Richards JG. Molecular neuroanatomy of human monoamine oxidases A and B revealed by quantitative enzyme radioautography and in situ hybridization histochemistry. Neurosci 1996; 70: 755-74.

[193] Fowler JS, Logan J, Wang G-J, Franceschi D, Volkow LD, Telang F, Pappas N, Ferrieri R, Shea C, Garza V, Xu Y, King P, Schlyer D, Gatley SJ, Ding Y-S, Warner D, Netusil N, Carter P, Jayne M, Alexoff D, Zhu W, Vaska P. Monoamine oxidase A imaging in peripheral organs in healthy human subjects. Synapse 2003; 49: 178-87.

[194] Fowler JS, Logan J, Wang G-J, Volkow LD, Zhu W, Franceschi D, Pappas N, Ferrieri R, Shea C, Garza V, Xu Y, MacGregor RR, Schlyer D, Gatley SJ, Ding Y-S, Alexoff D. PET imaging of monoamine oxidase B in peripheral organs in humans. J Nucl Med 2002; 43: 1331-8.

[195] Schildkraut JJ. The catecholamine hypothesis of affective disorders: a review of supporting evidence. Am J Psychiatry 1965; 122: 509-22.

[196] Anderson MC, Hasan F, McCrodden JM, Tipton KF. Monoamine oxidase inhibitors and the cheese effect. Neurochem Res 1993; 18: 1145-9.

[197] Tetrud JW, Langston JW. The effect of deprenyl (selegiline) on the natural history of Parkinson's disease. Science 1989; 245: 519-22.

[198] Parkinson's Study Group. The effect of deprenyl on the progression of disability in early Parkinson's disease. N Eng J Med 1989; 321: 1364-71.

[199] Abeles RH, Maycock AL. Suicide Enzyme Inactivators. Acc Chem Res 1976; 9: 313-9.

[200] Fowler JS, Volkow ND, Logan J, Wang G-J, MacGregor RR, Schlyer D, Wolf AP, Pappas N, Alexoff D, Shea C, Dorflinger E, Kruchowy L, Yoo K, Fazzini E, Patlak C. Slow recovery of human brain MAO B after L-Deprenyl (Selegeline) withdrawal. Synapse 1994; 18: 86-93.

[201] Zhuang Z, Hogan M, McCauley R. The in vitro insertion of monoamine oxidase B into mitochondrial outer membranes. FEBS Lett 1988; 238: 185-90.

[202] Fowler JS, Volkow ND, Logan J, Schlyer DJ, MacGregor RR, Wang G-J, Wolf AP, Pappas N, Alexoff D, Shea C, Gatley SJ, Dorflinger E, Yoo K, Morawsky L, Fazzini E. Monoamine oxidase B (MAO B) inhibitor therapy in Parkinson's disease: the degree and reversibility of human brain MAO B inhibition by Ro 19-6327. Neurology 1993; 43: 1984-92.

[203] Cesura AM, Galva MD, Imhof R, Kyburz E, Picotti GB, Da Prada M. [^{3}H] Ro 19-6327: a reversible ligand and affinity labelling probe for monoamine oxidase B. Eur. J. Pharmacol 1989; 162: 457-65.

[204] Bergstrom M, Westerberg G, Langstrom B. ^{11}C-Harmine as a tracer for monoamine oxidase A (MAO-A): in vitro and in vivo studies. Nucl Med Biol 1997; 24: 287-94.

[205] Bergstrom M, Westerberg G, Kihberg T, Langstrom B. Synthesis of some ^{11}C-labelled MAO-A inhibitors and their in vivo uptake kinetics in rhesus monkey brain. Nucl Med Biol 1997; 24: 381-8.

[206] Fowler JS, Ding Y-S, Logan J, Macgregor RR, Shea C, Garza V, Gimi R, Volkow ND, Wang G-, Schlyer D, Ferrieri R, Gatley SJ, Alexoff D, Carter P, King P, Pappas N, Arnett CD. Species differences in [^{11}C]clorgyline binding in brain. Nucl Med Biol 2001; 28: 779-85.

[207] Beer HF, Frey LD, Haberli M, Schubiger PA. [^{123}I/^{18}F] N-(2-aminoethyl)-5-halogeno-2-pyridinecarboxamides, site specific tracers for MAO-B mapping with SPECT and PET. J Nucl Med Biol 1995; 22: 999-1004.

[208] Bernard S, Fuseau C, Schmid L, Milcent R, Crouzel C. Synthesis and in vivo studies of a specific monoamine oxidase B inhibitor: 5-[4-(benzyloxy)phenyl]-3-(2-cyanoethyl)-1,3,4-oxadiazol-[^{11}C]-2(^{3}H)-one. Eur J Nucl Med 1996; 23: 150-6.

[209] MacGregor RR, Fowler JS, Wolf AP, Halldin C, Langström B. Synthesis of suicide inhibitors of monoamine oxidase: Carbon-11 labeled clorgyline, L-deprenyl and D-deprenyl. J Labeled Compd Radiopharm 1988; 25: 1-9.

[210] Fowler JS, MacGregor RR, Wolf AP, Arnett CD, Dewey SL, Schlyer D, Christman D, Logan J, Smith M, Sachs H, Aquilonius SM, Bjurling P, Halldin C, Hartvig P, Leenders KL, Lundqvist H, Oreland L, Stalnacke C-G, Langström B. Mapping human brain monoamine oxidase A and B with ^{11}C-labeled suicide inactivators and PET. Science 1987; 235: 481-5.

[211] Logan J, Fowler JS, Ding Y-S, Franceschi D, Wang G-J, Volkow ND, Felder C, Alexoff D. Strategy for the formation of parametric images under conditions of low injected radioactivity applied to PET studies with the irreversible monoamine oxidase A tracers [^{11}C]clorgyline and deuterium-substituted [^{11}C]clorgyline. J Cereb Blood Flow Metab 2002; *22*: 1367-76.

[212] Fowler JS, Wang G-J, Logan J, Xie S, Volkow ND, MacGregor RR, Schlyer DJ, Pappas N, Alexoff DL, Patlak C, Wolf AP. Selective reduction of radiotracer trapping by deuterium substitution: comparison of carbon-11-l-deprenyl and carbon-11-deprenyl-D_2 for MAO B mapping. J Nucl Med 1995; 36: 1255-62.

[213] Fowler JS, Logan J, Ding Y-S, Franceschi D, Wang G-J, Volkow ND, Pappas N, Schlyer D, Gatley SJ, Alexoff D, Felder C, Biegon A, Zhu W. Non-MAO A binding of clorgyline in white matter in human brain. J. Neurochem 2001; 79: 1039-46.

[214] Nakamura S, Kawamata T, Akiguchi I, Kameyama M, Nakamura N, Kimura H. Expression of monoamine oxidase B activity in astrocytes of senile plaques. Acta Neuropathol 1990; 80: 419-25.

[215] Kumlien E, Bergstrom M, Lilja A, Andersson J, Szekeres V, Westerberg CE, Westerberg G, Antoni G, Långström B. Positron emission tomography with [^{11}C]deuterium-deprenyl in temporal lobe epilepsy. Epilepsia 1995; 36: 712-21.

[216] Fowler JS, Volkow ND, Wang G-J, Logan J, Pappas N, Shea C, MacGregor RR. Age-Related Increases in Brain Monoamine Oxidase B in Living Healthy Human Subjects. Neurobiol Aging 1997; 18: 431-5.

[217] Saura J, Andres N, Andrade C, Ojuel J, Eriksson K, Mahy N. Biphasic and region-specific MAO-B response to aging in normal human brain. Neurobiol Aging 1997; 18: 497-507.

[218] Fowler JS, Volkow ND, Wang G-J, Pappas N, Logan J, Shea C, Alexoff D, MacGregor RR, Schlyer DJ, Zezulkova I, Wolf AP. Brain monoamine oxidase A inhibition in cigarette smokers. Proc Natl Acad Sci USA 1996; 93: 14065-9.

[219] Fowler JS, Wang J-K, Volkow ND, Pappas N, Logan J, MacGregor RR, Alexoff D, Shea C, Schlyer D, Wolf AP, Waener D, Zezulkova I, Cilento R. Inhibition of monoamine oxidase B in the brains of smokers. Nature 1996; 379: 733-6.

[220] Fowler JS, Wang G-J, Volkow ND, Franceschi D, Logan J, Pappas N, Shea C, MacGregor RR, Garza V. Smoking a single cigarette does not produce a measurable reduction in brain MAO B in non-smokers. Nicotine Tob Res 1999; 1: 325-9.

[221] Morens DM, Grandinetti A, Reed D, White LR, Ross GW. Cigarette smoking and protection from Parkinson's disease: false association or etiologic clue? Neurology 1995; 45: 1041-51.

[222] Baron JA. Beneficial effects of nicotine and cigarette smoking: the real, the possible and the spurious. Br Med Bull 1996; 52: 58-73.

[223] South MS. Synthesis and reactions of halogenated thiazole isocyanates. J Heterocyclic Chem 1991; 28: 1003-11.

[224] Blank B, DiTullio NW, Owings FF, Deviney L, Miao CK, Saunders HL. Mercapto heterocyclic carboxylic acids, analogs of 3-mercaptopicolinic acid. J Med Chem 1977; 20: 572-6.

[225] Murayama T, Kano Y, Ando T, Sasaki T, Sawabe T, Baba N, Takata H, Suzuki H, Aihara K, Fujita T. 2-Thioethenyl Carbaphenem Derivative. 2006; WO2006109823.

[226] Kanao M, Watanabe Y, Kimura Y, Saegusa J, Yamamoto K, Kanno H, Kanaya N, Kubo H, Ashida S-I, Ishikawa F. Thromboxane A2 synthetase inhibitors. 2. Synthesis and activities of tetrahydro-naphthalene and indan derivatives. J Med Chem 1989; 32: 1326-34.

[227] Hodgetts KJ, Kershaw MT. Regiocontrolled synthesis of substituted thiazoles. Org Lett 2002; 4: 1363-5.

[228] Thompson WJ, Gaudino J. A general synthesis of 5-arylnicotinates. J Org Chem 1984; 49: 5237-43.

[229] Oh C-H, Cho H-W, Baek D, Cho J-H. Synthesis and antibacterial activity of 1β-methyl-2-(5-substituted thiazolopyrrolidin-3-ylthio)carbapenem derivatives. Eur J Med Chem 2002; 37: 743-54.

[230] Höefl G, Steglich W. 4-Dialkylaminopyridine as acylation catalysts; III. Acylation of sterically hindered alcohols. Synthesis 1972; 11: 619-21.

[231] Egli RA. Katalysierte nitrilreduktionen mit natriumborhydrid. Helv Chim Acta 1970; 53: 47-53.

[232] See Ro 41-1049 HCl Salt MSDS. http://www.sigmaaldrich.com/catalog/search/P**ro**ductDetail/SIGMA/R107 accessed by Internet on 10/16/2007

[233] Jones RCF, Smallridge MJ. Tetrahydrofolate coenzyme models: synthesis of tetrahydroimidazo-isoquinolines and tetrahydroimidazoquinolines. J Chem Soc Perkin Trans 1 1990; 385-91.

[234] Graf R. Über die 4,6-Dichlor- und die 4,5,6-Trichlor-picolinsäure. J Prakt Chem 1932; 133: 36-50.

[235] Miyaura N, Suzuki A. Palladium-catalyzed cross-coupling reactions of organoboron compounds. Chem Rev 1995; 95: 2457-83.

[236] Gassner W, Imhof R, Kyburz E. Preparation of N-(2-aminoethyl) azolecarboxamides as monoamine oxidase inhibitors. EP0352581, 1990.

[237] Cesura AM, Bös M, Galva MD, Imhof R, Prada MDA. Characterization of the binding of [^{3}H]Ro41-1049 to the active site of human monoamine oxidase-A. Mol Pharmacol 1989; 37: 358-66.

[238] Engbersen JFJ, Koudijs A, Joosten MHA, van der Plas HC. Synthesis of 2-aminomethyl-1, 10-phenanthroline. A new chelating agent and versatile synthon for other chelating compounds. J Heterocyclic Chem 1986; 23: 989-90.

[239] Satoh T, Suzuki S. Reduction of organic compounds with sodium borohydride-transition metal salt system (1). Tetrahedron Lett 1969; 52: 4555-8.

[240] Klenke B, Gilbert IH. Nitrile reduction in the presence of Boc-protected amino groups by catalytic hydrogenation over palladium-activated Raney-Nickel. J Org Chem 2001; 66: 2480-3.